University of Strathclyde
Glasgow
Strathclyde Institute of Pharmacy and Biomedical Sciences

Investigations of the Physicochemical Properties of Waxes and Wax Matrix Pellet Formulations

Wipapan Phajongwiriyathorn
B.Sc. Pharm (Hons)

Ph.D. Thesis
April 2008

DECLARATION

This PhD thesis is dedicated to my Mum and Dad,

for all love and support throughout my life.

ACKNOWLEDGEMENTS

I would like to thank my academic supervisors, Professor Howard N.E. Stevens and Dr. Alexander B. Mullen for their excellent supervision, guidance and encouragement during the course of my PhD.

Thank you to my mum and dad, Naowarat and Mongkongnam Phajongwiriyathorn as well as my older brothers, Chaiwat and Nirut P. for their constant love and support.

Thank you to Professor Alastair Florence for help with X-ray powder diffraction.

Thank you to The Thailand Government Pharmaceutical Organisation for financial support throughout my PhD studies.

Thank you to my fabulous laboratory friends, Drs. Fiona McInnes & Manish Ghimire, Jung Kim, Jacob Frum, Jing Yan, Utsana Puapermpoonsiri, Gemma Coombs, Sarah Connolly, Yoon Wong Sim, Omar Sarheed, Shiow Fern Ng and Kar Wai Chooi for a most memorable time working at SIBS 218.

Thank you especially to Rachit Rungrongthanin for the constant care and encouragement.

Thank you to my Thai friends, Veerades, P., Sakchai, S., Thanundorn, P., Bongkoj S., Pornpisut, W., Wimonmat, B., for your hospitality and friendship during my 3 years in Glasgow.

Thank you to Dr. Lawrence Tetley and Margaret Mullen at the Institute of Biological Life Sciences, University of Glasgow for help with SEM.

Thanks to Anne Goudie, Steve Steer, Peter Constable, Tommy McGrory, John Nevin and Ian Simpson for excellent technical help throughout my PhD.

ABSTRACT

The research resulted in the development of wax matrix pellet systems using a direct warm spheronisation method for use as sustained release devices in oral drug delivery. The effect of altering process parameters on resultant pellet morphology, size distribution and in vitro dissolution performance was evaluated. Changes in the physicochemical and morphological properties of glyceryl monostearate (GMS) and glyceryl palmitostearate (GPS) used in pellet formulations following ageing were monitored by use of FT-IR spectrophotometry, differential scanning calorimetry, hot stage microscopy, X-ray powder diffraction, texture analyses, polarised light microscopy, scanning electron microscopy and dissolution testing.

Use of the direct warm spheronisation process resulted in the production of the unstable α-form of GMS that slowly reverted to the stable β-polymorph upon storage at 25°C but GPS exhibited changes in crystallinity upon storage. Thermal annealing of GMS and GPS formulations at 46°C resulted in the melt-solidified GMS (α-form) more rapidly transforming to the stable ß-form whereas melt-solidified GPS crystallised faster when compared to 25°C. The thermal annealing cycle at 46°C caused divergent effects in GMS and GPS pellet formulation dissolution performance with decreased drug release rates observed for GMS pellet formulations and increased drug release rates observed for GPS pellet formulations. Moreover, dissolution performance of pellet formulations after annealing was dependent on both wax and drug composition. The inclusions of excipients that stabilised the thermal properties of wax were only effective in preventing modification in pellet dissolution performance for short periods (2 weeks) post-annealing. The combined use of excipients and thermal annealing to stabilise the properties of waxes and provide consistent performance of the delivery device requires further optimisation before it can be a truly useful application for the industrial manufacture of pharmaceutical wax-based oral delivery devices.

PUBLICATIONS

Phajongwiriyathorn, W., Stevens, H.N.E., Mullen, A.B., (2006) Polymorphic transformation of glyceryl monostearate. *British Pharmaceutical Conference Science Proceedings*.

Phajongwiriyathorn, W., Stevens, H.N.E., Mullen, A.B., (2006) Processing factors in glyceryl monostearate matrix pellets based on direct warm spheronisation. *British Pharmaceutical Conference Science Proceedings*.

Phajongwiriyathorn, W., Stevens, H.N.E., Mullen, A.B., (2006) Polymorphic transformation of glyceryl monostearate. *AAPS Annual Meeting and Exposition Proceedings*.

Phajongwiriyathorn, W., Stevens, H.N.E., Mullen, A.B., (2007) Stability of glyceryl monostearate (GMS) and glyceryl palmitostearate (GPS). *AAPS Annual Meeting and Exposition Proceedings*.

CONTENTS

ABBREVIATIONS

DCP	Dibasic calcium phosphate dihydrate (Emcompress®)
DSC	Differential scanning calorimeter
DTA	Differential thermal analysis
DTZ	Diltiazem hydrochloride
FT-IR	Fourier Transform Infra Red spectrophotometer
GDB	Glyceryl dibehenate (Compritol 888 ATO®)
GMS	Glyceryl monostearate (Galeol®)
GPS	Glyceyl palmitostearate (Precirol®)
HCl	Hydrochloric acid 37%
HLB	Hydrophile-lipophile balance
$HPMC_{K15M}$	Hydroxylpropryl methyl cellulose (Methocel® K15 M)
HSM	Hot stage microscope
HSPM	Hot stage polarising microscope
KBr	Potassium bromide
PCM	Paracetamol
PEG	Polyethylene glycol
PEG 1450	Polyethylene glycol 1450 flake (Carbowax®)
PG8BX	Polyethylene glycol-8 beeswax (Apifil®)
RH	Relative humidity
SEM	Scanning electron microscope
XRPD	X-ray powder diffraction

CHAPTER 1

INTRODUCTION

The aim of this study is the development of a sustained release wax matrix pellet formulation using a direct warm spheronisation method. This introduction reviews sustained release matrix pellets in general, drug monographs, wax materials, wax matrix pelletisation, wax stability and factors affecting in vivo drug release and biopharmaceutical studies of wax formulations.

1.1 Sustained release matrix pellets in general

The term "sustained release" is used to explain a dosage form that delays drug release so that its plasma profile is sustained for a longer duration. The onset of pharmacologic action can also often be retarded and plasma levels manipulated (Chien, 1992). A significant aim of sustained release drug systems is to improve therapeutic efficacy by increasing patient compliance and decreasing incidences of adverse effect from untoward plasma drug concentrations. Ideally, a sustained release dosage form provides predictable and constant therapeutic concentration of drug in the body. Fluctuation of drug levels in the blood cause unwanted side effects and toxicity if the concentration is above desired therapeutic levels (Gandhi et al., 1999).

Matrix drug delivery systems consist of heterogeneous dispersion of drug particles in the matrix and their advantages and disadvantages are compared with polymeric coating systems. Matrix systems are cheaper and easier to manufacture than utilising film coating processes. Matrix systems are also reported to avoid irreproducible drug release profiles (Gandhi al., 1999). In contrast, polymeric coating systems exhibit greater variability than matrix systems because of issues surrounding film thickness, film cracking, polymer ageing and other parameters during the production leading to variations between individual batches. Spray coating processes in polymeric coating

systems may use organic solvents which are hazardous to health and environmental pollutants (Maejima et al., 1997). A stated disadvantage of matrix systems is that they are difficult to manufacture as small wax matrix pellets or granules because of aggregation of granules during production (Miyagawa et al., 1996). In some cases, drug release rate is difficult to control accurately from matrix systems because of the variable nature of the waxes themselves. In addition, excipient concentrations and drug particle size distribution will also contribute to overall variability (Miyagawa et al., 1996; Maejima et al., 1997).

Sustained release drug systems are broadly divided into two types: single unit dosage forms and multiparticulate systems. Multiparticulate systems consist of a multiplicity of small discrete units referred to as pellets, beads or spheroids. Pellets are spheres that differ in their diameters depending upon their specific applications. In pharmaceutical applications for subsequent filling into capsules, they are typically between 500 to 1500 μm (Vervaet et al., 1995). Pellets provide numerous therapeutic and technological advantages. In terms of therapeutic action, pellets result in enhanced drug absorption due to their being freely dispersed in the gastrointestinal tract which minimises local potential high drug concentrations, decreasing irritation of the gastrointestinal tract. By abolishing dose dumping, systemic side effects are minimised. From a technological perspective, pellets provide good flow properties, are robust and have a narrow particle size distribution (Gandhi et al., 1999).

Drug release from oral sustained release systems occurs by several mechanisms such as diffusion, erosion, dissolution, osmotic pressure and swelling. The mechanisms controlling drug release from sustained release matrix systems are diffusion, erosion or a combination of both diffusion and erosion as discussed below.

Diffusion. Diffusion mechanisms operate with non-disintegrating dosage forms. Such matrix dosage forms permit the drug to dissolve in dissolution media and diffuse out from the matrix and can be described by Fick's laws. The rate of drug release is controlled by the rate of water penetration into matrix and drug solubility

(Akiyama et al., 1993; Duclos et al., 1999; Peh et al., 2000; Frenning and Stromme, 2003).

Erosion. Drug is homogeneously distributed in an erodible matrix. Water interacts with the surface of the dosage form and erodes with drug liberation into bulk diffusion medium. The composition of the erodible formulation, geometry and mass transport phenomena affect the rate of drug release (Siepmann and Gopferich, 2001; Shen et al., 2002; Acemoglu, 2004).

Drug release from oral dosage forms can be explained by a kinetic model as shown below.

$$Q = f(t) \qquad \text{[Eqn. 1.1]}$$

$$Q = Kt^n \qquad \text{[Eqn. 1.2]}$$

[where Q = Amount of drug release (fraction or % drug dissolved from total drug present); t = duration of drug release (minute); K, n = constant values]

Value of n (release exponent) depends on the type of drug release kinetic in the dosage form as shown in Figure 1.1 (Costa and Sousa Lobo, 2001).

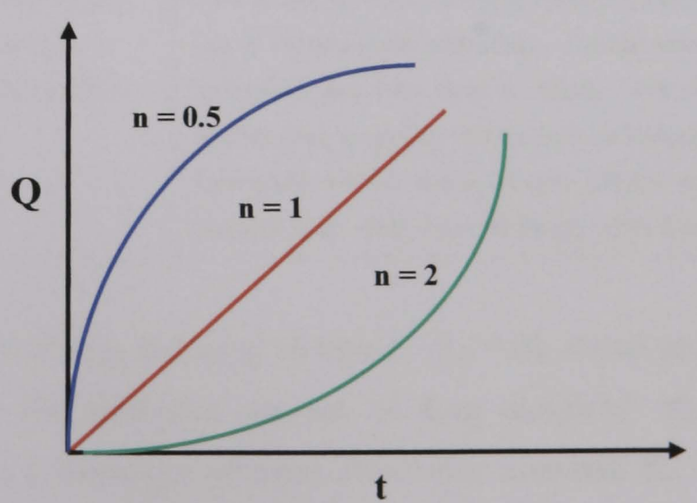

Figure 1.1. Effect of the release exponent (n) on characteristic profiles of drug release.

A summary of drug release kinetics is shown in Table 1.1 below.

Table 1.1. The type of drug release kinetic in the oral sustained release dosage forms.

Release exponent (n)	**Drug release kinetic**	**Equation**	**Characteristics**
0.5	Higuchi (Fickian)	$Q_t = K_H t^{1/2}$	The mechanism of drug release indicates a diffusion pathway. This model is used to study the release of water soluble and low soluble drug in semi-solid and/or solid matrix dosage form (Siepmann and Peppas, 2001; Rinaki et al., 2003; Crowley et al., 2004; Galal et al., 2004).
0.5<n<1.0	Anomalous (non-Fickian)	$Q_t / Q_\infty = K_k t^n$	Anomalous transport can be applied by Korsmeyer-Peppas model as shown in the equation. The mechanism of drug release indicates the combination of diffusion and erosion pathway. This model is used to describe the drug release in hydrophobic or polymeric dosage form which is unknown and/or combination of release mechanisms (Bodea and Leucuta, 1997; San Vicente et al., 2000; Roy and Xu, 2001; Khan and Craig, 2003; Jannin et al., 2006).
1.0	Zero order (linear)	$Q_t = Q_0 + K_0 t$	This model is used to describe systems which the drug release rate is independent of concentration. Dosage forms do not disintegrate and drug dissolution rate is slow assuming no area change. For examples: matrix tablets with low soluble drug, coated dosage forms, osmotic systems and transdermal systems (Danckwerts, 1994; Kim, 1995; Varelas et al., 1995; Caraballo et al., 1996; Chidambaram et al., 1998; Qiu et al., 1998; Galal et al., 2004).
2.0	First order (non-linear)	$Q_t = Q_0 e^{-K_1 t}$ $\ln Q_t =$ $\ln Q_0 + K_1 t$	This model is used to describe systems which the drug release rate is concentration dependent. Dosage forms absorb water and swell, then force drug to release. For examples: water-soluble drug in porous matrix such as hydrogel polymer and hydrophilic HPMC matrix systems (Mulye and Turco, 1995; Ehtezazi et al., 2000; Nur and Zhang, 2000; Rao et al., 2000).

[where Q_t = the amount of drug dissolved in time t, Q_0 = the initial amount of drug in the solution, Q_∞ = the maximum amount of drug dissolved, K_H = Higuchi dissolution constant, K_k = Korsmeyer-Peppas dissolution constant, K_0 = Zero order release constant, K_1 = First order release constant]

1.2 Drug monographs

1.2.1 Paracetamol

Paracetamol or acetaminophen, known also as N-acetyl-p-aminophenol, consists of a benzene ring core, substituted 1,4 (para) by one hydroxyl group and the nitrogen atom of an amide group. Molecular weight is 151.2 g/mol and chemical formula is $C_8H_9NO_2$ as given below.

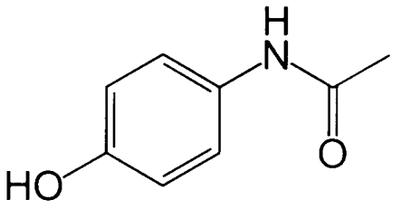

Figure 1.2. Chemical structure of paracetamol ($C_8H_9NO_2$) (Mills, 2006).

Paracetamol is a white, crystalline powder, slightly soluble in water (solubility = 14 mg/ml at 20°C), freely soluble in alcohol, very slightly soluble in ether and methylene chloride as well as insoluble in petroleum ether, pentane and benzene. The melting point is 168 - 172°C. Paracetamol should be stored in a well-closed container and protected from light. It is a common analgesic and antipyretic drug that is used for the relief of fever, headaches and other minor pains (British Pharmacopoeia, 1999; Moffat et al., 2004).

1.2.2 Diltiazem hydrochloride

Diltiazem hydrochloride is 1,5-Benzothiazepin-4(5H)-one, 3-(acetyloxy)-5[2-(dimethylamino)ethyl]-2,-3-dihydro-2(4-methoxyphenyl)-, mono-hydrochloride, (+)-cis. Molecular weight is 451 g/mol and chemical formula is $C_{22}H_{26}N_2O_4S{\cdot}HCl$ as shown below.

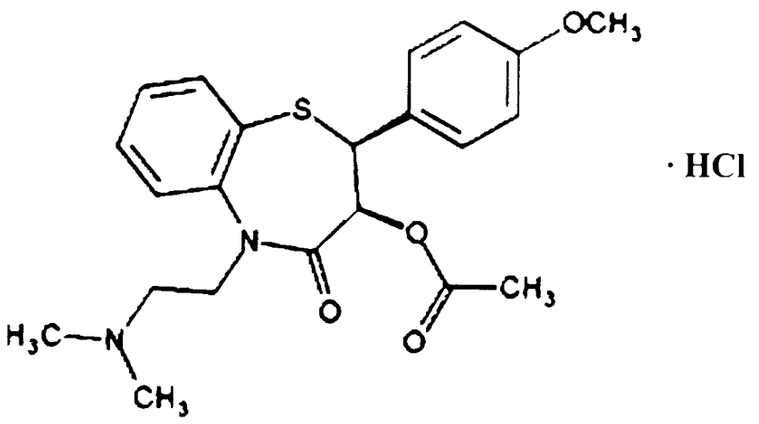

Figure 1.3. Chemical structure of diltiazem hydrochloride ($C_{22}H_{26}N_2O_4S{\cdot}HCl$) (GIMP, 2004).

Diltiazem hydrochloride is a white, crystalline powder, freely soluble in water, methanol, chloroform and methylene chloride as well as slightly soluble in ethanol. The melting point is 207.5 - 212.0°C. In storage condition, diltiazem hydrochloride should be stored in a tightly closed container and protected from light. It is a calcium channel blocker used in the treatment of hypertension, angina pectoris and some types of arrhythmia (British Pharmacopoeia, 1999; Moffat et al., 2004).

1.3 Wax materials

1.3.1 Characteristics

General characteristics of waxes are their lipophilic properties, insolubility in water and limited solubility in non-polar solvents such as ether, chloroform and dimethyl sulfoxide. These materials may feel greasy and appear slightly yellowish. From their properties, wax materials provided both advantages and disadvantages as formulation excipients as shown below.

Advantages

- Drug release of highly soluble drugs can be sustained by using a wax controlled-release system (Peh et al., 2000; Reitz and Kleinebudde, 2007).
- Enhancement of bioavailability of poorly soluble drugs can be controlled by using a wax formulation (Chauhan et al., 2005a).

- Taste masking of bitter tasting drugs can be produced by a wax system (Yajima et al., 2003).
- Floating wax dosage forms can prevent the gastric irritation of drugs (Shimpi et al., 2004; Chauhan et al., 2005a).
- The wide range of physicochemical properties of waxes provides opportunity for manipulating drug release profiles and formulation strategies (Gren and Nystrom, 1999).
- Waxes are generally non-toxic and chemically inert hydrophobic materials (Miyagawa et al., 1996; Gren and Nystrom, 1999).
- They are relatively inexpensive materials and do not require use of organic solvents (Gren and Nystrom, 1999).

Disadvantages

- High drug loadings or large particle sizes may result in poor drug uniformity (Gren and Nystrom, 1999).
- Manufacture at large scale can be problematic due to variation in the chemical composition of waxes as well as the drug concentration (Gren and Nystrom, 1999).
- Drug release may not be constant during storage but may change during ageing (Gren and Nystrom, 1999).
- Since processing requires elevated temperatures, it is unsuitable for thermolabile drugs (Miyagawa et al., 1996).
- Strict temperature control is required during the manufacturing process because waxes must be processed at temperatures above their melting points (Miyagawa et al., 1996).
- Many waxes have unstable physicochemical properties that change during storage (Craig, 1995).

1.3.2 Classification

Hydrophobic pharmaceutical materials are divided into 3 main types, i.e. lipids, waxes and glycerides.

1.3.2.1 Lipids

Lipids are subdivided into non-polar and polar lipids. The non-polar lipids contain oils with aliphatic hydrocarbon chains such as paraffin oil, hydrogenated castor oil and hydrogenated rape oil. Examples of polar lipids are fatty acids such as stearic acid and myristic acid or fatty alcohols such as cetostearyl alcohol, stearic alcohol and cetyl alcohol.

1.3.2.2 Waxes

A wax is normally described as a substance which is a plastic solid at room temperature and a liquid of low viscosity at temperatures above its melting point. Examples of waxes are carnauba wax, beeswax, paraffin wax and microcrystalline wax.

1.3.2.3 Glycerides

Glycerides are esters formed between glycerol and fatty acids. The basic structure of a glyceride is shown below.

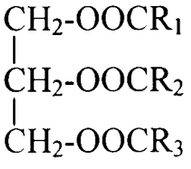

Figure 1.4. Basic structure of a glyceride.

R_1, R_2 and R_3 are the hydrocarbon moieties of the saturated fatty acids such as capric, lauric, myristic, palmitic and stearic acids or unsaturated fatty acids such as oleic, linoleic and palmitoleic acids. The alcohol groups can be esterified with fatty acids referred in terms of mono-, di- and triglycerides (Craig, 1995).

Gelucires are a commercial family of glyceride based materials composed of mixtures of glycerides and esters of polyethylene glycol (PEG; molecular weight =

300 - 1500 g/mol) providing a wide range of different HLB values and functionalities. They are identified by two numbers. The first number refers to the approximate melting point of the substance and the second number refers to the HLB value (range from 1 - 18) (Craig, 1995). The components of some hydrophobic materials are provided in Table 1.2.

Table 1.2. Approximate chemical compositions (%w/w) of hydrophobic materials (Gatteffosse s.a.).

Hydrophobic materials	Glycerides (% w/w)			PEG esters (% w/w)		Fatty acid compositions (%)
	Mono-	Di-	Tri-	Mono-	Di-	
GMS	40-55	30-45	5-15	-	-	C16(40-60); C18(40-60)
GPS	8-17	50-52	31-34	-	-	C14(2); C16(49); C18(47)
GDB	13-21	40-60	21-35	-	-	C22(>80)
Gelucire 43/01	-	-	100	-	-	C8(3); C10(2); C12(29); C14(11); C16(17); C18(36)
Gelucire 50/02	5	30	45	-	20	C12(10); C14(7); C16(40); C18(40)
Gelucire 50/13	5	8	8	29	43	C8(<3); C10(<3); C12(<5); C14(<5); C16(40-50); C18(48-58)
Gelucire 44/14	20% w/w mono-, di- and triglycerides			72 % w/w mono- and diPEG ester and 8 % w/w free PEG		C8(<15); C10(<12); C12(30-50); C14(5-25); C16(4-25); C18(5-35)
Gelucire 55/18	-	-	-	15.2	84.1	C16; C18

Gelucires can be divided to 3 groups which are lipophilic, amphiphilic and water dispersible. Lipophilic Gelucires such as glyceryl monostearate (GMS), glyceryl palmitostearate (GPS), glyceryl dibehenate (GDB), Gelucire 43/01, 33/01 and 39/01 are composed of glycerides alone that provide hydrophobic properties and are therefore useful in controlled drug release. Amphiphilic Gelucires such as Gelucire 50/13 and 53/10 consist of glycerides and polyethylene glycol (PEG) ester. Water dispersible Gelucires such as Gelucire 44/14 and Gelucire 55/18 are made of water soluble base which exhibit rapid drug release (Galal et al., 2004).

GMS, GPS. GDB, polyethylene glycol-8 beeswax (PG8BX) and Gelucire 50/13 which are employed in formulations developed within this thesis, are discussed in more detail in Sections 1.3.2.3.1-1.3.2.3.4 below.

1.3.2.3.1 Glyceryl monostearate (GMS)

The chemical name of GMS (known commercially as Geleol®) is octadecanoic acid, monoester with 1,2,3-propanetriol. However, in the European Pharmacopoeia (2007), it is recognised that GMS is not a pure material and GMS 40-55 is described as a mixture of monoacylglycerols, chiefly 40 - 55% monostearoylglycerol, 30 - 45% diacylglycerols and 5 - 15% triacylglycerols.

Important physical properties of GMS are its melting range of 55 - 60°C, HLB value of 3 (Personal communication, Gattefosse 2008). It typically exists as white to cream colour, with slight fatty odour and taste. It presents as wax-like solid in the form of beads, flakes or powders. GMS should be stored in a tightly closed container in a cool, dry place and protected from light.

GMS is widely used as nonionic emulsifier, stabiliser, emollient and plasticiser in food, pharmaceutical and cosmetic preparations. Furthermore, it has been used in the formulation of sustained release matrices for solid dosage forms (Rowe et al., 2003).

1.3.2.3.2 Glyceryl palmitostearate (GPS)

The chemical name of GPS (known commercially as Precirol®) is octadecanoic acid, 2,3-dihydroxypropyl ester mixed with 3-hydroxy-2-[(1-oxohexadecyl)-oxy] propyl octadecanoate, 2-[(1-oxohexadecyl)-oxy]-1,3-propanediyl dioctadecanoate and 1,2,3-propane triol. GPS consists of a mixture of mono-, di- and triglycerides of fatty acids, mainly palmitic acid (49%) and stearic acid (47%).

Major properties of GPS are its melting range of 52 - 55°C, HLB value of 2 (Personal communication, Gattefosse 2008) and it presents as fine white powder with

faint odour. GPS should be stored at a temperature below 35°C and preserved in a tightly closed container protected from light and moisture.

GPS is used as lubricant and in lipophilic matrix for sustained release tablet and capsule formulations (Rowe et al., 2003).

1.3.2.3.3 Glyceryl dibehenate (GDB)

Chemical name of GDB (known commercially as Compritol®) is docosanoic acid, (mono-, di- or tri-) ester with glycerin. In USPNF 24 (2000), GDB is described as a mixture of glycerides of fatty acids, mainly behenic acid with specification limits of 12 - 18% of 1-monoglycerides. Additionally, in European Pharmacopoeia (2007), GDB is described as a mixture of diacylglycerols, chiefly dibehenoylglycerol (40 - 60%) with various amounts of monoacylglycerols (15 - 23%) and triacylglycerols (21 - 35%).

Significant physical properties of GDB are its melting range of 65 - 77°C, HLB value of 2 (Personal communication, Gattefosse 2008) and it physically exists as fine white powder with faint odour. GDB should be stored in a tightly closed container at a temperature less than 35°C.

GDB is widely used as viscosity-increasing agent, lubricant, lipidic coating excipient in food, cosmetic and pharmaceutical preparations (Rowe et al., 2003).

1.3.2.3.4 Polyethylene glycol-8 beeswax (PG8BX)

PG8BX (known commercially as Apifil®) is composed of ~ 99% non-ionic white beeswax derivative with polyethylene glycol. Melting range and HLB value are 59 - 70°C and 9 (Personal communication, Gattefosse 2008) respectively. It typically exists as waxy solid with faint odour.

1.3.2.3.5 Stearoyl macrogolglycerides (Gelucire 50/13)

Gelucire 50/13 (known as stearoyl macrogolglycerides EP and stearoyl polyoxylglycerides USPNF) is composed of a well-defined mixture of mono-, di- and triglycerides and mono- and di- fatty acid esters of polyethylene glycol.

Melting range and HLB value are 50°C and 13 respectively. It should be preserved in a tightly closed container protected from air, light, heat and moisture.

Gelucire 50/13 is widely used as an excipient for hard gelatin capsules, as a bioavailability enhancer and controlled-release agent.

1.3.3 Hydrophile-lipophile balance (HLB) system

The HLB system (Griffin, 1949) is the balance between hydrophilic and hydrophobic moieties within various non-ionic surface active agents (including oils and waxes). Each surfactant is assigned a number (between 0 to 18) to represent the size and strength of the polar region relative to the non-polar portion of the molecule. The HLB number is an expression of the weight percentage of the hydrophilic portion to the hydrophobic portion calculated theoretically from the surfactant molecular weight. A high HLB value displays high hydrophilicity and water solubility whereas a low value reflects the reverse.

The HLB value for a mixture of oils, fats and/or waxes in a formulation can be calculated theoretically from the proportion of each component. The HLB value for a combination of high and low HLB agents can be determined by alligation. The HLB of a mixture of surfactants consisting of mole fraction x of wax A and (1-x) of wax B is assumed to be the algebraic mean of the two HLB numbers (Attwood, 2007).

$$HLB_{MixtureAB} = x.HLB_A + (1-x).HLB_B \qquad \text{[Eqn. 1.3]}$$

1.4 Wax matrix pelletisation

Wax pellets can be divided into two types that are matrix and coated pellets. The wax matrix pellets offer the advantage of a one-step production process that can be produced from various techniques as shown below.

Spray congealing. A drug is suspended in the molten wax. The suspension is sprayed and cooled gradually until molten droplets solidified to pellets. A significant requirement is that the materials have a narrow melting range (Rodriguez et al., 1999; Passerini et al., 2003; Albertini et al., 2004).

Melt pelletisation or granulation. The drug, wax and excipients are mixed in a high speed mixer that is controlled carefully temperature by heated jacket above the wax melting point, speed and time of impeller and chopper until pellets are formed. The advantages of this method are that a drying process is avoided and the consuming time and energy reduced compared to wet granulation or film coating processes (Zhou et al., 1996; Zhou et al., 1997; Voinovich et al., 2000; Vergote et al., 2001; Hamdani et al., 2002).

Extrusion and spheronisation. Waxes can be added to traditional wet-granulation / extrusion-spheronisation processes (Blanque et al., 1995; Montouss et al., 1999; Chatchawalsaisin et al., 2005).

Hot-melt extrusion and spheronisation. The dry mixtures of drug, wax and excipients are extruded using a single-screw extruder that is controlled at a temperature above the wax melting point in the feeding, melting and metering parts and operated optimum speed. Subsequently, extrudates are passed through the screen into granules and cooled at room temperature and then granules are spheronised and dried. This method is simple, efficient and continuous and offers avoidance of the use of water or solvents (Liu et al., 2001; Young et al., 2002).

Direct warm spheronisation without extrusion. The wax is melted at temperature above the wax melting point and then mixed with drug and excipients. The wax mixtures are cooled down, milled to reduce particle size and the desired size fraction transferred to a spheroniser operating at a controlled temperature slightly below the wax melting point. This leads to the formation of pellets. This novel pelletisation technique utilises granulation and warm-spheronisation procedures instead of employing traditional extrusion-spheronisation techniques (Lee, 2003). As the direct warm spheronisation method offered the prospect of a one-step manufacturing process and avoided the complication of extrusion, this method was selected for further study in this thesis.

The spheronisation method is discussed in more detail in Section 1.4.1. Subsequently, factors affecting wax matrix pellet formulations are reviewed in Section 1.4.2.

1.4.1 Spheronisation method

The technique of spheronisation is one of the most popular methods of forming pellets and demonstrates numerous advantages over other available methods.

Advantages

- Narrow particle size distribution.
- Convenience of production.
- Low friability of pellets.
- Production of controlled and sustained drug release system.

Disadvantages

- Not suitable for pellet production with high drug loading.
- Requirement for special types of equipment.

Spheronisation or marumerisation (Nakahara, 1964) is a technique to chop and roll granules into spheres by centrifugal and frictional forces. The spheroniser consists of

a vertical static cylinder (bowl) that can be jacketed for temperature control which is fitted with a horizontal rotating disk (friction plate) with a grooved surface to increase frictional force (Vervaet et al., 1995; Gandhi et al., 1999). The schematic diagram of a spheroniser (Model 120; Caleva) is shown in Figure 1.5.

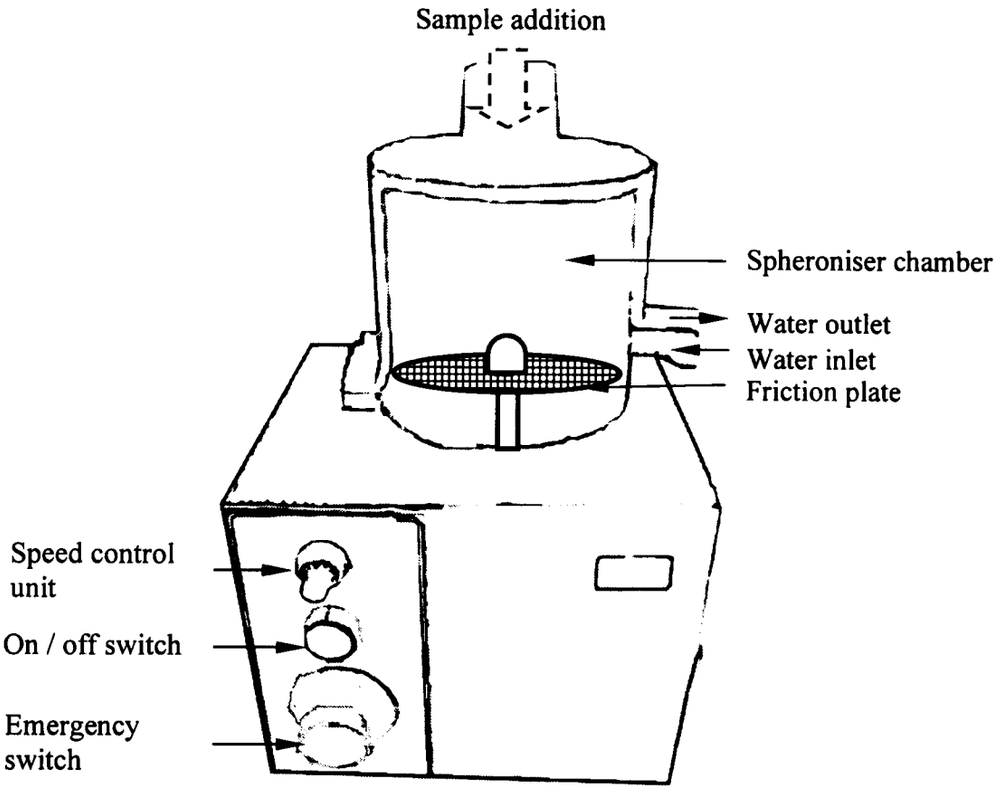

Figure 1.5. Schematic diagram of spheroniser (Model 120, Caleva).

1.4.1.1 Concept of spheronisation

In a spheronisation process, cylindrical extrudates are transformed into spheres. Extrudates are placed onto a friction plate which rotates in the spheroniser chamber. Rowe (1985) proposed a mechanism of pellet formation whereby cylindrical granules are transformed into cylinders with rounded edges, dumb-bells, elliptical particles and eventually spheres because of frictional forces as shown in Figure 1.6. However, Baert and Remon (1993) suggested an alternate mechanism based on frictional and rotational forces. This mechanism adds the twisting of the cylinder after the formation of cylinders with rounded edges. Finally, the cylinder particles break into two individual parts, which have a round and flat side as shown in Figure 1.7.

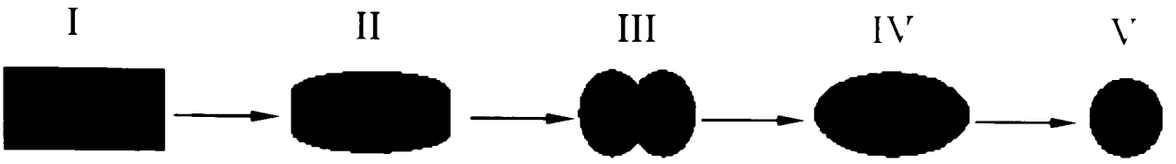

Figure 1.6. Schematic diagram of spheronisation mechanism according to Rowe (1985): (I) cylinder, (II) cylinder with round edges, (III) dumb-bell, (IV) ellipse, (V) sphere.

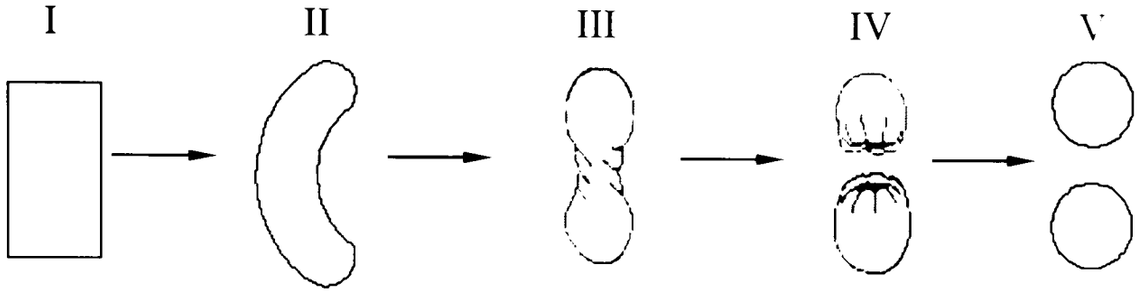

Figure 1.7. Schematic diagram of spheronisation mechanism according to Baert and Remon (1993): (I) cylinder, (II) rope, (III) dumb-bell, (IV) sphere with a cavity outside, (V) sphere.

1.4.1.2 Factors affecting spheronisation

Spheronisation speed. Spheronisation speeds of 200 to 400 rpm are normally employed. Too low a rotational speed results in unchanged granule shape whilst too high a spheronisation speed reduces the particle size and accelerates the agglomeration of pellets. Hence, the optimal speed achieves the toroidal flow of pellets inside the spheroniser chamber (Newton et al., 1995). Pellet size, hardness, roundness, friability, porosity, flow rate, surface structure, bulk and tapped density are influenced by the spheronisation speed (Vervaet et al., 1995).

Spheronisation time. Spheronisation time range is generally between 2 to 10 minutes. Increasing spheronisation time leads to larger, more spherical pellets with narrow pellet size distribution (Wan et al., 1993). Furthermore, changes in bulk and tapped densities as well as pellet yield at certain size ranges are obtained during long spheroniation time. Pellets will begin to agglomerate to larger particles if over-spheronised (Vervaet et al., 1995).

Spheronisation load. Increasing spheronisation load reduces the size and sphericity of pellets but increases in hardness, bulk and tap density whereas the major yield of size range is unchanged (Barrau et al., 1993; Hellen et al., 1993a; Hellen et al., 1993b). When spheronisation speed increases at a low spheronisation load and spheronisation time increases at a high spheronisation load, the yield of pellets of a required size may be decreased and increased respectively (Chariot et al., 1987).

Friction plate design. Different types of friction plate and their design can affect pellet sphericity and density. A friction plate having a grooved surface increases the frictional forces (Vervaet et al., 1995).

1.4.2 Factors affecting wax matrix pellet formulations

Whereas extrusion-spheronisation has been generally restricted to the processing of extruded wet powder masses, previous experience within this research group has demonstrated its applicability to the spheronisation of wax matrix granules prepared by melt-granulation followed by a milling process (Lee, 2003). In general, the spheronisation temperature range necessary for conversion of wax granules to spheres was approximately 7 to 10°C below the melting point of wax materials. Too high a spheronisation temperature results in sticking the granules to the spheroniser chamber and agglomerating to larger aggregates. Moreover, other factors affecting wax matrix pellet formulations are discussed below.

1.4.2.1 Types of wax materials

Different types of wax materials used in formulations can provide wide ranging drug release profiles for sustained and immediate release dosage forms. For example, the drug release from Gelucire 33/01, 39/01, 43/01 or 54/02 formulations provides for slow drug release by diffusion control with no incidence of swelling or erosion mechanisms. However, with Gelucire 50/13 and 53/10 formulations, the mechanism of drug release is swelling and erosion and results in faster drug release. However, formulations of Gelucire 55/18 composed of only PEG esters (water dispersible

Gelucires) show swelling, erosion and diffusion mechanisms, leading to the fastest drug release (Sutananta et al., 1995b; Galal et al., 2004).

1.4.2.2 Wax content

The quantity of wax materials in a formulation can affect overall drug release rates. As the microcrystalline wax (Lunacera® P) content of matrix pellets using a melt pelletisation process increased from 35 to 45%, ibuprofen release decreased from 95 to 75% after 12 hours (Zhou et al., 1996).

In contrast, the addition of GMS in matrix pellet formulations prepared by a wet granulation (followed by extrusion and spheronisation) process did not influence sustained drug release of four model drugs (paracetamol, diclofenac sodium, ibuprofen and indometacin). However, it was protective against moisture ingress rendering such a formulation suitable for a moisture sensitive drug (Chatchawalsaisin et al., 2005).

1.4.2.3 HLB value

The decrease in HLB value of wax materials correlated well with drug release from wax matrix pellets (Lee et al., 2001). Similarly, San Vicente et al. (2000) working with Gelucire 35/10, 48/09 and 46/07 found similar effects in matrix formulations. They suggested the predominant mechanism of drug release was diffusion with slight erosion for higher HLB preparations whereas low HLB preparations released solely by diffusion. Moreover, increasing HLB value from polyol behenate 70/02 (Compritol 888®; GDB) to polyol behenate 57/13 (Compricoat®) in matrix capsules accelerated drug release rate, although, interestingly, increasing HLB value from polyol behenate 70/02 to polyol behenate 63/05 (Compritol HD5®) in formulations resulted in a decreased drug release rate (Duclos et al., 1999).

1.4.2.4 Melting point

Wu et al. (2002) studied the release of potassium chloride (KCl) from semi-solid wax matrices based on Gelucires. With formulations containing 10% Gelucire, drug release decreased as the melting point increased (Gelucire 44/14 < 46/07 < 48/09 < 53/10 < 62/05). When the melting range of microcrystalline waxes in pellets increased by changing from Lunacera® P (58 - 62°C) to Lunacera® M (68 - 72°C), ibuprofen release slowed down from wax matrix formulations (Zhou et al., 1996).

1.4.2.5 Drug content and properties

As ibuprofen content increased in wax matrix pellets produced by a melt pelletisation process, the drug release rate decreased. Zhou et al. (1996) proposed that this was caused by the decrease of starch content in the formulation from 55 to 12 % w/w (more hydrophobic). Incorporation of caffeine and paracetamol into Gelucire 50/13 solid dispersions was observed to affect the physicochemical properties of the wax. Paracetamol acted as a nucleation agent to stabilise the lower melting fraction of Gelucire 50/13 and consequently affected drug release rate. However, caffeine systems exhibited wax polymorphic transformation to more stable forms (Khan and Craig, 2003).

1.4.2.6 Excipient content and properties

Blanque et al. (1995) reported that the inclusion of insoluble barium sulfate in place of soluble lactose resulted in prolonged drug release from matrix pellets prepared by extrusion and spheronisation. Miyagawa et al. (1996) demonstrated that accelerated diclofenac release was achieved by addition of hydroxypropylcellulose (HPC-SL) or methacrylic acid copolymer L (Eudragit® L-100) in a carnuba wax matrix granule formulation and attributed this to the swelling and solubility of the excipient. In addition, the same authors also found that inclusion of sodium chloride had minimal effect on drug release as although it was freely soluble, it had no swelling capacity.

In studies with Gelucire formulations, Galal et al. (2004) noted that the addition of 10 and 20% polyvinyl pyrrolidone (PVP; channeling agent) to a Gelucire 33/01 matrix provided retardation of carbamazepine release as PVP formed a gel inhibiting penetration of water. Moreover, the inclusion of 2% aerosil 200 (thixotropic gel forming agent) in Gelucire 33/01 formulation retarded the drug release. In contrast with the use of an alternative Gelucire 53/10, the addition of 20% PVP in matrix increased the rate of drug release due to erosion of the matrix with diffusion highlighting that the same excipient can impart different functionalities depending upon the wax used. Furthermore, 1 - 10% croscarmellose, a superdisintegrant agent, when added to Gelucire 53/10 formulations increased drug release.

1.4.2.7 Processing time

Increasing melt-granulation time during manufacture of matrix pellets by a melt pelletisation process resulted in an increase in mean pellet size, with narrow size distribution, particle densification and agglomeration growth of pellets as well as adhesion between pellets and instrument (Hamdani et al., 2002). Similarly, Zhou et al. (1997) reported that as high shear granulator mixing time increased, larger pellet were formed, having lower porosity and slower ibuprofen release from matrix pellets.

1.4.2.8 Temperature

Hamdani et al. (2002) noted that the temperature of instrument and product needed to be carefully controlled in order to avoid an increase in particle size and agglomeration. They found that controlling jacket temperature (~ 45°C) which was below the melting point of GDB and GPS provided for optimal granule formation in melt granulation process using a high shear mixer.

1.5 Wax stability

Wax materials and formulations often change physicochemical and morphological properties when they are melted, cooled and subsequently stored (Laine et al., 1988; Sutananta et al., 1994b; Craig, 1995; Galal et al., 2004; Shimpi et al., 2004). Various changes during storage are summarised below.

Oxidation. Chemical reaction occurs in the presence of oxygen resulting in rancidity. It leads to the formation of decomposition products such as aldehydes, ketones and acids. Increasing the amount of unsaturated molecules in wax materials, storage temperature and light exposure accelerate oxidation (Gunstone and Norris, 1983; Berger and Hamilton, 1995).

Crystallisation. Crystallisation occurs in the initial processing stage. When liquid wax is cooled, a solid phase separates whose composition and amount depends on the temperature or supercooling. As the solid fraction increases, nucleation occurs with crystal growth (Garti and Sato, 1988; Timms, 1995; Vippagunta et al., 2001; Lawler and Dimick, 2002; Himawan et al., 2006).

Polymorphism. Polymorphs are different crystalline forms of the same substance that have different crystalline arrangements and/or conformation of the molecules in the crystal lattice which then provide different physicochemical, morphological, thermodynamic, spectroscopic and kinetic properties. In general, waxes crystallise first in the least stable polymorphic form having higher solubility or vapour pressure and which transform or recrystallise to a more stable polymorph having lower solubility or vapour pressure (Garti and Sato,1988; Grant, 1999; Vippagunta et al., 2001; Himawan et al., 2006).

Polymorphic transformation and crystallisation are the main changes of wax substance during ageing as discussed in Sections 1.5.1 to 1.5.2.

1.5.1 Wax polymorphic transformation

Thermodynamically, a less stable wax polymorph will transform into a more stable polymorph. The rate of transformation to a more stable form is normally slow. The mechanism of this transformation involves rearrangement of intermolecular forces (Grant, 1999). Different polymorphic forms have different physical properties such as density, hardness, refractive index, melting point, enthalpy of fusion, vapour pressure, colour, solubility and dissolution rate (Vippagunta et al., 2001).

1.5.1.1 Wax polymorphic classification

Wax polymorphic forms can be divided into 2 types on the basis of stability: unstable and stable polymorphs. Unstable polymorphs (α, β') generally transform to stable polymorphs (β) as discussed below. The long spacings of XRPD patterns indicate the distance between crystal planes (chain length packing) whereas the short spacings indicate subcell structure (interchain distances) showing the differences between polymorphs (Garti and Sato, 1988; Larsson, 1994; Garti et al., 2001; Himawan et al., 2006).

α form. The α form (least stable form) appears macroscopically with smooth surfaces and has small thin crystal size (smaller than several micrometers) with high Gibbs free energy. This form is characterised by a single short spacing line in the XRPD pattern at 0.415 - 0.42 nm. The chains are arranged in loosely hexagonal subcell packing with no specific chain plane. Moreover, the α form of wax material generates during cooling after melting and transforms directly to the most stable β form via β' form with better chain packing following storage.

β' form. The β' form (metastable form) appears as long needle crystals (< 5 μm) and provides intermediate Gibbs free energy. This form is characterised by two strong short spacing lines at 0.37 - 0.40 nm and at 0.42 - 0.43 nm. The chains are arranged in an orthorhombic subcell packing with perpendicular hydrocarbon chain

planes. Furthermore, the β' form gives good plasticity and softness and transforms quickly to the most stable β form.

β form. The β form (most stable form) appears as large crystals (20 - 100 μm) with the lowest Gibbs free energy and often grows in clumps causing grainy microstructure. This form is characterised by a strong short spacing line near 0.46 nm and a number of other strong lines around 0.36 - 0.39 nm. The chains are arranged in triclinic subcell packing with all chain planes parallel providing the densest form.

Some examples and studies of wax polymorphism are shown below.

1.5.1.2 Study in polymorphic transformation of monoglycerides

For 1-monostearin and 1-monopalmitin, four polymorphs were found: sub-alpha, alpha, beta prime and beta forms. The melting point progressively increased during transformation through alpha to beta prime and to beta forms. The stable beta form was obtained by slow crystallisation from solvent or by transformation of alpha and beta prime form. Reversible alpha-subalpha transitions were observed during repeating cooling and heating cycles using differential thermal analysis (Luttton, 1948; Maruyama et al., 1971).

1.5.1.3 Study in polymorphic transformation of glyceryl monostearate (GMS)

GMS showed four crystal forms which are sub-alpha, alpha, beta' and beta (Maruyama et al., 1971; Maruyama et al., 1973). Following rapid cooling, GMS transformed from α-form to ß-form via ß'-form at ambient temperature. The stable ß-form of GMS had a higher melting point, higher density, was a poorer foaming and wetting agent than the α-form. The optimal heat treatment temperature for transformation of GMS from α-form to ß-form was 50°C for 90 minutes since this yielded the maximum stable ß-form content as confirmed by DSC and powder X-ray diffraction (Yajima et al., 2002). Moreover, the optimal condition for transformation

from the α- to ß-form of GMS in a clarithromycin-wax matrix formulation was heat treatment at 40°C for 5 hours (Yajima et al., 2003).

1.5.2 Wax crystallisation

In natural lipids, the common packing structure is a bilayer arrangement with parallel hydrocarbon chains. The polar groups form sheets and the molecules in adjacent layers are oriented head-to-head with a methyl end group gap in the middle and with polar head groups on the surface (Larsson, 1994; Kaneko, 2001; Lawler and Dimick, 2002). Some examples and studies in the crystallisation of wax substances are shown below.

1.5.2.1 Study in crystallisation of triglycerides

The common structures of triglycerides such as tricaprin, trilaurin, tripalmitin, tristearin and trimyristin show a layered appearance. Fresh triglycerides solidified in a layered amorphous form which changed to the crystal form during storage. The size of the wax molecules and their mechanical treatment influenced crystallisation rate. Polymorphic transformations were not found with triglycerides on ageing (Laine et al., 1988).

1.5.2.2 Study in crystallisation of glyceryl palmitostearate (GPS) and glyceryl dibehenate (GDB)

Untreated and freshly solidified GPS and GDB samples showed partially amorphous layered structures which gradually crystallised after storage. This was confirmed by DSC, X-ray diffraction and hot-stage microscopy (HSM). The crystallisation rate of GPS which consisted of shorter fatty acid chain (after 2 weeks at 40°C or 24 h at 50°C) was faster than the rate of crystallisation of GDB (after 5 weeks storage at 50°C) confirming that crystallisation rate relied on molecular size (Laine et al., 1988; Hamdani et al., 2003).

Increasing the extrusion temperature resulted in a narrow melting peak of GPS with appearance of a shoulder peak (at a lower temperature) owing to partial melting of the wax and/or recrystallisation of lower melting crystal structures. When GPS was processed at temperatures above its melting point, a melting peak at low temperature was observed and transformed to higher melting crystal structures upon storage (Reitz and Kleinebudde, 2007).

When wax components in formulations transform to alternative crystal form or crystallise during storage, their characteristics may change as summarised below. These are discussed in greater detail in Sections 1.5.3 to 1.5.12.

- FT-IR spectrum
- Melting point, DSC profile and XRPD pattern
- Morphological properties
- Hardness (e.g. suppositories)
- Softening time (e.g. suppositories)
- Viscosity
- Solid fat content
- Drug release (in vitro and in vivo)

1.5.3 FT-IR spectrophotometry investigation of wax stability

In early stages of storage at a temperature below the transition point of the sub-α, the hydroxyl (–OH) absorption band and the carbonyl (=CO) absorption band of 1-monostearin were observed at 3342 cm^{-1} and 1730 cm^{-1} indicating the sub-α form. Upon further storage, the –OH absorption band (3360 cm^{-1}, α form) progressively shifted to 3342 cm^{-1} and 3243 cm^{-1} (β' form) and then to 3243 cm^{-1} and 3307 cm^{-1} (β form). Similarly the =CO absorption band (1721 cm^{-1}, α form) shifted to 1736 cm^{-1} (β'and β form) (Maruyama et al., 1971). The IR spectrum of α-, β'- and β form in saturated monoacid triglycerides showed single band at 720 cm^{-1}, doublet at 719 and 727 cm^{-1} as well as single band at 717 cm^{-1} respectively (Garti and Sato, 1988). Moreover, Bresson et al. (2006) using Raman spectroscopy, suggested that in

polymorphs of saturated monoacid triglycerides, the C=O stretching mode was split into two components for α form packing or three components for β'- or β form.

1.5.4 Differential scanning calorimetry (DSC) investigation of wax stability

In a study of GMS, the α form obtained from melting and solidification showed a melting endotherm at 67.9°C which transformed to the β form at room temperature with a melting endotherm at 71.9°C (Yajima et al., 2002).

Hamdani et al. (2003) demonstrated that freshly solidified GPS provided two endothermic peaks (~ 48 and 54°C) which after storage at 40°C for 2 weeks, changed with disappearance of the lower endothermic peak and a shift to a higher endothermic peak (~ 57°C) implying that a duration of 2 weeks at 40°C might be sufficient time for GPS crystallisation. However, GDB showed only a slight change of single endothermic peak (from ~ 70 to 72°C) after storage at 40°C for 2 weeks.

The melting point of fatty suppository bases (Witepsol W35, Witepsol E75 and Suppocire A) increased during storage (1, 7, 33 or 70 days) at various temperatures (3, 22, 30, 40, or 50°C) as observed by Liversidge et al. (1981) using differential thermal analysis (DTA). The authors attributed this to polymorphic transformations from the less stable form (α form) to the more stable form (β form). The increase in the rate of change was dependent on a decrease in the molecular weight of the fatty acid chain length in triglycerides such as tristearin << tripalmitin < trimyristin < trilaurin < tricaprin. The shorter side–chain of the fatty acids resulted in greater molecular mobility or an ability of the molecules to reorganise from unstable to stable polymorphs. Moreover, an increase in the storage temperature decreased the time required for changes to occur.

In studies with Gelucires, Gelucire 43/01, 50/02 and 54/02 containing glycerides alone and Gelucire 50/13 containing a mixture of glycerides and PEG esters changed thermally during storage (28, 112 or 228 days). However, Gelucires 55/18 containing PEG esters exhibited small changes in DSC profiles resulting from chain

folding. Such alternations of DSC curves in Gelucires were assigned to changes in the crystal structure of the glyceride components (Sutananta et al., 1994b). In addition, aged Gelucire 43/01 matrices showed broader peak and higher enthalpy of fusion than fresh samples (Shimpi et al., 2004; Chauhan et al., 2005a). Furthermore, Gelucire 50/13 presented two forms composed of form I (two melting peaks at 40 and 46°C) and form I' (one melting peak at 48°C) observed by DSC. Form I was found in post-production and then transformed to form I' after storage at 40°C (Roussin and Duddu, 2001).

1.5.5 X-ray powder diffraction (XRPD) investigation of wax stability

XRPD patterns in aged fatty suppository base (tricaprin, trimyristin, tripalmitin, tristearin and mixture of trilaurin and trimyristin) showed the development of new peaks after storage at room temperature for up 3 months. The change was caused by the gradual crystallisation of fresh triglycerides which had partially amorphous layered structures and they had no found any sign of polymorphism transformation (Laine et al., 1988).

Hamdani et al. (2003) demonstrated that freshly solidified GPS exhibited one narrow peak at 2θ angle of 21.5° but the aged samples (stored 2 weeks at 40°C or 24 hours at 50°C) showed three peaks at 2θ angle of 19.5°, 21.5° and 23.5°. Similarly, fresh solidified GDB showed two peaks at 2θ angle of 21° and 23° whereas the aged samples (stored 2 weeks at 40 or 50°C) exhibited an increase in height of two peaks. However, GDB showed three major peaks at 2θ angle of 19.2°, 21° and 23.5° in aged samples stored for longer times (5 weeks at 50°C). They concluded that GDB (longer fatty acid chain; C_{22}) crystallised more slowly (after 5 weeks storage at 50°C) than GPS (shorter fatty acid chain; $C_{16\text{-}18}$) after 2 weeks at 40°C or 24 hours at 50°C.

However, solid dispersion formulations containing nifedipine, Pluronic® F68 and Gelucire 50/13 (1:1:1) showed no changes in physicochemical properties after storage at 4 or 25°C over 8 weeks. No new peak was observed in the XRPD

indicating no phase change of drug and matrix system and no shift in the peak position indicating no interaction between drug and matrix (Vippagunta et al., 2002).

1.5.6 Polarised light microscopy investigation of wax stability

Under polarising microscopy, the α form of triglycerides showed bright spherulites with no colour with isogyres perpendicular to one another called "maltese cross". The ß' form exhibited coloured and featherlike spherulites whereas the ß form showed a disappearance of spherulites with "maltese cross" (Whittam and Rosano, 1975).

Hot stage polarising microscope (HSPM) is a semi-quantitative method involving heating samples on a hot stage and observing changes under a polarised light microscope. At 45°C, Gelucire 43/01 had completely melted but in aged samples (stored at room temperature for 30 days), there were residual unmelted particles. This was attributable to increased energy being required to overcome enthalpy changes relating to crystallisation of Gelucire during storage (Shimpi et al., 2004; Chauhan et al., 2005a). In addition, Hamdani et al. (2003) reported that fresh GPS and GDB showed slightly lower melting temperatures (~ 55 and 72°C) than aged samples (56 and 73°C) stored for 2 weeks at 40°C observed by HSPM photographs.

1.5.7 Scanning electron microscope (SEM) investigation of wax stability

SEM images of fresh granules containing Gelucire 43/01 and drug (diltiazem HCl or risedronate sodium) exhibited smooth surfaces with no evidence of crystalline forms. However, in aged samples, rough surfaces were apparent owing to phase transformations in Gelucire 43/01 (Shimpi et al., 2004; Chauhan et al., 2005a). In a study of Gelucire 50/13, form I (the unstable form) with smooth surfaces was transformed after storage to form I' showing cracks, fissures, gaps and spaces on the surface. Therefore, an increase in drug release rate upon ageing was facilitated by enhanced penetration of dissolution medium into the wax (Roussin and Duddu, 2001; Galal et al., 2004).

Khan and Craig (2004) reported that Gelucire 50/13-caffeine dispersions had microcracks due to matrix contraction after solidification but this event was not observed in Gelucire 50/13-paracetamol samples owing to greater plasticity. After storage at 20°C, the cracks disappeared in Gelucire 50/13-caffeine dispersions and scale-like structures were observed. Following storage at 37°C, scale-like structures developed into leaf-like structures for both caffeine and paracetamol matrices. This suggested a general mechanism of changes in surface morphology on storage.

1.5.8 Texture Analyser investigation of wax stability

The Texture Analyser is used to determine hardness (required force to achieve a given deformation) which is one of the important factors to determine mechanical and rheological properties of pharmaceutical semi-solid products (Jones et al., 2002). The hardness (evaluated by needle penetration distance) of petroleum waxes and wax fractions depended on temperature and the carbon number. When temperature of the wax samples increased near to the phase transition temperature, the waxes became very soft. Moreover, the wax fractions with a higher concentration of paraffin (high melting point) were less sensitive to temperature increases than samples having lower concentrations of paraffin (Srivastava et al., 1993).

1.5.9 Viscosity investigation of wax stability

During storage, atmospheric exposure can result in hydrolysis of high HLB PEG esters such as Gelucire 55/18 into PEG and fatty acids and degradation of PEG into lower molecular weight fractions resulting in a reduction in viscosity. However, the viscosity of lower HLB Gelucire 50/13 remained constant after storage 220 days (Sutananta et al., 1995a).

1.5.10 Solid fat content investigation of wax stability

The endotherm area from DSC data is directly proportional to the solid fat content of the wax. A high proportion of slow cooled Gelucire 43/01 (10°C/hour) was in the

molten state at the room temperature compared to a fast cooled sample (cooled in liquid nitrogen). Consequently, waxes transformed from segregated to homogeneous wax microstructures upon storage (Sutananta et al., 1994b). Shimpi et al. (2004) and Chauhan et al. (2005a) reported that when solid fat content was plotted semi-log graph versus temperature of Gelucire 43/01, the rate of decrease in the solid content in fresh samples was higher than that of aged samples (stored at room temperature for 30 days). Similarly, Khan and Craig (2004) noted that solid dispersions containing Gelucire 50/13 and drug (10% paracetamol or caffeine) showed an increase in the solid fat proportion when stored at 37°C for 180 days.

1.5.11 In vitro drug release investigation of wax stability

Drug release from wax formulations after ageing may increase, decrease or remain unchanged in individual formulations as shown the data below.

1.5.11.1 Increased drug release following wax stability

Drug release of diltiazem hydrochloride granules (containing drug and Gelucire 43/01 (1:1.5)) prepared by melt granulation increased after storage at room temperature for 10 or 30 days due to phase transformation of wax (Shimpi et al., 2004). In addition, an increase in risedronate sodium release was observed from Gelucire 43/01 formulations containing wax and drug as well as wax, drug and Caprol PGE (surfactant). Aged samples with high surfactant content exhibited increases in drug release rates owing to transformation of Gelucire 43/01 (Chauhan et al., 2005a). Hamdani et al. (2002) demonstrated in wax matrix pellets that drug release from phenylephrine hydrochloride pellets (10% drug, 30% lactose, 45% GDB and 15% GPS) stored at 40°C and 75% RH for 6 weeks increased significantly due to sensitivity of Gelucires at high temperature and humidity.

A significant increase in drug release was observed with theophylline capsules containing 40% drug and 60% Gelucire 50/13 upon storage at 40°C for 9 days and 25°C for 2 months. Increasing dissolution rate profiles were caused by physical and

morphological changes of Gelucire 50/13 resulting from phase seperation and crystallisation (Roussin and Duddu, 2001). Furthermore, theophylline capsules consisting of 14.7% drug, 60.3% GPS and 25% Lutrol® F127 (poloxamer 407) showed a slightly increased drug release rate after storage at 40°C/75% RH and 25°C/60% RH for up to 1 month probably due to crystallisation of GPS. The addition of Lutrol® F127 led to increased drug release and improved wax stability (Jannin et al., 2006).

Choy et al. (2005) noted that an increase in drug release from capsules composed of paracetamol and Gelucire 50/13 was observed during storage for 22 weeks at 37°C because the wax components formed large crystals upon polymorphic transformation to the more stable form leading to increase porosity and accelerated drug dissolution. Similarly, Galal et al. (2004) demonstrated that ageing of Gelucire 50/13 matrix formulations for 1 year at room temperature (25°C) resulted in increased carbamazepine release due to possible phase separation into discrete chemical compositions within the matrix and rearrangement into microsegregated structures.

1.5.11.2 Decreased drug release following wax stability

The dissolution rate of salbutamol from capsules containing Gelucire 35/10 (capsule size numbers 1, 3 and 4) or Gelucire 48/09 (capsule size numbers 3 and 4) decreased upon storage for 1 year at room temperature whereas Gelucire 46/07 formulations (capsule size numbers 1, 3 and 4) exhibited no dissolution changes upon ageing. San Vicente et al. (2000) suggested that increasing drug release in formulations (Gelucire 46/07 < Gelucire 48/09 < Gelucire 35/10) was related to changes brought about during wax ageing. Moreover, an increase in capsule size (number 1 > 3 > 4) also increased the rate of change in wax stability and influenced dissolution performance.

In addition, temperature and humidity conditions during storage of wax formulations affect the drug dissolution rate. Hamdani et al. (2002) reported that pellets containing phenylephrine hydrochloride, lactose, GPS and GDB stored at 30°C and 60% RH or at 25°C and 60% RH for 6 weeks had a noticeable decrease in drug

release profiles whereas pellets stored at 4°C (fridge) for 38 weeks exhibited no significant differences in drug release profiles compared to the initially made samples. Similarity, Remunan et al. (1992) noted that nifedipine release in tablets containing Gelucire 53/10 decreased when stored at high temperature and humidity (40°C and 80% RH) for 6 months. They suggested that the changes in drug dissolution could be caused by formation of drug microcrystals and wax structural changes.

Both increase and decrease in drug dissolution rates has been reported with solid extrusion formulations containing GPS and theophylline (50:50) upon storage at 40°C. The drug dissolution decreased over the first eight days but after 9 months, the dramatic increase in drug release profiles and melting enthalpy from wax extrudates were observed. This was caused by effect of ageing process in heterogeneous compositions of GPS (Reitz and Kleinebudde, 2007).

1.5.11.3 Unchanged drug release following wax stability

The solid dispersions of glibenclamide containing wax (Gelucire 50/13 or 44/14) and silicon dioxide (non-porous Aerosil® 200)prepared by spray drying technique exhibited no changes in dissolution rate or wax crystallinity during storage at 30°C and 65% RH for 3 months. The unchanged dissolution rate may have resulted from stability improvements gained from hydrogen bonding between the glibenclamide and the Gelucire with absorption of amorphous silicon dioxide onto the formulation surface (Chauhan et al., 2005b).

Galal et al. (2004) reported that Gelucire 53/10 matrix formulations containing carbamazepine had no alteration in release profiles following storage at room temperature for 1 year, which was proposed to be due to no changes in the wax matrix composition or surface appearance. Moreover, Reitz and Kleinebudde (2007) noted that theophylline release in a solid extrusion formulation containing glyceryl trimyristate (Dynasan®) stored at 40°C up to 9 months was constant compared to fresh samples. They suggested that the homogeneous composition of glyceryl

trimyristate led it to crystallise faster after extrusion providing a formulation with consistent performance.

1.5.12 In vivo drug release investigation of wax stability

Choy et al. (2005) demonstrated during an in vivo study recruiting 12 healthy male adults that drug bioavailability from capsules composed of paracetamol and Gelucire 50/13 was not significantly affected by the storage conditions (4 or 37°C for 22 weeks). However, the highest maximum plasma concentration (C_{max}) and the lowest mean residence time (MRT) of samples stored at 37°C showed a statistically significant difference. No correlation between mean dissolution time (MDT) values from an in vitro study and MRT values from in vivo study was observed. In addition, Dennis et al. (1990) also reported that wax ageing (stored at 30°C for 1 month) of capsule containing ketoprofen, Gelucires 50/13 and 50/02 had no significant effects ($p > 0.05$) on drug bioavailability, C_{max}, t_{max} and MRT observed in a trial involving 7 healthy male volunteers. The increased in vitro drug release during storage was not paralleled by changed in vivo drug release.

1.5.13 Effect of processing methods and conditions on wax stability

Processing methods and conditions such as cooling or solidification, melting, milling, granulation and shearing can result in changes in the physicochemical characteristics of waxes as monitored by DSC, XRPD, viscosity and dissolution (Sutananta et al., 1994a) as shown some cases in Sections 1.5.13.1 to 1.5.13.2.

1.5.13.1 Effect of wax processing methods

Pelletisation using spray drying from an organic solvent system and spray congealing methods produces the unstable polymorphic α-form of glycerol tristearate which gradually transformed into stable β-form upon storage at elevated temperatures (25 or 37°C) for 6 months (Eldem et al., 1991). Moreover, carnuba wax products prepared by rapid cooling using a spray congealed process were polymorphically

unstable due to imperfect crystallisation and transformed to the stable β-form during ageing (Emas and Nyqvist, 2000).

In addition, mechanical treatment of small molecular weight triglycerides can induce changes in crystallinity. For example, freshly milled tricaprin after solidification becomes more crystalline when comparing to fresh melt-solidified material (Laine et al., 1988).

1.5.13.2 Effect of wax cooling rate

Recrystallisation and/or polymorphic transformation of a wax and its subsequent alteration in properties can be affected by its cooling rate. For example, fast cooling (cooled in liquid nitrogen) of Gelucires 43/01, 50/02, 54/02, 50/13 or 55/18 provided solidification of larger proportions of metastable or lower melting form than slow cooled (10°C/hour) samples which formed larger spherulites (Sutananta et al., 1994a). Moreover, slow cooled Gelucire 43/01 (10°C/hour) resulted in slower transformation of wax to the stable form than fast cooled material due to segregation of both low and high melting point glyceride components into discrete microscopic regions. However, fast cooled wax had a rapid transformation to the stable form owing to it having a homogeneous chemical structure with facilitated reorganisation during storage (Sutananta et al., 1994b; Craig, 1995). Laine et al. (1988) also reported that rapidly cooled triglycerides such as trimyristin (stored in refrigerator) was more amorphous than slow cooled samples (stored at room temperature).

Changes in drug release rate and mechanism caused by wax cooling rate have been observed for Gelucire 50/13 or 55/18 (Sutananta et al., 1995a). For example, drug release of 2% w/w theophylline from Gelucire 55/18 or 50/13 matrices prepared by slow cooling (10°C/hour) was faster than samples cooled at ambient temperature. The mechanism of drug release from slow cooled Gelucire 55/18 formulations was diffusion whereas a combination of both diffusion and erosion was observed in fast cooled samples. However, the cooling rate had no effect in formulations with higher (> 30% w/w) drug loading.

Phuapradit et al. (2002) suggested that cooling rate is the critical factor in controlling wax viscosity and the manufacture processes. Wax formulations (containing hydrogenated soybean oil flakes, hydrogenated vegetable oils and purified yellow beeswax) which were rapidly cooled (15°C/min) had higher viscosities than samples slowly cooled (1.3°C/min) due to greater recrystallisation and polymorph transitions of the triglycerides and fatty alcohol components from wax.

1.5.14 Inhibition of wax transformation

As physicochemical properties and drug release profiles of wax formulations can alter upon ageing, considerable research has been undertaken to inhibit polymorphic transformation and crystallisation of wax materials used in pharmaceutical formulations. Thermal annealing and stabilising agents are utilised to inhibition the wax transformation as discussed below.

1.5.14.1 Effect of thermal annealing on wax stability

Thermal annealing is the process of using elevated storage temperature to accelerate stabilisation in the properties of a material. For example, carnuba wax samples prepared by the rapid cooling using a spray congealing technique were annealed at elevated temperature (40, 50 or 60°C) for 2 days. Increased annealing temperature decreased the exothermic reaction as observed by isothermal microcalorimetry due to rearrangement of the wax components to a more stable form. However, wax was in closely complete stable state and still changed upon storage. Emas and Nyqvist (2000) suggested that at each annealing temperature, carnuba wax had different equilibrium states.

In addition, in a study with Gelucire 43/01 that was rapidly cooled in liquid nitrogen and then annealed at 29 or 36°C for 1 - 3 days, samples annealed at 36°C showed larger proportions of high melting temperature than those at 29°C as observed from DSC measurements of the samples. Sutananta et al. (1994b) suggested that annealing at a temperature ~ 9°C below the melting temperature or fast cooling in

samples provided the most opportunity for rapid transformation from the unstable to stable polymorphs.

1.5.14.2 Effect of stabilising agents on wax stability

With Gelucire 50/13–theophylline formulations, drug release increased after storage (Roussin and Duddu, 2001). Attempts to inhibit dissolution changes upon storage focussed on avoiding or accelerating phase transformation post-manufacture. Nucleation inhibitors such as polyvinyl pyrrolidone (PVP), carboxy methyl cellulose (CMC) and Cab-O-Sil (fumed silica) were added to the Gelucire 50/13–theophylline matrix formulations. These nucleation inhibitors had no effect on stabilising the dissolution performance of the formulations during storage. Consequently, thermal annealing at 40°C was utilised for expediting phase transformation. However, complete transformation took 2 weeks and was considered impractical for industrial manufacture. Combination of thermal annealing at 40°C and addition of nucleation enhancers (GMS and PEG 1450) were employed and were observed to be successful in inhibiting dissolution changes following storage at 25 or 40°C for up to 2 months.

Galal et al. (2004) demonstrated that incorporation of 50% or 80% Gelucire 53/10 into a Gelucire 50/13-carbamazepine matrix formulation inhibited dissolution changes during storage for 1 year at room temperature. They proposed that Gelucire 53/10 might act as a bridge former between Gelucire 50/13 microcrystals which led to inhibition of phase transformations with a resultant homogeneous matrix and surface. Moreover, the addition of 10% PVP (a polymorphic transformation inhibitor) in Gelucire 33/01 matrix formulations stabilised drug release profiles upon ageing.

Eldem et al. (1991) reported that some emulsifiers such as lecithin, mono- and diglycerides could be used as stabilising agents to prevent or delay the wax polymorphic transformations from the unstable to more stable form due to the emulsifiers being incorporated into the wax crystal lattice and molecular spacial arrangements. Furthermore, Jannin et al. (2006) noted that inclusion of 25% w/w

poloxamer 407 (Lutrol® F127; hydrophilic polymer) into theophylline-GPS capsule formulations stabilised drug release profiles during 6 months storage.

1.6 Factors affecting in vivo drug release

The in vivo performance of oral dosage forms can be influenced by drug physicochemical properties and gastrointestinal physiological & anatomy as well as the performance of the oral delivery vehicle (Rubinstein et al., 1988; Mayersohn, 2002). A summary of the drug physicochemical variables that can impact on in vivo availability is showed below. Anatomical & physiological and dosage form variables are discussed in Sections 1.6.1 to 1.6.2.

Drug solubility and gastrointestinal permeability. The Biopharmaceutics Classification System (BCS) describes gastrointestinal drug bioavailability in terms of aqueous drug solubility and drug gastrointestinal permeability, classifying into 4 classes (Class I - high solubility and high permeability; Class II - low solubility and high permeability; Class III - high solubility and low permeability; Class IV - low solubility and low permeability) (Amidon et al., 1995; Yu et al., 2002).

Mechanism of drug absorption. In general, all drugs are absorbed by a passive diffusion mechanism. A high concentration gradient facilitates diffusion across the gastrointestinal membrane (Chambin et al., 2002; Mayersohn, 2002).

Oil/water partition coefficient ($K_{o/w}$) and chemical structure. Membrane permeability can be expressed in terms of $K_{o/w}$. Lipid soluble drugs (≥ log P value of 3) penetrate the lipid regions of the membrane whereas water-soluble drugs (low log P values) enter via aqueous pores (Rubinstein et al., 1988; Alhamami, 2002; Mayersohn, 2002).

pK_a value and pH. Since the proportion of drug ionised or unionised is in dynamic equilibrium, the small intestine is always the major site of drug absorption regardless of drug charge due to its larger surface area relative to the stomach and colon. The

proportion of drug in unionised form is influenced by gastrointestinal pH and can be quantified by the Henderson-Hasselbalch equation. When unionised drug diffuses across the intestinal wall into the systemic circulation via the portal vein, equilibrium in the intestinal lumen is re-established to provide additional unionised drug for absorption and so the process continues until the concentration (diffusional) gradient is exhausted (Rubinstein et al., 1988; Mayersohn, 2002).

1.6.1 Anatomical and physiological variables

Anatomical and physiological variables affect the drug absorption from the gastrointestinal tract as discussed below.

1.6.1.1 Gastric emptying rate

The gastric emptying rate is often the rate limiting step in drug absorption. When gastric emptying time is delayed, systemic bioavailability decreased due to slow drug absorption from the small intestine and limited hepatic presentation (Wilding et al., 1992). Gastrointestinal emptying rate is influence by types of meal & calorific content, timing of meal, formulation viscosity, physical state, patient's health, body posture and co-administration of drugs (Rubinstein et al., 1988).

1.6.1.2 Gastrointestinal tract motility

The stomach and small intestines have motility to propel and mix food (or chyme) along the digestive tract towards the aboral end. Transit and residence time within the stomach and small intestinal can influence the amount of time a given dosage form can reside in a particular part of the digestive tract. The mean transit time through the stomach and small intestines is around 2 hours and 3 - 4 hours respectively (Rubinstein et al., 1988; Yu et al., 1996; Mayersohn, 2002). As the small intestine is the principal site of drug absorption, less intestinal motility results in longer residence time in the small intestine and maximises drug absorption across surface epithelium (Mayersohn, 2002). Gastrointestinal motility is influence by the

degree of physical activity, age, disease state and emotional condition of the patient (Hoener and Benet, 2002).

1.6.1.2.1 Fasted state (Interdigestive state)

In the stomach, the motility pattern is characterised by the migrating motor complex (MMC) sequence which occurs every 2 - 3 hours to clear any contents within the stomach into the small intestine. The MMC can be characterised by 4 phases, which are minimal activity for ~ 1 hour, irregular contraction for 30 - 45 minutes, intense peristaltic wave for 5 - 15 minutes (housekeeping wave) and then transition of decreasing activity leading to next cycle. The housekeeping wave results in emptying of dosage forms or residual content (including non-disintegrating dosage forms) of the stomach to the small intestine (Rubinstein et al., 1988; Mayersohn, 2002). The gastric emptying of an individual dosage form in the fasted state is dependent on the time of dosing relative to the MMC status and presentation to the duodenum can vary between 10 minutes and 3 hours (Washington and Wilson, 1994).

1.6.1.2.2 Fed state (Digestive state)

The ingestion of light, heavy or small meals is referred to as the fed state. The fed state delays gastric emptying and can reduce drug absorption (Rubinstein et al., 1988; West et al., 1990). The stomach and intestinal motility sequence can be divided to two types: mixing (segmental) and propulsive (peristaltic). The former mixes the food content with secretions in circular movements while the latter propels the food content in the gastrointestinal tract towards the aboral end. Increasing intestinal segmentation in the presence of drug will increase contact area between drug and an absorbing membrane and increase drug absorption rate (Mayersohn, 2002).

1.6.1.3 Effect of food on gastric emptying and intestinal drug absorption

The presence of food in the gastrointestinal tract may reduce gastric emptying rate and subsequently decrease the rate of drug absorption. Drug may bind to food particles or react with gastrointestinal fluid resulting in lower drug absorption (Mayersohn, 2002). Some studies investigating the effect of food on gastric emptying and intestinal drug absorption from pellet formulations are shown below.

Wilding et al. (1991) reported that the presence of food decreased the gastric emptying of diltiazem pellet formulations but not the small intestinal transit time. Pellets reached the caecum within 3 - 4 hours after leaving the stomach. Bioavailability of sustained release pellets was also unaffected by food in the 8 volunteers studied. Moreover, Yuen et al. (1993) observed that food had no effect on the rate and extent of gastrointestinal theophylline absorption even though the ingestion of food had delayed gastric emptying and caecum arrival of the pellets. Gastrointestinal absorption of theophylline from pellets was variable and slowest in the colon (important absorption site), followed by the stomach then the small intestine.

The size of meal ingested has an influence on the gastric emptying of pellets. Gastric emptying of pellets containing tiaprofenic acid after a light breakfast was faster than that from pellets after a heavy meal but small intestinal transit remained similar (Davis et al., 1987). In addition, following ingestion of a heavy meal, pellets whose densities were close to that of the food became entrapped with the food, prolonging digestion and delaying gastric emptying. However, following ingestion of a light meal, light and heavy pellets did not caught up in antral flow and emptied after bulk of digestible solid, delaying gastric emptying (Meyer et al., 1985b; Washington and Wilson, 1994).

1.6.2 Dosage form variables

Different dosage forms can affect drug absorption. For example, gastric emptying times increase in the following order: solution < pellets < single unit dosage forms

such as tablets or capsules (Abrahamsson et al., 1996). However, Wilding et al. (1991) reported that diltiazem absolute bioavailability between sustained release pellet and solution were similar but they had different rates of absorption. For sustained release matrix pellet systems, factors of dosage form variables affecting drug absorption are provided below.

Size of pellets. In a dog study, increasing pellet diameter from 1 to 5 mm slowed gastric emptying but pellets of 0.015 mm had similar gastric emptying to pellets of size 1 mm (Meyer et al., 1985a). Moreover, in human studies, pellet sizes between 1 - 3 mm with a density of 1 gcm^{-3} were more influenced on the gastric emptying rates than quantity of food ingested (100 or 420 g/meals). The critical size of a pellet required to prolong gastric residence was suggested to be 1.4 $\pm$ 0.3 mm in diameter with a density of 1 gcm^{-3} (Meyer et al., 1988).

Density. The gastrointestinal transit time is affected by the pellet density. Devereux et al. (1990) reported that 1 mm pellets with higher density (2.8 gcm^{-3}) prolonged gastric emptying and caecum arrival time more than 1 mm pellets with lower density (1.5 gcm^{-3}) in both fed and fasted states. In contrast, Clarke et al. (1995) demonstrated that there were no significant differences in gastrointestinal transit between 1.2 - 1.4 mm pellets with varied densities of 1.5, 2.0 and 2.4 gcm^{-3} when observed in 8 healthy males. Therefore, the critical density range to delay gastrointestinal transit might lie in the range 2.4 - 2.8 gcm^{-3}.

1.7 Biopharmaceutical studies of wax formulations

The biopharmaceutical studies of wax formulations involve two approaches that the use of simulated gastric fluids for in vitro assessment and pharmacokinetic & scintigraphic studies in animals or humans as discussed below (Craig, 1995). In pharmacokinetic study, the term "bioavailability" is used to describe the rate and extent of a therapeutically active drug that reaches the systemic circulation. The extent of bioavailability is presented by the area under the concentration–time curve

(AUC) and maximum plasma concentration (C_{max}) and the rate of bioavailability is expressed by the time to reach C_{max} (t_{max}) (Metzler, 1991).

1.7.1 Simulated gastric fluid studies of wax formulations

The dissolution media which were simulated gastric fluids with high content of lipid affected drug dissolution rate more than aqueous fluids observed from formulations containing tetracycline hydrochloride and Gelucire 50/02 (Buckton et al., 1989). Moreover, various dissolution media (simulated gastric fluid pH 1.2, phosphate buffers pH 4.5 and 6.8 as well as water) were investigated in three formulations (capsule filled with piroxicam powder, semi-solid dispersion formulations containing piroxicam, Gelucire 44/14 and Labrasol® in capsules and commercial tablets containing a complex of piroxicam:ß-cyclodextrin). The drug release of capsules filled with piroxicam was depended on pH of media that drug dissolution profiles at pH 1.2 and 6.8 were faster than that of pH 4.5 and water. In wax formulations, drug dissolution at pH 4.5 and water increased compared to capsules filled with piroxicam indicating improvement of drug solubility. However, commercial tablets showed the fastest drug dissolution due to the most development of piroxicam solubility (Yuksel et al., 2003).

1.7.2 Pharmacokinetic and scintigraphic studies of wax formulations

The bioavailability of ibuprofen from a pellet formulation containing 60% drug, 25% microcrystalline wax(es) and 15% waxy maltodextrin could be manipulated by the inclusion of different proportions of wax to control release rate. Formulations containing both microcrystalline waxes (Lunacera® P and M, weight ration 3:7, total content of 25% w/w) had a lower C_{max} and AUC compared to formulations composed of Lunacera® P alone as the microcrystalline wax component, although the t_{max} values were similar (Zhou et al., 1998).

Dennis et al. (1990) reported that a rapid oral release matrix system consisting of Gelucire 44/14 and ketoprofen might be absorbed due to the rapid dispersal of the

Gelucire 44/14 base in the stomach following by emptying of gastric contents into small intestine where drug absorption occurs as observed by gamma scintigraphy. Sustained release could be achieved by formulation of ketoprofen (17% w/w) with 60% Gelucire 50/13 and 20% Gelucire 50/02 with resultant drug absorption occurring in the intestine. Bioavailability decreased with decreased gastric dispersion as this led to slower gastric emptying and reduced drug absorption. Moreover, the floating behaviour of wax pellet formulations in the stomach have been reported by Shimpi et al. (2004) and Chauhan et al. (2005a) respectively for diltiazem and risedronate formulations containing Gelucire 43/01 as assessed by human gamma scintigraphic studies.

An improvement in the oral bioavailability of piroxicam (Class 2 drug with high permeability – low solubility) by dispersion in a matrix formulation containing Gelucire 44/14 and Labrasol® (caprylocaproyl macrogolglycerides) was reported by Yuksel et al. (2003). The bioavailability parameters (C_{max} and AUC) of piroxicam were significant higher than that of capsule filled with piroxicam powder but they were similar to that of commercial tablet containing a complex of piroxicam:ß-cyclodextrin. The drug bioavailability from a wax formulation was reported as being of more rapid onset but of shorter duration than the commercial product. In addition, Barker et al. (2003) demonstrated that the addition of Gelucire 44/14 in a α-tocopherol formulation led to improved drug bioavailability. The bioavailability parameters (C_{max} and AUC) of α-tocopherol from Gelucire 44/14 formulation were significantly higher ($P < 0.01$) than that of commercial sample but they found no significant differences in t_{max} ($P > 0.05$) between the two formulations when tested in 6 healthy males. The Gelucire 44/14 formulations also showed a noticeable increase in the extent of absorption with a more rapid onset compared to commercial samples.

1.8 Aims and objectives

The aims of the PhD studies were to develop sustained release wax matrix pellets based on a direct warm spheronisation method and to record physicochemical and morphological changes in glyceryl monostearate (GMS) and glyceryl palmitostearate

(GPS) used in the formulations during subsequent storage. Processes capable of preventing any physicochemical or morphological changes in GMS and GPS formulations upon ageing were also explored. In order to achieve these aims, the research had the following objectives:

1. To optimise the composition and processing conditions required to produce wax matrix pellets using a direct warm spheronisation technique.

2. To investigate any physicochemical changes in GMS and GPS materials during ageing.

3. To investigate any physicochemical changes in GMS and GPS formulations during ageing.

4. To investigate any morphological changes in GMS and GPS as raw materials and in formulations during ageing.

5. To identify suitable processes incorporating thermal annealing and/or stabilising agents to inhibit any changes observed in the dissolution performance of GMS and GPS formulations.

CHAPTER 2

MATERIALS AND METHODS

Chemicals, reagents and equipment with suppliers are listed in Section 2.1 to 2.3. Abbreviations for chemicals and some equipment are shown in bold type. These abbreviations are used throughout the thesis.

2.1 Materials

2.1.1 Excipients

Adizem® XL capsule (Diltiazem HCl 120 mg) batch no. BN 121916	Napp Pharmaceuticals Ltd., Cambridge, UK.
Dibasic calcium phosphate dihydrate (Emcompress®) (**DCP**) batch no. G13A	JRS Pharma, Rosenberg, Germany.
Gelucire 50/13 batch no. 22783	Supplied by Gattefosse, Cedec, France.
Glyceryl dibehenate (Compritol 888 Ato®) (**GDB**) batch no. 23225	Supplied by Gattefosse, Cedec, France.
Glyceryl monostearate (Galeol®) (**GMS**) batch no. 25388	Supplied by Gattefosse, Cedec, France.
Glyceyl palmitostearate (Precirol®) (**GPS**) batch no. 22363	Supplied by Gattefosse, Cedec, France.
Hydrochloric acid 37% (**HCl**)	Sigma Chemical Co., St.Louis, USA.
Hydroxylpropyl methyl cellulose (Methocel® K15 M Premium; high viscosity) ($\mathbf{HPMC_{K15M}}$) batch no. KE03012N12	Dow Chemicals Ltd., Midland, MI, USA.
Polyethylene glycol 1450 flake (Carbowax®) (**PEG 1450**) batch no. B114E	Union Carbide Chemicals and Plastics Company Inc., Danbury, USA.
Polyethylene glycol-8 beeswax (Apifil®) (**PG8BX**) batch no. 23165	Supplied by Gattefosse, Cedec, France.
Potassium bromide (**KBr**)	Sigma-Aldrich Co. Ltd., Poole, Dorset, UK.
Potassium dihydrogen phosphate ($\mathbf{KH_2PO_4}$)	Sigma-Aldrich Co. Ltd., Poole, Dorset, UK.
Sodium hydroxide ≥ 98% (**NaOH**)	Sigma Chemical Co., St.Louis, USA.

2.1.2 Drugs

Diltiazem HCl (**DTZ**) batch no. 97EXC077	Pfizer Limited, Surrey, UK.
Paracetamol (**PCM**) batch no. 34H0249	Sigma Chemical Co., St.Louis, USA.

2.1.3 Consumables

Aluminium crucible with lids (40 µl)	Mettler-Toledo Ltd., Leicester, UK.
Aluminium foil (Aluchef® foil)	Terinex Limited, Bedford, UK.
Glass capillary (Ø 0.7 mm; wand 0.01)	Hilgenberg, Germany.
Microscope cover glass (22 x 22 mm; thickness 1)	VWR International Ltd., Leicestershire, UK.
Microscope slide (76 x 26 mm; 1.0 - 1.2 mm thick)	VWR International Ltd., Leicestershire, UK.
Microscope slide (Ø 16 mm; thickness 1)	VWR International Ltd., Leicestershire, UK.
Petri dishes (Ø 100 mm; height 15)	VWR International Ltd.., Leicestershire, UK.

2.2 Equipment

2.2.1 Manufacture

Hand blender (Mode no. HM-918)	Cookworks, UK.
pH meter (pH 211)	Hanna Instruments, Italy.
Sieves (brass; sizes 850, 1000 and 1180 µm)	Endecotts Ltd., London, UK.
Sieve shaker (Model EFL 2)	Endecotts Ltd., London, UK.
Sonicator (Transsonic T310)	Camlab Serving Science, Cambridge, UK.
Spheroniser (Model 120)	Caleva, Process Solutions Ltd., Sturminster Newton, Dorset, UK.
Turbula™ mixer	Willy A. Bachofen AG, Basel, Switzerland.
Water bath (Type SE-15)	Grant Instruments Ltd., Cambridge, UK.

2.2.2 Analysis

Aluminium crucible-lid sealer	Mettler-Toledo Ltd., Leicester, UK.
Automated dissolution apparatus (Model ST 7)	Copley Scientific Limited, Nottingham, UK.
Crucible sealing press	Mettler-Toledo Ltd., Leicester, UK.
Differential scanning calorimeter system (**DSC**; DSC 822^e Module; TA controller TC15)	Mettler-Toledo Ltd., Leicester, UK.

Fourier Transform Infra Red spectrophotometer (**FT-IR**)(Bench.101 : Genesis 1)	Mattson Instruments, Madison, USA.
Hot stage microscope (**HSM**; TMS 91)	Linkam Scientific Instruments Ltd., Surrey, UK.
IR Press	Research & Industrial Instrument Company, London, UK.
Polarised light microscope (Polyvar®)	Reichert-Jung, Arnsberg, Germany.
Pump of dissolution apparatus (Ismatec®) type ISM931 V4.00	Ismatec SA, Labrtechnik-Analytik, Glattbrugg-Zurich, Switzerland.
Scanning electron microscope (**SEM**; SEM 515)	Philips Ltd., Eindhoven, Netherlands.
Sieves (brass; sizes 500, 850, 1000, 1180, 1400, 1700 and 2360 μm)	Endecotts Ltd., London, UK.
Sputter coater (Polaron SC 515)	Bio-Rad sputter coater, Bio-Rad Ltd., Hemel Hempstead, UK.
UV spectrophotometer (Cecil CE 3021)	Cecil instruments, Cambridge, UK.
Texture Analyser (TA-XT2)	Stable Micro Systems, Surrey, UK.
X-ray powder diffraction (**XRPD**; Bruker-AXS D8)	Bruker AXS GmBH, Karlsruhe, Germany.

2.3 PC software

Differential scanning calorimeter software (Star^e system)	Mettler-Toledo Ltd., Leicester, UK.
Dissolution software (Erweka dissolution V2.17)	Erweka Co. Ltd., Heusenstamm, Germany.
FT-IR software (Winfirst V3.5)	Mattson Instruments, Madison, USA.
Polarised light microscope software (Leutron vision V1.95.002)	Reichert-Jung, Arnsberg, Germany.
Texture Analyser software (Texture Exponent V2.07)	Stable Micro Systems, Surrey, UK.
SEM software (Image Slave)	Meeco-Dindema, Sydney, Australia.
X-ray software (EVA 9.0.0.2)	Socabim, Germany.

2.4 Analytical techniques

2.4.1 Sieve and size distribution analysis

2.4.1.1 Sieve and size distribution analysis of solidified mixtures

Size distribution of solidified samples was performed using sieves of size 500, 850, 1000, 1180, 1400, 1700 and 2360 μm (stacked descending to this order) on the sieve shaker (Model EFL 2; Endecott) for 5 minutes. Characteristics of the resultant granules were observed visually and recorded. The quantity of granules retained on each sieve after shaking was weighed and recorded.

2.4.1.2 Sieve and size distribution analysis of pellets

Size distribution of pellets was performed using sieves of size 850, 1000 and 1180 μm (stacked descending to this order) on the sieve shaker (Model EFL 2; Endecott) for 5 minutes. Characteristics of the resultant pellets were observed visually and recorded. The quantity of pellets retained on each sieve after shaking was weighed and recorded.

2.4.1.3 Data analysis of size distribution

Data analysis was presented as tables or graphs. In tables, the percentages retained fractions on each sieve are reported.

For graphical presentations, cumulative weight percentages of oversize and undersize against sieve aperture size were plotted on a semilogarithmic scale. The two graphs are mirror images of each other and cross over at 50 cumulative percent indicating the median size or mid-point (half of particles are smaller than the median size and half are larger).

When data was graphically represented in arithmetic-probability format, the cumulative weight percent undersize or oversize was plotted on the probability scale and the sieve aperture sizes on the arithmetic scale. They are used to assess the characteristic of crystal size distribution in terms of two properties, the median size (MS) and the coefficient of variation (CV) following Equation 2.1 (Mullin, 1996).

$$CV = \frac{100\,(d_{84} - d_{16})}{2d_{50}} \qquad \text{[Eqn. 2.1]}$$

[where d_{84}, d_{50}, and d_{16} are the equivalent sieve aperture values corresponding to 84, 50 and 16 cumulative percentages respectively as well as d_{50} is the median size]

2.4.2 Ultraviolet spectroscopy

When ultraviolet (UV) or visible light passes through the chemical solution, the energy of the photons in the region 200 - 800 nm is allowed to excite electrons and move to higher energy level. The excitation is measured as absorption-wavelength spectrum in a UV/visible spectrophotometer.

The UV/visible spectrophotometer is utilised to determine concentrations of chemical solution, according to Beer Lambert Law. This stated that the amount of absorbed incident light is directly proportional to the number of absorbing molecules relating to concentration of the solution and is not depended on the intensity of the source as following Equation 2.2.

$$\text{Absorbance (A)} = \text{Log } I_0 / I_t = \varepsilon.\, b.\, c \qquad \text{[Eqn. 2.2]}$$

[where I_0 = intensity of incident light; I_t = intensity of transmitted light; ε = molar extinction coefficient; b = cell pathlength in cm (usually 1 cm); c = concentration of absorbing solution in mol/L]

If ε and b are constants, the following equation can be rearranged to give:

$$\frac{A_1}{A_2} = \frac{C_1}{C_2} \qquad \text{[Eqn. 2.3]}$$

[where A_1, A_2 = absorbance of solutions 1 and 2; C_1, C_2 = concentration of solutions 1 and 2]

This is the basic equation used to determine concentration of a solution, correlating to the absorbance from UV/visible spectrophotometer (Thorburn Burns, 1993).

2.4.2.1 Generation of an absorbance linearity curve based on drug concentration using UV spectroscopy

The drug was dissolved in a distilled water to obtain a stock solution. This stock solution was diluted to prepare five concentrations of drug and each solution was scanned within a pre-determined wavelength range to obtain the UV spectrum. From the UV spectrum, an appropriate analytical fixed wavelength was selected.

At a fixed wavelength, all the solutions were measured the absorbance values which were plotted against the concentration. According to Beer Lambert Law, the absorbance value at any specific wavelength is proportionate to the concentration of the solution. A linear regression was fitted to present the relationship between absorbance value and solution concentration. This linear relationship was used in further dissolution studies to determine the concentration of drug solution.

2.4.3 Dissolution test

Dissolution tests were performed following USP Method XXIV, Apparatus 2 method using paddles set at speed 50 rpm and peristaltic pump set at 30 rpm with dissolution media maintained at 37°C. Each dissolution run was performed using six dissolution pots each containing 900 ml dissolution media (distilled water used in general). Drug release was typically performed for 8 or 24 hours.

2.4.4 Statistical analysis

Statistical analysis was performed using Fit Factors (difference factor f_1 and similarity factor f_2) in dissolution profile comparisons (Moore and Flanner, 1996). One graph was set as the reference (pre-change) graph while the other was assigned the test (post-change) graph. This method is also employed by FDA in scale-up and post approval changes (SUPAC-IR) (FDA, 1997).

2.4.4.1 Difference factor (f_1)

The f_1 value measures the relative error calculating the percentage difference between all time points of two curves as following Equation 2.4.

$$f_1 = \frac{\sum_{j=1}^{n} |Rj - Tj|}{\sum_{j=1}^{n} Rj} \qquad \text{[Eqn. 2.4]}$$

[where n = numbers of sampling time; R_j = percentage drug dissolved of reference batch at time j; T_j = percentage drug dissolved of test batch at time j]

If the f_1 value is close to zero, two curves can be considered similar. Normally, f_1 value less than 15 (0 - 15) indicates no significant difference between two graphs (equivalence between reference and test curves).

2.4.4.2 Similarity factor (f_2)

The f_2 value measures the dissolution percentage similarity between all time points for two curves as following Equation 2.5.

$$f_2 = 50 \text{ Log } \{ [1 + 1/n \sum_{t=1}^{n} w_t (R_t-T_t)^2]^{-0.5} \text{ x } 100 \} \qquad \text{[Eqn. 2.5]}$$

[where n = numbers of sampling time; w_t = optional weight factor * ; R_t = percentage drug dissolved of reference batch at time t; T_t = percentage drug dissolved of test batch at time t]

(For example, if time point 10 minutes is more important, then a higher weighting could be given at this point)*

If the f_2 value is nearly 100, two curves can be considered similar. Normally, f_2 value more than 50 (50 - 100) indicates no significant difference between two graphs (equivalence between reference and test curves).

The suggestion of dissolution profile comparison should be considered as following.

- Dissolution time points should be more than 4 points and perform under the same condition.
- Only one measurement should be considered after 85% drug dissolution of both reference and test samples.
- Using the mean data, the percent coefficient of variation should not be more than 20% at the earlier time points and should not be more than 10% at other time points.

2.4.5 Fourier-Transform infrared (FT-IR) spectrophotometry

FT-IR spectrophotometry is the study of the interaction of electromagnetic radiation with molecule structure causing vibration of chemical bond. The region of electromagnetic wavelength (λ) is 0.8 to 1000 μm (infrared spectrum) and the frequency (ν) is number of cycles that the wave undergoes in a second. The frequency, wavelength and speed of light are related to each other responding to following equation.

$$c = \nu . \lambda \qquad \text{[Eqn. 2.6]}$$

[where c = the speed of light ($3x10^{10}$ cm/second); ν = frequency in Hertz (sec^{-1}); λ = wavelength in cm]

The unit called the wavenumber (W) is usually used to indicate different types of light. The relationship between wavenumber and wavelength is shown in Equation 2.7.

$$W = 1/\lambda \qquad \text{[Eqn. 2.7]}$$

[where W = wavenumber in cm^{-1}; λ = wavelength in cm]

Therefore, the light wave can be described by frequency, wavelength or wavenumber as in the relationship in Equation 2.8.

$$c = \nu / W \quad \text{or} \quad \nu = c . W \qquad \text{[Eqn. 2.8]}$$

The IR spectra are divided into three regions which are near IR, mid IR and far IR. The mid IR (4000 – 400 cm^{-1}) is the most commonly used region in pharmaceutical analysis. The IR spectra are plotted as wavenumber (X axis) with absorbance or transmittance (Y axis).

2.4.5.1 Instrumentation

The foundation of FT-IR spectrophotometry is the change in rotational and vibrational energy levels of electrons following the absorption of IR spectrum. The absorption is caused by a change in the dipole moment of a molecule. The dipole moment is a measurement of the charge asymmetry of molecules that distribute positive (δ^+) and negative (δ^-) charges between two atoms. The bond bending and stretching affect the symmetry of a molecule, change the dipole moment and result in the IR spectrum.

The group wavenumber indicates the functional groups of molecules in the specific absorption bands at a particular wavenumber. The important functional groups and band position are shown in Table 2.1. The specific and unique region of the IR spectrum from 1600 to 1000 cm^{-1} (fingerprint region) is used in the qualitative analysis (Smith, 1999).

Table 2.1. Functional groups in the IR spectrum.

Band position in cm^{-1}	Functional groups
3500 - 3200	O-H or N-H
3200 - 2800	C-H
2250 - 2000	C≡N, C≡C
1800 -1600	C=O
< 1000	C=C, Benzene rings

2.4.5.2 Sample preparation for FT-IR

FT-IR analysis can be applied to samples in gas, liquid and solid phases. In solid samples, the KBr disc is the most useful and widely used technique. Advantages of this method are very low absorption from the KBr and the small amount of sample required. Sample preparation for KBr disc is explained below.

1. The fine particle of sample (~ 1 mg) was mixed with ~ 250 mg of KBr and grounded together on an agate mortar until the sparkle disappeared.
2. The mixture was put in 'press assembly' (consisting of base, barrel, dies and piston).
3. The 'press assembly' was placed into the hydraulic press and then pumped until required pressure (~ 10 tonnes) for 3 minutes.
4. The barrel-piston assembly was removed from the base and turned upside down.
5. The KBr sample disc was carefully removed from the 'press assembly' and scanned by the FT-IR spectrophotometer.

2.4.6 Differential scanning calorimetry (DSC)

The DSC is one of several techniques of thermal analysis. Other techniques of thermal analyses include differential thermal analysis (DTA), thermogravimetric analysis (TG), thermomechanical analysis (TMA), dynamic mechanical analysis (DMA) and hot stage microscopy (HSM; as explained in Section 2.4.9). DSC has many advantages such as fast analysis time, easy sample preparation, small amount of required samples (0.1 μm – 10 mg), wide temperature range of applicability, applicability to solid, liquid or semi-solid and excellent quantitative and qualitative capability (Hatakeyama and Quinn, 1999).

2.4.6.1 Instrumentation

The principle of DSC involves heating up a sample (usually above the melting point of samples) and comparing it to a reference. The required heat flow is recorded. As the sample and reference are heated, there can be a different heat flows which can be expressed as exothermic or endothermic events. These events are represented as peaks or curves of energy flux unit (Joules/time) versus temperature. The area under the curve is directly proportional to absorption or emission of heat from the sample. The area is integrated and calculated a heat of fusion (ΔH) or enthalpy change. The melting point can also be determined from the main peak.

Generally, there are two types of DSC instrument: the power compensation DSC typified by the Perkin-Elmer systems and the heat flux DSC exemplified by the Dupoint and Mettler systems. The differences between two kinds of systems are that sample and reference pans are heated by individual heaters in power compensation system but there is one heater to heat both sample and reference pans in heat flux system (Ford and Timmins, 1989). The system used in the following studies is based on the heat flux principle that is the Mettler Toledo Star^e DSC 822^e system consisted of a TA controller (TC 15) and a measuring cell (DSC 822^e Module). The measuring cell is cooled by liquid nitrogen and purged with dry nitrogen gas. The schematic cross section through the measuring cell (DSC 822^e Module) is shown in Figure 2.1.

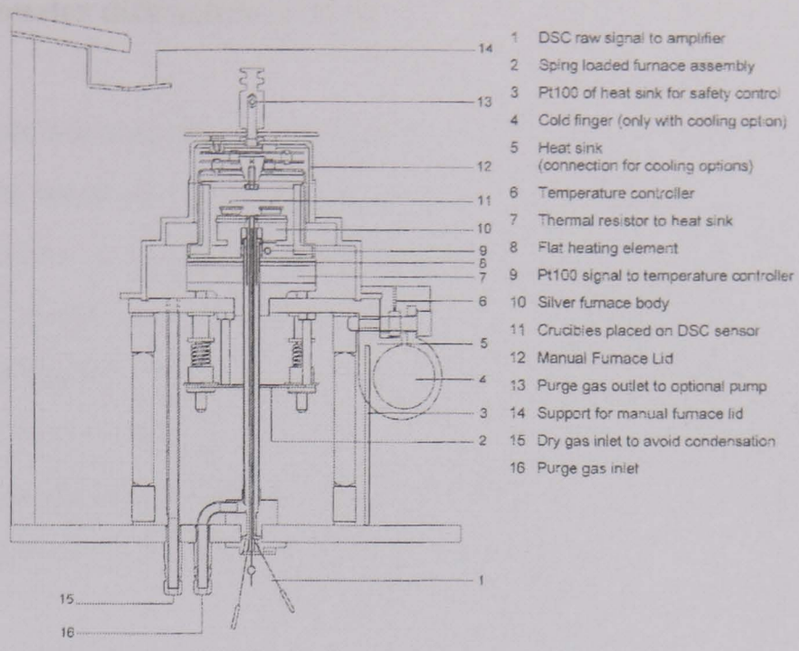

Figure 2.1. Schematic cross sectional view of the DSC 822^e measuring cell (Obtained from Mettler Teledo instrument handbook).

2.4.6.2 Sample preparation for DSC

The aluminium standard crucibles pans (40 µl) were used. Sample preparation for DSC studies is presented below.

1. The empty crucible was weighed before sample addition.
2. The sample (approximately 2 - 5 mg) was added and weighed by difference.
3. The crucible lid was pierced using a pin to allow gas exchange during heating.
4. The crucible containing the sample was placed in a crucible sealing press by tweezers and then rotated slowly the hand wheel twice for sealing.
5. The sealed crucible was placed in the sample pan of the DSC instrument.

The reference crucible was prepared identically without sample addition. The same reference was used for all samples in DSC studies.

GMS samples were heated from 30 to 85°C at a heating rate of 10°C/min for one cycle whereas GPS samples were heated from 30 to 75°C at a heating rate of 5°C/min for one cycle. The DSC plots were normalised against the weight of each sample.

2.4.7 X-ray powder diffraction (XRPD)

X-rays are short wavelength, high energy beams of electromagnetic radiation with a wave frequency between UV and gamma rays in the electromagnetic spectrum. The x-rays incident on a crystalline solid become scattered in all directions. When objects scatter x-rays, the interference at specific angles is called diffraction. The angles of diffraction are dependent on the relationships between the atoms making up a molecule in a crystalline form. Bragg's law describes x-ray diffraction by the assumption of perfectly parallel and monochromatic x-rays. At a wavelength (λ) and an angle (θ) of the x-ray beams on the crystalline sample,

$$n\lambda = 2d \sin\theta \qquad \text{[Eqn. 2.9]}$$

[where d = distance between the planes in the crystals; n = order of reflection]

The wavelength of X-rays can be expressed in Angstrom (Å) units with $1 Å = 10^{-10}$ m and can be used to determine atomic, molecular and ionic distances within a crystal lattice. The x-ray pattern is described by the θ angle. Crystalline materials present sharp peak characteristic whilst amorphous compounds express diffuse peaks in the x-ray pattern. The set of d-spacing (the distance between adjacent planes of atoms) shows the unique "fingerprint" of the crystal using for identification of the compound.

2.4.7.1 Instrumentation

The single crystal x-ray diffraction is used for small single crystals (less than 100 atoms) but it can not analyse large single crystals (up to 2000 atoms). Therefore, powder diffraction is an excellent alternative for the investigation of polycrystalline and complex compounds. The XRPD used in this thesis is the Bruker-AXS D8 X-ray powder diffractometer consisted of three basic parts shown in Figure 2.2.

1. A source of radiation consisting of an X-ray tube and a high voltage generator
2. The detector and counting equipment
3. The diffractometer

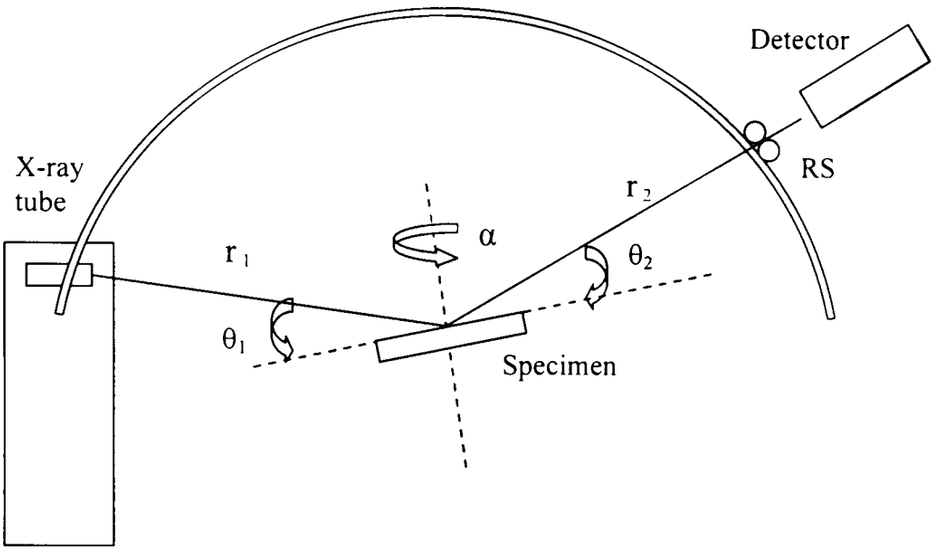

Figure 2.2. Operating principle of powder diffraction (Obtained from Jenkins and Snyder, 1996).

Crystal structure determination involves packing powder into a cell, collection of data, determination of unit cell parameters, space group determinations, prior to structure solution and refinement of the data set (Jenkins and Snyder, 1996).

2.4.7.2 Sample preparation for XRPD

The samples were placed in 0.7 mm borosilicate glass capillaries. The radiation source was monochromatic copper (CuK_{a1}), λ = 1.54056 Å and data collection ranged from 3 to 40° 2θ at a step size of 0.017° and time per step of ~ 4 minutes.

2.4.8 Polarised light microscopy

Polarised light is light in which the waves are all vibrating in one fixed direction. Polarisation involves decreased oscillation of natural light consisting of an infinite number of planes to only a single plane by the use of a filter as shown in Figure 2.3.

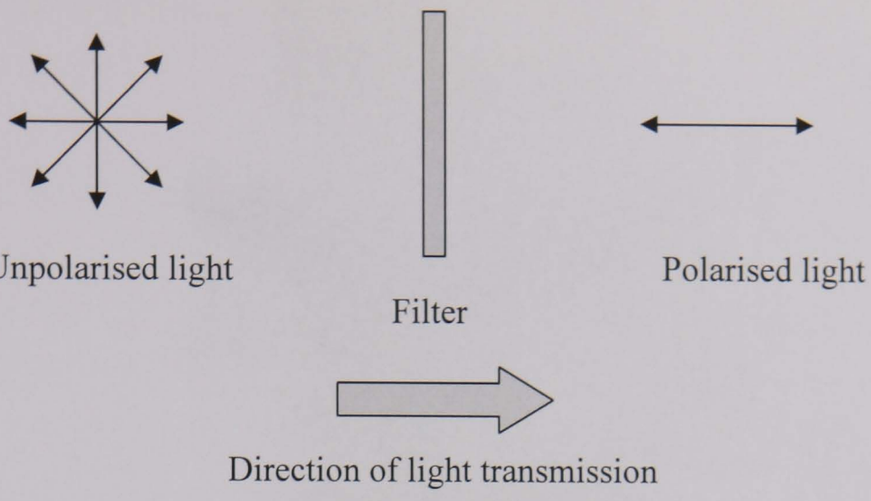

Figure 2.3. Polarisation of natural light.

In general, materials can be divided as isotropic and anisotropic. A substance in which light has the same refractive index (velocity) in all directions is called isotropic. Isotropic materials are completely dark when viewed under polarised light. However, anisotropic materials exhibit birefringence that could have two refractive indices. Birefringence is described as the difference between the two refractive indices of ordinary and extraordinary rays. When anisotropic materials are viewed under polarised light, they express a coloured image of the birefringent material owing to splitting of beams (Patzelt, 1985).

2.4.8.1 Instrumentation

Polarised light microscope (Polyvar; Reichert-Jung, Germany) as shown in Figure 2.4 was used to observe the morphology.

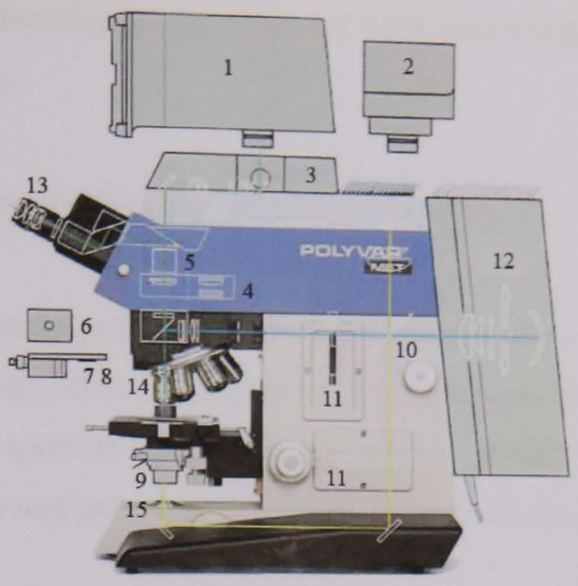

1. Polaroid camera	6. Incident light module	11. Filter module
2. 35 mm camera	7. Interference contrast module	12. High intensity lamp
3. Camera module	8. Interferometer module	13. Eyepieces
4. Magnification module	9. Transmitted light condenser	14. Objectives
5. Dual relex module	10. Mirror module	15. Transmitted light filter polariser

Figure 2.4. Schematic diagram of a Polyvar microscope (modified from http://www.materials.co.uk/optical.htm).

The polariser and filter are parallel to each other when the angle between them is 0^{o}, 180^{o} or 360^{o} exhibiting maximum brightness intensity. In contrast, the polariser and filter are vertical to each other when the angle between them is 90^{o} or 270^{o} showing minimum brightness intensity and no transmitted light (Slayter and Slayter, 1992). Total magnification values x250 and x1000 were used to view samples.

2.4.8.2 Sample preparation for polarised light microscopy

1. Wax sample was melted at a water bath maintained at 70°C (above the melting point of wax)
2. The glass slide was warmed on a water bath.
3. One drop of the sample was placed on the warm glass slide.
4. A glass slide cover slip was gently lowered onto the sample.

5. Sample slide was investigated by polarised light microscopy and stored at 25 or 46°C for fixed times.

2.4.9 Hot stage microscopy (HSM)

HSM, known as thermoanalytical microscopy, is a valuable supportive tool when used in conjunction with other techniques such as polarised light microscopy, DSC or thermogravimetric analysis (TG). The changes in sample morphology such as melting, crystallisation and polymorphic transformation can be observed by HSM.

HSM analysis in this study was performed using a Linkam TMS 91 (UK.) hot stage assembled on a polarised light microscopy (Polyvar, Germany). The samples were observed under polarised light by using a scanning speed of 1°C/min from room temperature to approximately 65°C (above the wax melting point). Images were captured to observe changes as a function of temperature.

2.4.10 Scanning electron microscope (SEM)

SEM is a useful instrument for studying three-dimensional samples and surface topography. It has many advantages over traditional microscopes. SEM has a large depth of field, which allows more samples to be in focus at one time. It also has higher resolution of images such that closely spaced features can be resolved at higher magnifications. The SEM uses electromagnets (instead of lenses in optical microscopes) to bend an electron beam to generate an image on a monitor.

2.4.10.1 Instrumentation

SEM images are produced by generating a fine beam of electrons at the top of the microscope from a heated tungsten filament (electron gun). The electron beam follows a vertical path through the column of the microscope within a vacuum. The beam travels through magnetic lens and scanning coils, which focus the beam at the surface of sample and scans the beam across in a raster or pattern of parallel lines

(the electron beam in an x-y coordinate system collecting data points). When the electron beam hits the sample, secondary electrons (low energy), backscattered electrons and X-rays are ejected from the sample. These electrons are collected by different detectors and converted into a signal and then sent to a monitor. It is possible to choose different detectors for use with samples of different properties. The secondary electron detector generates a clear and focused topographical image of the sample but the backscatter electron detector produces an image used to observe the elemental component of the sample (Watt, 1997). The SEM 515 microscope (Philips, Eindhoven, Netherlands) and a Polaron SC 515 SEM sputter coating system were used in this thesis. The schematic diagram of SEM main component is shown in Figure 2.5.

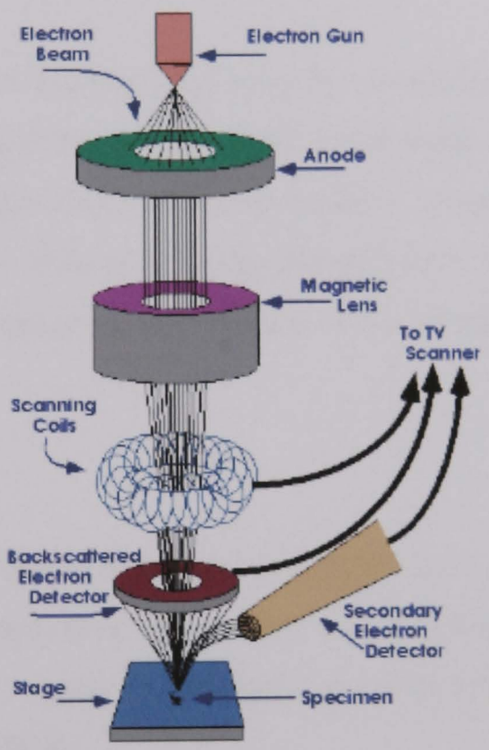

Figure 2.5. Schematic diagram of SEM principle (Reproduced from http://mse.iastate.edu/microscopy/home.html (website of department of Materials Science and Engineering at Iowa State University)).

2.4.10.2 Sample preparation for SEM

Since the SEM utilises electrons to form an image and uses vacuum conditions, specific sample preparation is necessary. If samples are metals that are conductive,

they do not require preparation. However, non-conductive samples must be modified to have a conductive property by coating with a thin layer of conductive materials using a device known as a sputter coater. The sputter coater uses an electric field and argon gas in a small vacuum chamber. The argon gas and electric field cause an electron to be removed from the argon to produce positive charge ions. The argon ions are attracted to a gold foil with negative charge and knock gold atoms from the surface of the gold foil. The gold atoms fall and settle onto the surface of the sample forming a gold coating. Coating a sample with a heavy metal allows optimisation of the signal, which protects from charge effect, improves image contrast and provides a consistent source of secondary electrons. The gold coating also prevents mass loss due to damage by the beam, provides a layer of thermal conductivity and avoids overheating of samples (Slayter and Slayter, 1992).

Two types of sample were analysed, the wax raw materials and pellet formulations. Firstly, samples were mounted on 10 mm aluminium stubs with double-sided carbon or copper tape. The samples were then gold coated (~ 10 nm) using a sputter coating system (Polaron SC 515). The gold coated samples were placed at the base of the SEM. All samples were imaged at three or four levels of magnification.

2.4.11 Texture Analyser

Texture Analyser uses a penetration test to measure the force during insertion of a probe into a sample to a specified depth. The test determines both compression and shearing properties of a sample as the probe penetrates the surface layers of the sample (Lu and Abbott, 2004).

2.4.11.1 Instrumentation

In the present study, analysis was performed by using a TA.XT2 Texture Analyser (Stable Microsystems, UK.) fitted with 5 kg load capacity cell and Texture Expert Exceed real-time graphics and data acquisition software as shown in Figure 2.6. This instrument has been used to characterise morphological changes in wax materials.

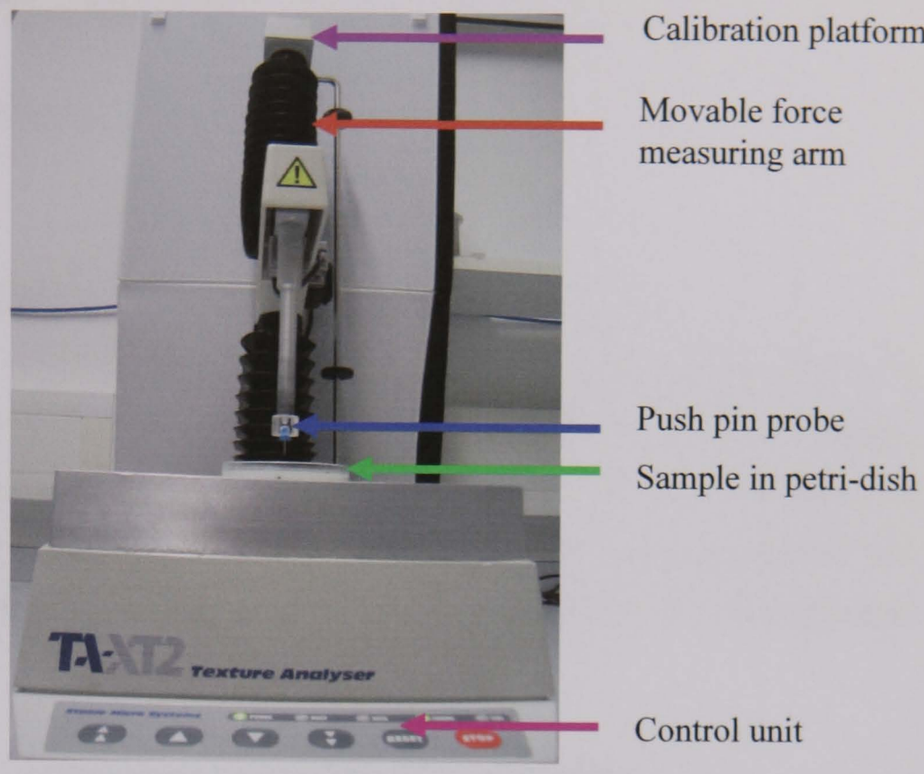

Figure 2.6. Schematic diagram of a TA.XT2 Texture Analyser.

Sample preparation for Texture Analyser is described in more detail in Section 6.2.1.

2.4.11.2 Operation of Texture Analyser

- Calibration

The force and height calibrations were required to perform before testing. The force calibration was performed by placing load cell 2 kg on the calibration platform of Texture Analyser. The height calibration was conducted by moving the position probe closely to base and ensuring that the space between the probe and the test bed of the attachment is clear of obstructions.

- Software programme

Mode: Compression

Pre-test speed: 1.0 mm/sec

Test speed: 0.10 mm/sec

Post-test speed: 10.00 mm/sec

Target mode: Distance

Distance: 1.0 mm

Trigger type: Auto (Force)

Trigger force: 0.1 g

- Sample handling

Samples were removed from storage temperatures and allowed to equilibrate at room temperature for 1 hour. Samples were penetrated by a sharp, clean and dry pointed metal probe (push pin) to a depth of 1 mm during a 10 seconds period as shown in Figure 2.7. Six replicates of each wax sample were tested ensuring that the test surfaces were separated by a distance of 40 mm from each other and from the edge of the container.

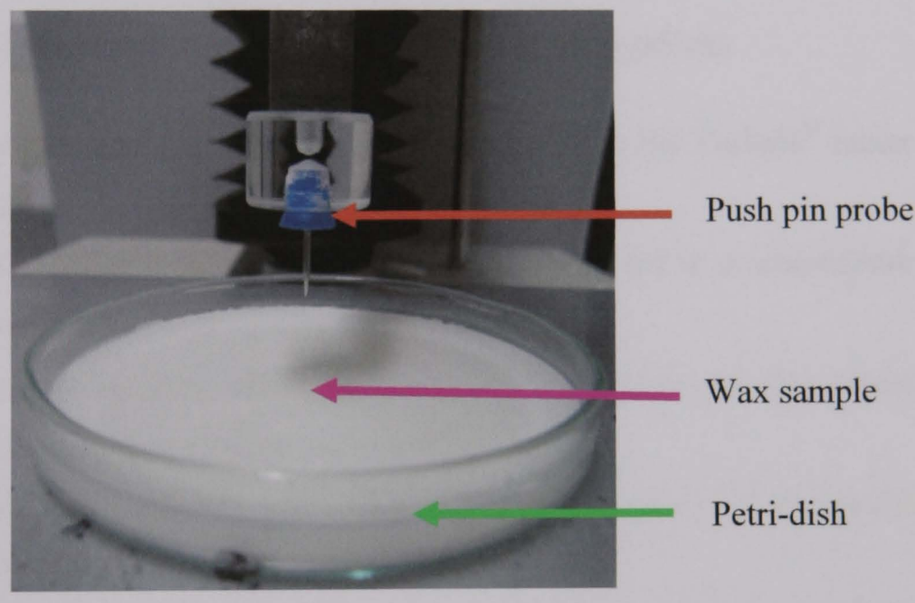

Figure 2.7. Schematic diagram of penetration test of a TA.XT2 Texture Analyser.

2.5 Pellets prepared by direct warm spheronisation

Pellets were produced by addition of drug and excipient powders into melted wax and then spheronised in a spheroniser controlled a constant temperature as explained a diagram in Figure 2.8 and manufacturing steps below.

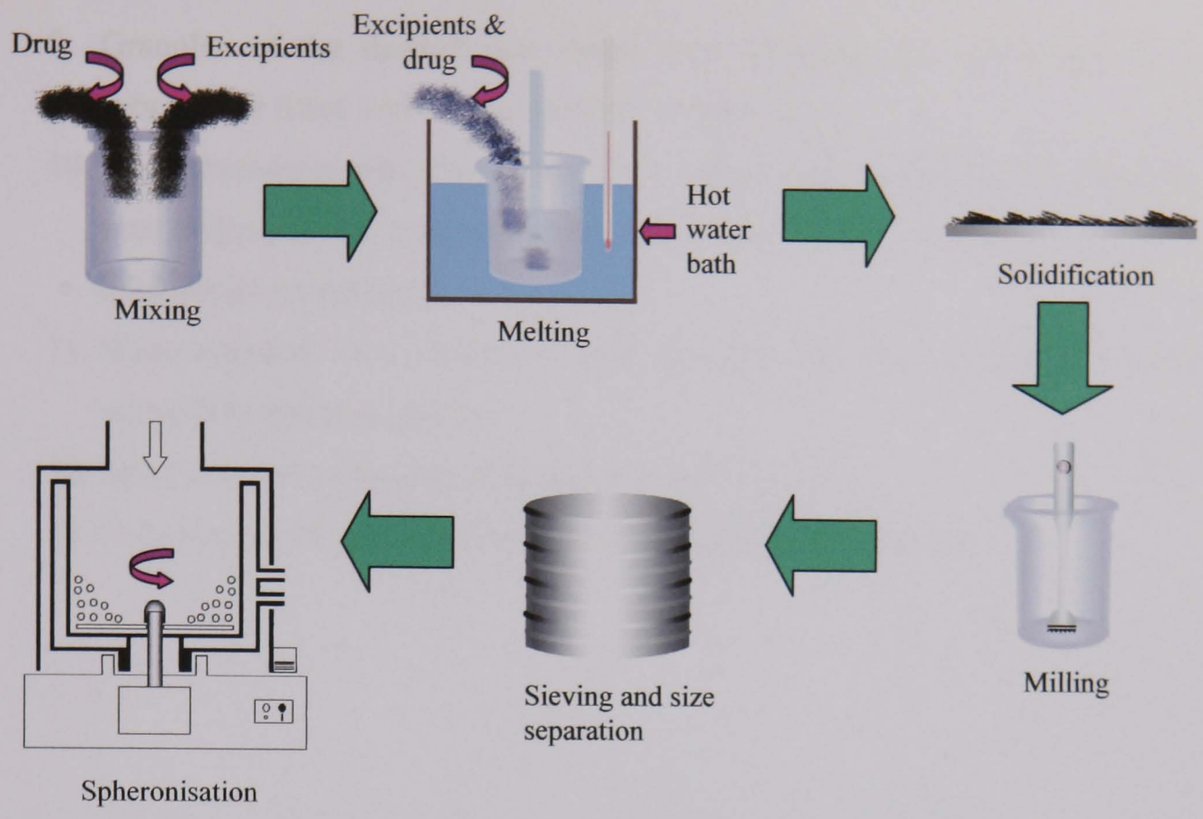

Figure 2.8. Manufacturing steps in the preparation of wax matrix pellets.

1. Powder excipients and drug were weighed and mixed in the Turbula® mixer for 15 minutes.
2. Wax was weighed and melted in a water bath maintained at a temperature above the wax melting point.
3. The powder mixtures were added gradually into the melted wax and stirred until a homogeneous formulation was obtained.
4. The formulation was then transferred onto an aluminium foil and allowed to cool to 3°C for 1 hour.
5. The solidified mixture was transferred into a hand blender and milled for 50 seconds.
6. The resulting granules were then sieved and separated according to size range using sieve sizes 1000 and 1180 μm.
7. Granules of size less than 1001 μm were remelted, solidified, milled and sieved again. Granules of size greater than 1180 μm were directly transferred back into the hand blender to be further milled.
8. Steps 4 to 7 were repeated until the whole formulation existed as granules of size range 1001 to 1180 μm.

9. Granules of the desired size range were weighed and spheronised in a spheroniser fitted with a cross-hatched surface plate.
10. The spheroniser was pre-warmed to a temperature around 10°C below the wax melting point, using a constant temperature water bath maintained at an appropriate temperature.
11. Spheronisation was continued until granules had been transformed into reasonably spherical pellets.
12. Spheronisation time and temperature were recorded.
13. Pellets were visually inspected, weighed and size distribution.

CHAPTER 3

THE INFLUENCE OF PROCESSING ON THE CHARACTERISTICS OF WAX MATRIX PELLETS

3.1 Introduction

This chapter investigates the influence of process change on the resultant characteristics and performances of wax granules and pellets arising from the manufacturing operations. Factors studied include m+illing time in granulation, formulation composition, storage time (ageing), spheronisation (time, temperature and speed) and their impact on pellet morphology and drug release. Wax matrix formulations comprising glyceryl monostearate (GMS) were utilised in this study in comparison to wax admixtures with alternative components having the same HLB value. A direct warm spheronisation method was used to form pellets from milled granules. Paracetamol was chosen as a slightly water soluble model drug which was easy to analyse by UV spectrophotometry.

All formulations contained wax (30 - 90% w/w), dicalcium phosphate (0 - 60% w/w) and paracetamol (10% w/w).

3.2 Methods

Pellet manufacture and analytical methods are provided below and referenced where appropriate to Chapter 2.

3.2.1 Effect of milling time on granule size distribution

Five batches of GMS granules containing 50% GMS, 40% DCP and 10% paracetamol were prepared by following the general granule preparation steps 1 - 4 (Section 2.5, Page 65). The solidified mixture was transferred into a hand blender

and milled for 10, 30, 50, 70 or 100 seconds. The resultant granules were analysed by sieve and size distribution analysis of solidified mixtures (Section 2.4.1.1, Page 48)

3.2.2 Effect of spheronisation time and speed on pellet dissolution

Pellets of size range 1001 to 1180 μm containing 50% GMS, 40% DCP and 10% paracetamol were prepared by following the general warm spheronisation method (Section 2.5, Page 65) with some modifications as listed below.

- Spheronisation times of 1, 2, 3, 4, 5 or 6 minutes at a fixed speed setting of 5 were utilised.
- Spheronisation speed settings of 4, 5, 6 or 7 at a fixed time of 4 minutes were employed.

The resultant pellets were analysed by dissolution test (Section 2.4.3, Page 50).

3.2.3 Effect of GMS content and pellet ageing on pellet dissolution

All pellet formulations were prepared by following the general warm spheronisation method (Section 2.5, Page 65) using a spheronisation speed setting of 6 and a spheronisation time of 4 minutes. The composition of these variants is described below.

- Pellets of varied GMS, DCP and paracetamol compositions (3:6:1, 4:5:1, 5:4:1, 6:3:1, 7:2:1 and 9:0:1).
- Freshly prepared pellets were stored in a sealed glass vessel in the dark at ambient temperature for 75 days and then evaluated by dissolution test.

Pellets in the size range of 1001 to 1180 μm were employed in subsequent dissolution studies (Section 2.4.3, Page 50).

3.2.4 Effect of wax compositions of identical HLB on pellet dissolution

Pellet formulations (nominal HLB value of 3) containing 60% wax admixture, 30% DCP and 10% paracetamol (see compositions and processes in Table 3.1 below) were prepared by the general warm spheronisation method (Section 2.5, Page 65). Pellets in the size range of 1001 to 1180 μm were employed in subsequent dissolution studies (Section 2.4.3, Page 50).

Table 3.1. Pellet formulations containing 60% wax admixture, 30% DCP and 10% paracetamol.

Formulation	Wax admixture content (% w/w)	Spheronisation temperature (°C)	Spheronisation time (minutes)
A	60 (GMS)	50	4
B	51.6 (GDB) : 8.4 (PG8BX)	50	4
C	54.6 (GDB) : 5.4 (Gelucire 50/13)	50	4
D	51.6 (GDB) : 8.4 (PG8BX)	45	2
E	51.6 (GPS) : 8.4 (PG8BX)	45	2

3.2.5 Effect of spheronisation time and temperature as well as pellet ageing on pellet dissolution

Pellet formulations (HLB value = 3) of size range 1001 to 1180 μm containing 51.6% GDB, 8.4% PG8BX, 30% DCP and 10% paracetamol were prepared by following the general direct warm spheronisation method (Section 2.5, Page 65) except for some modifications as listed.

- Spheronisation times of 2, 4 or 6 minutes at a fixed temperature of 50°C were utilised.
- Spheronisation temperatures of 50, 55, 58, 60 or 63°C were employed at a fixed spheronisation time of 4 minutes.

- Freshly prepared pellets (using a spheronisation temperature of 50°C and a spheronisation time of 4 minutes) were stored in sealed glass containers in the dark at room temperature for 75 days and then evaluated by dissolution test.

The resultant pellets were analysed by dissolution test (Section 2.4.3. Page 50).

3.3 Results and Discussion

3.3.1 Effect of milling time on granule size distribution

3.3.1.1 Sieve and size distribution analysis

The size distribution resulting from milling of solidified mixtures is shown in Table 3.2 and graphically represented in Figure 3.1.

Table 3.2. Fractional mass percentage of solidified samples varied milling times as 10, 30, 50, 70 or 100 seconds.

Size aperture (μm)	Fractional mass percentage (% retained) (Milling time)				
	10 sec.	30 sec.	50 sec.	70 sec.	100 sec.
2360	65.8	52.4	13.0	20.6	15.5
1700	8.1	11.7	8.3	7.3	5.5
1400	3.9	8.0	7.1	3.7	3.6
1180	5.0	9.1	9.1	4.5	2.6
1000	2.6	3.3	7.1	4.9	3.6
850	3.0	3.9	7.4	3.6	4.1
500	6.8	6.3	23.7	20.2	19.7
< 500	4.8	5.3	24.3	35.2	45.4

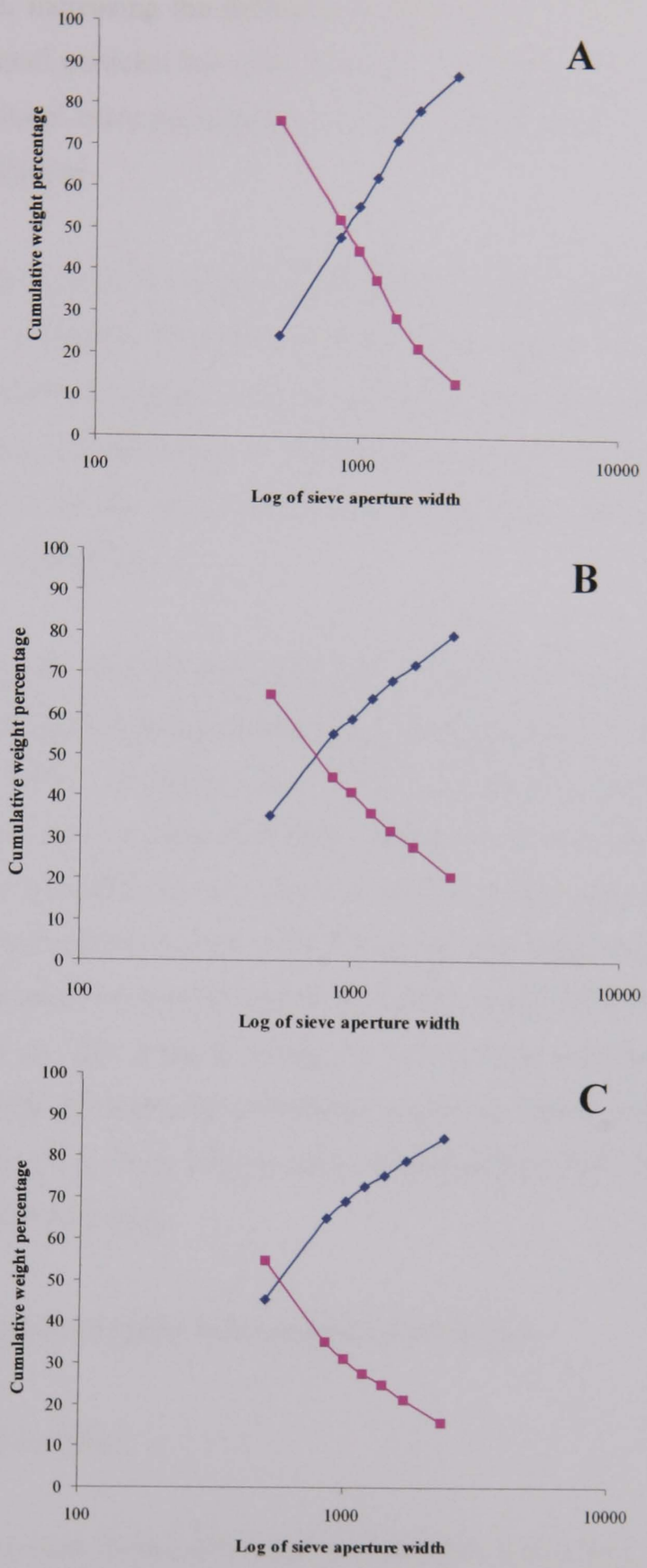

Figure 3.1. Size distribution of milled granules plotted semilogarithmically in the form of cumulative oversize (—■—) and undersize (—◆—) percentages (A – 50 sec; B – 70 sec; C – 100 sec of milling time).

From Table 3.2, increasing the milling time from 10 to 100 seconds increased the proportion of small particles less than 500 μm. At a milling time of 50 seconds, the maximum fractional mass percentage (7.1%) of desired granule size range 1001 to 1180 μm was obtained.

At milling times of 10 or 30 seconds, determination of the 50 cumulative percentages could not be calculated from the semilogarithmic graph plot because particle aggregation resulted in granules ≥ 2360 μm (figures are not shown). The median sizes (mid-points), defined from 50 cumulative percentages of the semilogarithmic graph (Figure 3.1), of 50, 70 or 100 seconds milling time were approximately 885, 750 or 580 μm respectively.

Two parameters, the median size (MS) and the coefficient of variation (CV), are significant values provided from arithmetic-probability graph of sieve test data (not shown; Mullin, 1996). At milling times of 10 or 30 seconds, median size could not be determined on the arithmetic-probability graph due to particle aggregation. The median sizes of cumulative percent undersize and oversize at the milling time 50, 70 or 100 seconds were approximately 875, 750 or 540 μm respectively. In cumulative undersize of arithmetic-probability graph, d_{16} values could not be found at the milling times of 50, 70 or 100 seconds owing to narrow size distributions. Similarly, cumulative oversize of arithmetic-probability graph, d_{84} values could not be found at the milling times of 50, 70 or 100 seconds. Consequently, the CV values could not be calculated from these data.

3.3.2 Effect of spheronisation time on pellet dissolution

3.3.2.1 Dissolution studies

As spheronisation times increased from 1 to 3 minutes, a decrease in drug dissolution rate was observed (Figure 3.2). Using Fit factor for statistical analysis (with $f_1 > 15\%$ and $f_2 < 50\%$; Appendix I, Table I.1.1), there were significant differences in dissolution profiles observed between granules and pellets.

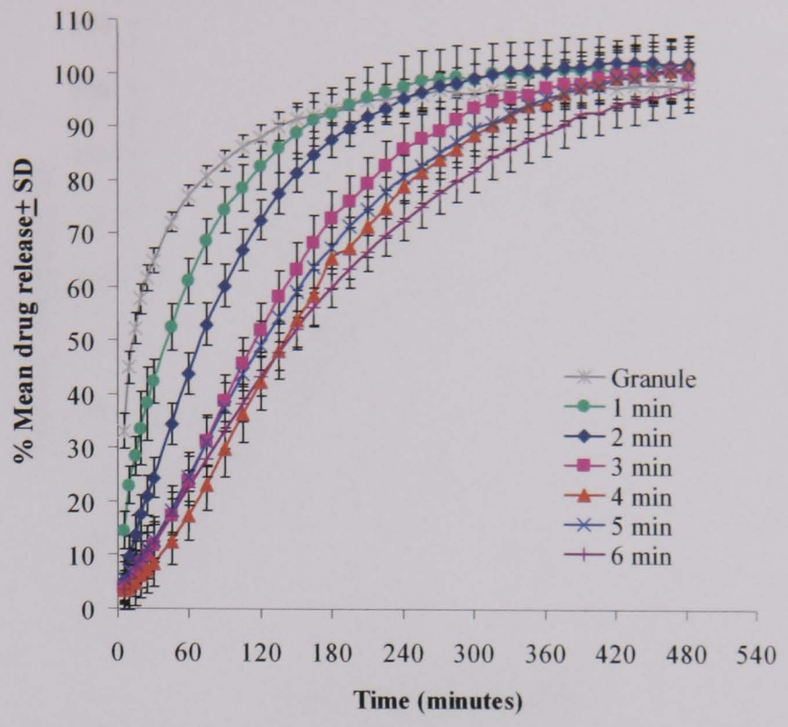

Figure 3.2. Dissolution profiles of formulations containing 50% GMS, 40% DCP and 10% paracetamol prepared at different spheronisation times (n = 6).

However, increasing spheronisation times from 3 to 6 minutes had no significant further effect on dissolution rate. At spheronisation times of 5 to 6 minutes, significant agglomeration occurred resulting in low yields of pellets with the desired size range. For this reason, a spheronisation time of 3 - 4 minutes was selected as it afforded the appropriate spherical pellets with high yields and demonstrable sustained release profiles. From the individual dissolution curves in Figure 3.2, the relationship between spheronisation time and mean time to 50% drug release can be obtained as shown in Figure 3.3.

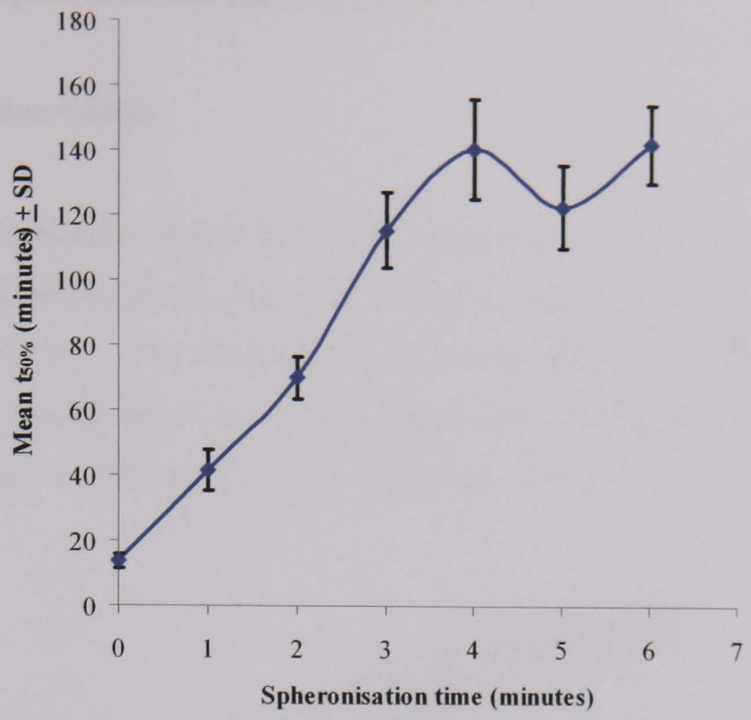

Figure 3.3. Effect of spheronisation time on mean time to 50% drug release ($t_{50\%}$) of formulations containing 50% GMS, 40% DCP and 10% paracetamol (n = 6).

The observed profile suggests that the increase in spheronisation time may prolong the $t_{50\%}$ by a combination of events. These may include densification the matrix (reduced diffusional pathways) (Vervaet et al., 1995) and by reduction of surface irregularities during transformation from granules with jagged irregular surfaces (Figure 3.4A) to pellets (Figure 3.4B) possessing more spherical forms.

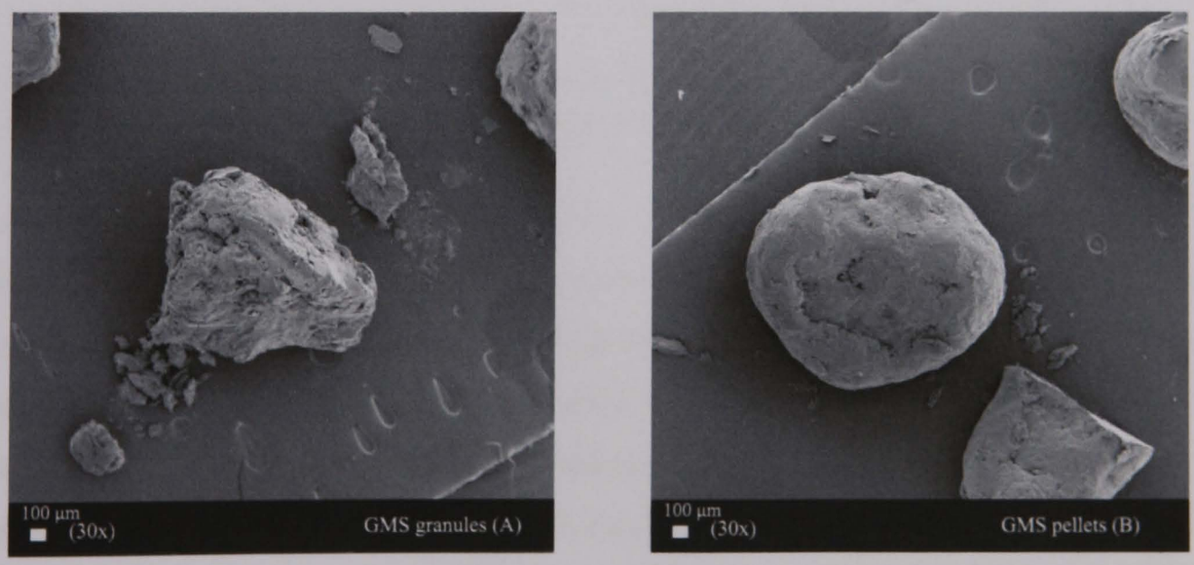

Figure 3.4. SEM photographs of GMS granules (**A**) and pellets (**B**) at magnification 30X.

3.3.3 Effect of spheronisation speed on pellet dissolution

3.3.3.1 Dissolution studies

Increasing spheronisation speeds from 4 to 5 significantly decreased drug dissolution rate but spheronisation speeds from 5 to 7 resulted in similar dissolution profiles as shown in Figure 3.5. The dissolution profiles of pellets at spheronisation speed between 4 and other speeds (5 to 7) were significantly different when analysed using Fit factors (with $f_1 > 15\%$ and $f_2 < 50\%$; Appendix I, Table I.1.2).

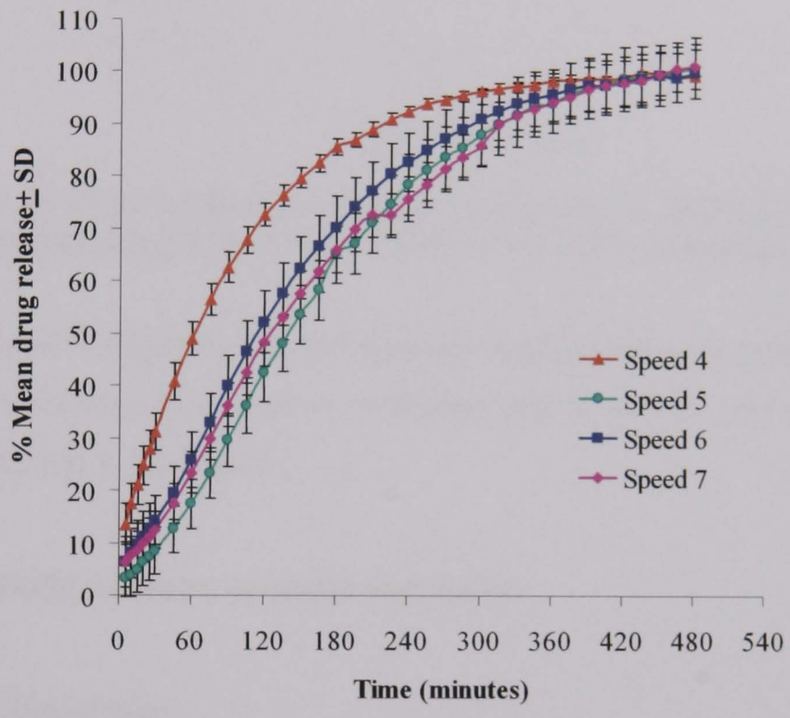

Figure 3.5. Dissolution profiles of formulations containing 50% GMS, 40% DCP and 10% paracetamol prepared at different spheronisation speeds (n = 6).

As spheronisation speed increased from 4 to 5, pellet spheronicity increased although there were no further differences with pellets manufactured at speeds 5 to 7 (data not shown). Moreover, increasing the spheronisation speed more than to 7 was unsuccessful due to extensive agglomeration and pellet massing. Therefore, the most appropriate spheronisation speed was selected to be 5 - 7 and it provided suitably spherical pellets with sustained drug release. From the individual dissolution curves in Figure 3.5, the relationship between spheronisation speed and mean time to 50% drug release can be obtained as shown in Figure 3.6.

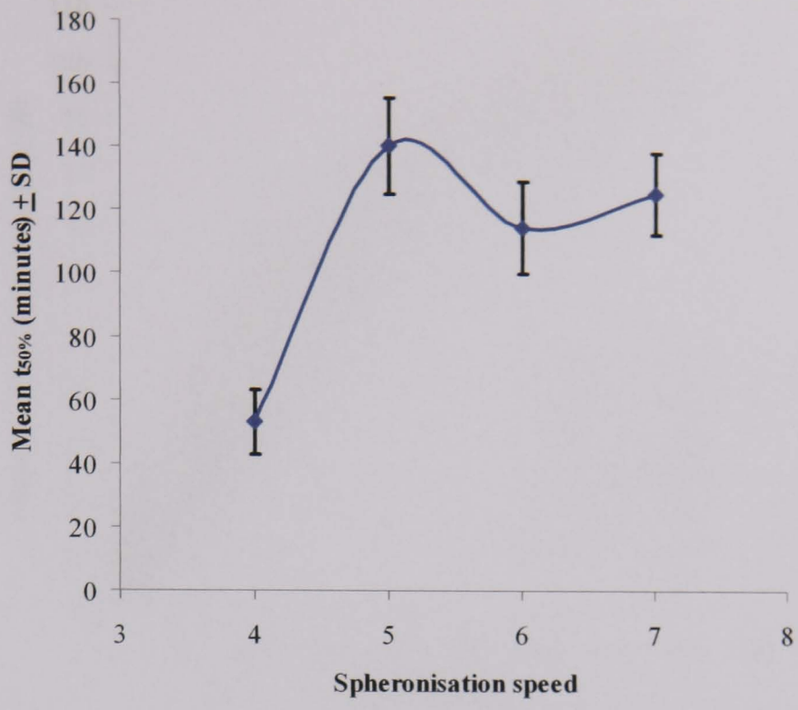

Figure 3.6. Effect of spheronisation speed on mean time to 50% drug release ($t_{50\%}$) of formulations containing 50% GMS, 40% DCP and 10% paracetamol (n = 6).

The observed profile suggests that the increase in spheronisation speed may prolong the $t_{50\%}$ by a combination of events, including matrix density and surface area as discussed in Section 3.3.2.1 above.

3.3.4 Effect of GMS content on pellet dissolution

3.3.4.1 Dissolution studies

The results of the dissolution studies are shown in Figure 3.7 below.

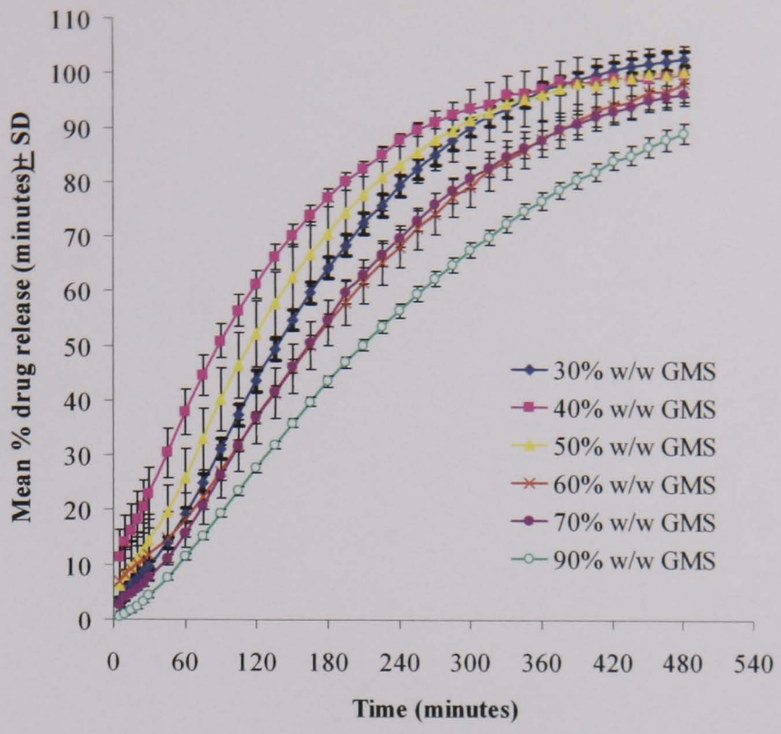

Figure 3.7. Dissolution profiles of formulations containing GMS (30 – 90%), DCP (0 – 60%) and paracetamol (10%) (n = 6).

As the amount of GMS increased from 40% to 90% w/w, a reduction of drug dissolution release was observed with the exception of the formulation containing 30% w/w GMS. The difference in pellet dissolution profiles between 30% and 40% w/w GMS was significant; however the difference between the dissolution profiles of pellets containing 30% and 50% w/w GMS was not significant when analysed using Fit factors (Appendix I, Table I.1.3). From Figure 3.7, the relationship between GMS content and mean time to 50% drug release can be obtained as shown in Figure 3.8.

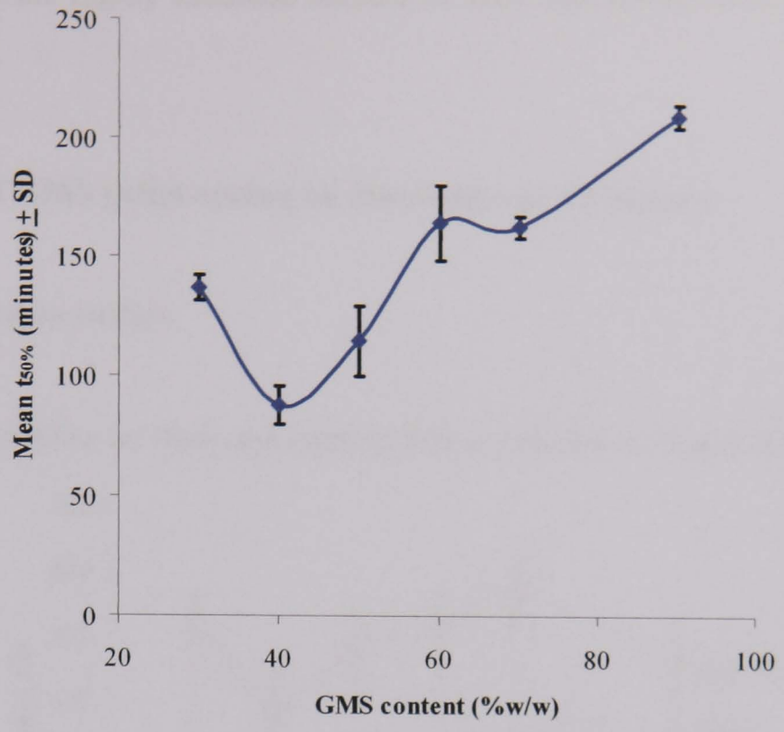

Figure 3.8. Effect of GMS content on mean time to 50% drug release ($t_{50\%}$) of formulations containing GMS (30 – 90%), DCP (0 – 60%) and paracetamol (10%) (n = 6).

Increasing GMS content from 40% to 90% w/w of formulation accelerated the $t_{50\%}$ relating to a decrease in the dissolution profiles. Similar effects on the ibuprofen release were reported when the microcrystalline wax (Lunacera® P) content of matrix pellets increased from 35 to 45% w/w, drug release decreased from 95 to 75% after 12 hours (Zhou et al., 1996). Peh et al. (2000) investigating a similar formulation of GMS pellets containing microcrystalline cellulose, postulated a mechanism that increasing GMS content had the effect of enhancing lipophilicity of the matrix, resulting in reduced wettability and decreased drug diffusion, prolonging drug release.

However, in these current studies, the formulation containing 30% w/w GMS demonstrated anomalous behaviour with respect to dissolution rate. The reduced wax content within the matrix may permit greater interactions between paracetamol and DCP (ratio 1:6) which compromises anticipated drug dissolution. Similar effects have been reported previously for DCP–drug interactions within tablet formulations (Sallam et al., 1988; Sallam et al., 1991; Khaili and Sallam, 2000), where it was

suggested that the highly indented surface of DCP can entrap drug particles and/or drug mixtures.

3.3.5 Effect of GMS pellet ageing on dissolution performance

3.3.5.1 Dissolution studies

The results of studies on fresh and aged pellets are shown in Figure 3.9 below.

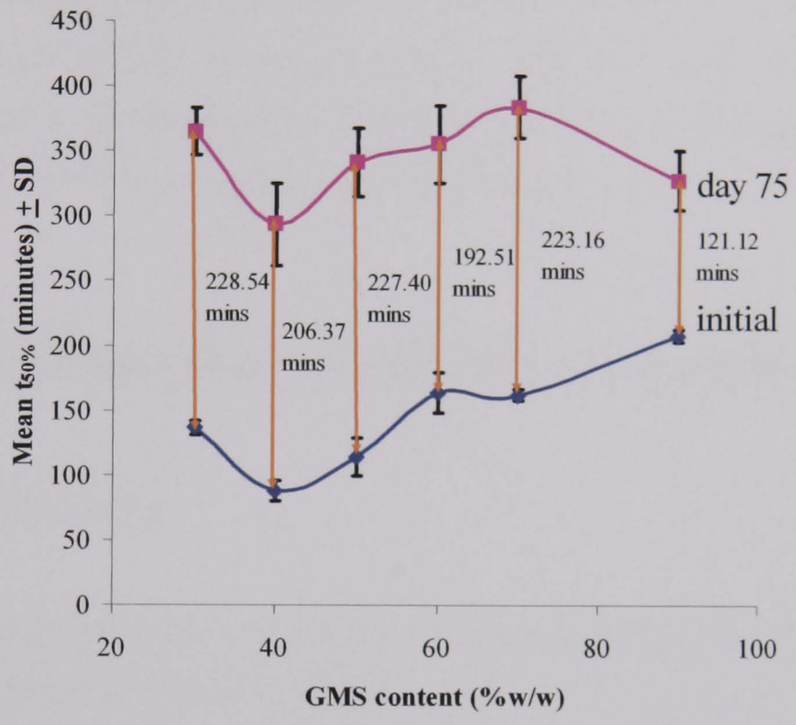

Figure 3.9. Effect of pellet ageing on mean time to 50% drug release ($t_{50\%}$) of formulations containing GMS (30 – 90%), DCP (0 – 60%) and paracetamol (10%) after storage for 75 days at room temperature (n = 6). Vertical bands represent the numerical difference in $t_{50\%}$ values on storage.

A significant decreased rate of drug release was observed upon storage for all formulation compositions when analysed using Fit factors (with $f_1 > 15\%$ and $f_2 < 50\%$; Appendix I, Table I.1.4).

Other researchers have reported similar results with wax matrix formulations with reductions of drug release upon storage and have attributed this to polymorphic transitions to more stable polymorphs or conversions of amorphous to crystalline forms (Remunan et al., 1992; San Vicente et al., 2000; Hamdani et al., 2002).

Moreover. Yajima et al. (2002) found that melt solidification of GMS yielded the α-form that was successively transformed to the stable ß-form via the ß'-form under ambient conditions. Further investigations of physicochemical changes in GMS formulations are reported in Chapter 5.

The increase in $t_{50\%}$ values between fresh and aged samples containing GMS content from 30% to 70% were similar (192 - 228 minutes), however for the formulation containing 90% GMS, a smaller effect was observed (121 minutes). This formulation was significantly different from the others in that it was devoid of DCP, however it is not known mechanistically how this factor can contribute to the observed result. It can be postulated that DCP may promote the ageing process and transformation of GMS although such confirmatory thermal analyses were not performed.

3.3.6 Effect of wax compositions of identical HLB on pellet dissolution

3.3.6.1 Dissolution studies

The dissolution performances of individual wax admixture (HLB = 3) formulations are shown in Figures 3.10 and 3.11 below.

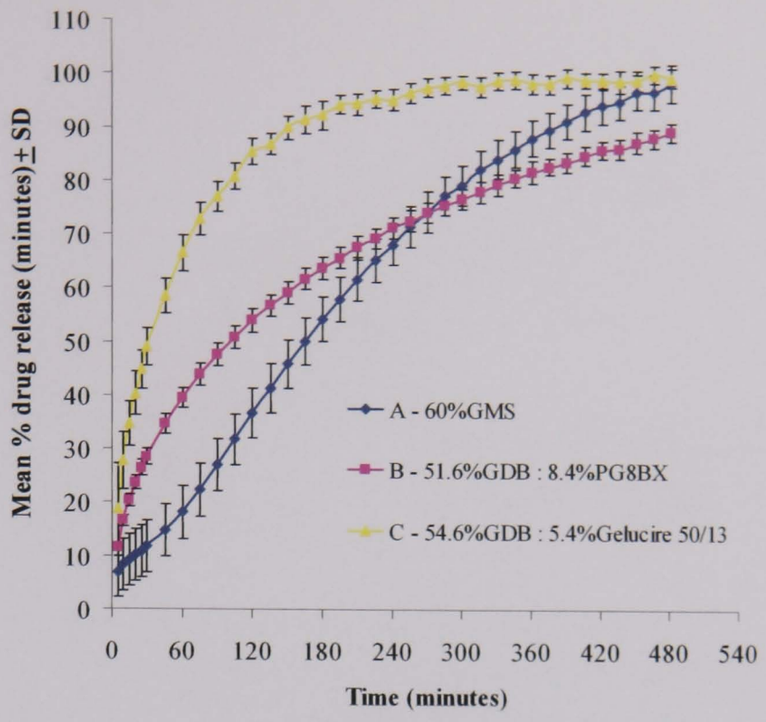

Figure 3.10. Dissolution profiles of formulations containing GMS or wax admixtures (60%), DCP (30%) and paracetamol (10%) with HLB value 3 prepared using a spheronisation temperature of 50°C and a spheronisation time of 4 minutes (n = 6).

The manipulation of HLB value has been previously demonstrated to be an effective way of modifying drug dissolution from a wax matrix formulation (Lee et al., 2001).

In the current study, the dissolution performances of the wax formulations (Figure 3.10) of identical HLB had significantly different dissolution profiles when analysed using Fit factors (with $f_1 > 15\%$ and $f_2 < 50\%$; Appendix I, Table I.1.5.1). Mechanistically, drug release was consistent with the HLB value of the minor wax component with faster release observed for Gelucire 50/13 (HLB 13) than for PG8BX (HLB 9) and for the GMS alone. The inclusion of a wax with a higher HLB value appears to facilitate the dissolution process. This may be a consequence of enhanced particle wetting and/or formation of a pore structure, swelling or water channels within the matrix during the dissolution process. Although the three formulations had identical HLB values, the relative contribution of the components can significantly different when considering functionality.

The dissolution profiles of two further batches of formulation nominally composed of wax admixtures of identical HLB values are shown in Figure 3.11.

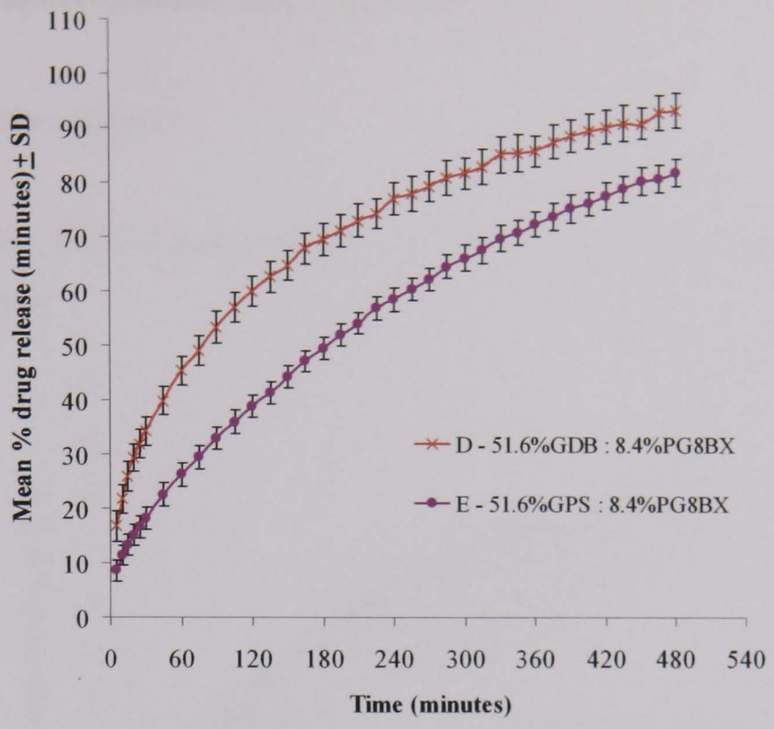

Figure 3.11. Dissolution profiles of formulations containing wax admixtures (60%), DCP (30%) and paracetamol (10%) with HLB value 3 prepared using a spheronisation temperature of 45°C and a spheronisation time of 2 minutes (n = 6).

Interestingly, despite the GDB and GPS having identical HLB values of 2, and the formulations each having the same minor component (PG8BX) at the same concentration (8.4%) and both being identically processed, their dissolution profiles were significantly different using Fit factors (with $f_1 > 15\%$ and $f_2 < 50\%$; Appendix I, Table I.1.5.2). Generally, GDB formulation provides slower drug release than GPS formulation because GDB is composed of longer fatty acids (C_{22}) and as a consequence has a higher melting point (65 - 77°C) compared to GPS (52 - 55°C). The addition of PG8BX (surfactant) into GDB might have a more pronounced effect on accelerating drug release compared to an admixture of GPS and PG8BX.

This would suggest that HLB alone is a rather crude instrument in describing the hydrophobic index of a material and further consideration of physicochemical properties must be taken into account.

3.3.7 Effect of spheronisation time and temperature on pellet dissolution

3.3.7.1 Dissolution studies

The result of the effect of spheronisation time on wax admixture pellets is shown in Figure 3.12 below.

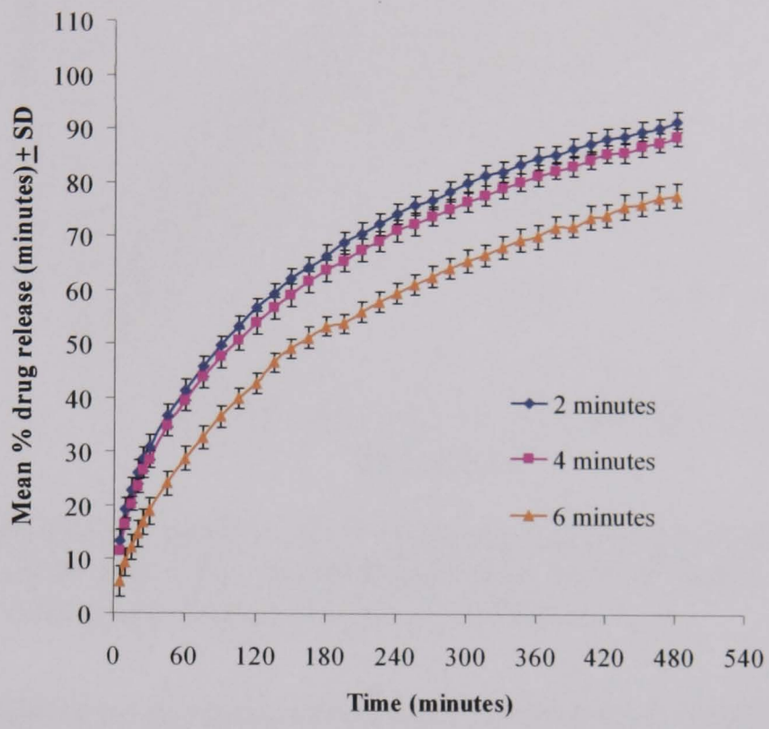

Figure 3.12. Dissolution profiles of formulations containing 51.6% GDB, 8.4% PG8BX, 30% DCP and 10% paracetamol prepared at different spheronisation times at a fixed temperature of 50 °C (n = 6).

This followed a similar trend to GMS formulations (Figure 3.2) with increasing spheronisation time resulting in slower dissolution rate. Although increasing spheronisation times from 2 to 4 minutes resulted in only slight changes, the additional process time between 4 to 6 minutes significantly reduced drug dissolution when analysed using Fit factor (with $f_1 > 15\%$ and $f_2 < 50\%$; Appendix I, Table I.1.6.1). It was concluded that the increase in spheronisation time decreased drug release by reduction of surface area as the irregular surfaces were transformed into more spherical forms with increasing densification of the matrices. This was confirmed by observations of tapped density which increased from $0.6897 < 0.7018 < 0.7143$ mg/ml with increasing spheronisation times from $2 < 4 < 6$ minutes.

The result of the influence of spheronisation temperature on wax admixture pellets is shown in Figure 3.13 below.

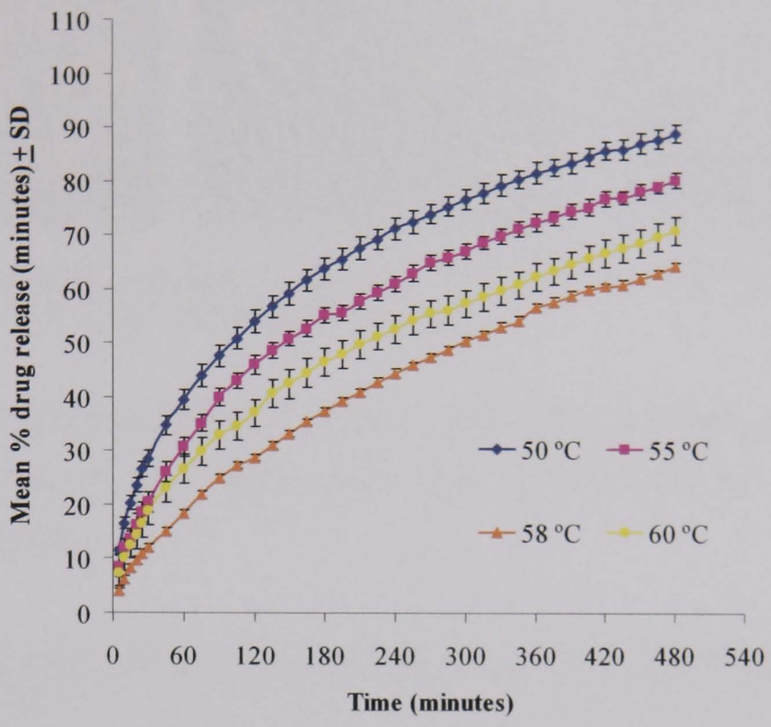

Figure 3.13. Dissolution profiles of formulations containing 51.6% GDB, 8.4% PG8BX, 30% DCP and 10% paracetamol prepared at different spheronisation temperatures at a fixed spheronisation time of 4 minutes (n = 6).

As the spheronisation temperatures increased from 50 to 58°C, a significant decrease in drug release rate was observed when analysed using Fit factor (with $f_1 > 15\%$ and $f_2 < 50\%$; Appendix I, Table I.1.6.2) consistent with the changes of surface area and density as discussed in the study of effect of spheronisation time above.

However, the drug dissolution profile of pellets prepared at spheronisation temperature of 60°C was faster than those at 58°C. Observation of the pellets revealed progressive sphere formation from 55°C (Figure 3.14A) to 58°C (Figure 3.14B), however those pellets processed at 60°C (Figure 3.14C) appeared different, with less regular surfaces as well as some evidence of adherent smaller particle fractions. The higher spheronisation temperature (60°C) is close to the melting point of PG8BX (59 - 70°C) and it is suggested that at 60 °C, the pellets in the spheroniser are softer and could give rise to the formation of both smaller particles by attrition against the spheroniser wall as well as bigger particles by agglomeration.

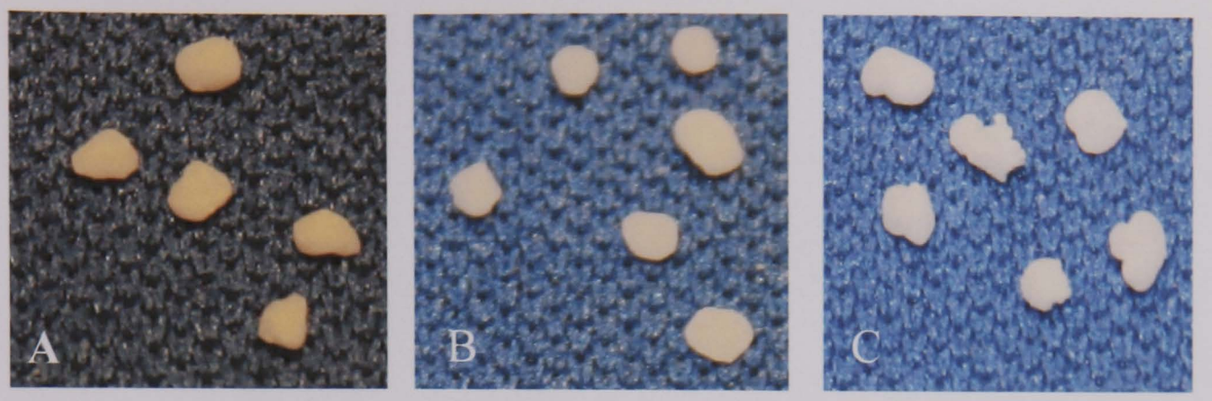

Figure 3.14. Digital photographs of wax admixture pellets at different spheronisation temperatures of 55°C (**A**), 58°C (**B**) and 60°C (**C**).

The sieve analysis results (Table 3.3 below) confirm the agglomeration effect with a significant increase in the fraction more than 1180 μm as the spheronisation temperature increases.

Table 3.3. Fractional mass percentage of pellets varied spheronisation temperature as 50, 55, 58, or 60°C.

Size aperture (μm)	Fractional mass percentage (% retained) (Spheronisation temperature)			
	50°C	55°C	58°C	60°C
1180	1.0	4.2	62.7	80.3
1000	20.0	21.8	19.2	9.9
850	38.9	32.5	7.8	4.5
< 850	40.1	41.5	10.3	5.3

Furthermore, increasing the spheronisation temperature to 63°C (above the melting temperature of PG8BX) was unsuccessful due to extensive agglomeration and pellet massing.

3.3.8 Effect of GDB-PG8BX pellet ageing on dissolution performance

3.3.8.1 Dissolution studies

The results of studies on fresh and aged pellets are shown in Figure 3.15 below.

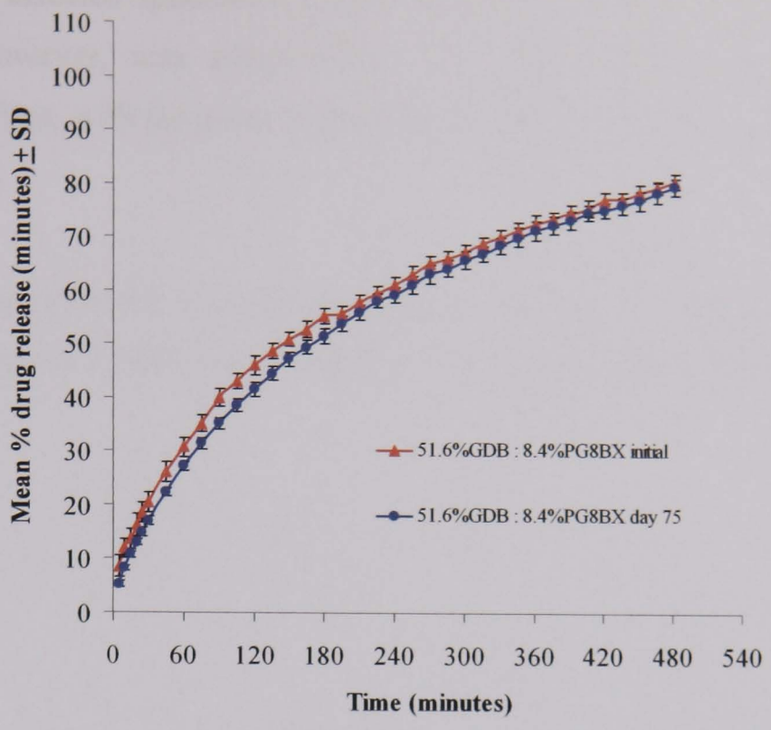

Figure 3.15. Dissolution profiles of formulations containing of 51.6% GDB, 8.4% PG8BX, 30% DCP and 10% paracetamol after storage for 75 days at room temperature (n = 6).

The GDB–PG8BX formulations exhibited no changes of dissolution profiles after 75 days storage at room temperature using Fit factor (with $f_1 < 15\%$ and $f_2 > 50\%$; Appendix I, Table I.1.7). This observation is consistent with the report by Galal et al. (2004) who noted that a carbamazepine formulation containing Gelucire 53/10 was stable to dissolution on storage at room temperature for 1 year.

3.4 Conclusion

Wax matrix pellets have been readily produced via a direct warm spheronisation method without resort to extrusion. The granulation and warm spheronisation techniques have been utilised to produce matrix pellets. The composition and processing conditions can be readily manipulated to provide pellets with definable performance characteristics.

The yield of granules in the desirable size range was dependent on the blender milling time. In the spheronisation process, spheronisation time, speed and

temperature all affected spheronicity, size distribution and dissolution performance of pellets. However, wax compositions at identical HLB values did affected dissolution profiles, with the more hydrophilic additives accelerating drug release to a greater extent.

Pellet ageing was observed with certain formulations with a resultant impact on drug dissolution. This will be described in greater detail in Chapters 5 and 7.

CHAPTER 4

PHYSICOCHEMICAL EVALUATIONS OF GMS AND GPS AS RAW MATERIALS

4.1 Introduction

From the previous chapter, the dissolution profiles of wax matrix pellets containing GMS, DCP and paracetamol decreased significantly upon storage. It is widely recognised that waxes often undergo physicochemical changes when they are melted, cooled and subsequently stored (Laine et al., 1988; Sutananta et al., 1994b; Craig, 1995; Galal et al., 2004). Polymorphic transformation and crystallisation of the wax are the main changes observed during ageing. The aim of this chapter is to investigate the physicochemical properties of GMS and GPS materials following processing and subsequent ageing. Furthermore, the potential advantage of thermally annealing materials as a means of accelerating the ageing process is investigated. A number of analytical techniques were employed to aid in the characterisation of the materials. This included FT-IR, DSC, X-ray powder diffraction and hot stage microscopy.

4.2 Methods

Sample preparation and analytical methods are provided below and referenced where appropriate to Chapter 2.

4.2.1 Effect of storage temperature on the physicochemical properties of GMS

Untreated GMS samples were studied without any thermal treatment and served as controls. Other GMS samples were melted by heating at 70°C (higher than the melting point) and solidified at 3°C, room temperature or 50°C for 1 hour and then

analysed by FT-IR spectrophotometry (Section 2.4.5, Page 52) and DSC (Section 2.4.6, Page 55). Each sample was stored in an air-tight amber glass container at constant temperatures (3°C, room temperature or 50°C) and for fixed times (0, 7, 28, 60 or 180 days) and then evaluated by FT-IR spectrophotometry and DSC.

4.2.2 Effect of storage temperature on the physicochemical properties of GPS

Untreated GPS was used as a control. Other GPS samples were melted by heating at 70°C (higher than the melting point) and solidified at 3, 25 or 50°C for 1 hour and then analysed by FT-IR spectrophotometry (Section 2.4.5, Page 52) and DSC (Section 2.4.6, Page 55). Each sample was stored in an air-tight amber glass container at constant temperature (3, 25 or 50°C) for fixed times (0, 7, 14 or 180 days) and then evaluated by FT-IR spectrophotometry and DSC.

4.2.3 Effect of cooling rate on thermal properties of GMS

GMS samples in the DSC pan were melted in situ by heating to 70°C at a heating rate of 3°C/min. This temperature was maintained for 1 hour before cooling the sample at 0.17°C/min to 30°C (slow cooling) or cooled rapidly to -50°C (fast cooling). Both samples were stored in desiccators at room temperature for 0, 7, 60 or 180 days and then evaluated by DSC (Section 2.4.6, Page 55).

4.2.4 Effect of thermal annealing temperature on thermal properties of GMS

GMS samples in the DSC pan were melted in situ by heating to 70°C at a heating rate of 3°C/min. This temperature was maintained for 1 hour before cooling the sample rapidly to -50°C prior to storage in desiccators at 37, 46 or 55°C for 0, 2 days and then evaluated by DSC (Section 2.4.6, Page 55).

4.2.5 Effect of thermal annealing on GMS

Untreated GMS samples were used as a control. Other GMS samples were melted by heating at 70°C (higher than the melting point) and solidified at 3°C for 1 hour and then analysed by FT-IR spectrophotometry (Section 2.4.5, Page 52) and DSC (Section 2.4.6, Page 55), hot stage microscopy (HSM; Section 2.4.9, Page 61) and X-ray powder diffraction (XRPD; Section 2.4.7, Page 57). Each sample was annealed in an air-tight amber glass container at 25 or 46°C for fixed times (0, 7 or 28 days for FT-IR, DSC and HSM as well as 0, 4 or 28 days for XRPD).

4.2.6 Effect of thermal annealing on GPS

Untreated GPS samples were used as a control. Other GPS samples were melted by heating at 70°C (higher than the melting point) and solidified at 3°C for 1 hour and then analysed by FT-IR spectrophotometry (Section 2.4.5, Page 52) and DSC (Section 2.4.6, Page 55) and X-ray powder diffraction (XRPD; Section 2.4.7, Page 57). Each sample was annealed in an air-tight amber glass container at 25 or 46°C for fixed times (0, 4, 7, 14 or 28 days for FT-IR and DSC as well as 0, 4 or 28 days for XRPD).

4.3 Results and Discussion

4.3.1 Effect of storage temperature on the physicochemical properties of GMS

4.3.1.1 FT-IR spectrophotometry of GMS

FT-IR spectra were analysed within the region of wavenumber 400 to 4000 cm^{-1}. The typical FT-IR spectrum of untreated GMS is shown in Figure 4.1.

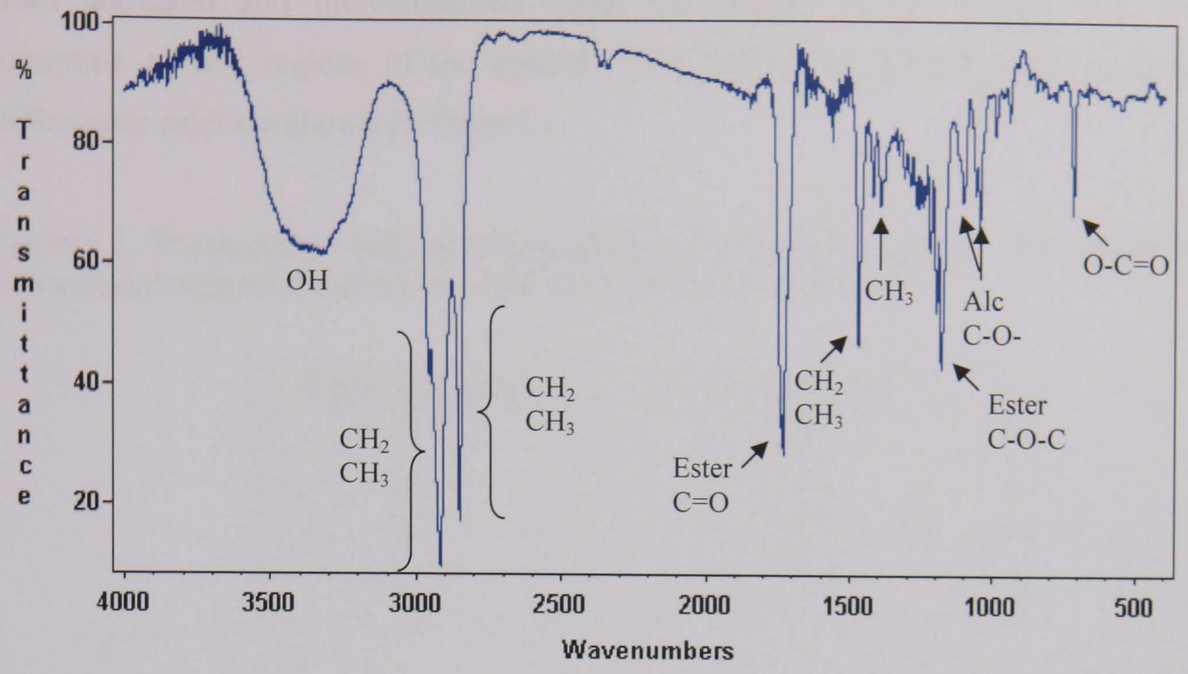

Figure 4.1. Typical FT-IR spectrum of the untreated GMS showing functional groups as attributed by Hemming and Hawthorne (1996).

The fingerprint region from 1000 to 1600 cm^{-1} is frequently used for qualitative analysis (Smith, 1999). Hence this specific region of the IR spectrum was examined in the untreated and melt-solidified (at room temperature) GMS materials shown in Figure 4.2.

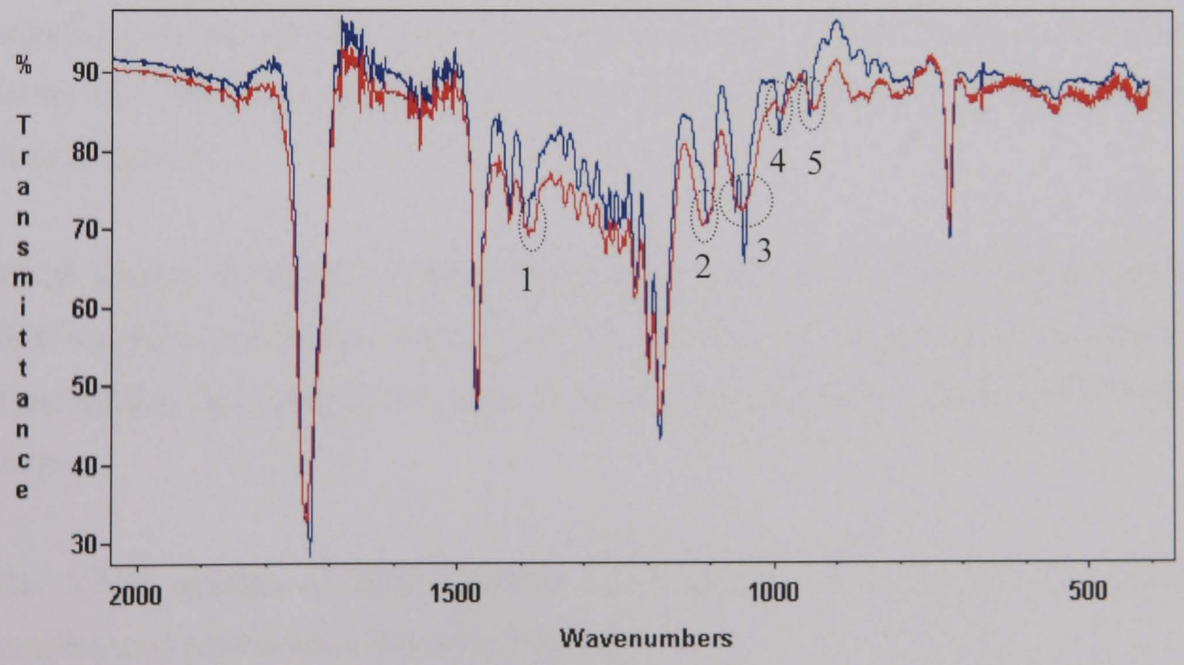

Figure 4.2. FT-IR spectra of GMS (— untreated; — melt-solidified) at room temperature.

Both untreated and melt-solidified GMS had similar FT-IR spectra with the exception of few regions of the spectra. The regions of interest where spectral differences exist are shown in Table 4.1.

Table 4.1. Wavenumber regions where differences in FT-IR spectra were observed between the untreated and melt-solidified GMS (from Figure 4.2).

Region number	Wavenumber (cm^{-1})
1	1386
2	1110
3	1049
4	992
5	945

From Figure 4.2 and Table 4.1, the spectral differences between untreated and melt-solidified GMS were attributed by Hemming and Hawthorne (1996) to the glyceryl alcohol C-OH observed from peaks at wavenumber 1049 and 1110 cm^{-1}. The FT-IR spectrum of the untreated GMS showed a more noticeable shoulder and sharper peaks than observed in melt-solidified GMS. Moreover, sharper peaks at wavenumber 1386 (position of CH_3), 992 and 945 cm^{-1} were observed for the untreated materials. The three peaks at wavelength 1049, 1110 and 1386 cm^{-1} were selected as being indicators of differences between the untreated and melt-solidified forms of GMS and were applied to the evaluation of waxes receiving different thermal cycles.

FT-IR spectra of untreated GMS samples when stored at 3°C, room temperature or 50°C exhibited no changes throughout the 180 days of storage (data not shown). This implies that commercial material as supplied exists in a stable polymorphic form.

The FT-IR spectra of melt-solidified GMS samples after storage at different temperatures are shown in Figure 4.3 below.

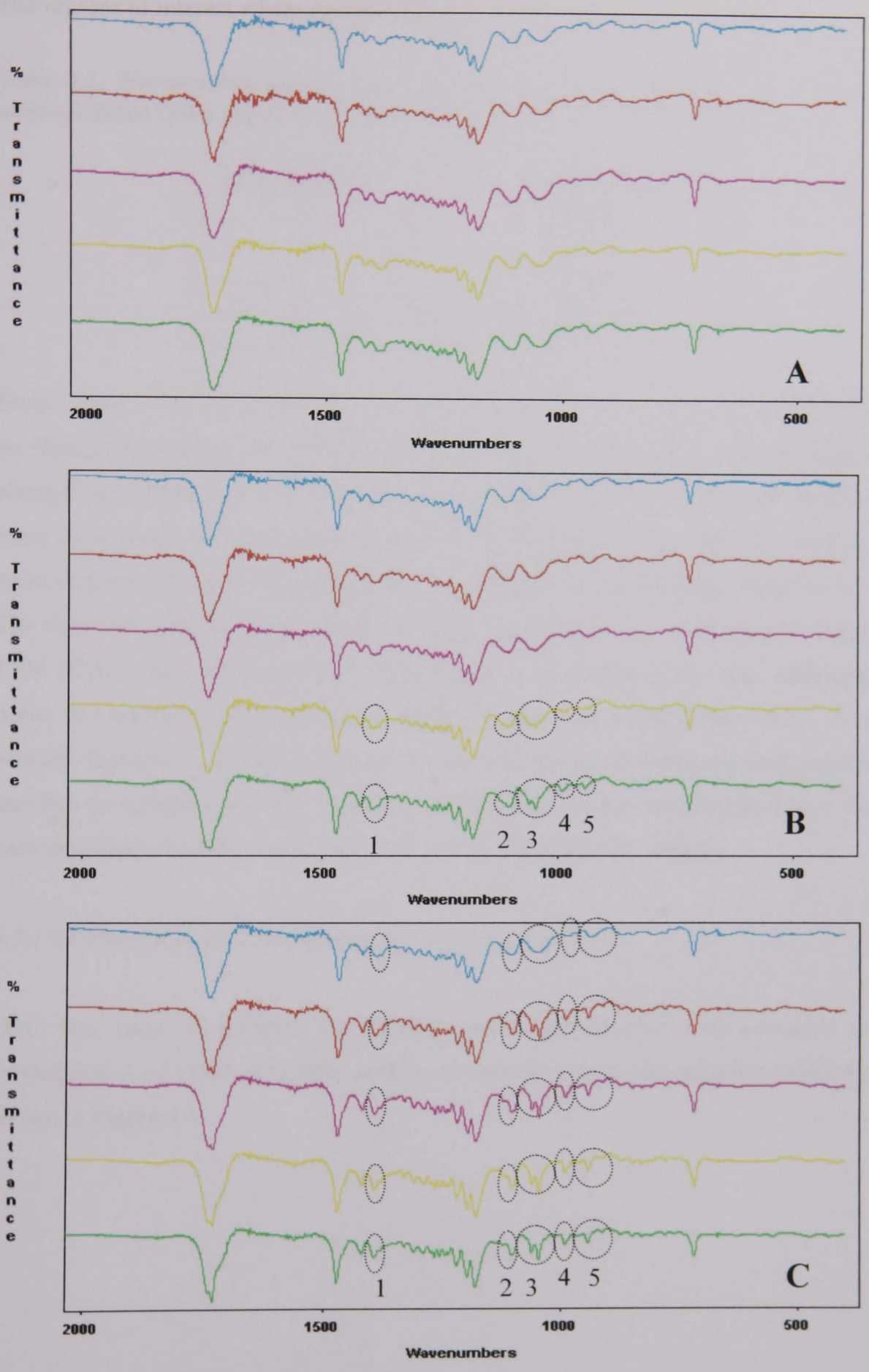

Figure 4.3. FT-IR spectra of melt-solidified GMS samples stored at 3°C (**A**), room temperature (**B**) or 50°C (**C**) for various time intervals (—0 day; —7 days; — 28 days; — 60 days; — 180 days).

The regions of interest where spectral differences exist are shown in Table 4.2.

Table 4.2. Wavenumber regions where differences in FT-IR spectra were observed melt-solidified GMS stored at room temperature or 50°C (from Figure 4.3).

Region number	Wavenumber (cm^{-1})
1	1394
2	1105
3	1048
4	992
5	943

From Figure 4.3A, the FT-IR spectra of melt-solidified GMS stored at 3°C exhibited no changes throughout the 180 day storage period suggesting that physicochemical changes are inhibited at low temperature. However, melt-solidified GMS stored at room temperature demonstrated changes in FT-IR spectra at the 60 days analysis point (Figure 4.3B) and when stored at 50°C, changes were immediate (Figure 4.3C). The observed spectral changes at wavenumber 1048 (Alc C-O), 1105 (Alc C-O) and 1394 (CH_3) were characterised by development of sharper peaks and additional peaks as observed previously in the spectra of untreated GMS (Figure 4.2). It is possible that inter- and intra-molecular bonds were disrupted during the melt process and that on solidification and subsequent ageing the structure reverted to that of the untreated form of GMS (Maruyama et al., 1971; Bresson et al., 2006).

4.3.1.2 Differential scanning calorimetry (DSC) of GMS

DSC was used to monitor the melting point, polymorphic transformation or crystallisation of GMS. The DSC profiles of untreated and melt-solidified GMS are shown in Figure 4.4.

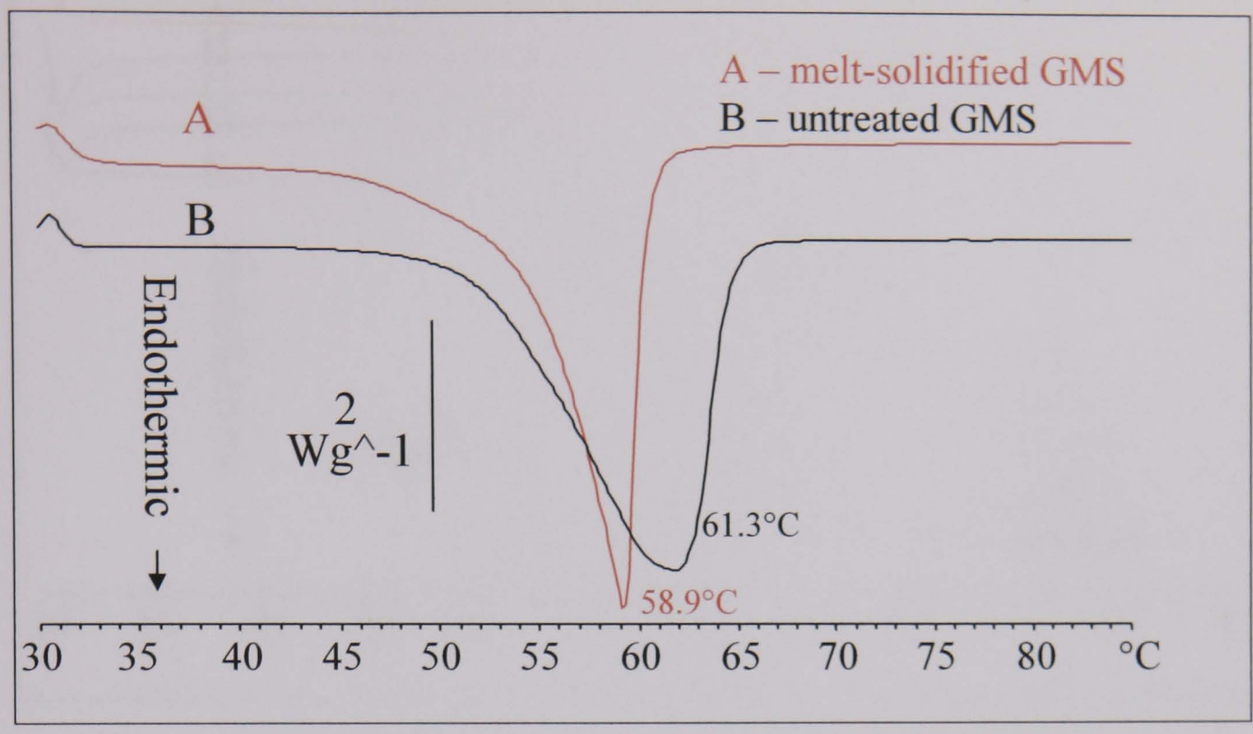

Figure 4.4. Effect of melt-solidification on DSC profiles of GMS (solidification at room temperature) (scale bar = heat flow (2 watts per gram)).

The melting temperatures for samples were determined from the DSC profiles and found to be 61.3°C for untreated GMS and 58.9°C for melt-solidified GMS respectively. The untreated GMS showed a broader melting range compared to the melt-solidified sample which exhibited a sharp and narrower melting range.

DSC profiles of untreated GMS samples after storage at 50°C are shown in Figure 4.5. At this temperature, noticeable changes in thermal profiles are observed, whereas at the lower storage conditions (3°C and room temperature), only very slight changes were observed (data not shown). The numerical values for melting point and enthalpy at individual temperatures and times are shown in Table 4.3. Enthalpy (ΔH) represented the amount of energy absorbed by the sample during melting as measured by onset and offset values.

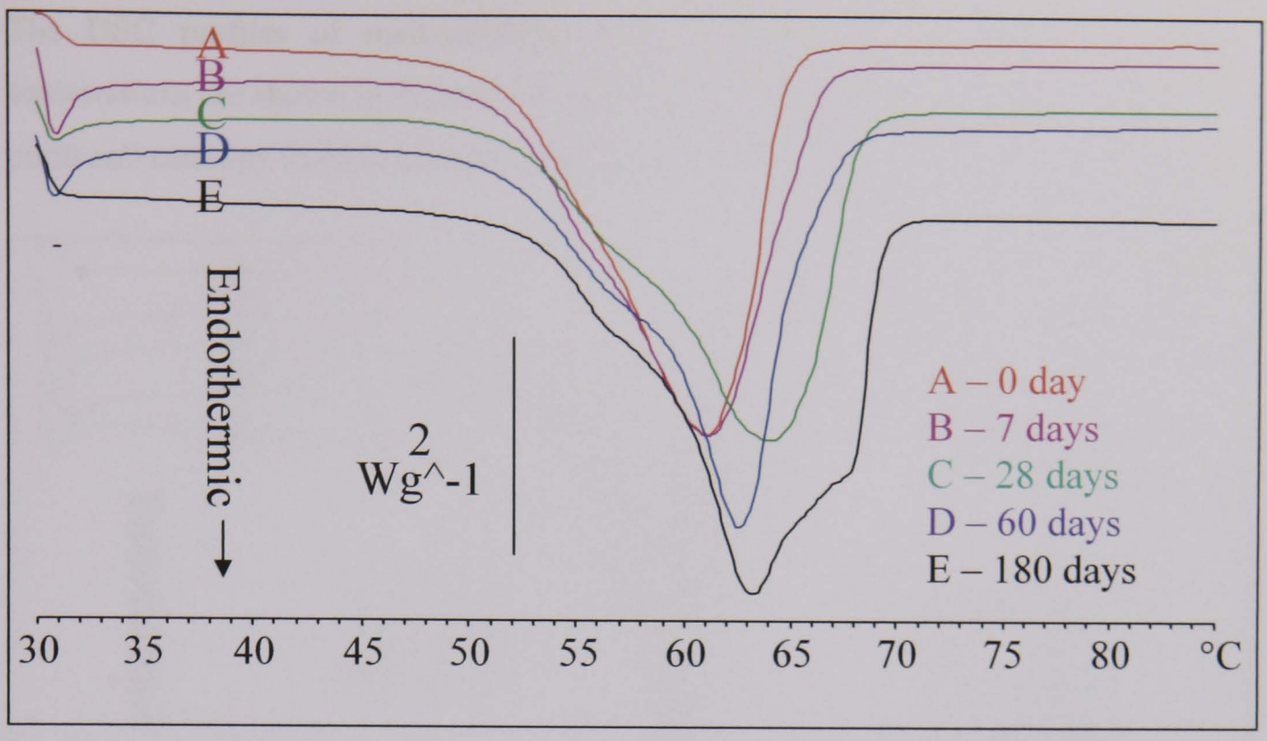

Figure 4.5. Effect of storage at 50°C on DSC profiles of untreated GMS (scale bar = heat flow (2 watts per gram)).

Table 4.3. Effect of storage time and temperature on the thermal characteristics of untreated GMS.

Storage temperature Storage duration (days)	Melting point (°C)			Enthalpy (ΔH) (J/g)		
	3°C	*Room temp.*	*50°C*	*3°C*	*Room temp.*	*50°C*
0	60.9	60.9	60.9	158.8	158.8	158.8
7	60.7	61.6	60.8	169.5	157.7	168.8
28	61.9	62.9	63.7	145.8	142.6	165.4
60	62.1	62.2	62.9	146.2	144.1	157.2
180	61.4	62.2	62.9	152.8	166.5	189.8

For untreated GMS stored at 3°C and room temperature, small fluctuations in melting point and enthalpy (ΔH) were observed over the 180 day storage. However, DSC profiles of samples stored at 50°C (Figure 4.5) for 28 days and greater showed a 2 - 3°C increase in peak temperature with a broadening of the melting transition. This was particularly evident after storage for 180 days, with corresponding increase in enthalpy. These thermal changes were not highlighted in parallel FT-IR studies (Section 4.3.1.1), demonstrating the importance of using complementary techniques for such analyses.

The DSC profiles of melt-solidified GMS samples after storage at different temperatures are shown in Figures 4.6 - 4.8 below. The numerical values for melting point and enthalpy (ΔH) at individual temperatures and times are shown in Table 4.4.

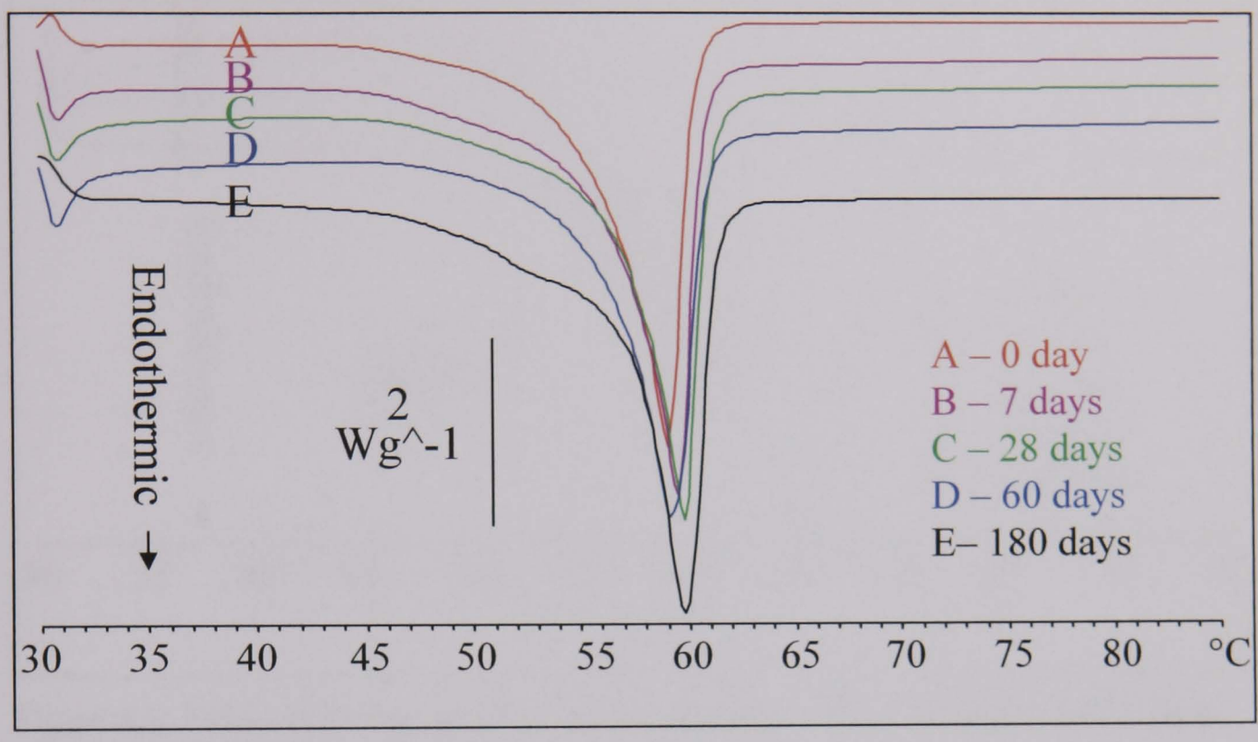

Figure 4.6. Effect of storage at 3°C on DSC profiles of melt-solidified GMS (scale bar = heat flow (2 watts per gram)).

There were no significant changes in the DSC profiles obtained after storage at 3°C.

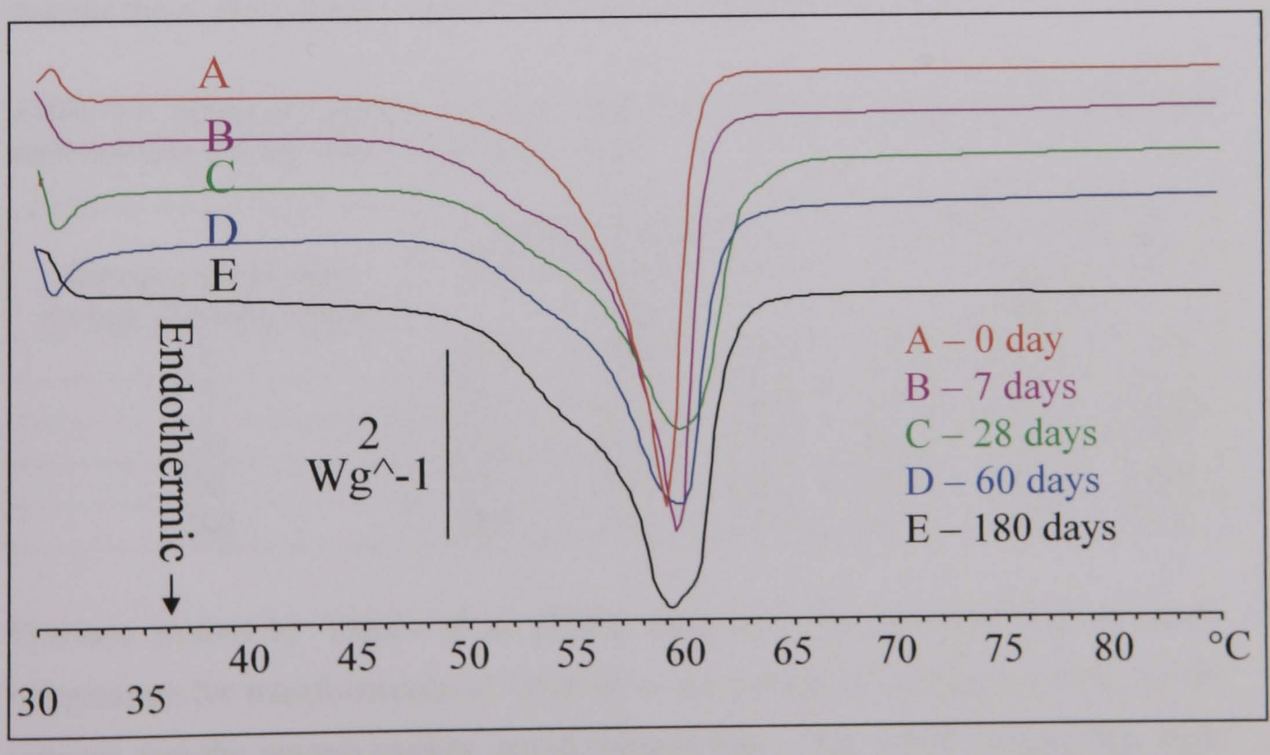

Figure 4.7. Effect of storage at room temperature on DSC profiles of melt-solidified GMS (scale bar = heat flow (2 watts per gram)).

After prolonged storage at room temperature, there were noticeable broadening of the thermal profiles, although melting point remained relatively constant (Table 4.4).

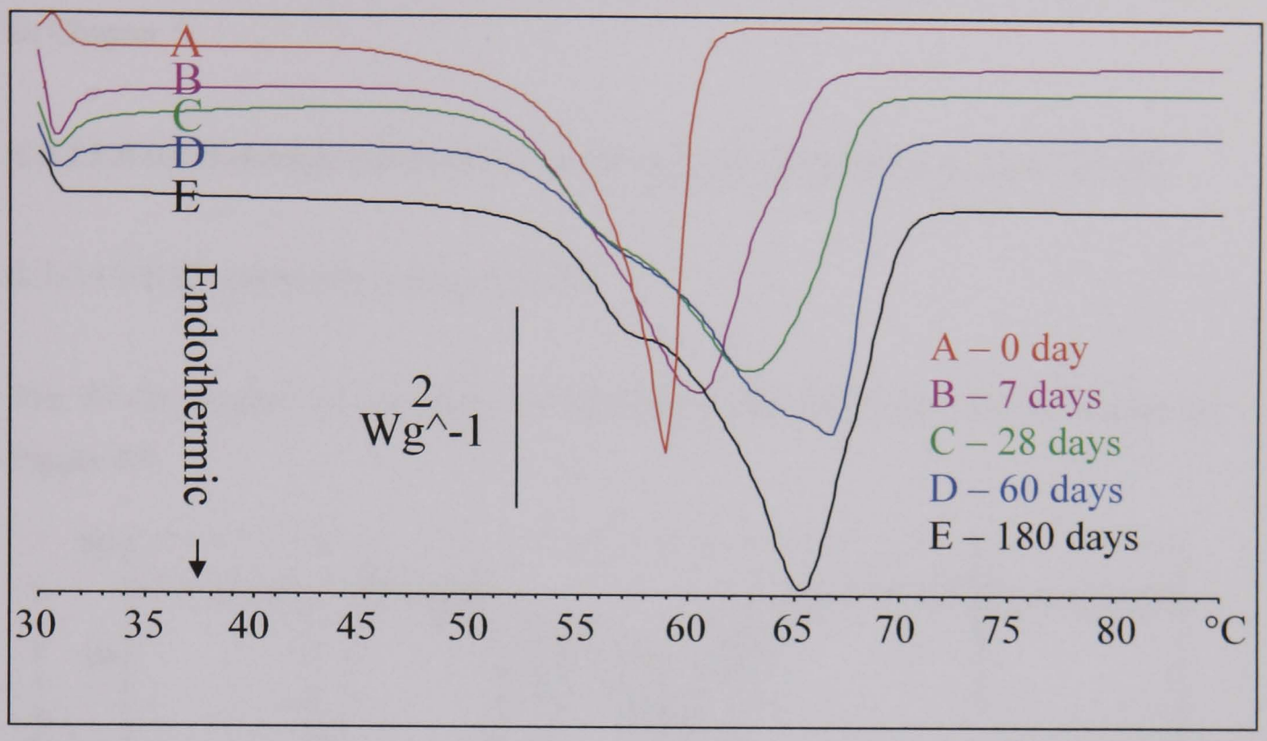

Figure 4.8. Effect of storage at 50°C on DSC profiles of melt-solidified GMS (scale bar = heat flow (2 watts per gram)).

Immediately following storage at 50°C there was an upward trend in the melting point which appeared to stabilise after about 60 day storage. However at the longer storage times, the enthalpy values were noticeably higher (Table 4.4).

Table 4.4. Effect of storage time and temperature on the thermal characteristics of melt-solidified GMS (from Figures 4.6 - 4.8).

Storage temperature Storage duration (days)	Melting point (°C)			Enthalpy (ΔH) (J/g)		
	3°C	*Room temp.*	*50°C*	*3°C*	*Room temp.*	*50°C*
0	58.6	58.6	58.6	107.6	107.6	107.6
7	59.0	59.3	60.2	115.5	119.2	150.0
28	59.7	60.5	64.5	105.2	115.8	160.7
60	59.3	59.6	66.0	100.9	110.4	168.8
180	59.3	59.3	65.0	115.2	124.9	190.4

Previous studies by Yajima et al. (2002) suggested that optimum heat treatment temperature for transformation of GMS from the α-form to ß-form was 50°C for 90 minutes and the present studies would support that. This would suggest that high

temperature (50°C) storage will accelerate transformation of GMS from an unstable α-form to stable ß-form. The influence of these physical transformations on the dissolution performance of the waxes within the pellet dosage form will be discussed in Chapter 5.

4.3.2 Effect of storage temperature on the physicochemical properties of GPS

4.3.2.1 FT-IR spectrophotometry of GPS

The FT-IR spectra of untreated and melt-solidified GPS materials are shown in Figure 4.9.

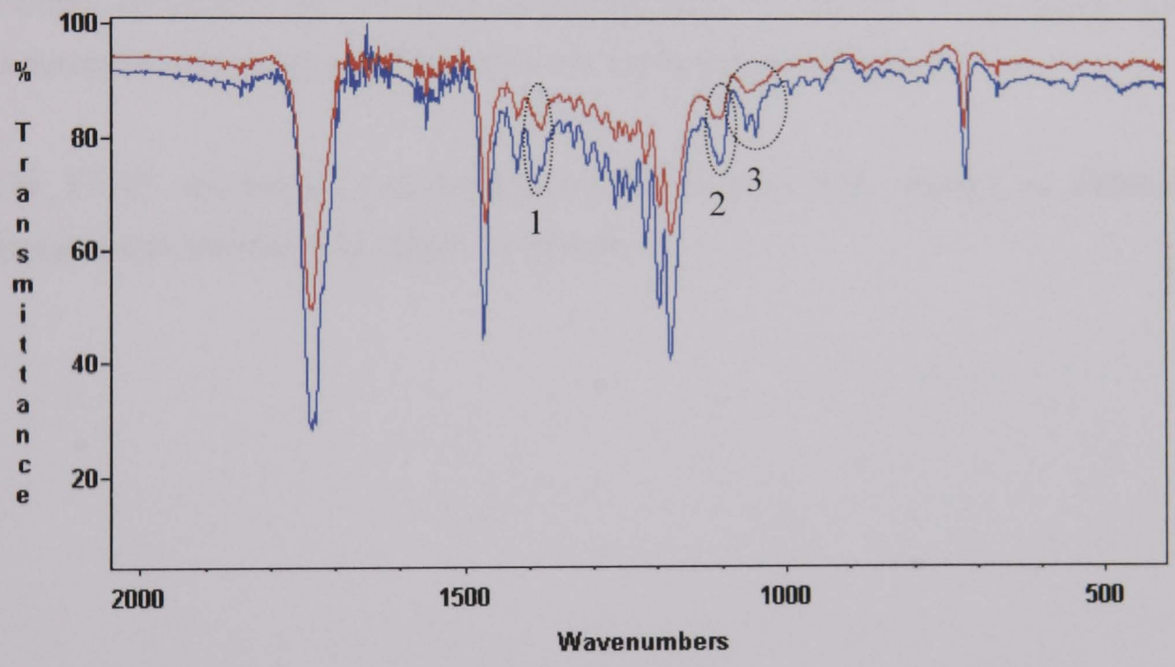

Figure 4.9. FT-IR spectra of GPS (— untreated; — melt-solidified) at 25°C.

The regions of interest where spectral differences exist are shown in Table 4.5.

Table 4.5. Wavenumber regions where differences in FT-IR spectra were observed between the untreated and melt-solidified GPS (from Figure 4.9).

Region number	Wavenumber (cm^{-1})
1	1392
2	1105
3	1062

From Figure 4.9 and Table 4.5, the spectral differences between untreated and melt-solidified GPS occurred at position of alcohol C-O observed from peaks at wavenumber 1062 and 1105 cm^{-1} (Hemming and Hawthorne, 1996). The FT-IR spectrum of the untreated GPS showed a more noticeable shoulder and sharper peaks than observed in melt-solidified GPS. Furthermore, a small additional peak at wavenumber 1392 (position of CH_3) was observed in the untreated GPS. The three peaks at wavelength 1062, 1105 and 1392 cm^{-1} were selected as being indicators of differences between the untreated and melt-solidified forms of GPS and were applied to the evaluation of waxes receiving different thermal cycles.

FT-IR spectra of untreated GPS samples when stored at 3, 25 or 50°C exhibited no changes throughout the 180 days of storage (data not shown). This implies that commercial material as supplied exists in a stable polymorphic form.

The FT-IR spectra of melt-solidified GPS samples after storage at different temperatures are shown in Figure 4.10 below.

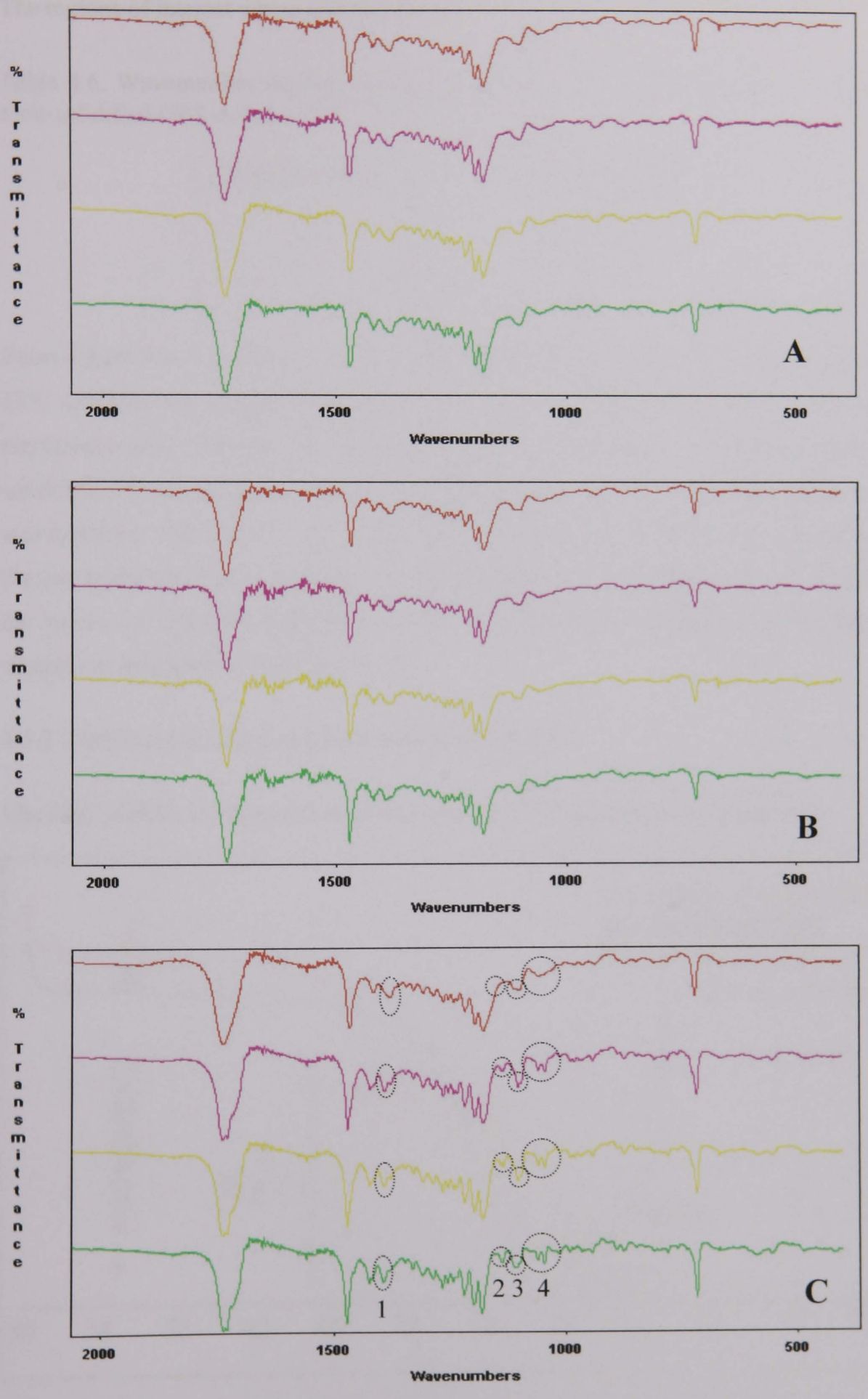

Figure 4.10. FT-IR spectra of melt-solidified GPS samples stored at 3°C (**A**), 25°C (**B**) or 50°C (**C**) for various time intervals (— 0 day; — 7 days; — 14 days; — 180 days)

The regions of interest where spectral differences exist are shown in Table 4.6.

Table 4.6. Wavenumber regions where differences in FT-IR spectra were observed melt-solidified GPS stored at 50°C (from Figure 4.10).

Region number	Wavenumber (cm^{-1})
1	1394
2	1144
3	1106
4	1062

From Figure 4.10 (A - B), the FT-IR spectra of melt-solidified GPS stored at 3 and 25°C exhibited no changes throughout the 180 day storage period suggesting that physicochemical changes are inhibited at low temperatures. However, melt-solidified GPS stored at 50°C showed spectral changes after 7 days (Figure 4.10C) at wavenumbers 1062 (Alc C-O), 1106 (Alc C-O) and 1394 (CH_3) from broad to sharper peaks with the development of the additional peaks as observed previously in the spectra of untreated GPS (Figure 4.9). This followed a similar trend to GMS samples as discussed in Section 4.3.1.1.

4.3.2.2 Differential scanning calorimetry (DSC) of GPS

The DSC profiles of untreated and melt-solidified GPS are shown in Figure 4.11.

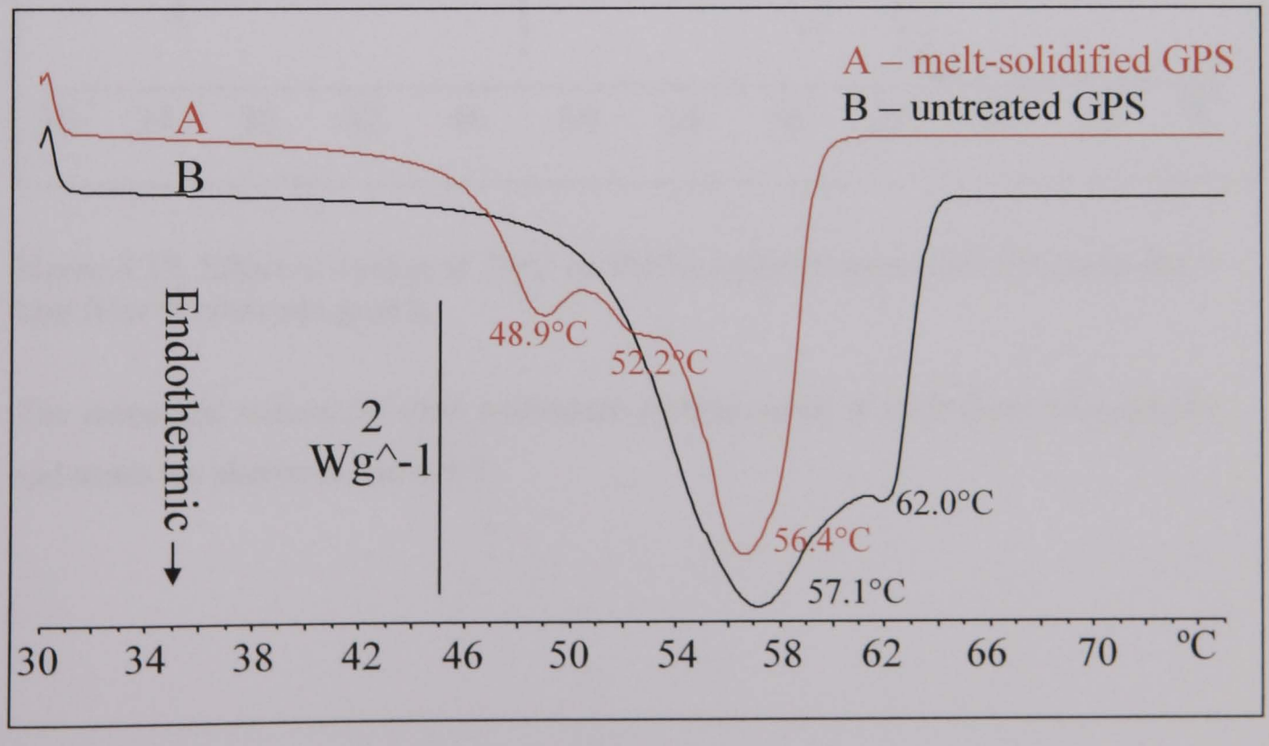

Figure 4.11. Effect of melt-solidification on DSC profiles of GPS (solidification at 25°C) (scale bar = heat flow (2 watts per gram)).

The DSC profiles of melt-solidified GPS showed two shoulder peaks at 48.9 and 52.2°C as well as a main peak at 56.4°C whereas untreated GPS showed a shoulder peak at 62.0°C and a main peak at 57.1°C. The untreated GPS showed a broader melting range and higher melting temperature compared to the melt-solidified sample which exhibited a narrower melting range and more additional peaks.

DSC profiles of untreated GPS samples after storage at 50°C are shown in Figure 4.12. At this temperature, noticeable changes in thermal profiles are observed, whereas at lower temperature storage conditions (3 and 25°C), only very slight changes were observed (data not shown).

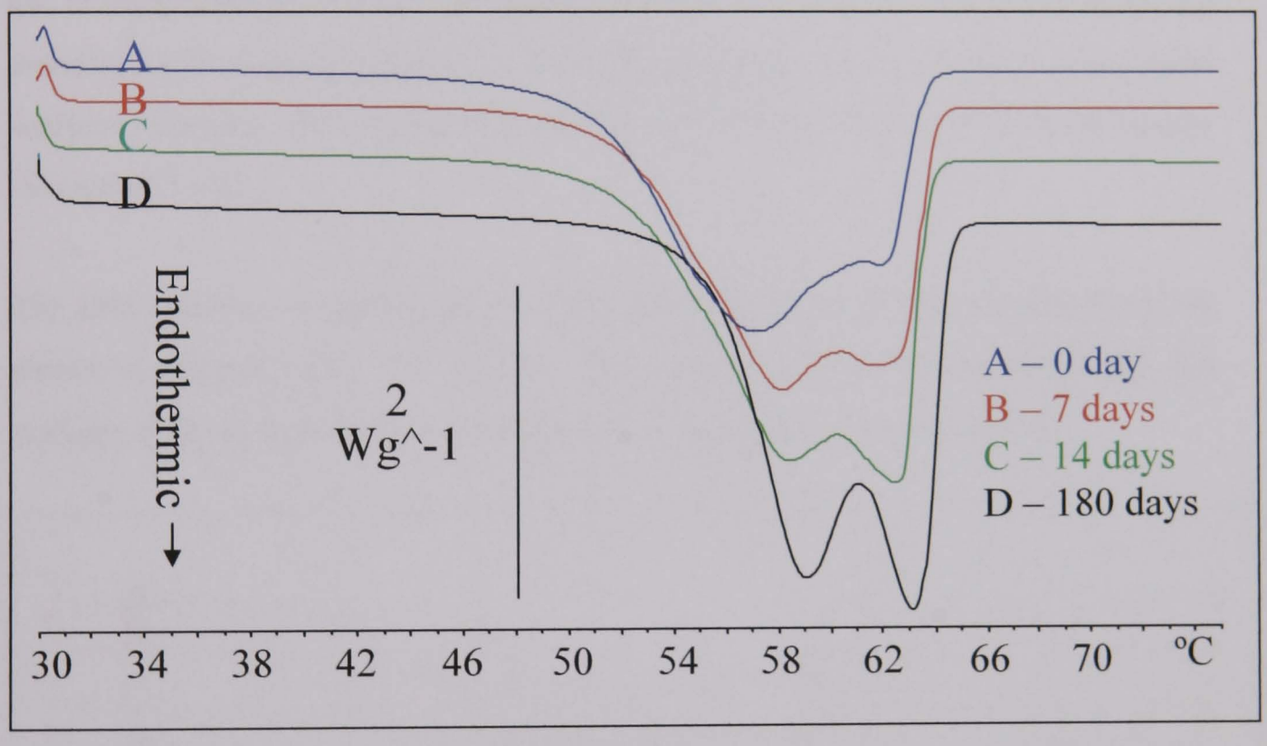

Figure 4.12. Effect of storage at 50°C on DSC profiles of untreated GPS (scale bar = heat flow (2 watts per gram)).

The numerical values for each individual melting event at individual temperatures and times are shown in Table 4.7.

Table 4.7. Effect of storage time and temperature on the thermal characteristics of untreated GPS.

Storage temperature Storage duration (days)	Melting point (°C)			Enthalpy (ΔH) (J/g)		
	3°C	*25°C*	*50°C*	*3°C*	*25°C*	*50°C*
0	57.1, 62.0	57.1, 62.0	57.1, 62.0	183.9	183.9	183.9
7	57.6, 62.6	56.9, 61.9	57.9, 61.6	184.1	185.3	191.9
14	56.8, 61.4	57.8, 62.4	58.2, 62.5	160.1	187.5	203.5
180	57.1, 62.3	57.4, 62.1	58.9, 63.1	183.2	186.3	201.2

For untreated GPS stored at 3 and 25°C, small changes in melting point and enthalpy (ΔH) were observed over the 180 day storage. However, GPS samples stored at 50°C (Figure 4.12) for 7 days and longer demonstrated changes to the DSC profiles with the development of a second prominent peak at around 62°C. After 180 days, the enthalpy (ΔH) of samples stored at 50 °C increased noticeably compared to the initial untreated sample. This change detected by DSC was not observed in FT-IR studies (Section 4.3.2.1).

The DSC profiles of melt-solidified GPS after storage at different temperature are shown in Figures 4.13 - 4.15 below. The numerical values for melting point and enthalpy (ΔH) at individual temperatures and times are shown in Table 4.8.

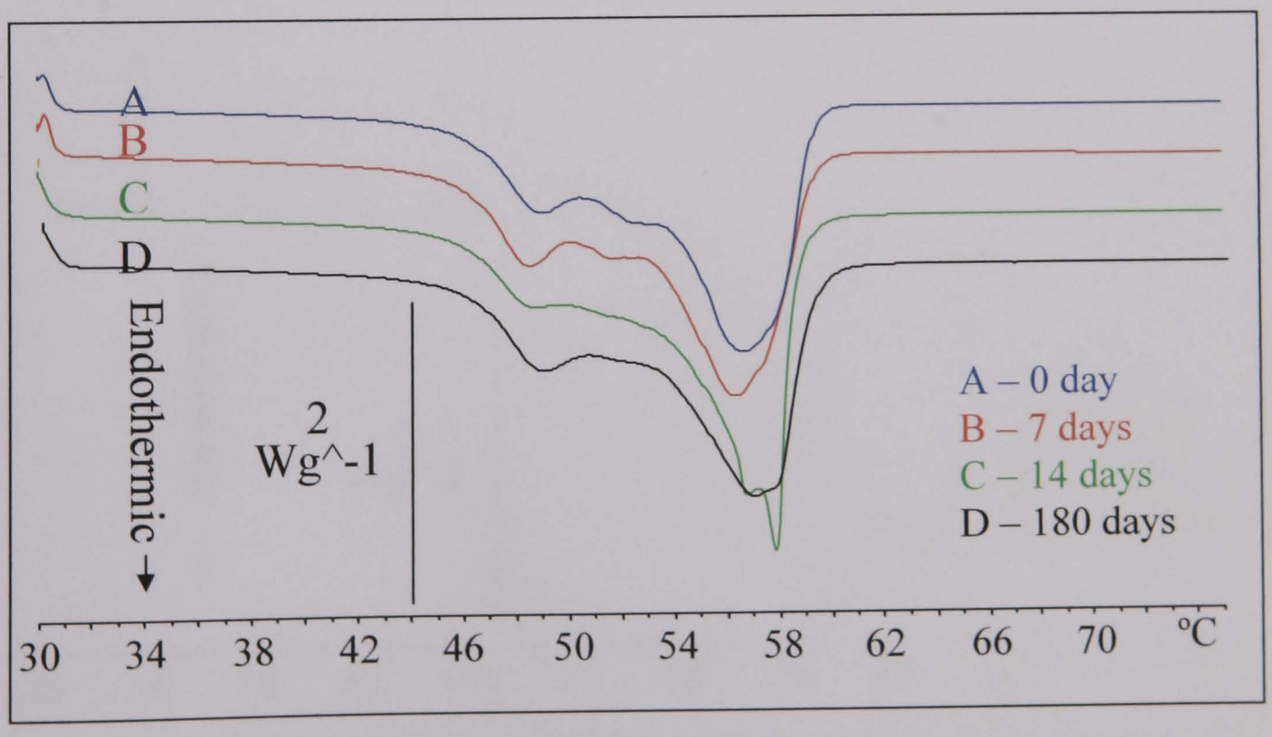

Figure 4.13. Effect of storage at 3°C on DSC profiles of melt-solidified GPS (scale bar = heat flow (2 watts per gram)).

During storage at 3°C, the spectra were essentially unchanged with the exception of the 14 days sample which exhibited a sharp endothermic transition at 57.7°C.

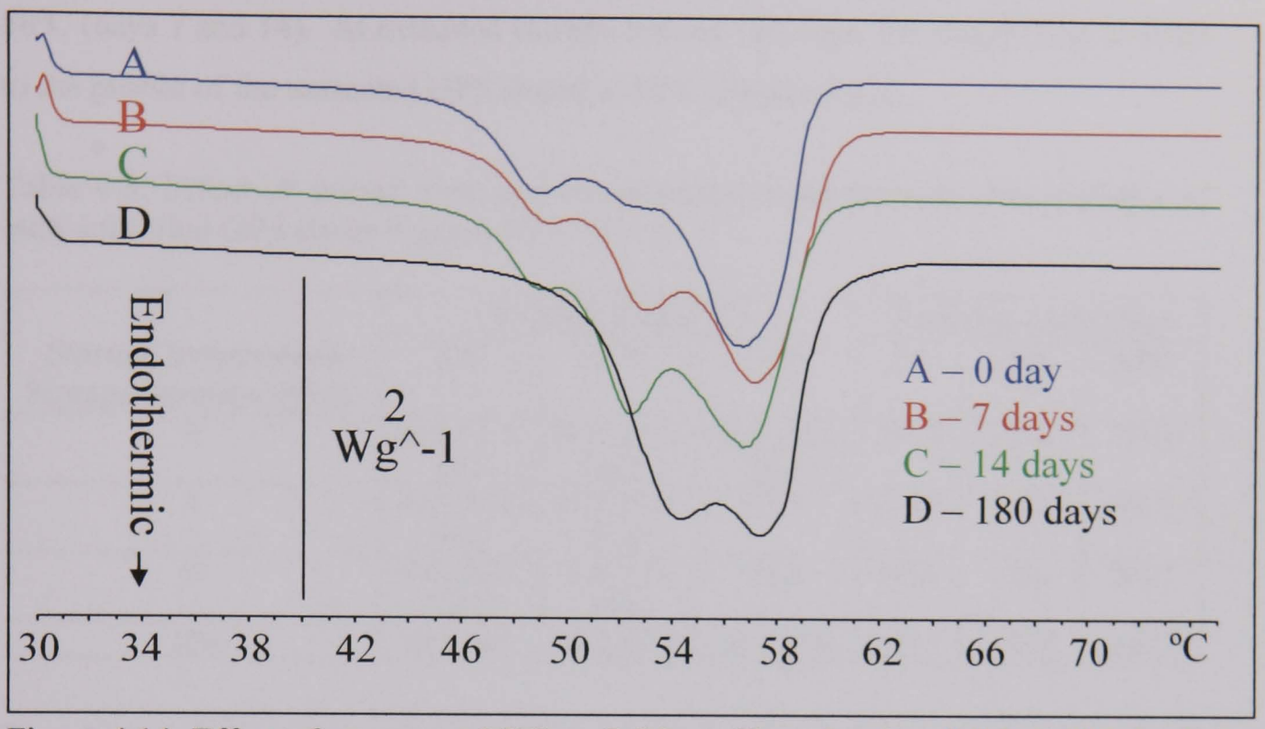

Figure 4.14. Effect of storage at 25°C on DSC profiles of melt-solidified GPS (scale bar = heat flow (2 watts per gram)).

Storage at 25°C resulted in the material exhibiting three definable endothermic transitions at days 0 – 14. By day 180, the endothermic transition at ~ 49°C disappeared leaving the two peaks with transitions at 54.2 and 57.2°C.

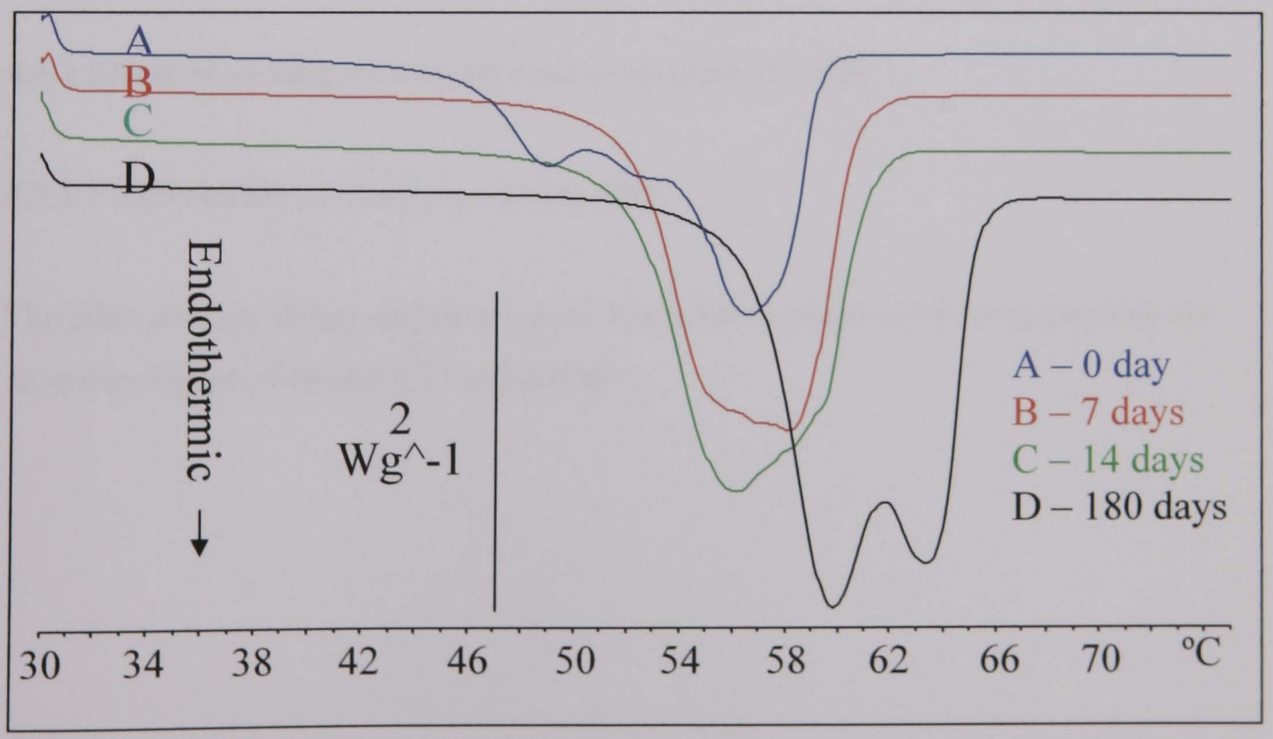

Figure 4.15. Effect of storage at 50°C on DSC profiles of melt-solidified GPS (scale bar = heat flow (2 watts per gram)).

Immediately following storage at 50°C the material lost the endothermic transition at 48.9 and 52.3°C and reverted to a material with a single broad endotherm at ~ 56 - 58°C (days 7 and 14). At extended storage time of 180 days, the sample had reverted to the profile of the untreated GPS stored at 50°C (Figure 4.12).

Table 4.8. Effect of storage time and temperature on the thermal characteristics of melt-solidified GPS (from Figures 4.13 – 4.15).

Storage temperature Storage duration (days)	Melting point (°C)			Enthalpy (ΔH) (J/g)		
	3°C	*25°C*	*50°C*	*3°C*	*25°C*	*50°C*
0	48.9, 52.3, 56.5	48.9, 52.3, 56.5	48.9, 52.3, 56.5	139.8	139.8	139.8
7	48.4, 51.4, 56.2	49.2, 52.9, 57.0	57.7	139.5	147.6	166.5
14	48.5, 56.4, 57.7	49.0, 52.4, 56.9	55.8	146.6	152.6	200.2
180	48.7, 56.6	54.2, 57.2	59.7, 63.9	137.5	152.4	196.7

The change of aged melt-solidified GPS stored at 50°C was also observed in FT-IR studies. Some of the triglyceride components of GPS have been previously reported to convert from an amorphous to crystalline form following thermal processing (Laine et al., 1988). This may account for some of the thermal changes observed in the DSC profiles of melt-solidified GPS and subsequently stored at 3, 25 or 50°C.

4.3.3 Effect of cooling rate on thermal properties of GMS

4.3.3.1 Differential scanning calorimetry (DSC)

The DSC profiles of fast and slow cooled GMS after storage at room temperature are shown in Figures 4.16 and 4.17 respectively.

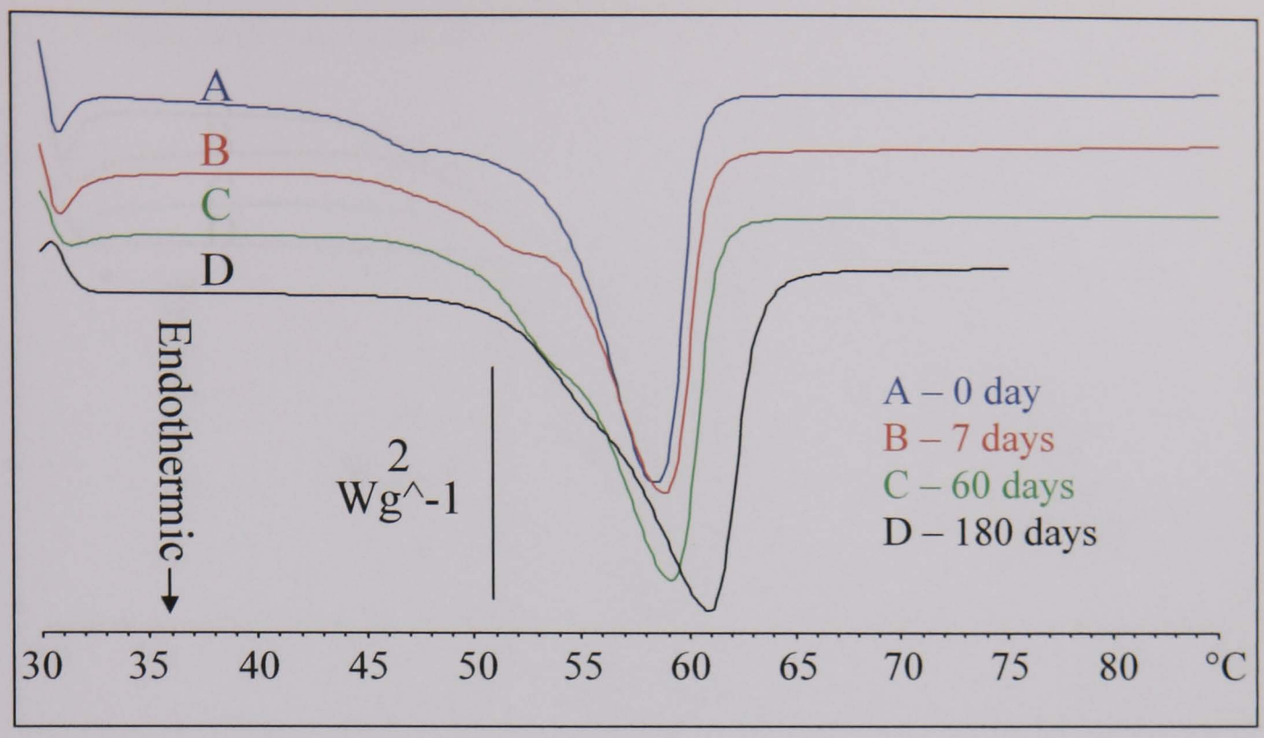

Figure 4.16. Effect of storage time at room temperature on DSC profiles of fast cooled GMS (scale bar = heat flow (2 watts per gram)).

Sutananta et al. (1994b) using identical methodology, noted that fast cooled Gelucire 43/01 brought about homogeneous chemical structure with facilitated reorganisation during storage, while slow cooled wax led to fractionation of low and high melting point of glyceride components into discrete regions at the microscopic level. In the present study of fast cooled GMS, the shoulder peak temperature moved from 46.9°C to 56°C and the main endotherm shifted from 58°C to 60.4°C.

The results of the slow cooling runs are shown below.

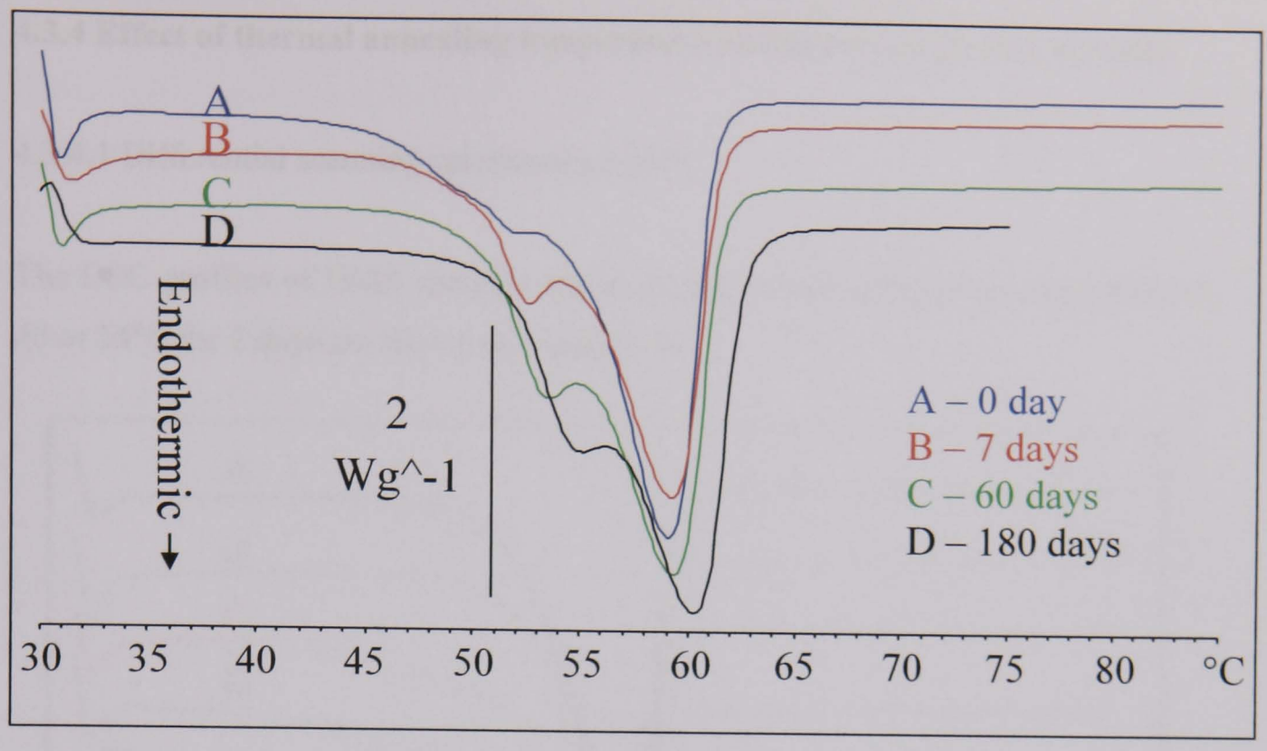

Figure 4.17. Effect of storage time at room temperature on DSC profiles of slow cooled GMS (scale bar = heat flow (2 watts per gram)).

The DSC profiles of slow cooled GMS stored for up to 180 days demonstrated a broadening in the shoulder. Sutananta et al. (1994b) attributed such thermal characteristics with the segregation of wax components into different melting fractions.

The rate of thermal change was affected by the cooling rate with faster cooling rates accelerating the transformation of GMS to more stable polymorphs. A summary of the thermal characteristics of GMS in both methods is shown in Table 4.9.

Table 4.9. Effect of storage time after fast and slow cooling on the thermal characteristics of GMS (from Figures 4.16 - 4.17).

Method Storage duration (days)	Melting point (°C)		Enthalpy (ΔH) (J/g)	
	Fast cooling	*Slow cooling*	*Fast cooling*	*Slow cooling*
0	46.9, 58.0	51.0, 58.8	123.7	123.3
7	51.7, 58.5	52.2, 59.0	102.8	106.0
60	53.8, 58.7	53.0, 59.1	116.3	115.9
180	56.0, 60.4	54.5, 60.1	114.5	118.9

4.3.4 Effect of thermal annealing temperature on thermal properties of GMS

4.3.4.1 Differential scanning calorimetry (DSC)

The DSC profiles of GMS samples stored at thermal annealing temperatures of 37, 46 or 55°C for 2 days are shown in Figure 4.18.

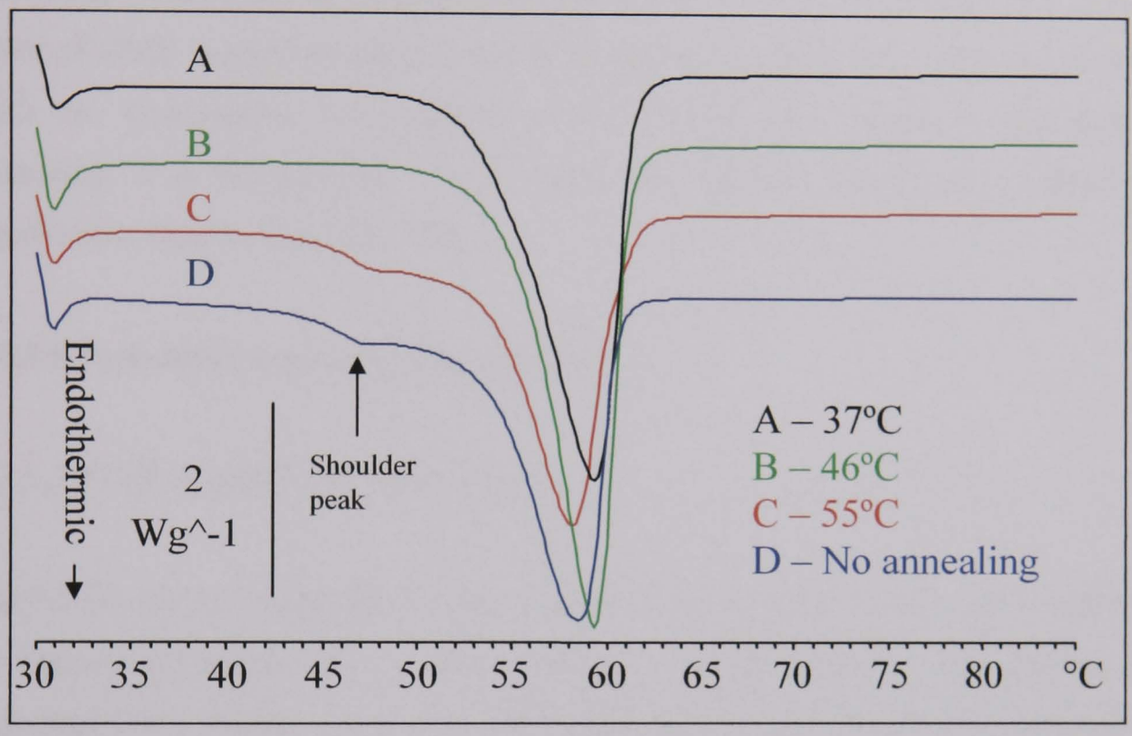

Figure 4.18. Effect of annealing temperature (37, 46 or 55°C) for 2 days on DSC profiles of GMS (scale bar = heat flow (2 watts per gram)).

The thermal changes are summarised in Table 4.10.

Table 4.10. Effect of annealing temperature on the thermal characteristics of GMS (from Figure 4.18).

Temperature of thermal annealing	Melting point (°C)		Enthalpy (ΔH) (J/g)
	Main peak	Shoulder peak	
No annealing	58.0	46.9	123.7
55°C	57.7	47.4	114.7
46°C	58.8	-	125.5
37°C	58.7	-	127.8

In this present study, thermal annealing was carried out at a range of temperatures below the melting temperature of GMS (55 - 60°C). Annealing at 55°C afforded the unstable form with a shoulder peak as observed in the profile of the initial sample.

The temperature of 46°C was found to be the optimum temperature for annealing to afford rapid conversion to the stable form (disappearance of a shoulder peak) and this process was selected to be employed in further studies.

As the temperature of the annealing process approaches the melting temperature of GMS, no structural modifications are observed compared to material not undergoing annealing. However, at temperatures approximately 9°C lower than the melting point of GMS, a rapid transformation in structure was observed. This is consistent with the observations of Sutananta et al. (1994b) who suggested that thermal annealing at a temperature ~ 9°C below the melting temperature formed the equilibrium structure at a rapid rate.

4.3.5 Effect of thermal annealing on GMS

4.3.5.1 FT-IR spectrophotometry of GMS

The FT-IR spectra of untreated GMS samples when annealed at 25 or 46°C exhibited no changes throughout the 28 days of storage (data not shown). This implies that untreated GMS already exists in a stable polymorphic form which is not affected by annealing. The FT-IR spectra of melt-solidified GMS samples after annealing at 25 or 46°C are shown in Figure 4.19. The regions of interest where spectral differences exist are shown in Table 4.11.

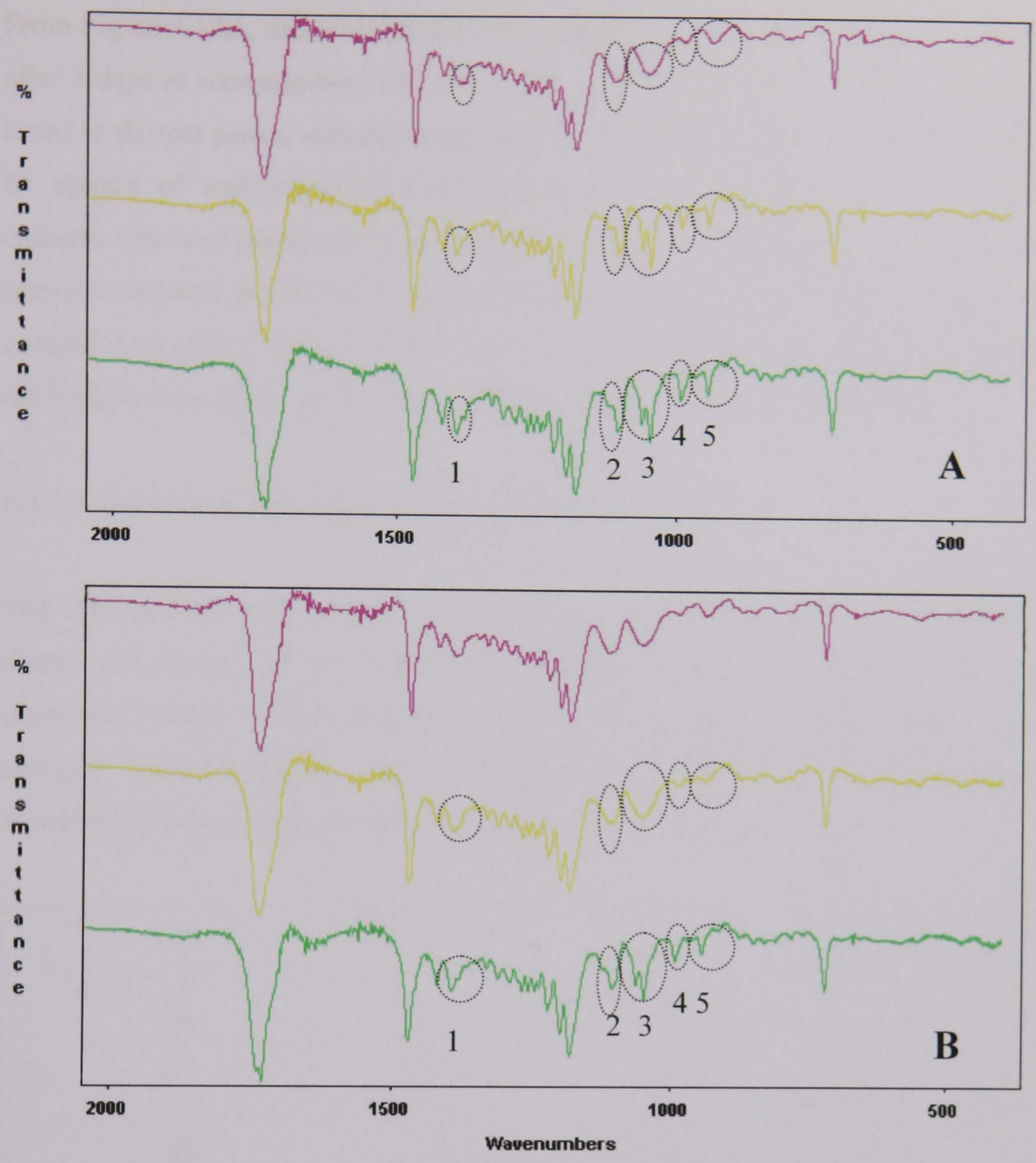

Figure 4.19. FT-IR spectra of melt-solidified GMS samples annealed at 46°C (**A**) and 25°C (**B**) for various time intervals (— 0 day; — 7 days; — 28 days).

Table 4.11. Wavenumber regions where differences in FT-IR spectra were observed between the melt-solidified GMS samples annealed at 25 or 46°C (from Figure 4.19).

Region number	Wavenumber (cm^{-1})
1	1394
2	1105
3	1051
4	992
5	943

From Figure 4.19A, melt-solidified GMS annealed at 46°C showed spectral changes after 7 days at wavenumber 1051 (Alc C-O), 1105 (Alc C-O) and 1394 (CH_3) from broad to sharper peaks, with the development of additional peaks. Moreover, the FT-IR spectra of melt-solidified GMS annealed at 25°C (Figure 4.19B) exhibited changes observed previously in the spectra of GMS annealed at 46°C, however, the samples annealed at 25°C took longer (28 days) for the spectral changes to develop compared to only 7 days at 46°C. This confirms that high annealing temperature (46°C) had more effect on the structure change than low temperature (25°C).

4.3.5.2 Differential scanning calorimetry (DSC) of GMS

The DSC profiles of untreated GMS samples after annealing at 46°C are shown in Figure 4.20 below. At this temperature, noticeable changes in thermal profiles are observed, whereas at annealing temperature (25°C), only very slight changes were observed (data not shown). The numerical values for each individual melting event at individual temperatures and times are shown in Table 4.12.

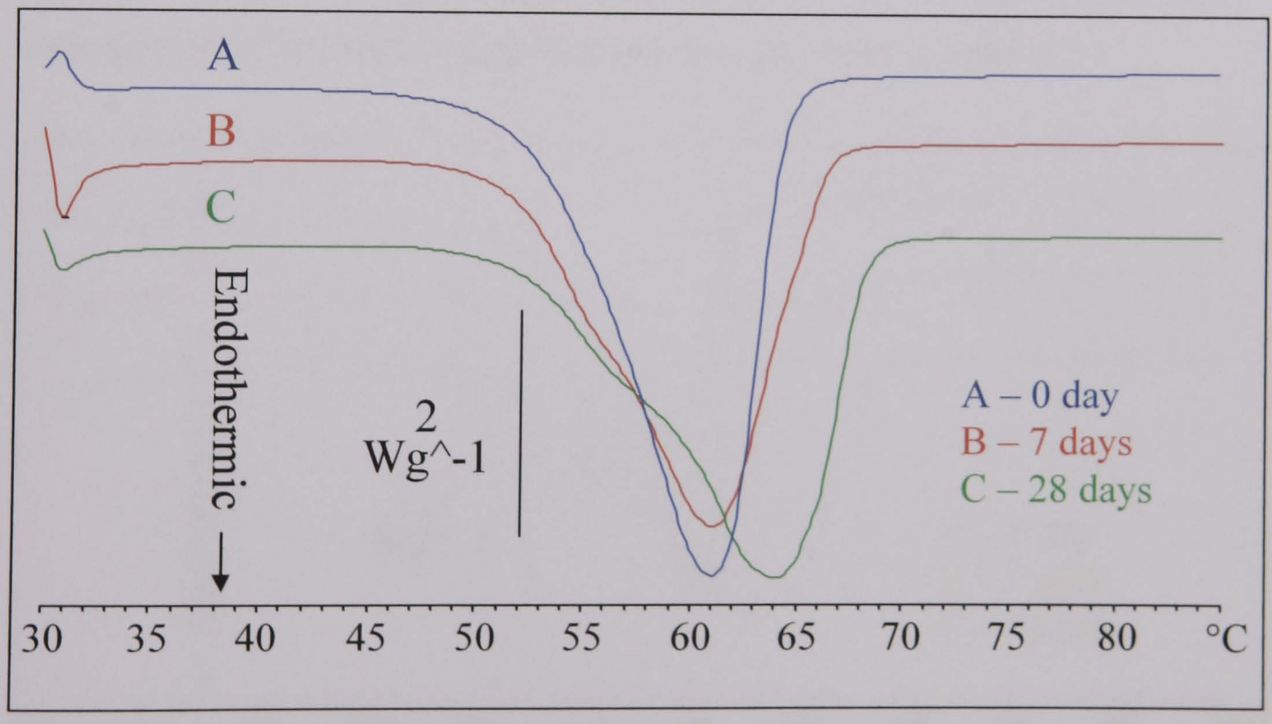

Figure 4.20. Effect of annealing at 46°C on DSC profiles of untreated GMS (scale bar = heat flow (2 watts per gram)).

Table 4.12. Effect of annealing time and temperature on the thermal characteristics of untreated GMS.

Annealing temperature Storage duration (days)	Melting point (°C)		Enthalpy (ΔH) (J/g)	
	25°C	*46°C*	*25°C*	*46°C*
0	60.9	60.9	158.8	158.8
7	61.6	60.8	157.7	168.8
28	62.9	63.7	142.6	165.4

The DSC profiles of untreated GMS annealed at 46°C (Figure 4.20) for 28 days showed a ~ 3°C increase in peak temperature with a broadening of the melting transition and an increase of enthalpy (ΔH). For untreated GMS at 25°C, small fluctuations in melting point and enthalpy (ΔH) were observed over the 28 days storage. These thermal changes were not found in parallel FT-IR studies (Section 4.3.5.1), demonstrating the importance of using complementary techniques for such analyses.

The DSC profiles of melt-solidified GMS samples after annealing at 46 or 25°C are shown in Figures 4.21 - 4.22 below. The numerical values for melting point and enthalpy (ΔH) at individual temperatures and times are shown in Table 4.13.

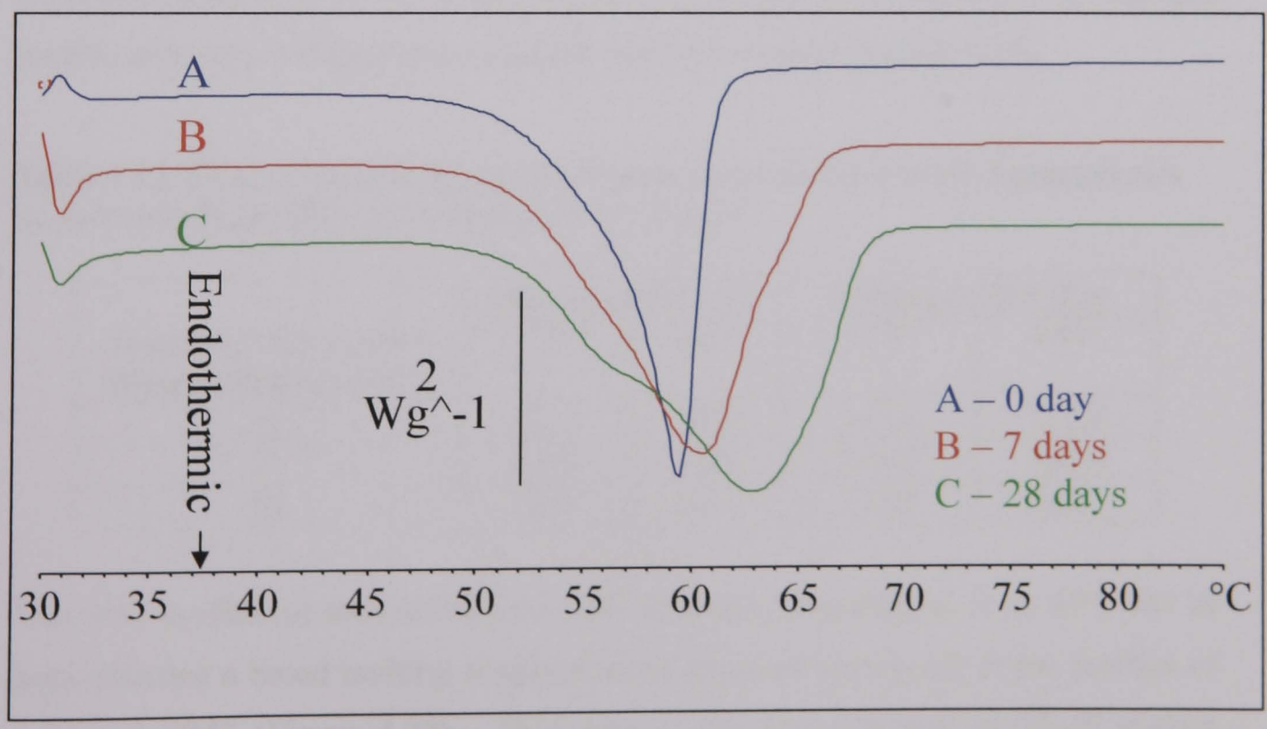

Figure 4.21. Effect of annealing at 46°C on DSC profiles of melt-solidified GMS (scale bar = heat flow (2 watts per gram)).

Immediately following annealing at 46°C there was an upward trend in the melting point. Moreover, a remarkable increase of enthalpy (ΔH) and a noticeable shoulder peak was found during annealing over a 28 day period.

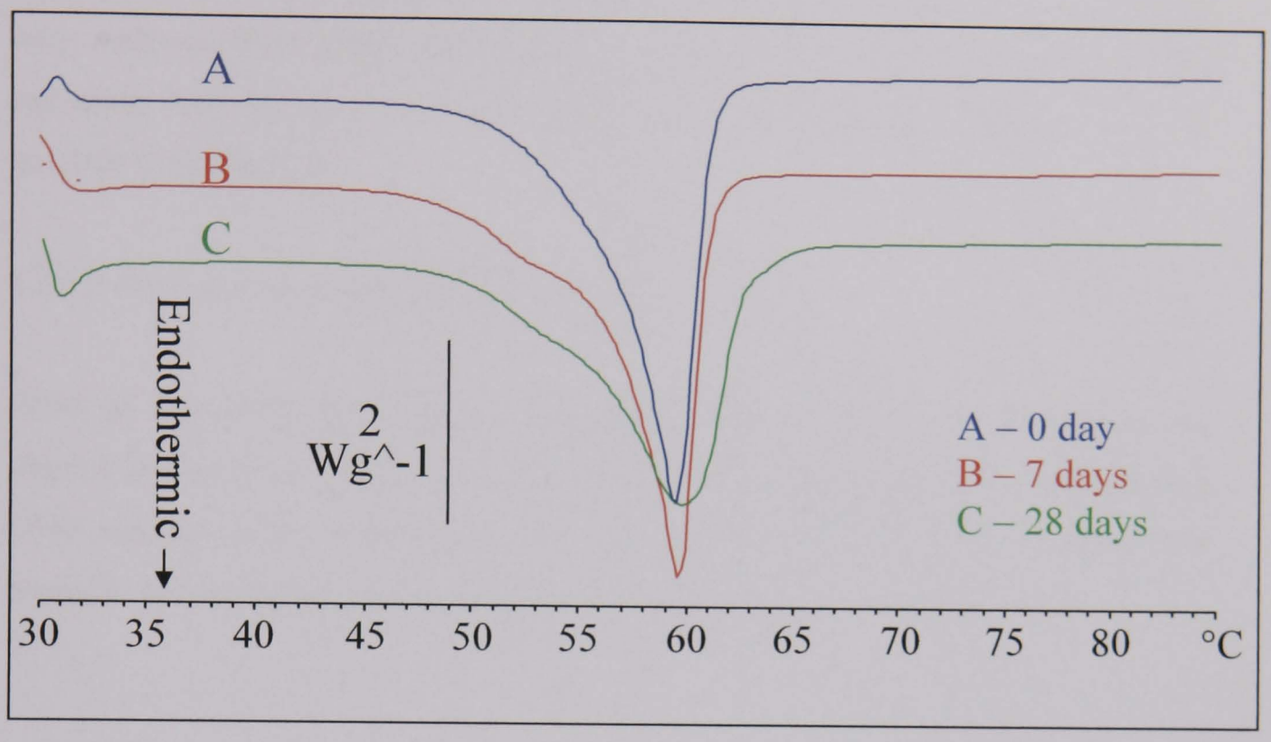

Figure 4.22. Effect of annealing at 25°C on DSC profiles of melt-solidified GMS (scale bar = heat flow (2 watts per gram)).

After annealing at 25°C for 28 days, there was noticeable broadening of the thermal profile, although melting point remained relatively constant (Table 4.13).

Table 4.13. Effect of annealing time and temperature on the thermal characteristics of melt-solidified GMS (from Figures 4.21 – 4.22).

Annealing temperature Storage duration (days)	Melting point (°C)		Enthalpy (ΔH) (J/g)	
	25°C	*46°C*	*25°C*	*46°C*
0	59.3	59.3	112.8	112.8
7	59.3	60.2	119.2	150.0
28	60.5	64.5	115.8	160.7

The DSC profiles of melt-solidified GMS following annealing at 25 or 46°C for 28 days afforded a broad melting temperature as observed previously in the profiles of untreated GMS (Figure 4.20). This change was also observed in FT-IR studies (Section 4.3.5.1). This suggests that untreated GMS when melted and cooled

afforded the less stable α-form which transformed during annealing to the ß-form similar to the untreated form of GMS.

The annealing temperature of 25°C had less effect on the change of thermal profiles with melt-solidified GMS than at 46°C. Consequently, high temperature (46°C) annealing will be used in further studies to accelerate transformation from an unstable to stable form.

4.3.5.3 Hot stage microscopy (HSM) of GMS

HSM in this study was used in conjunction with polarised light microscopy to observe the nature of the physical changes. The HSM photographs of melt-solidified GMS samples after annealing at 46°C are shown in Figure 4.23. Images were recorded to observe any changes during the temperature range of 50 to 65°C.

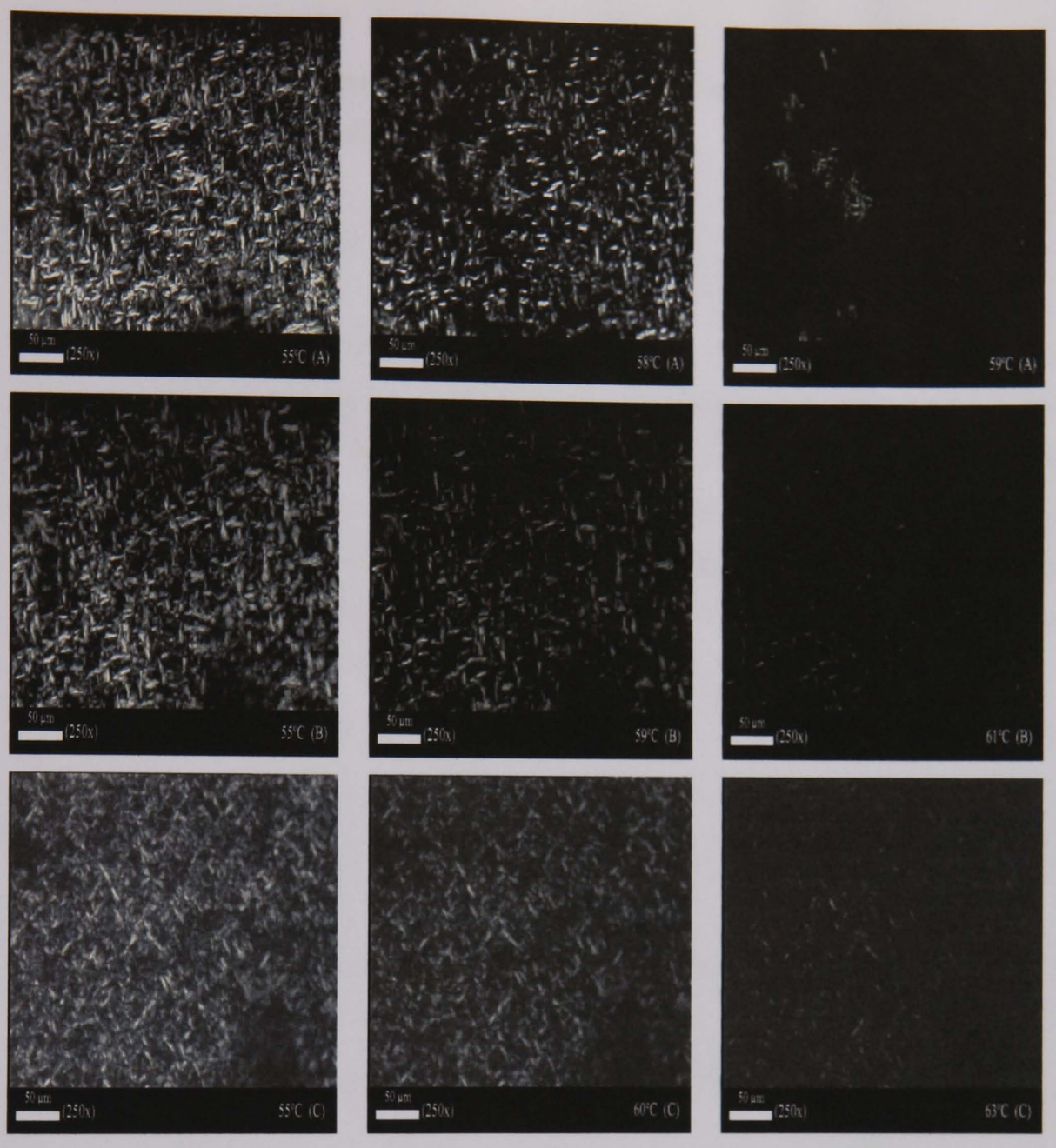

Figure 4.23. Hot stage polarising microscope photographs of melt-solidified GMS following (**A**) no annealing, (**B**) annealing for 7 days at 46°C or (**C**) annealing for 28 days at 46°C.

From Figure 4.23A, when heated up to 58°C, the majority of the sample of melt-solidified GMS formed a liquid, with some crystallites still visible. At 59°C, the entire sample had melted. When melt-solidified GMS were annealed at 46°C for 7 days (Figure 4.23B), the GMS melting temperature increased substantially to 61°C. When annealed at 46°C for 28 days (Figure 4.23C), the GMS melting temperature had further increased to 63°C. This illustrated that the annealing time at 46°C

affected to the melting temperature of processed GMS and correlated with the DSC results (Figure 4.21 and Table 4.13).

4.3.5.4 X-ray powder diffraction (XRPD) of GMS

XRPD is commonly employed to investigate the degree of crystallinity and polymorphic identity of materials. The long spacings of XRPD patterns refer to the distance between crystal planes (chain length packing) whereas short spacings correlate to subcell structure (interchain distances) highlighting differences between polymorphs (Himawan et al., 2006). In the present studies, the short spacing region was examined in the untreated and melt-solidified GMS materials after annealing as shown in Figures 4.24 and 4.25.

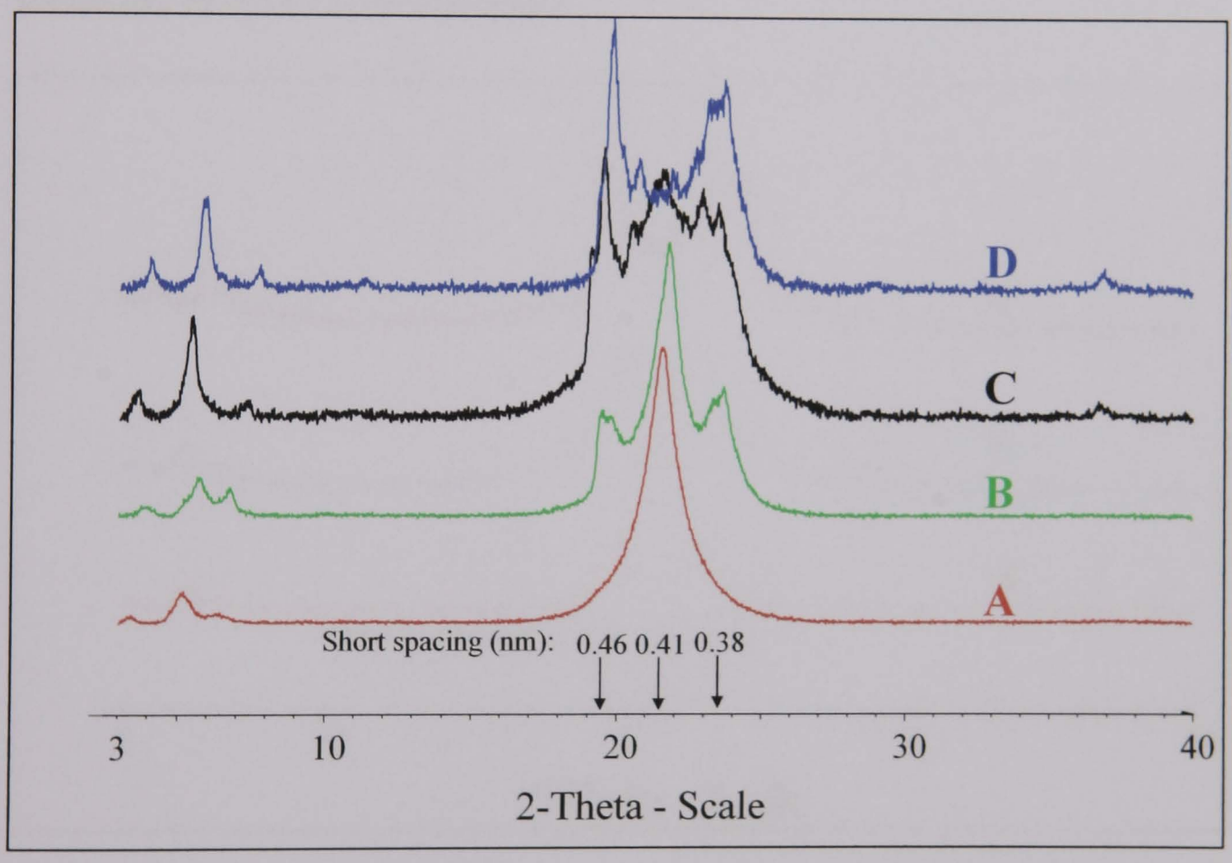

Figure 4.24. X-ray diffractograms of melt-solidified GMS following (**A**) no annealing, (**B**) annealing for 4 days at 46°C, (**C**) annealing for 28 days at 46°C or (**D**) untreated sample.

Yajima et al. (2002) reported that the XRPD pattern of α-form of GMS showed one distinct peak at 2θ angles of ~ 21.5° (d = 0.41 nm) whereas the ß-form of GMS

showed two peaks at 2θ angles of ~ 19.5° (d = 0.46 nm) and ~ 23.5°(d = 0.38 nm). From the present study, the XRPD pattern of melt-solidified GMS (Figure 4.24A) showed one narrow peak at 2θ angles of 21.5° (d = 0.41 nm) that was referred to the α-form of GMS. However, GMS aged for 4 days (Figure 4.24B) showed three peaks at 2θ angles of 19.5°, 21.5° (main) and 23.5°. The samples aged for 28 days (Figure 4.24C) exhibited four small peaks at 2θ angles of 19.5°, 21.5°, 23.0° and 23.5° suggesting a mixture of predominantly ß-form with some α-form detectable. The pattern of untreated GMS (Figure 4.24D) showed two peaks at 2θ angles of 19.5° (d = 0.46 nm) and 23.5° (d = 0.38 nm) confirming the presence of the ß -form. It could be concluded that untreated GMS (ß-form) when melted and cooled provides the α-form which then reverts progressively back to the stable form (ß-form) during annealing at 46°C. However, annealing at 46°C for 28 days was insufficient to completely reconvert to the stable form.

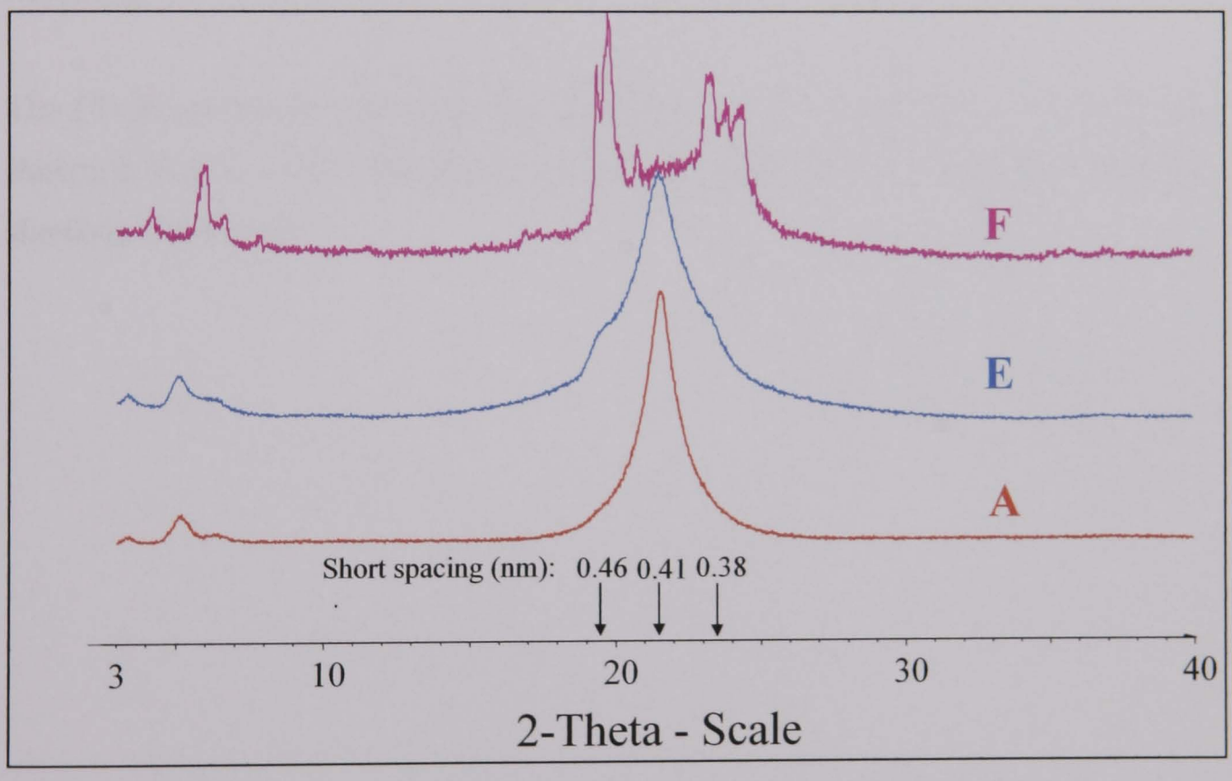

Figure 4.25. X-ray diffractograms of melt-solidified GMS following (**A**) no annealing, (**E**) annealing for 28 days at 25°C or (**F**) annealing for 90 days at 25°C.

The XRPD pattern of aged GMS at 25°C for 28 days (Figure 4.25E) retained one peak at 2θ angles of 21.5° (d = 0.41 nm) and began to exhibit polymorphic changes as observed from the appearance of shoulder peaks. After 90 days, aged GMS

(Figure 4.25F) showed six peaks at 2θ angles of 19.0°, 19.5° (d = 0.46 nm), 20.5°, 23.0°, 23.5° (d = 0.38 nm) and 24.5° indicating complete conversion to the ß-form as observed previously in the pattern of untreated GMS (Figure 4.24D). This confirms that a lower annealing temperature of 25°C prolonged the polymorphic change in GMS following melt solidification as demonstrated by XRPD patterns.

4.3.6 Effect of thermal annealing on GPS

4.3.6.1 FT-IR spectrophotometry of GPS

The FT-IR spectra of untreated GPS samples when annealed at 25 or 46°C exhibited no changes throughout the 28 days of storage (data not shown). This implies that untreated GPS already exists in a stable polymorphic form which is not affected by annealing.

The FT-IR spectra of melt-solidified GPS samples after annealing at 25 or 46°C are shown in Figure 4.26. The regions of interest where spectral differences exist are shown in Table 4.14.

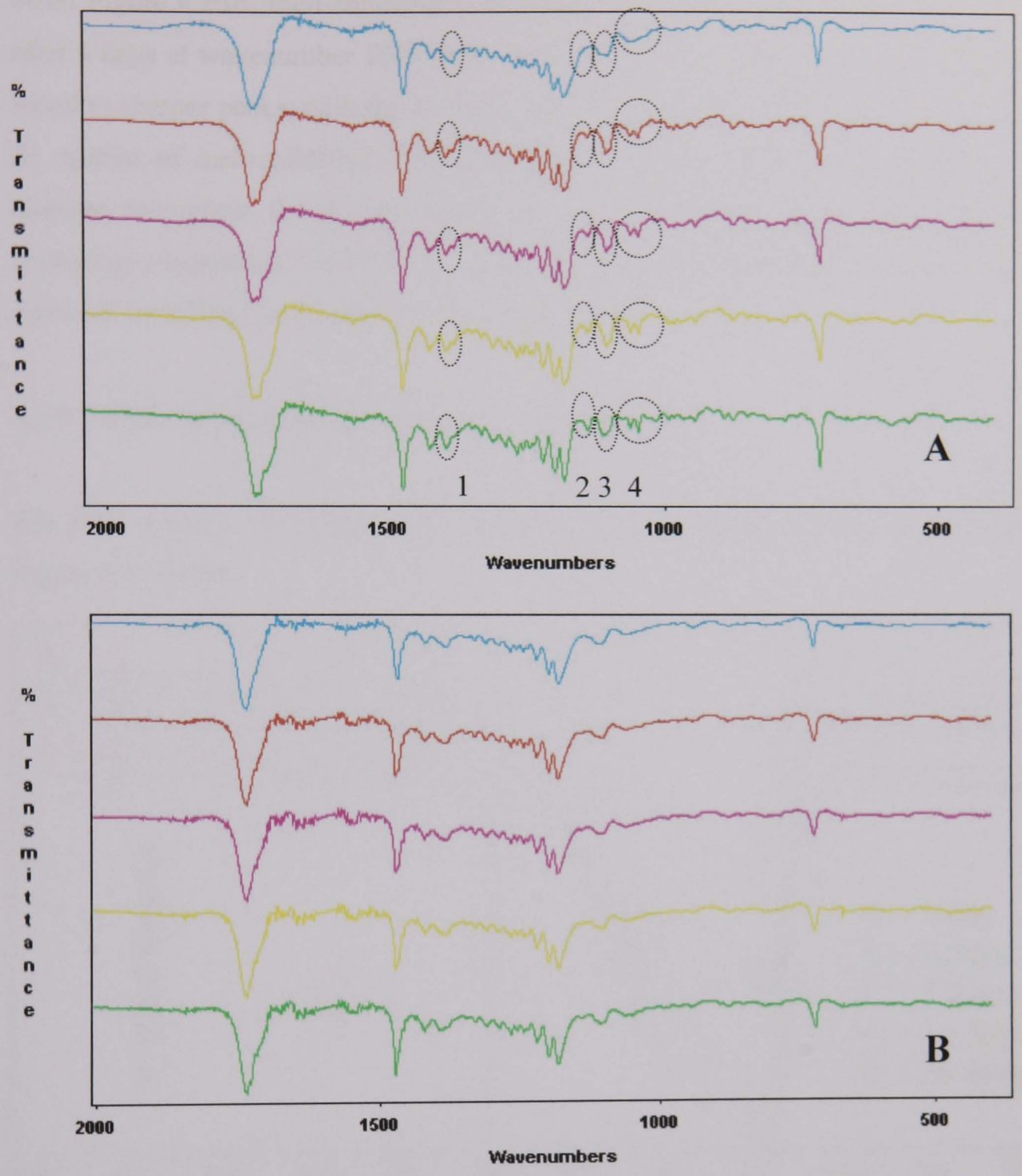

Figure 4.26. FT-IR spectra of melt-solidified GPS samples annealed at 46°C (**A**) and 25°C (**B**) for various time intervals (— 0 day; — 4 days; — 7 days; — 14 days; — 28 days).

Table 4.14. Wavenumber regions where differences in FT-IR spectra were observed between the melt-solidified GPS samples annealed at 46°C (from Figure 4.26).

Region number	Wavenumber (cm^{-1})
1	1394
2	1140
3	1099
4	1062

From Figure 4.26A, melt-solidified GPS annealed at 46°C showed spectral changes after 4 days at wavenumber 1062 (Alc C-O), 1099 (Alc C-O) and 1394 (CH_3) from broad to sharper peaks, with the development of additional peaks. However, the FT-IR spectra of melt-solidified GPS annealed at 25°C (Figure 4.26B) exhibited no changes throughout the 28 day annealing period. This might conclude that high annealing temperature (46°C) had more influence on the spectral changes of both melt-solidified GPS and GMS than low temperature (25°C).

4.3.6.2 Differential scanning calorimetry (DSC) of GPS

The DSC profiles of untreated GPS samples after annealing at 46°C are shown in Figure 4.27 below.

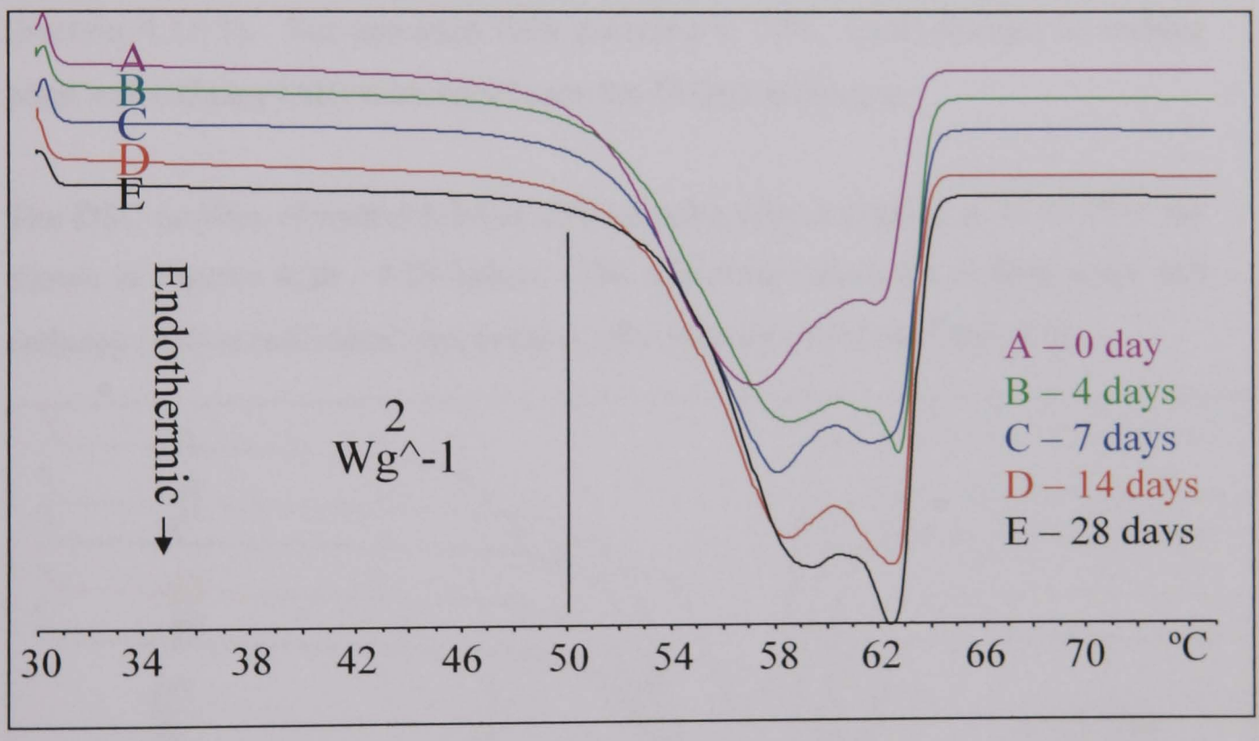

Figure 4.27. Effect of annealing at 46°C on DSC profiles of untreated GPS (scale bar = heat flow (2 watts per gram)).

At 46°C, noticeable changes in thermal profiles are observed, whereas at annealing temperature (25°C), only very slight changes were observed (data not shown).

The numerical values for each individual melting event at individual temperatures and times are shown in Table 4.15.

Table 4.15. Effect of annealing time and temperature on the thermal characteristics of untreated GPS.

Annealing temperature Storage duration (days)	Melting point (°C)		Enthalpy (ΔH) (J/g)	
	25°C	*46°C*	*25°C*	*46°C*
0	57.1, 62.0	57.1, 62.0	183.9	183.9
4	57.6, 62.5	58.3, 62.7	185.4	194.1
7	56.9, 61.9	57.9, 61.6	185.3	191.9
14	57.8, 62.4	58.2, 62.5	187.5	203.5
28	57.2, 61.5	59.0, 62.3	178.0	195.2

The untreated GPS annealed at 46°C (Figure 4.27) for 4 days and longer demonstrated changes in the DSC profiles with the development of a second prominent peak at ~ 62°C. After 28 days, melting temperatures increased in height and sharpness. In addition, the enthalpy (ΔH) increased compared to the initial untreated sample. The change detected by DSC was not observed in FT-IR studies (Section 4.3.6.1). For untreated GPS annealed at 25°C, small changes in melting point and enthalpy (ΔH) were found over the 28 days annealing.

The DSC profiles of melt-solidified GPS samples after annealing at 46 or 25°C are shown in Figures 4.28 - 4.29 below. The numerical values for melting point and enthalpy (ΔH) at individual temperatures and times are shown in Table 4.16.

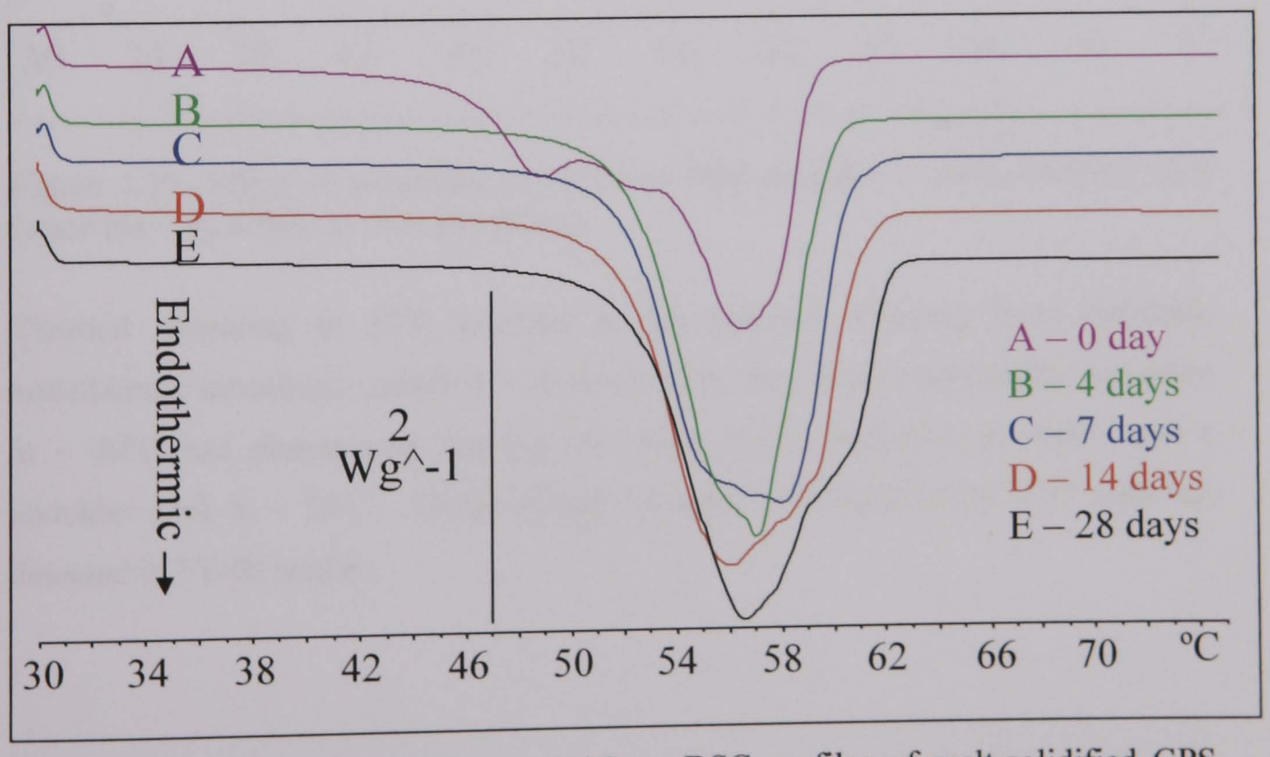

Figure 4.28. Effect of annealing at 46°C on DSC profiles of melt-solidified GPS (scale bar = heat flow (2 watts per gram)).

Immediately following annealing at 46°C the GPS lost the endothermic transition at 48.9 and 52.3°C and reverted to a material with a single broad endotherm at ~ 56 - 57°C (after day 4). The aggregation of three peaks into one peak and disappearance of exothermic peaks of annealed GPS at 46°C might be caused by the gradual crystallisation of GPS during annealing. Moreover, enthalpy (ΔH) of annealed GPS at 46°C for 4 days and longer increased substantially compared to the initial GPS. The change of aged GPS annealing at 46°C was also observed in FT-IR studies (Section 4.3.6.1).

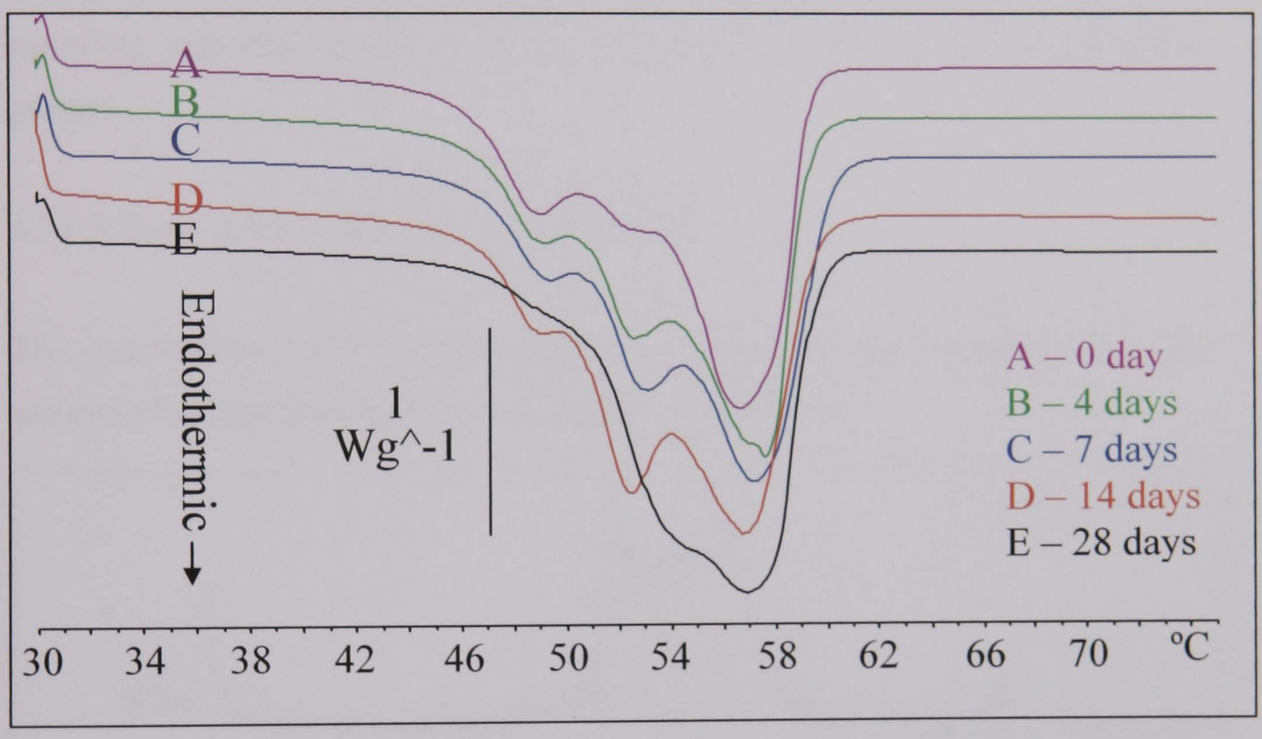

Figure 4.29. Effect of annealing at 25°C on DSC profiles of melt-solidified GPS (scale bar = heat flow (1 watt per gram)).

Thermal annealing at 25°C resulted in the material retaining three definable endothermic transitions at days 0 – 14, however by day 28 the endothermic transition at ~ 49°C had disappeared, leaving one peak with a transition at 56.8°C and a shoulder peak at ~ 54°C. These changes of aged GPS annealed at 25°C were not detected in FT-IR studies.

Table 4.16. Effect of annealing time and temperature on the thermal characteristics of melt-solidified GPS (Figures 4.28 – 4.29).

Annealing temperature Storage duration (days)	Melting point (°C)		Enthalpy (ΔH) (J/g)	
	25°C	*46°C*	*25°C*	*46°C*
0	48.9, 52.3, 56.5	48.9, 52.3, 56.5	139.8	139.8
4	49.0, 52.5, 57.5	57.0	145.6	155.8
7	49.2, 52.9, 57.0	57.7	147.6	166.5
14	49.0, 52.4, 56.9	55.8	152.6	200.2
28	54.2, 56.8	56.4	142.3	171.9

It could be concluded that melt-solidified GPS crystallised gradually during thermal annealing and that higher annealing temperatures accelerate the crystallisation process.

4.3.6.3 X-ray powder diffraction (XRPD) of GPS

The comparisons of X-ray diffractograms of untreated and melt-solidified GPS samples after annealing are shown in Figures 4.30 and 4.31.

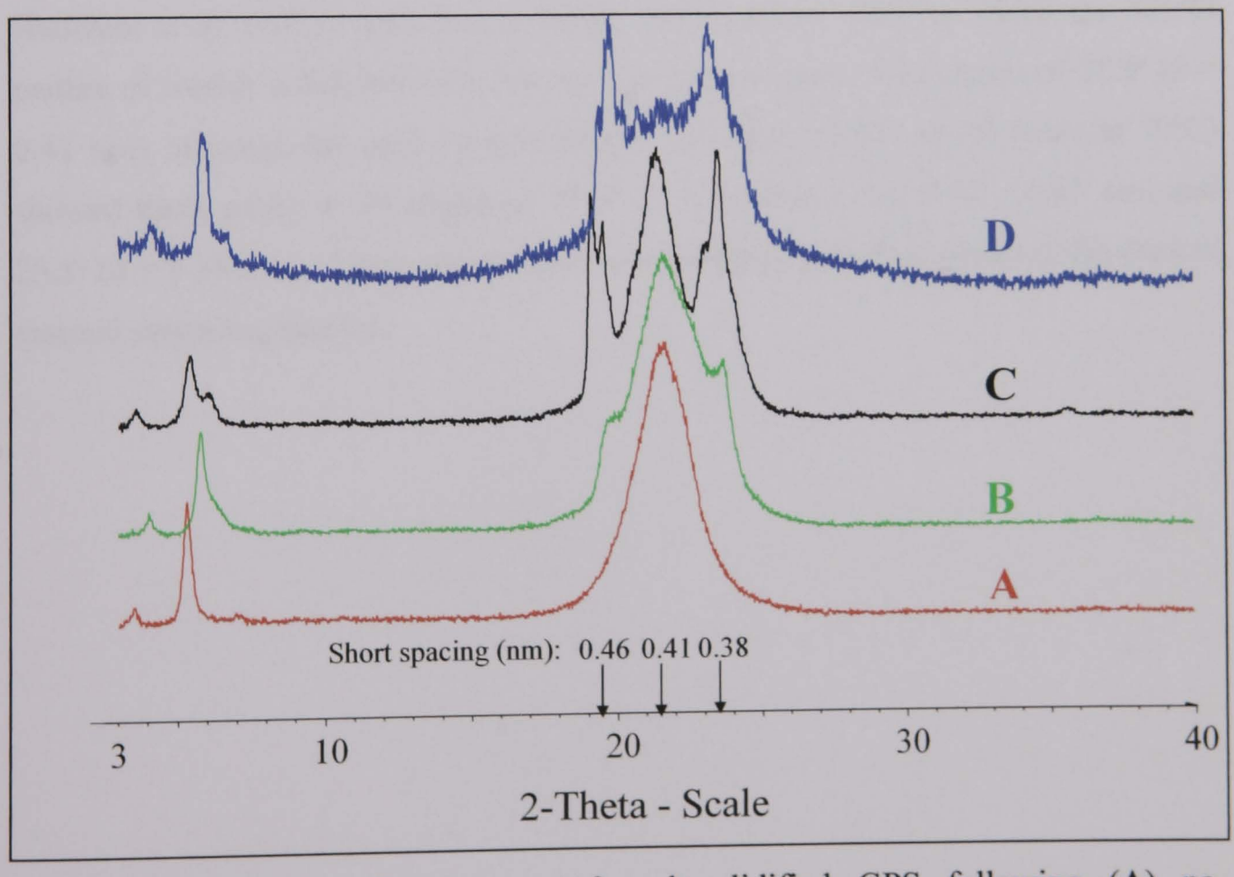

Figure 4.30. X-ray diffractograms of melt-solidified GPS following (**A**) no annealing, (**B**) annealing for 4 days at 46°C, (**C**) annealing for 28 days at 46°C or (**D**) untreated sample.

Previously triglyceride components of GPS, tripalmitin and tristearin, have been reported to show X-ray diffractograms peaks at 2θ angles of 21.6° (d = 0.41 nm) and 21.8° (d = 0.41 nm) respectively at initial time. Laine et al. (1988) proposed that freshly solidified samples exhibited a partially amorphous layered structure which gradually crystallised upon storage at room temperature. In the present study, the XRPD pattern of melt-solidified GPS (Figure 4.30A) showed one peak at 2θ angle of 21.5° (d = 0.41 nm) suggesting the presence of a layered amorphous form. The aged sample annealed at 46°C for 4 days (Figure 4.30B) showed two small shoulder peaks at 2θ angles of 19.5° and 23.5° and a main peak at 2θ angles of 21.5°. In addition, the aged sample for 28 days (Figure 4.30C) showed four distinct peaks at 2θ angles of 19.0°, 19.5°, 21.5° (main) and 23.5°. The peaks of the sample aged for 28 days, with the exception of a main peak, were similar to those of untreated GPS (Figure 4.30D) which showed two distinct peaks at 2θ angles of 19.5° (d = 0.46 nm) and 23.5° (d = 0.38 nm) attributable to development of the crystalline form. This would explain that the melt-solidified GPS annealed at 46°C gradually crystallised.

Hamdani et al. (2003) described a similar GPS stability study in which the XRPD pattern of freshly solidified GPS showed one narrow peak at 2θ angles of 21.5° (d = 0.41 nm), whereas the aged sample (stored 2 weeks at 40°C or 24 hours at 50°C) showed three peaks at 2θ angles of 19.5° (d = 0.46 nm), 21.5° (d = 0.41 nm) and 23.5° (d = 0.38 nm). These results were in accordance with the results of the present thermal annealing studies.

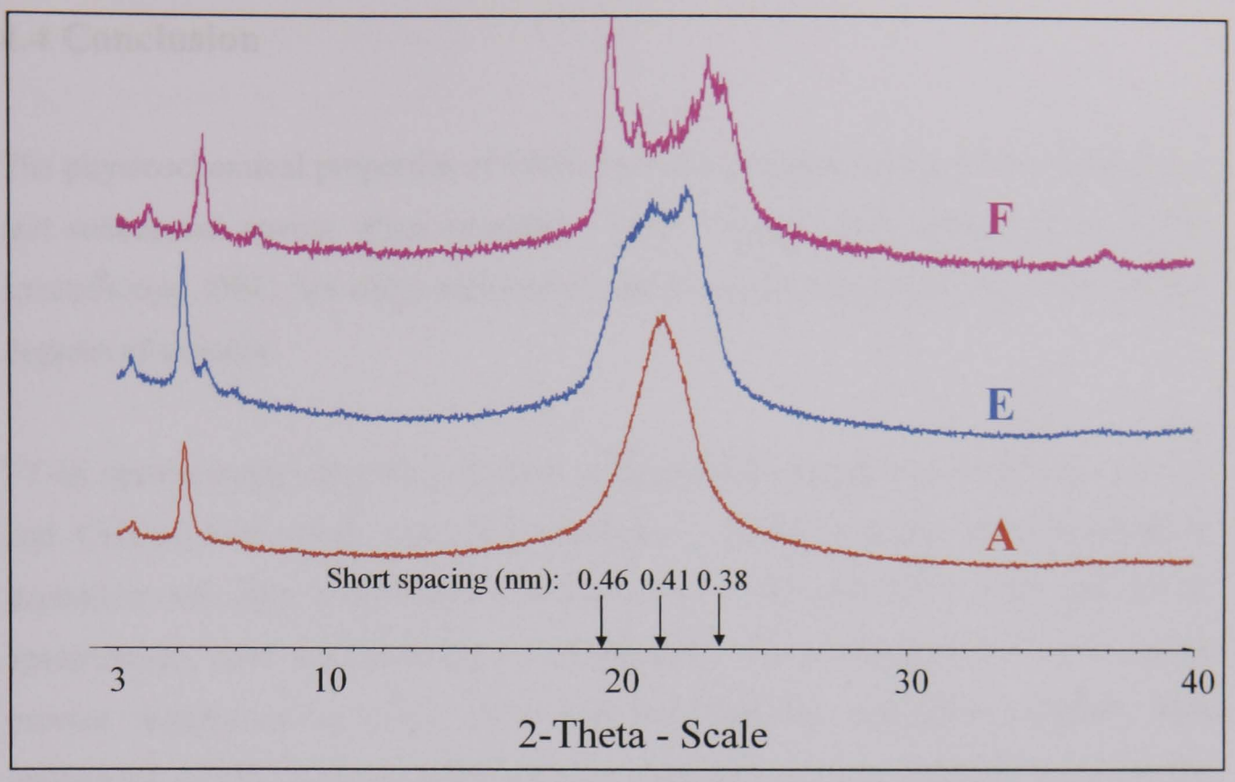

Figure 4.31. X-ray diffractograms of melt-solidified GPS following (**A**) no annealing, (**E**) annealing for 28 days at 25°C or (**F**) annealing for 90 days at 25°C.

The XRPD pattern of aged samples at 25°C for 28 days (Figure 4.31E) still retained two peaks at 2θ angles of 21.5° and 22.5°. Crystallisation was observed as demonstrated by splitting of the main peak and progressively developed by 90 days with 2θ angles of 19.5° (d = 0.46 nm), 20.5°, 23.5° (d = 0.38 nm) which was similar to untreated GPS (Figure 4.30D). This confirms that melt-solidified GPS annealed at 25°C for 90 days undergoes complete crystallisation with reversion to the XRPD pattern of untreated GPS and higher annealing temperatures (46°C) accelerated the crystallisation process and required longer than 28 days to complete crystallisation.

Comparison of GMS and GPS would indicate that GMS transforms more rapidly when subjected to identical thermal annealing cycles. This may be a consequence of the differences in chemical compositions with GMS, composed mainly of monoglycerides transforming more rapidly than GPS which is predominantly composed of mostly di- and triglycerides. The stabilisation rate has been previously reported to be dependent on the molecular size (Laine et al., 1988).

4.4 Conclusion

The physicochemical properties of GMS and GPS changed during melt-solidification and subsequent ageing when annealed. These changes were monitored by FT-IR spectroscopy, DSC, hot stage microscopy and X-ray powder diffraction, with varying degrees of success.

FT-IR spectroscopy identified changes in the spatial arrangement of the alcohol C-O and CH_3 of both GMS and GPS materials. These changes were temperature dependent and only manifested at temperatures of 25 and 50°C. DSC and FT-IR spectroscopy were complementary and indicated that a temperature of 3°C would prevent changes upon storage. DSC also indicated that with GMS materials, high temperature (50°C) storage accelerated transformation from an unstable α-form to the stable ß-form. However, with GPS materials, high temperature (50°C) storage expedited a change from amorphous to crystalline form of GPS.

Fast cooling of GMS materials affected the recombination of wax components and probably accelerated the change to the stable form, whilst slow cooling led to fractionation of wax components into different melting fractions. A temperature of 46°C was found to be the optimal for the annealing process to afford rapid conversion to the stable form.

For GMS, it could be concluded that the untreated GMS (ß-form) when melted and cooled provides the α-form which reverts progressively back to the stable ß-form during annealing. However in GPS, it could be concluded that the melt-solidified GPS presented a partially amorphous layered structure initially which then progressively crystallised after annealing.

XRPD proved a useful technique in characterising structural change of the wax materials. High temperature thermal annealing (46°C) of both GMS and GPS had more pronounced affects on structure and physicochemical property than when annealing was performed at low temperature (25°C) with melt-solidified GMS

(composed of smaller molecular weight materials) taking remarkably less annealing time compared to melt-solidified GPS (composed of larger molecular weight materials).

The present study confirms that three analytical techniques were suitable for monitoring changes in the physicochemical properties of the wax materials when subjected to pharmaceutical processing.

CHAPTER 5

PHYSICOCHEMICAL EVALUATIONS OF WAX MATRIX FORMULATIONS

5.1 Introduction

From Chapter 4, thermal annealing was shown to affect physicochemical properties of GMS and GPS materials with polymorphic transformation and crystallisation being the main changes observed. The impact of these changes on the resultant performance of these materials as components of a formulation is studied in this Chapter with the aim of investigating physicochemical changes of wax matrix formulations upon thermal annealing.

The techniques of DSC, HSM, XRPD and dissolution test were used to monitor the changes of the wax matrix formulations. Slightly soluble paracetamol and freely water soluble diltiazem HCl were chosen as model drugs for the formulations because they are easy to analyse by UV spectrophotometry.

5.2 Methods

Sample preparation and analytical methods are provided below and referenced where appropriate to Chapter 2.

5.2.1 Effect of thermal annealing on GMS pellet formulations containing paracetamol

Pellets composed of 60% GMS, 30% DCP and 10% paracetamol were prepared by following the general warm spheronisation method (Section 2.5, Page 65) using a spheronisation temperature of 50°C and a spheronisation time of 4 minutes. Pellets within the size range of 1001 to 1180 μm were annealed in an air-tight amber glass

container at 46°C for fixed times (0, 1, 2, 4, 7 or 28 days) and then analysed by DSC (Section 2.4.6, Page 55) and dissolution test (Section 2.4.3, Page 50).

5.2.2 Effect of thermal annealing on GPS pellet formulations containing diltiazem HCl

Pellets composed of 90% GPS and 10% diltiazem HCl were prepared by following the general warm spheronisation method (Section 2.5, Page 65) using a spheronisation temperature of 45°C and a spheronisation time of 5 minutes. Pellets within the size range of 1001 to 1180 μm were annealed in an air-tight amber glass container at 25 or 46°C for fixed times (0, 4, 7, 14 or 28 days) and then analysed by DSC (Section 2.4.6, Page 55) and dissolution test (Section 2.4.3, Page 50).

5.2.3 Effect of thermal annealing on GPS pellet formulations with high diltiazem HCl loading

Adizem® XL (diltiazem HCl 120 mg pellets from Napp Pharmaceuticals Ltd., Cambridge, UK.) capsule was selected as the reference commercial product for dissolution testing. In this present study, pellets composed of 60% GPS and 40% diltiazem HCl were used to provide 120 mg of diltiazem HCl in one capsule (total weight ~ 300 mg). The formulations were prepared by following the general warm spheronisation method (Section 2.5, Page 65) using a spheronisation temperature of 45°C and a spheronisation time of 5 minutes. Pellets within the size range of 1001 to 1180 μm were annealed in an air-tight amber glass container at 25 or 46°C for fixed times (0, 4, 7 or 28 days) and then analysed by dissolution test (Section 2.4.3, Page 50).

5.2.4 Effect of thermal annealing on wax-drug mixtures

The wax–drug mixtures were composed of 10% diltiazem HCl and 90% wax (GMS or GPS). The wax was melted at a temperature above its melting point and drug was added gradually into the melted wax and solidified at 3°C for 1 hour and then analysed by HSM (Section 2.4.9, Page 61) and XRPD (Section 2.4.7, Page 57). Each

sample was annealed in an air-tight amber glass container at 25 or 46°C for 0, 4 or 28 days and then evaluated by HSM and XRPD

5.2.5 Effect of wax type on thermal annealing

Pellets composed of 60% wax (GMS, GDB or GPS), 30% DCP and 10% diltiazem HCl were prepared by following the general warm spheronisation method (Section 2.5, Page 65) using spheronisation temperatures of 45 - 50°C and a spheronisation times of 4 - 5 minutes. Pellets within the size range of 1001 to 1180 μm were annealed in an air-tight amber glass container at 46°C for fixed times (0, 4, 7 or 28 days) and then analysed by dissolution test (Section 2.4.3, Page 50).

5.2.6 Effect of wax content on thermal annealing

GMS pellets composed of GMS (40 – 90%), DCP (0 – 50%) and paracetamol (10%) were prepared by following the general warm spheronisation method (Section 2.5, Page 65) using a spheronisation temperatures of 50°C and a spheronisation time of 4 minutes. GPS pellets composed of GPS (60 – 90%), DCP (0 – 30%) and diltiazem HCl (10%) were prepared by following the general warm spheronisation method (Section 2.5, Page 65) using a spheronisation temperatures of 45°C and a spheronisation time of 5 minutes. Pellets within the size range of 1001 to 1180 μm were annealed in an air-tight amber glass container at 46°C for fixed times (0, 4, 7 or 28 days for GMS pellets as well as 0, 4, 14 or 28 days for GPS pellets) and then analysed by dissolution test (Section 2.4.3, Page 50).

5.2.7 Effect of drug type and content on thermal annealing

Sample preparation is described using the two methods below.

- Pellets composed of 10% drug (PCM or DTZ), 60% GMS and 30% DCP were prepared by following the general warm spheronisation method (Section 2.5, Page 65) using a spheronisation temperatures of 50°C and a

spheronisation time of 4 minutes. Pellets within the size range of 1001 to 1180 μm were annealed in an air-tight amber glass container at 46°C for fixed times (0, 1, 2, 3, 4, 7 or 28 days) and then analysed by dissolution test (Section 2.4.3, Page 50).

- Pellets composed of DTZ (10 – 40%), DCP (0 – 30%) and GPS (60%) were prepared by following the general warm spheronisation method (Section 2.5, Page 65) using a spheronisation temperatures of 45°C and a spheronisation time of 5 minutes. Pellets within the size range of 1001 to 1180 μm were annealed in an air-tight amber glass container at 46°C for fixed times (0, 4, 7 or 28 days) and then analysed by dissolution test (Section 2.4.3, Page 50).

5.3 Results and Discussion

5.3.1 Effect of thermal annealing on GMS pellet formulations containing paracetamol

5.3.1.1 Differential scanning calorimetry (DSC)

DSC was used to monitor the melting point, polymorphic transformation and crystallisation of the wax formulations. The DSC profiles of GMS pellets after annealing at 46°C are shown in Figure 5.1.

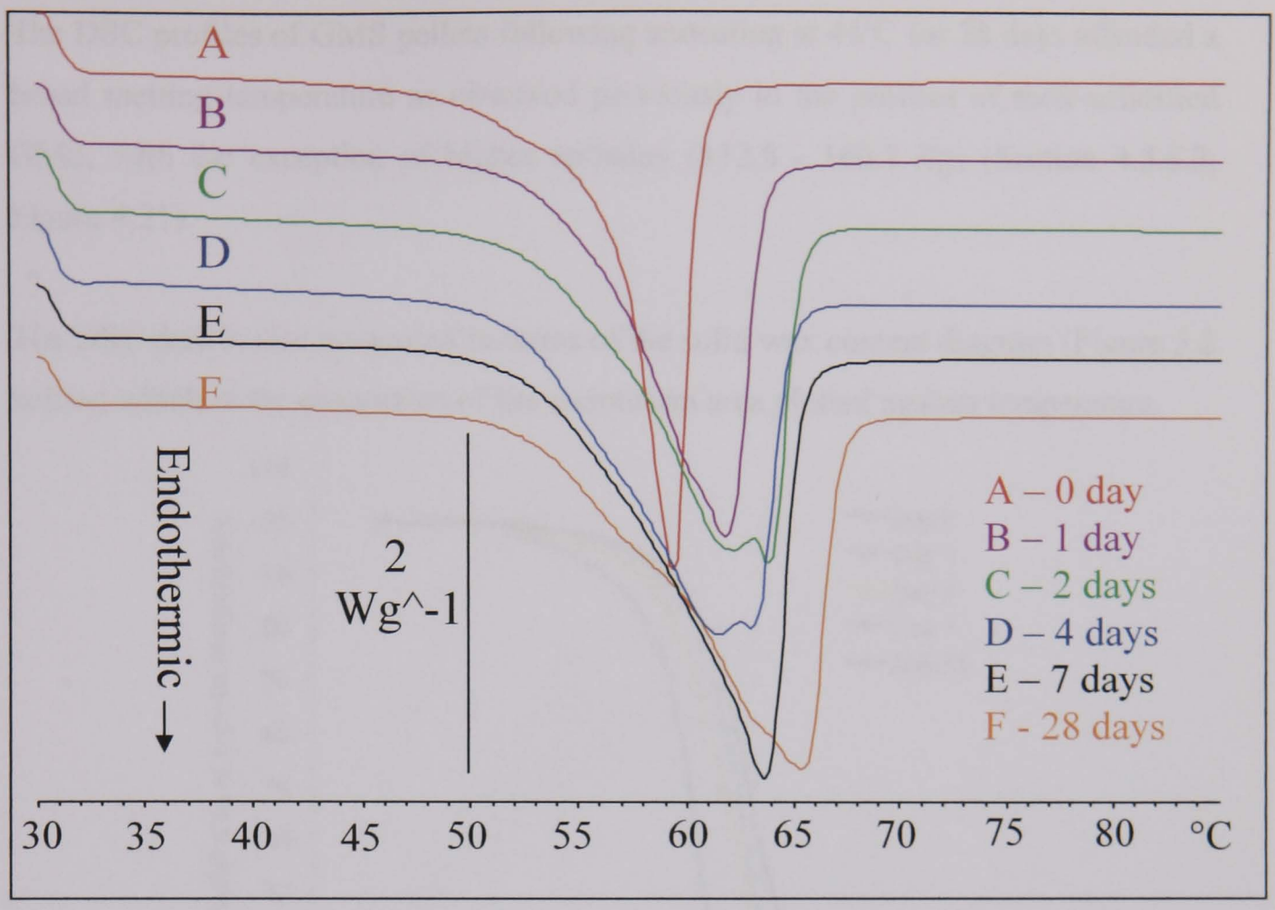

Figure 5.1. Effect of annealing at 46°C on DSC profiles of GMS-paracetamol pellets (scale bar = heat flow (2 watts per gram)).

Immediately following annealing at 46ºC there was an upward trend in the melting point together with a noticeable increase of enthalpy (ΔH) (Table 5.1). A shoulder peak was evident after 2 and 4 days annealing with endothermic broadening, however this transformed to a single peak at 7 days, with further development of a shoulder at 59.2ºC by the 28 day period.

Table 5.1. Effect of annealing time on the thermal characteristics of GMS-paracetamol pellets (from Figure 5.1).

Storage duration (days)	Melting point (ºC)	Enthalpy (ΔH) (J/g)
0	58.9	76.0
1	61.7	90.0
2	62.2, 63.6	101.9
3	62.1, 64.0	112.7
4	63.1, 62.0	107.2
5	62.5, 63.9	108.3
6	62.2	96.7
7	63.1	108.3
28	59.2, 65.2	108.9

The DSC profiles of GMS pellets following annealing at 46°C for 28 days afforded a broad melting temperature as observed previously in the profiles of melt-solidified GMS, with the exception of higher enthalpy (112.8 - 160.7 J/g) (Section 4.3.5.2, Figure 4.21).

The DSC data is also presented in terms of the solid wax content diagram (Figure 5.2 below) which is the proportion of the endotherm area plotted against temperature.

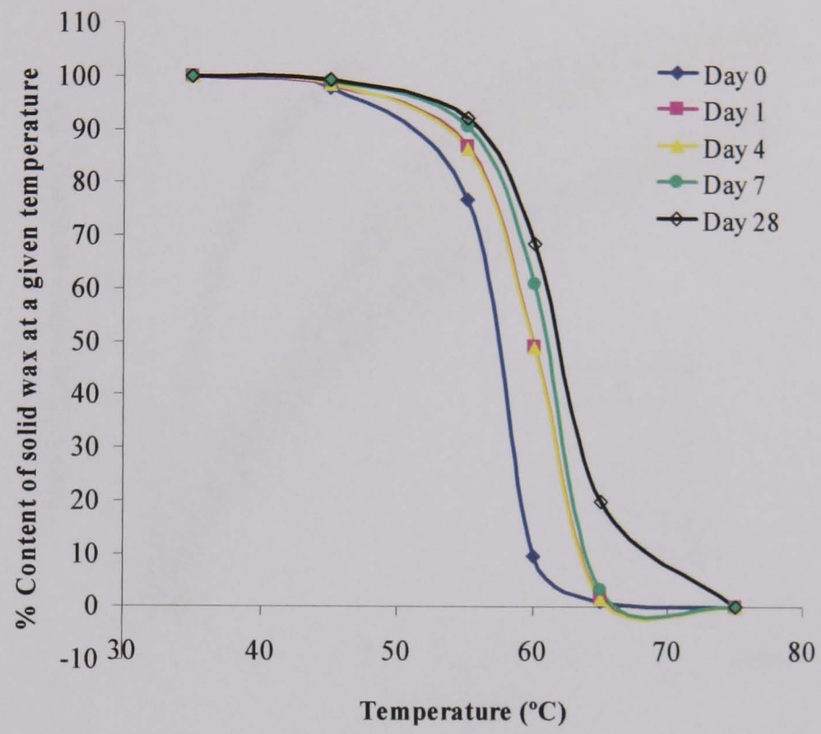

Figure 5.2. Percent content of solid wax as a function of temperature of GMS-paracetamol pellets after annealing at 46°C.

The proportion of the wax in the solid state at a given temperature increases with annealing time. The percent content of solid wax following application of heat was lower in those GMS pellets that had not been subjected to annealing than in the samples which had been subjected to annealing at 46°C for 28 days.

Khan and Craig (2004) reported a similar study in which a solid dispersion containing Gelucire 50/13 and drug (10% paracetamol or caffeine) showed an increase in melting point and in the solid fat proportion when stored at 37°C for 180 days. Moreover, Shimpi et al. (2004) reported similar findings in aged granules (30 days at room temperature) containing Gelucire 43/01.

5.3.1.2 Dissolution studies

As annealing time increased from initial to 4 days, there was a decrease in drug dissolution rate (Figure 5.3). From day 4 – 28, no further significant changes occurred in dissolution rate (Fit factor for statistical analysis with $f_1 < 15\%$ and $f_2 > 50\%$; Appendix I, Table I.2.1).

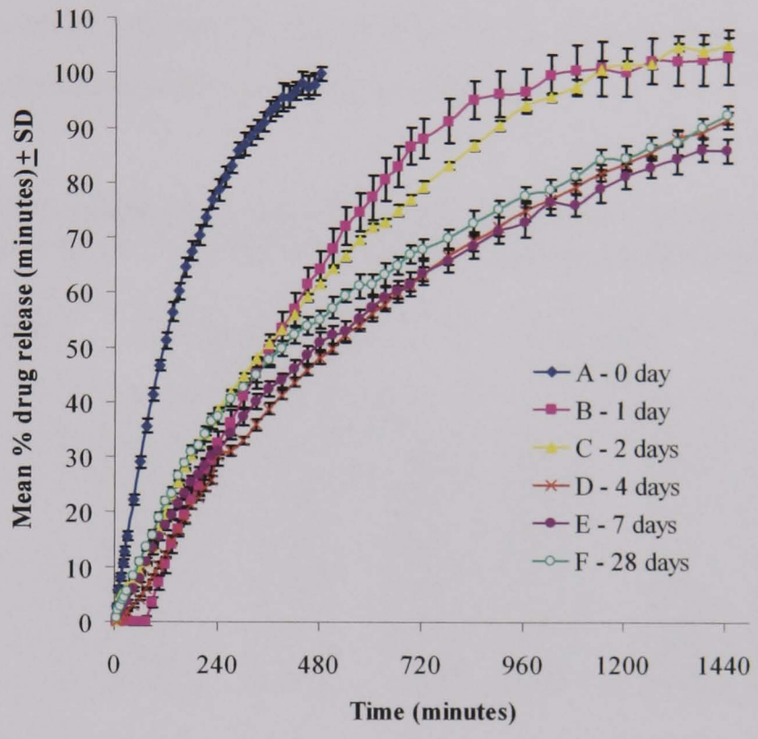

Figure 5.3. Dissolution profiles of formulations containing of 60% GMS, 30% DCP and 10% paracetamol after annealing for 1, 2, 4, 7 or 28 days at 46°C (n = 6).

The decrease in dissolution profiles of GMS pellets upon annealing was possibly caused by polymorphic transformation of the GMS component. Yajima et al. (2002) suggested that the melt-solidified GMS yielded the α-form that was continually transformed to the stable ß-form under ambient conditions. The α-form of GMS had better wetting and foaming properties as well as lower melting point and density compared to the ß-form. Consequently aged GMS pellets with annealing at 46°C provided the ß-form with decreased dissolution profiles.

A decrease in nifedipine release from wax tablet formulations containing Gelucire 53/10 was reported by Remunan et al. (1992) when stored at 40°C and 80% RH for 6

months. They suggested this was due to formation of drug microcrystals and polymorphic structural changes in the wax.

The dissolution profiles (from Figure 5.3) were fitted to Korsmeyer-Peppas ($Q_t/Q_\infty = K_k t^n$), zero order ($Q_t = Q_0 + K_0 t$) and Higuchi ($Q_t = K_H t^{1/2}$) models described in Section 1.1. The n (release exponent) describes the mechanism of drug release, with n nearer to 0.5 indicating a dominance of diffusion and n closer to 1.0 indicating a dominance of erosion whereas K_k, K_0 and K_H are Korsmeyer-Peppas, zero order and Higuchi constants respectively as shown in Table 5.2.

Table 5.2. Kinetic parameters describing the dissolution profiles of formulations containing of 60% GMS, 30% DCP and 10% paracetamol annealing at 46°C.

Storage duration (days)	Korsmeyer-Peppas model			Zero order model		Higuchi model	
	r^2	n	K_k	r^2	K_0	r^2	K_H
0	0.992	0.71	1.66	0.974	0.32	0.944	4.82
1	0.986	1.06	0.09	0.990	0.14	0.805	2.60
2	0.994	0.73	0.66	0.971	0.11	0.939	2.81
4	0.987	0.73	0.49	0.973	0.09	0.926	2.22
7	0.989	0.63	1.00	0.955	0.08	0.965	2.27
28	0.987	0.58	1.46	0.932	0.08	0.976	2.47

From the three models, the dissolution profiles of GMS pellets fitted the Korsmeyer-Peppas model the best, as observed from coefficient of determination (r^2) closest to 1. The initial GMS pellets showed the n value of 0.71 indicating a combination of diffusion and erosion of paracetamol release. After annealing at 46°C for 28 day, the drug release mechanism changed to a predominant diffusion mechanism as observed by a decrease in n value to 0.58.

From Figure 5.3, the relationship between annealing time and mean times to drug release can be obtained as shown in Figure 5.4.

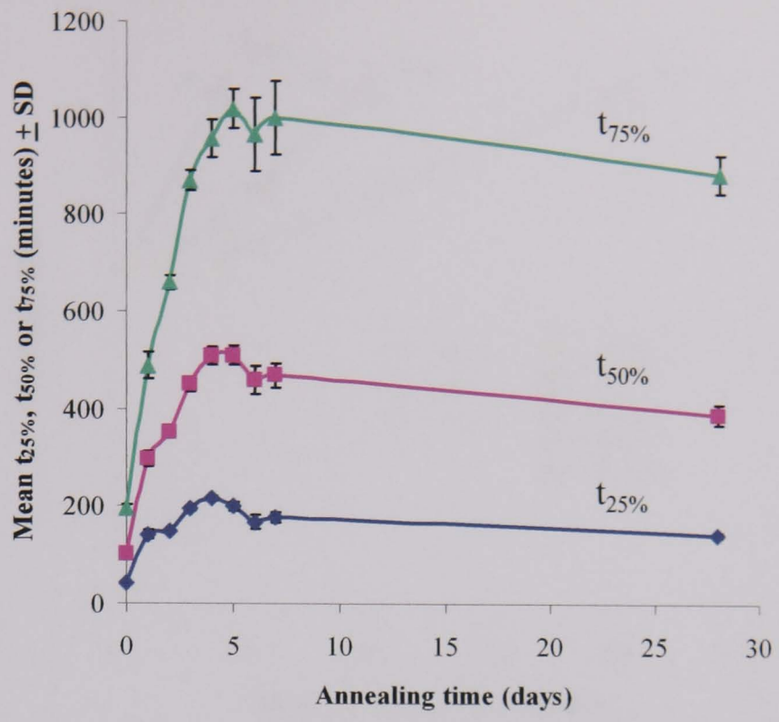

Figure 5.4. Effect of pellet annealing on mean times to 25%, 50% or 75% drug release ($t_{25\%}$, $t_{50\%}$ or $t_{75\%}$) of formulations containing 60% GMS, 30% DCP and 10% paracetamol after annealing for 1, 2, 4, 7 or 28 days at 46°C (n = 6).

The observed profiles for $t_{25\%}$, $t_{50\%}$ and $t_{75\%}$ were similar with a distinct change being observed over the first 4 days, followed by a plateau. Therefore thermal annealing at 46°C for up to 4 days provided an opportunity to transform GMS to its most stable polymorph and stabilise subsequent drug release profiles.

5.3.1.3 Correlation between DSC and dissolution profiles

A correlation between DSC and dissolution profiles is portrayed in Figure 5.5.

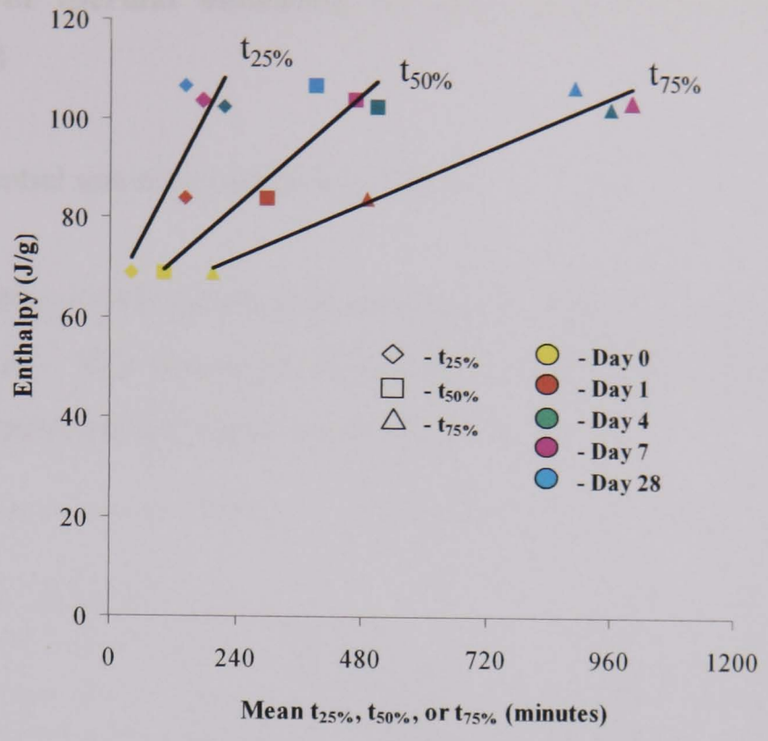

Figure 5.5. Plot of enthalpy vs mean times to 25%, 50% or 75% drug release ($t_{25\%}$, $t_{50\%}$ or $t_{75\%}$) for formulations containing 60% GMS, 30% DCP and 10% paracetamol after annealing at 46°C (n = 6).

The mathematical values derived from the plots in Figure 5.5 are shown in Table 5.3.

Table 5.3. Mathematical parameters relating to plots shown in Figure 5.5.

Time drug release	Slope (m)	Y-intercept (b)	Coefficient of determination (r^2)
$t_{25\%}$	0.208	62.967	0.694
$t_{50\%}$	0.093	60.021	0.864
$t_{75\%}$	0.046	60.789	0.960

From Figure 5.5, an increase in $t_{25\%}$, $t_{50\%}$ or $t_{75\%}$ from initial to 4 days was associated with an increase in enthalpy (ΔH) and followed plateau after 4 days. This demonstrates that enthalpy (ΔH) in GMS formulations annealed at 46°C correlated linearly to mean times to 25%, 50% or 75% drug release with the $t_{75\%}$ data showing the best correlation ($r^2 = 0.960$).

5.3.2 Effect of thermal annealing on GPS pellet formulations containing diltiazem HCl

5.3.2.1 Differential scanning calorimetry (DSC)

The DSC profiles of GPS pellets after annealing at 46 and 25°C are shown in Figures 5.6 – 5.7 below. The numerical values for melting point and enthalpy (ΔH) at individual temperatures and times are shown in Table 5.4.

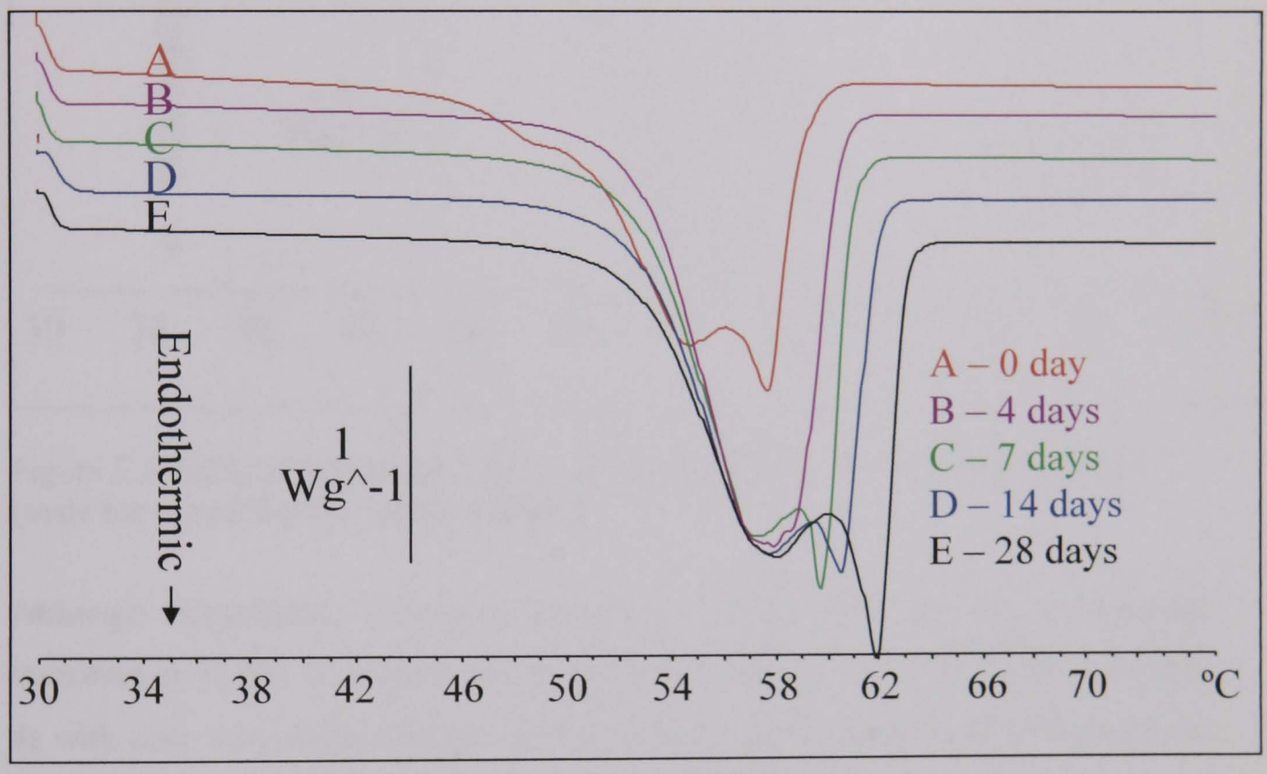

Figure 5.6. Effect of annealing at 46°C on DSC profiles of GPS-diltiazem pellets (scale bar = heat flow (1 watt per gram)).

Immediately following annealing at 46°C the GPS lost the endothermic transition at 47.9 and 54.5°C and reverted to a material with a single broad endotherm at ~ 58°C (day 4) as observed previously in the profiles of melt-solidified GPS (Section 4.3.6.2, Figure 4.28). The aggregation of three peaks into one peak and disappearance of exothermic peaks of annealed GPS pellets at 46°C could be caused by the gradual crystallisation of GPS during the 4 days annealing. Moreover, enthalpy (ΔH) of annealed GPS pellets at 46°C for 4 days and greater increased substantially compared to the initial GPS formulations. The DSC profiles of GPS pellets following

annealing at 46°C for 28 days afforded a higher melting temperature with higher enthalpy.

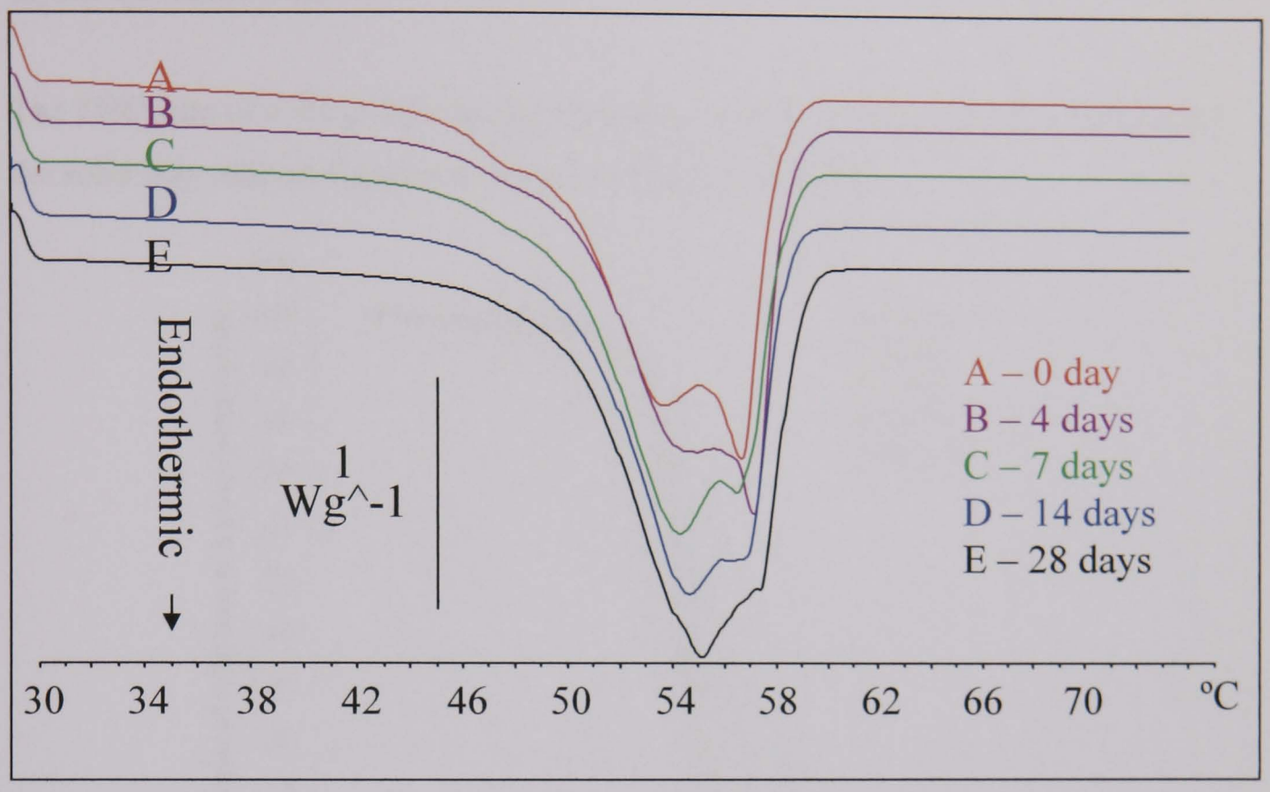

Figure 5.7. Effect of annealing at 25°C on DSC profiles of GPS-diltiazem pellets (scale bar = heat flow (1 watt per gram)).

Although immediately following annealing at 25°C GPS lost the endothermic transition at 47.9°C, it retained two endothermic peaks at 55.3 and 58.0°C (after day 4) with only very slight changes in the enthalpy (ΔH) of annealed GPS pellets at 25°C being observed at longer times of annealing (Table 5.4).

Table 5.4. Effect of annealing time and temperature on the thermal characteristics of GPS pellets (from Figures 5.6 – 5.7).

Annealing temperature Storage duration (days)	Melting point (°C)		Enthalpy (ΔH) (J/g)	
	25°C	*46°C*	*25°C*	*46°C*
0	47.9, 54.5, 57.6	47.9, 54.5, 57.6	125.9	128.3
4	55.3, 58.0	57.8	126.2	148.2
7	55.2, 57.4	57.0, 59.5	127.0	151.5
14	55.4, 57.6	57.4, 60.4	127.5	153.5
28	55.9, 57.5	57.8, 61.7	134.7	165.1

It is concluded that GPS component in pellets crystallised gradually during thermal annealing and that a higher annealing temperature (46°C) accelerated the crystallisation process.

The DSC data of GPS pellets during annealing at 46°C is also exhibited in terms of the solid wax content diagram as shown in Figure 5.8 below.

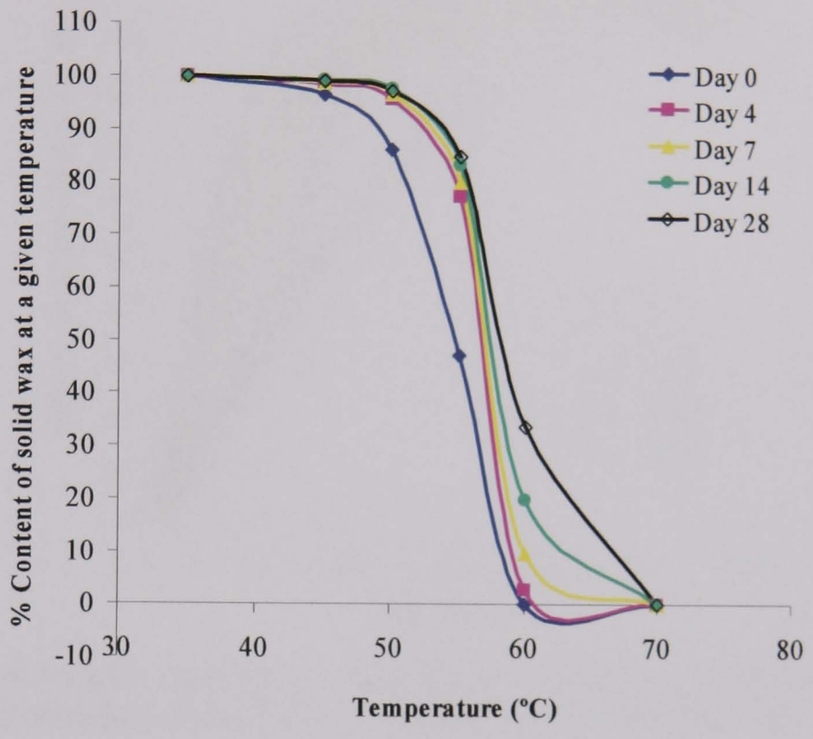

Figure 5.8. Percent content of solid wax as a function of temperature of GPS-diltiazem HCl pellets after annealing at 46°C.

This followed a similar trend to GMS-paracetamol pellets (Figure 5.2) with increasing annealing time resulting in an increase in the proportion of the wax in the solid state at a given temperature. The percent content of solid wax following application of heat was lower in those GPS pellets that had not been subjected to annealing than in the samples which had been subjected to annealing at 46°C for 28 days.

5.3.2.2 Dissolution studies

The result of the effect of annealing time and temperature (46°C) on GPS pellets is shown in Figure 5.9 below.

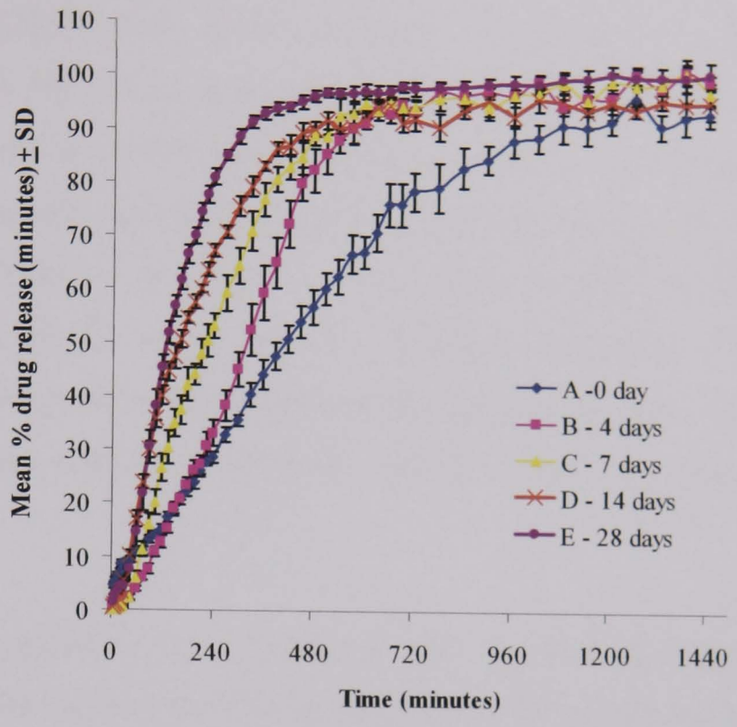

Figure 5.9. Dissolution profiles of formulations containing of 90% GPS and 10% diltiazem HCl after annealing for 4, 7, 14 and 28 days at 46°C (n = 6).

Increasing annealing time from 0 to 14 days significantly increased drug dissolution rate as shown in Figure 5.9 (with $f_1 > 15\%$ and $f_2 < 50\%$; Appendix I, Table I.2.2.1), however, the dissolution profiles of pellets annealed between 14 and 28 days were similar when analysed using Fit factors (with $f_1 < 15\%$ and $f_2 > 50\%$).

The increase in dissolution profiles of GPS pellets during annealing at 46°C was possibly caused by GPS crystallisation from a heterogeneous composition composed mainly of di- and triglycerides. Laine et al. (1988) found that the freshly melted triglycerides provided a partially amorphous layered structure which gradually crystallised with time. The formation of large wax crystals may result in enhanced porosity which then facilitates dissolution medium penetration with associated enhanced dissolution rate (Khan and Craig, 2004; Choy et al., 2005). The further

observation of morphological changes in annealed GPS pellets using Texture Analyser, scanning electron microscope (SEM) and polarised light microscopy is described in Chapter 6.

An increase in the drug release of GPS formulations was also observed by Reitz and Kleinebudde (2007) with solid extrusion formulations containing GPS and theophylline (50:50). Drug dissolution increased after 9 months of storage at 40°C and was attributed to a GPS ageing process. In addition, acceleration in drug release profiles from capsules containing paracetamol and Gelucire 50/13 was also observed during ageing (Choy et al., 2005). In that study, the drug dissolution profiles of samples stored for 22 weeks at 37°C increased noticeably. The authors also suggested that the wax formed large crystals upon polymorphic transformation to a more stable form, leading to increased porosity which then speeded up the drug release rate.

The dissolution profiles (from Figure 5.9) were fitted to Korsmeyer-Peppas, zero order and Higuchi models described in Section 1.1. The n (release exponent), K_k, K_0 and K_H were shown in Table 5.5.

Table 5.5. Kinetic parameters describing the dissolution profiles of formulations containing of 90% GPS and 10% diltiazem HCl after annealing at 46°C.

Storage duration (days)	Korsmeyer-Peppas model			Zero order model		Higuchi model	
	r^2	n	K_k	r^2	K_0	r^2	K_H
0	0.989	0.80	0.39	0.974	0.10	0.905	2.55
4	0.997	1.31	0.03	0.990	0.18	0.732	2.65
7	0.981	0.94	0.29	0.971	0.21	0.838	3.41
14	0.977	0.79	0.84	0.973	0.24	0.895	3.98
28	0.980	1.01	0.32	0.955	0.36	0.822	4.42

From the three models, the dissolution profiles of GPS pellets fitted the Korsmeyer-Peppas model the best, as observed from coefficient of determination (r^2) closet to 1. The initial GPS pellets showed the n value of 0.80 indicating a combination of diffusion and erosion of diltiazem HCl release. After annealing at 46°C for 28 day, the drug release mechanism changed to predominant erosion observed by an increase

in n value to 1.01. Khan and Craig (2004) reported that an increase in the ratio of erosion to diffusion of caffeine and paracetamol release from Gelucire 50/13 matrix formulations after storage 180 days at 37°C was observed. This implied that drug release mechanism changed from diffusion to erosion pathways.

The result of the effect of annealing time and temperature (25°C) on GPS pellets is shown in Figure 5.10 below.

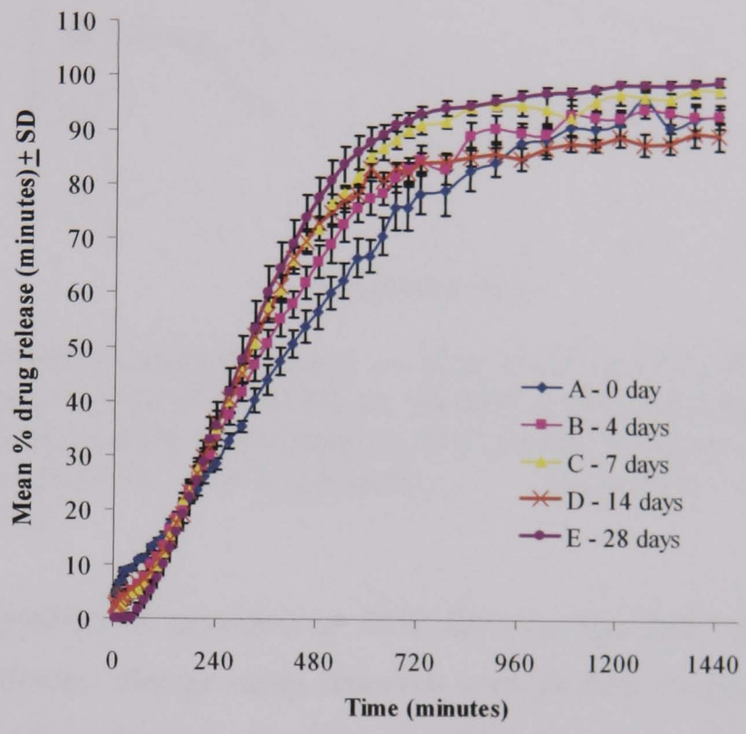

Figure 5.10. Dissolution profiles of formulations containing of 90% GPS and 10% diltiazem HCl after annealing for 4, 7, 14 and 28 days at 25°C (n = 6).

The GPS pellets exhibited no significant changes of dissolution profiles after annealing for 28 days at 25°C as assessed using Fit factor (with $f_1 < 15\%$ and $f_2 > 50\%$; Appendix I, Table I.2.2.2). At this annealing temperature, small changes in thermal profiles are observed (Figure 5.7 and Table 5.4). It is evident that a higher annealing temperature (46°C) had a more pronounced effect on the crystallisation process of GPS in the formulation than was seen at the lower temperature (25°C).

From Figures 5.9 - 5.10, the relationship between annealing time and mean times to drug release can be obtained as shown in Figure 5.11.

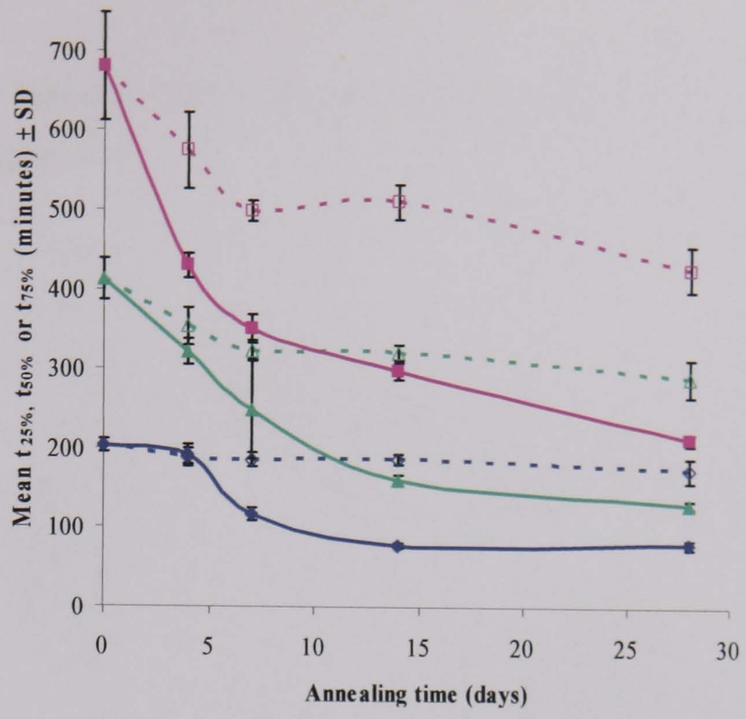

Figure 5.11. Effect of pellet annealing on mean times to 25%, 50% or 75% drug release ($t_{25\%}$, $t_{50\%}$ or $t_{75\%}$) of formulations containing 90% GPS and 10% diltiazem HCl after annealing at 46°C (solid lines) or 25°C (dotted lines) (n = 6) (—◆— $t_{25\%}$ at 46°C; - ◇ - $t_{25\%}$ at 25°C; —▲— $t_{50\%}$ at 46°C; - △ - $t_{50\%}$ at 25°C; —■— $t_{75\%}$ at 46°C; - □ - $t_{75\%}$ at 25°C).

The observed profiles of annealing at 46°C for $t_{25\%}$, $t_{50\%}$ and $t_{75\%}$ were generally similar with a distinct change being observed over the first 14 days, followed by a plateau. Therefore thermal annealing at 46°C for up to 14 days permitted stabilisation of drug release profiles of GPS pellets. However, the $t_{25\%}$, $t_{50\%}$ and $t_{75\%}$ in pellets annealed at 25°C were similar indicating constant drug release. In a similar situation, Roussin and Duddu (2001) noted that thermal annealing of a Gelucire 50/13–theophylline matrix at 40°C for about 2 weeks maintained a constant rate of drug release.

However, since thermal annealing is an impractical method for use at large scale in the pharmaceutical industry, alternative methods to stabilise drug release profiles are investigated in Chapter 7.

5.3.2.3 Correlation between DSC and dissolution profiles

A correlation between DSC and dissolution profiles for GPS formulations is portrayed in Figure 5.12.

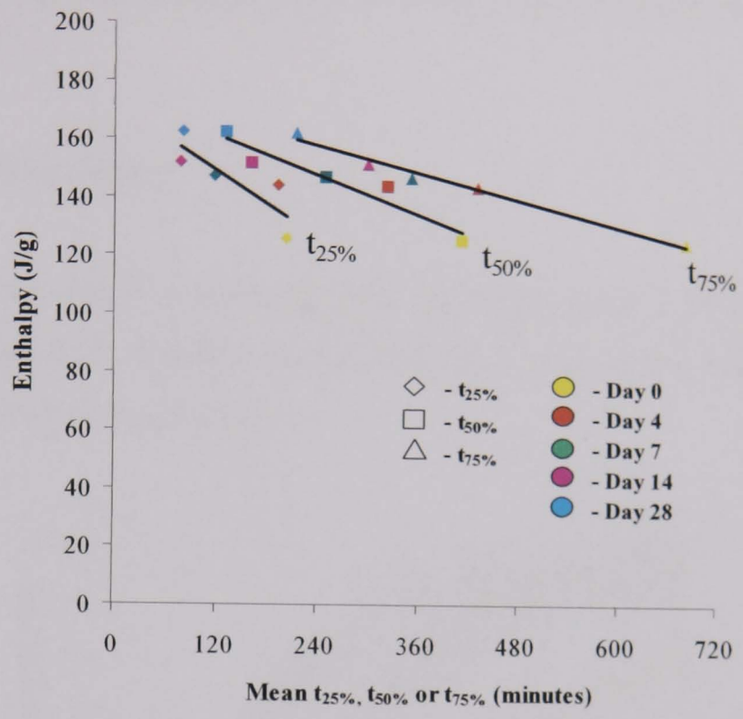

Figure 5.12. Plot of enthalpy vs mean times to 25%, 50% or 75% drug release ($t_{25\%}$, $t_{50\%}$ or $t_{75\%}$) for formulations containing 90% GPS and 10% diltiazem HCl after annealing at 46°C (n = 6).

The mathematical values derived from the plots in Figure 5.12 are shown in Table 5.6.

Table 5.6. Mathematical parameters relating to plots shown in Figure 5.12.

Time of drug release	Slope (m)	Y-intercept (b)	Coefficient of determination (r^2)
$t_{25\%}$	-0.190	171.98	0.719
$t_{50\%}$	-0.111	174.75	0.906
$t_{75\%}$	-0.075	175.92	0.977

From Figure 5.12, a decrease in $t_{25\%}$, $t_{50\%}$ or $t_{75\%}$ from initial to 28 days was associated with an increase in enthalpy (ΔH). The data demonstrates that enthalpy (ΔH) in GPS formulations annealed at 46°C correlated linearly with mean times to 25%, 50% or 75% drug release with $t_{75\%}$ showing the best correlation ($r^2 = 0.977$).

The slope of the correlation of GPS pellets with enthalpy was negative; being the opposite of the relationship previously reported for the GMS formulations (Figure 5.5 and Table 5.3).

5.3.3 Effect of thermal annealing on GPS pellet formulations with high diltiazem HCl loading

5.3.3.1 Dissolution studies

The results of the effect of annealing time and temperature at 46 and 25°C on GPS pellets with high dose loading are compared to a commercial product as shown in Figures 5.13 and 5.14 respectively.

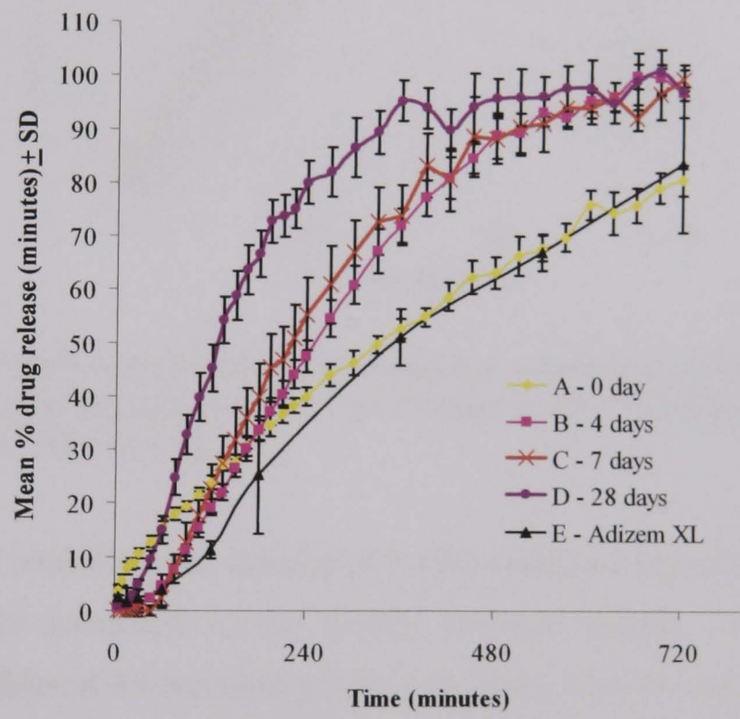

Figure 5.13. Dissolution profiles of formulations containing of 60% GPS and 40% diltiazem HCl after annealing for 4, 7 or 28 days at 46°C compared to commercial pellets (Adizem® XL) (n = 6).

The drug release profile of commercial product was similar to that of initial GPS pellets composed of 60% GPS and 40% diltiazem HCl. However, when GPS pellets were annealed at 46°C for 4 days or longer, their dissolution profiles exhibited significant differences with increasing drug release rates compared to the commercial

pellets (using Fit factor for statistical analysis with $f_1 > 15\%$ and $f_2 < 50\%$; Appendix I, Table I.2.3.1).

Such changes were previously attributed to crystallisation of the GPS in the 10% diltiazem formulation (see Section 5.3.2).

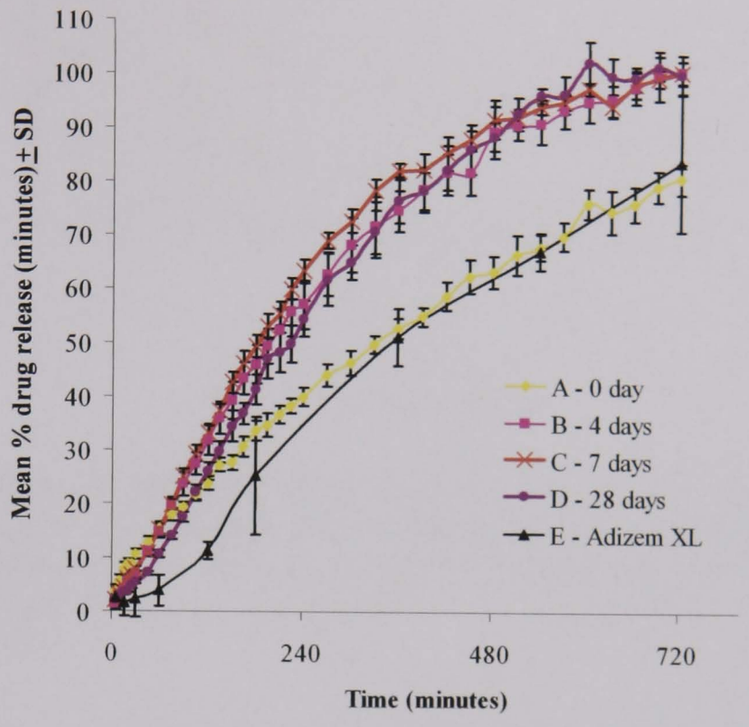

Figure 5.14. Dissolution profiles of formulations containing of 60% GPS and 40% diltiazem HCl after annealing for 4, 7 or 28 days at 25°C compared to commercial pellets (Adizem® XL) (n = 6).

After 4 days of annealing, the dissolution profile stabilised and afforded a faster rate of drug release compared to the freshly prepared sample. Furthermore, the dissolution profiles of the annealed pellets were faster than the commercial Adizem® XL formulation. This was statistically confirmed using Fit factor for statistical analysis (with $f_1 > 15\%$ and $f_2 < 50\%$; Appendix I, Table I.2.3.2) with significant differences in dissolution profiles observed between commercial pellets and annealed samples at 25°C, however, the dissolution profiles of initial GPS pellets and commercial products were similar.

From Figures 5.13 - 5.14, the relationship between annealing time and mean times to drug release can be obtained as shown in Figure 5.15.

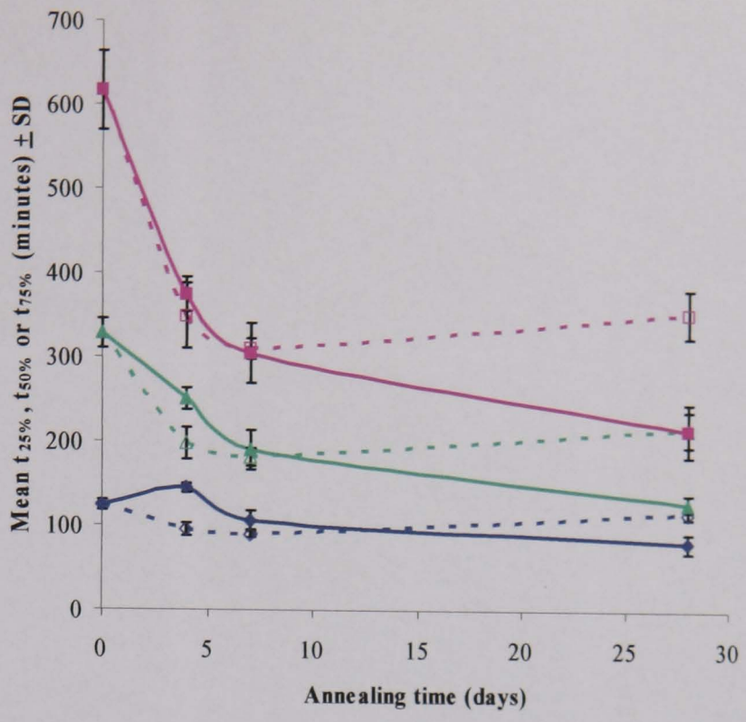

Figure 5.15. Effect of pellet annealing on mean times to 25%, 50% or 75% drug release ($t_{25\%}$, $t_{50\%}$ or $t_{75\%}$) of formulations containing 60% GPS and 40% diltiazem HCl after annealing at 46°C (solid lines) or 25°C (dotted lines) (n = 6) (—◆— $t_{25\%}$ at 46°C; - ◇ - $t_{25\%}$ at 25°C; —▲— $t_{50\%}$ at 46°C; - △ - $t_{50\%}$ at 25°C; —■— $t_{75\%}$ at 46°C; - □ - $t_{75\%}$ at 25°C).

The $t_{25\%}$, $t_{50\%}$ and $t_{75\%}$ profiles for pellets annealed at 46°C were similar with a distinct change being observed over the 28 days. In contrast the $t_{25\%}$, $t_{50\%}$ and t_{75} of pellets annealed at 25°C showed greater consistency reaching a plateau after 4 days of storage. Interestingly, the physicochemical transformations were observed to be more rapid with formulations containing 10% diltiazem (Section 5.3.2.2) and it could be suggested that annealing time is affected by the influence of drug content. This is further investigated in Section 5.3.7 below.

5.3.4 Effect of thermal annealing on wax-drug mixtures

5.3.4.1 Hot stage microscopy (HSM) of GMS-diltiazem mixtures

The HSM photographs of GMS-diltiazem mixtures after annealing at 25 or 46°C are shown in Figure 5.16. Images were recorded to observe any changes during the temperature range of 50 to 65°C.

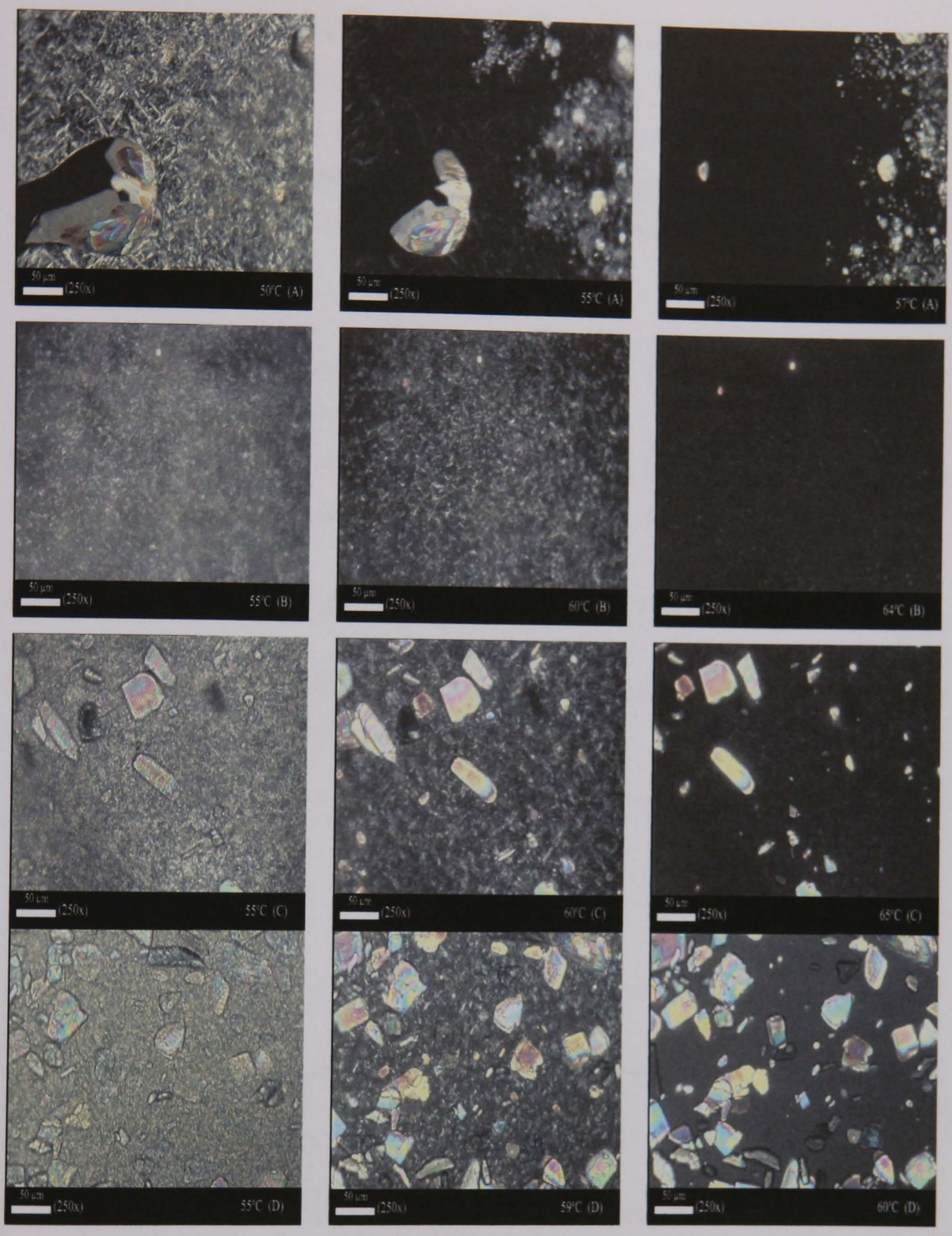

Figure 5.16. Hot stage polarising microscope photographs of melt-solidified GMS-diltiazem mixtures following (**A**) no annealing, (**B**) annealing for 4 days at 46°C, (**C**) annealing for 28 days at 46°C or (**D**) annealing for 28 days at 25°C.

The diltiazem crystals were clearly identifiable using HSM with polarised light. The formulations would appear to exist as solid dispersions (as opposed to a solid solution) as observed by the existence of birefringent crystals. Such a formulation was anticipated given the relative water solubility of diltiazem and its elevated

melting point (207.5 - 212.0°C). From Figure 5.16A, when heated from 50 to 55°C, GMS partially melted leaving residual crystals visible. By 57°C, the entire GMS sample had melted. With annealed product (46°C for 4 days, Figure 5.16B), the melting temperature of GMS increased substantially to 64°C. When annealed at 46°C for 28 days (Figure 5.16C), the GMS melting temperature had further increased to 65°C.

However, the GMS-diltiazem mixtures annealed for 28 days at 25°C (Figure 5.16D) only exhibited a small increase in melting temperature (60°C). This confirmed that the higher annealing time of 46°C exerted a more significant effect on the melting temperature of GMS in mixtures than occurred after lower temperature annealing.

5.3.4.2 X-ray powder diffraction (XRPD) of GMS-diltiazem mixtures

The comparisons of X-ray diffractograms in GMS-diltiazem mixtures after annealing at 25 or 46°C are shown in Figure 5.17 below

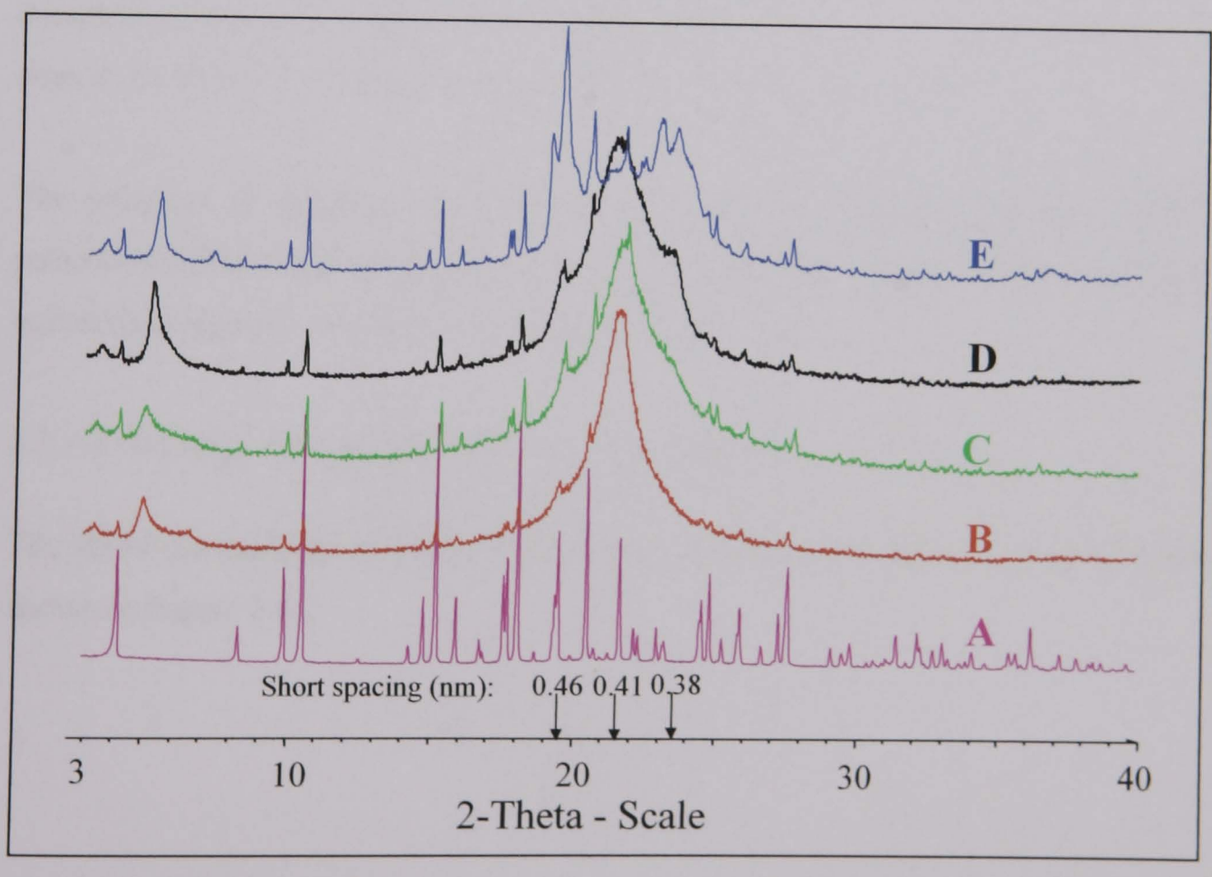

Figure 5.17. X-ray diffractograms of (**A**) diltiazem HCl or melt-solidified GMS-diltiazem mixture following (**B**) no annealing, (**C**) annealing for 28 days at 25°C, (**D**) annealing for 4 days at 46°C or (**E**) annealing for 28 days at 46°C.

The XRPD patterns of diltiazem HCl (Figure 5.17A) showed clusters of several small peaks at 2θ angles of around 15.5°, 18.0°, 19.5°, 20.5°, 22.0°, 22.0° and 25° - 28°. The XRPD patterns of melt-solidified GMS-diltiazem mixture (Figure 5.17B) showed a main peak at 2θ angles of 21.5° (d = 0.41 nm) indicating the α-form of GMS and three small peaks at 2θ angles of 18.0°, 19.5° and 20.5° indicating diltiazem in a crystalline form. The mixture annealed for 28 days at 25°C (Figure 5.17C) still retained four peaks at 2θ angles of 18.0°, 19.5°, 20.5° and 21.5° (main) which are similar to freshly melt-solidified sample.

However, XRPD patterns of annealed mixture at 46°C for 4 days (Figure 5.17D) retained four peaks at 2θ angles of 18.0°, 19.5°, 20.5° and 21.5° (main), with the development of a new peak at 2θ angles of 23.5° (d = 0.38 nm) suggesting the occurrence of polymorphic GMS changes while the characteristic diltiazem patterns remained. After annealing for 28 days at 46°C (Figure 5.17E), the patterns showed seven small peaks at 2θ angles of 18.0°, 19.0°, 20.5°, 22.0°, 22.5°, 23.0° and 23.5° (d = 0.38 nm) as well as a main peak at 2θ angles of 19.5° (d = 0.46 nm) indicating complete conversion to the ß-form of GMS as observed from the disappearance of a peak at 21.5° (d = 0.41 nm) with retention of the diltiazem patterns.

The presence of diltiazem HCl did not influence the physical changes of XRPD patterns of GMS-diltiazem mixtures which showed similar pattern to annealed GMS materials (Figures 4.24 and 4.25, Section 4.3.5.4).

5.3.4.3 Hot stage microscopy (HSM) of GPS-diltiazem mixtures

The HSM photographs of GPS-diltiazem mixtures after annealing at 25 or 46°C are shown in Figure 5.18.

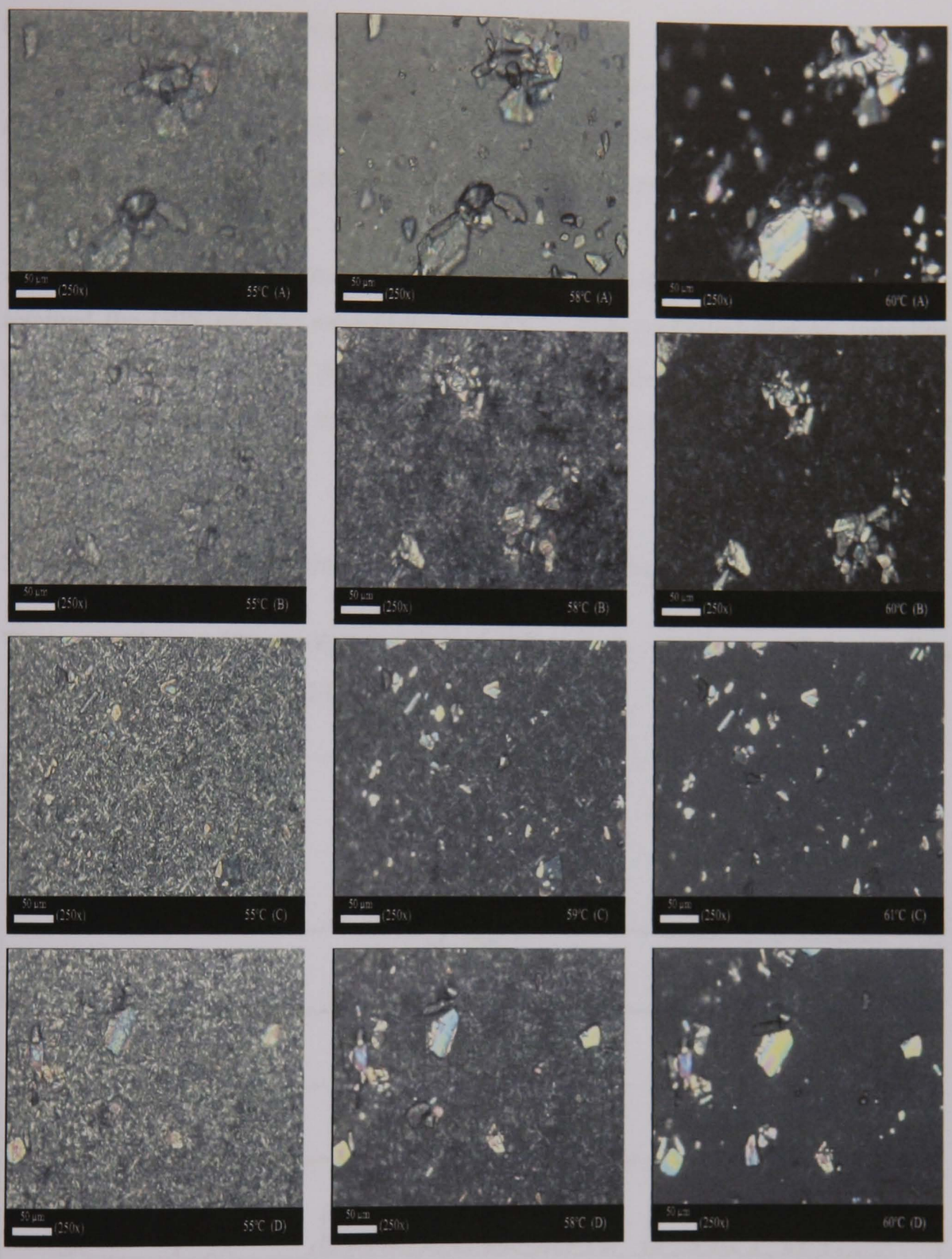

Figure 5.18. Hot stage polarising microscope photographs of melt-solidified GPS-diltiazem mixtures following (**A**) no annealing, (**B**) annealing for 4 days at 46°C, (**C**) annealing for 28 days at 46°C or (**D**) annealing for 28 days at 25°C.

The diltiazem crystals were clearly identifiable using HSM with polarised light. The GPS formulations appear to exist as solid drug dispersions as observed by the existence of birefringent crystals. From Figure 5.18A, when heated from 55 to 58°C,

GPS partially melted leaving residual crystals visible. By 60°C, the entire GPS sample had melted. With annealed product (46°C for 4 days, Figure 5.18B), the melting temperature of GPS remained at 60°C. When annealed at 46°C for 28 days (Figure 5.18C), the melting temperature of GPS had increased to 61°C.

However, the GPS-diltiazem mixtures annealed for 28 days at 25°C (Figure 5.18D) retained the GPS melting temperature of 60°C. This confirmed that an annealing temperature of 25 or 46°C had a small effect on the melting range temperature of GPS-diltiazem admixtures and correlated to the DSC results (Figures 5.6 - 5.7 and Table 5.4).

5.3.4.4 X-ray powder diffraction (XRPD) of GPS-diltiazem mixtures

The comparisons of X-ray diffractograms in GPS- diltiazem mixtures after annealing at 25 or 46°C are shown in Figure 5.19 below.

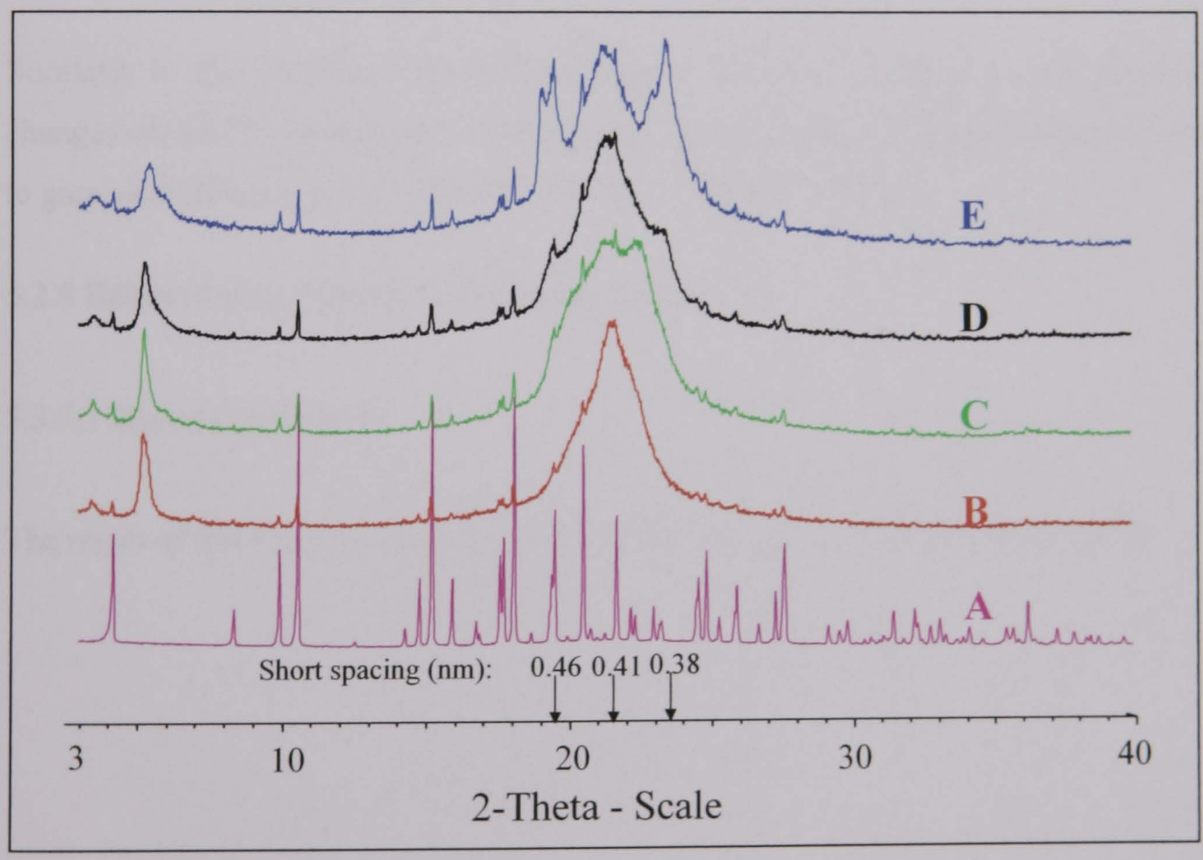

Figure 5.19. X-ray diffractograms of (**A**) diltiazem HCl or melt-solidified GPS-diltiazem mixture following (**B**) no annealing, (**C**) annealing for 28 days at 25°C, **(D)** annealing for 4 days at 46°C or **(E)** annealing for 28 days at 46°C.

The XRPD patterns of diltiazem HCl (Figure 5.19A) showed clusters of several small peaks at 2θ angles of around 15.5°, 18.0°, 19.5°, 20.5°, 22.0°, 22.0° and 25° - 28°. The XRPD patterns of melt-solidified mixture of GPS and diltiazem (Figure 5.19B) showed a main peak at 2θ angles of 21.5° (d = 0.41 nm) and three small peaks at 2θ angles of 18.0°, 19.5° and 20.5° indicating diltiazem in a crystalline form. The samples annealed for 28 days at 25°C (Figure 5.19C) showed four peaks at 2θ angles of 18.0°, 19.5°, 20.5° and 21.5°, with the development of two new peaks at 2θ angles of 21° and 22.5° attributable to development of a GPS crystalline form.

The XRPD patterns of annealed mixture at 46°C for 4 days (Figure 5.19D) showed little change, however after annealing for 28 days at 46°C (Figure 5.19E) eight peaks at 2θ angles of 18.0°, 19.0°, 19.5° (d = 0.46 nm), 20.5°, 21.5° (d = 0.41 nm), 22.5°, 23.0° and 23.5° (d = 0.38 nm) were evident indicating physical transformation of GPS. This change might reflect the increase in dissolution profiles of GPS pellets annealed for 28 days at 46°C as previously described in Figure 5.9.

Similarly to the situation with GMS, diltiazem HCl had no effect on the physical changes of XRPD patterns of GPS-diltiazem mixtures which showed similar pattern to annealed GPS materials (Figures 4.30 - 4.31, Section 4.3.6.3).

5.3.5 Effect of wax type on thermal annealing

5.3.5.1 Dissolution studies

The result of the effect of wax type on thermal annealing is shown in Figure 5.20.

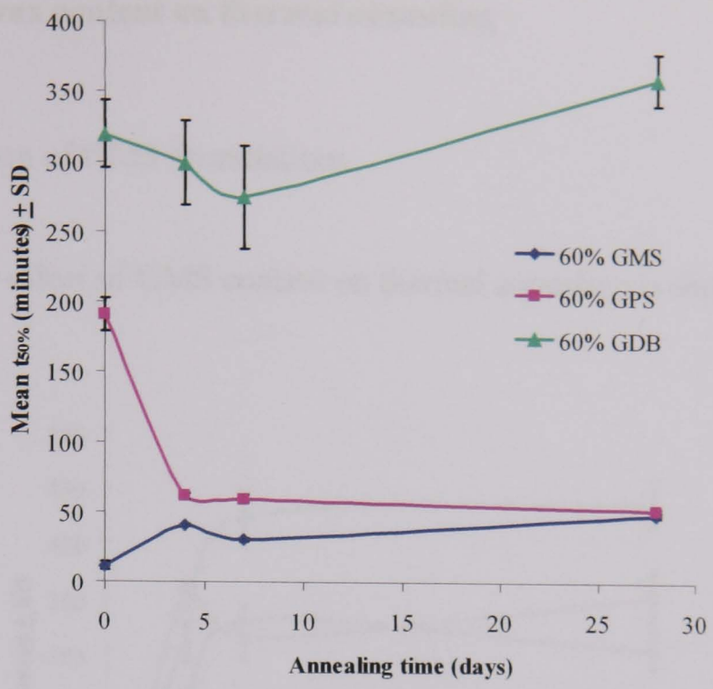

Figure 5.20. Effect of pellet annealing on mean time to 50% drug release ($t_{50\%}$) of formulations containing 60% wax, 30% DCP and 10% diltiazem HCl after annealing for 4, 7 or 28 days at 46°C (n = 6).

The annealing temperature of 46°C caused different effects in the $t_{50\%}$ for each wax formulation. With the GMS pellets, annealing time increased $t_{50\%}$ at 28 days suggesting a reduction of drug release rate caused by polymorphism transformation of the GMS component. In contrast, GPS pellets following annealing showed a marked increase in drug release rate (reduction in $t_{50\%}$) due to crystallisation of GPS component. However, in GDB pellets, annealing time had no statistically significant effect on the change of $t_{50\%}$.

In a similar situation, Reitz and Kleinebudde (2007) likewise reported an increase in the drug release of solid extrusion formulations containing GPS and theophylline (50:50) after 9 months of storage at 40°C, whereas no significant changes in the drug release of aged formulations containing glyceryl trimyristate and theophylline (50:50) were observed. They concluded that waxes with heterogeneous compositions (GPS) exhibited longer crystallisation time than homogeneous wax (glyceryl trimyristate).

5.3.6 Effect of wax content on thermal annealing

5.3.6.1 Dissolution of GMS formulations

The result of the effect of GMS content on thermal annealing is shown in Figure 5.21 below.

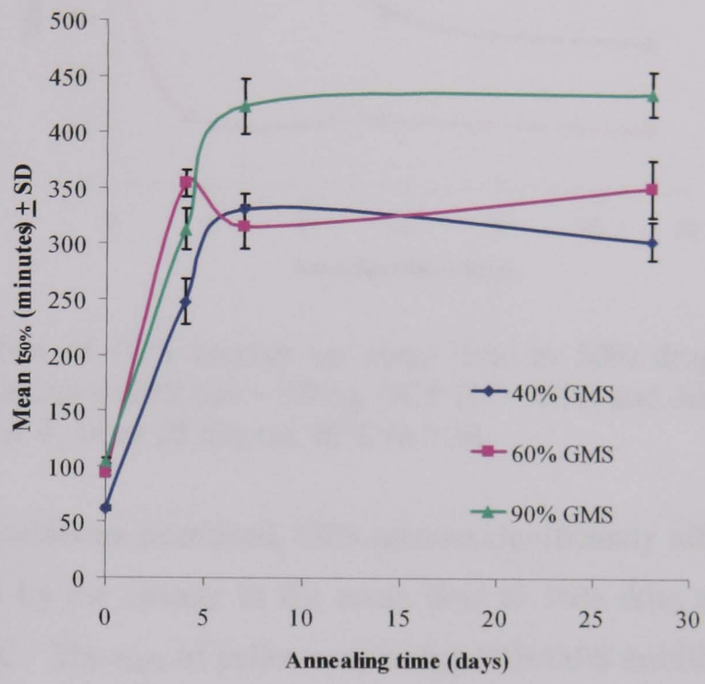

Figure 5.21. Effect of GMS content on mean time to 50% drug release ($t_{50\%}$) of formulations containing GMS (40 – 90%), DCP (0 – 50%) and paracetamol (10%) after annealing for 4, 7 or 28 days at 46°C (n = 6).

Before 7 days of annealing at 46°C, the $t_{50\%}$ for all GMS pellets increased. After 7 days the $t_{50\%}$ appeared to plateau suggesting that thermal annealing for up to 7 days at 46°C was sufficient to ensure reproducible drug release profiles.

5.3.6.2 Dissolution of GPS formulations.

The result of the effect of GPS content on thermal annealing is shown in Figure 5.22 below.

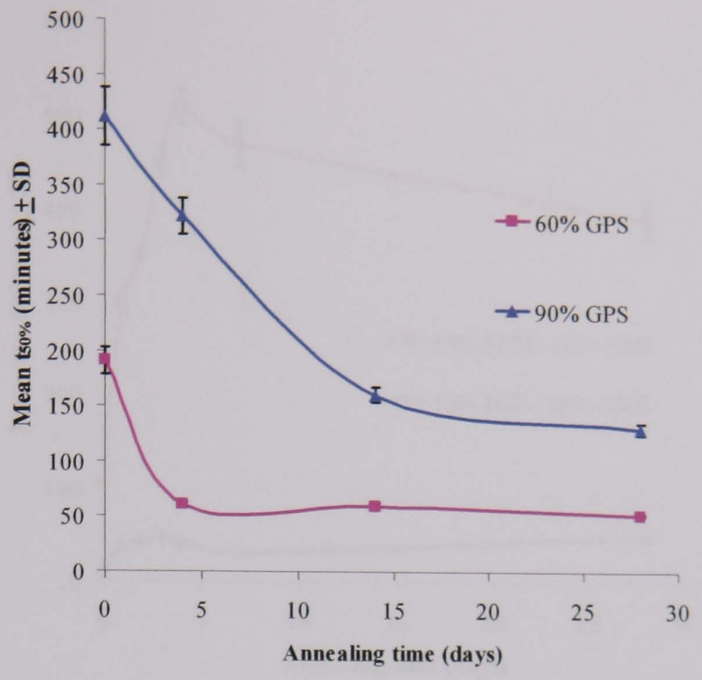

Figure 5.22. Effect of GPS content on mean time to 50% drug release ($t_{50\%}$) of formulations containing GPS (60 – 90%), DCP (0 – 30%) and diltiazem HCl (10%) after annealing for 4, 14 or 28 days at 46°C (n = 6).

For the two formulations examined, GPS content significantly affected drug release rate as observed by the change in the mean time to 50% drug release ($t_{50\%}$) upon annealing at 46°C. The $t_{50\%}$ of pellets containing 60% GPS stabilised after 4 days of annealing, whereas pellets containing 90% GPS stabilised after 14 days of annealing.

5.3.7 Effect of drug type and content on thermal annealing

Paracetamol (PCM, slightly soluble in water) and diltiazem HCl (DTZ, freely soluble in water) were used as model drugs in this study.

5.3.7.1 Dissolution studies

The results of the effects of drug type and content on thermal annealing are shown in Figures 5.23 and 5.24 respectively.

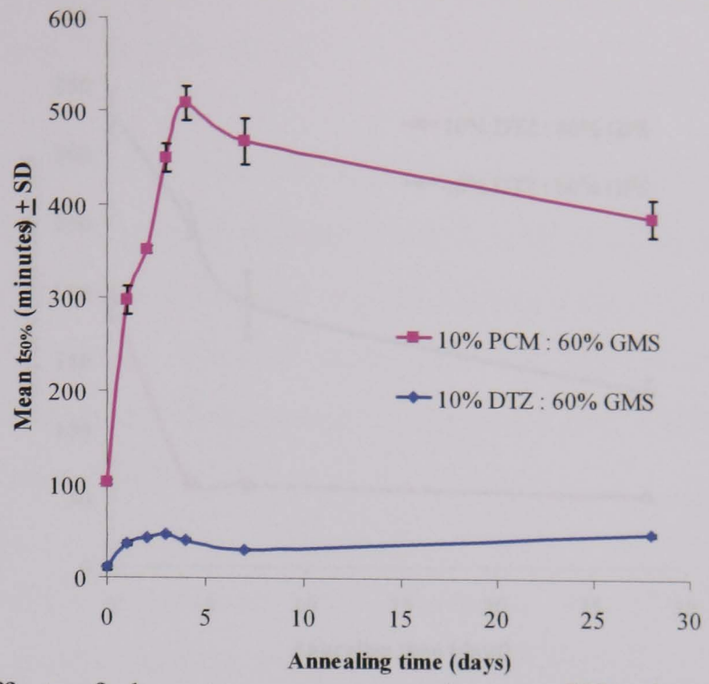

Figure 5.23. Effect of drug type on mean time to 50% drug release ($t_{50\%}$) of formulations containing GMS (60%), DCP (30%) and drug (10%) after annealing for 1, 2, 3, 4, 7 or 28 days at 46°C (n = 6).

PCM and DTZ pellets exhibited significantly different dissolution profiles with $t_{50\%}$ of PCM pellets higher than that of DTZ samples indicating slower drug release reflecting the relative water solubility of the two drugs. On annealing the $t_{50\%}$ value from PCM pellets between day 0 and 4 was dramatically increased with a more gradual reduction in $t_{50\%}$ value found from day 4 onwards. However, the dissolution curves of PCM pellets (data not shown) were similar between day 4 and 28 (using Fit factor with $f_1 < 15\%$ and $f_2 > 50\%$; Appendix I, Table I.2.6.1). In contrast, DTZ pellets demonstrated less pronounced differences in $t_{50\%}$ values but the dissolution curves of DTZ pellets (data not shown) were different between initial and day 4 (using Fit factor with $f_1 > 15\%$ and $f_2 < 50\%$), however were similar between day 4 and 28.

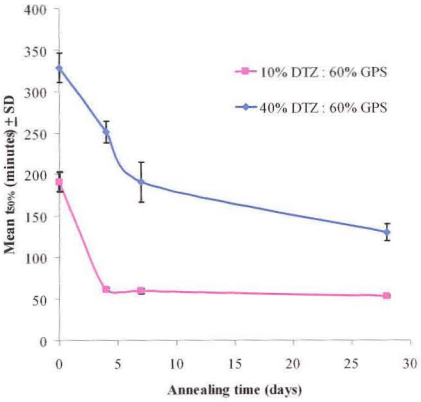

Figure 5.24. Effect of drug content on mean time to 50% drug release ($t_{50\%}$) of formulations containing GPS (60%), DCP (0 - 30%) and DTZ (10 – 40%) after annealing for 4, 7 or 28 days at 46°C (n = 6).

Pellets containing 10% drug content had a noticeably more rapid release compared to those containing 40% diltiazem HCl. This was completely unexpected and no explanation is offered even after consideration of the potential role of the DCP excipient. In both samples, the $t_{50\%}$ decreased upon annealing with the 10% formulation plateauing after 4 days whereas the 40% formulation continued to fall progressively over the 28 day period.

5.4 Conclusion

The physicochemical changes observed in GMS and GPS formulations during thermal annealing were monitored by DSC, HSM, XRPD as well as dissolution testing. Thermal annealing at 46°C produced divergent effects on GMS and GPS pellets with decreased release rates in GMS formulations and increased release rates in GPS formulations.

Annealing was associated with physicochemical transformations to the more stable GMS polymorph which has poorer wetting properties. The optimal annealing time

was 4 days at 46°C to stabilise the drug release of GMS pellets containing 60% GMS, 30% DCP and 10% paracetamol.

In contrast, drug dissolution from GPS pellets was accelerated during annealing at 46°C possibly due to a gradual crystallisation of GPS as demonstrated by XRPD. The formation of large crystals might lead to increased porosity which would then accelerate drug dissolution. Thermal annealing at 46°C for up to 14 days would be sufficient to afford constant drug release profiles from GPS pellets containing 90% GPS and 10% diltiazem HCl.

A higher annealing temperature (46°C compared to only 25°C) accelerated physicochemical changes as observed by HSM and XRPD.

Subsequent dissolution performance was dependent on wax type & content and drug type & content with each of these parameters responding differently to annealing.

CHAPTER 6

MORPHOLOGICAL EVALUATIONS OF GMS AND GPS AS RAW MATERIALS AND IN FORMULATIONS

6.1 Introduction

As previously discussed in Chapters 4 and 5, thermal annealing of GMS and GPS as raw materials and in formulations affected the chemical and physical properties as demonstrated by polymorphic transformation and crystallisation using FT-IR spectrum, DSC, X-ray diffraction and dissolution test. Structural changes in wax upon storage have been previously reported using scanning electron microscope (SEM), where morphological changes such as cracks, fissures, gaps, spaces (Roussin and Duddu, 2001) and rough surfaces (Shimpi et al., 2004) are representative of these intramolecular changes. This suggested that instruments such as the SEM, polarised light microscope and Texture Analyser may be useful in characterising and documenting such morphological changes.

6.2 Methods

Sample preparation and analytical methods are provided below and referenced where appropriate to Chapter 2.

6.2.1 Effect of thermal annealing in GMS or GPS materials on mechanical properties

Untreated GMS and GPS materials were melted in a 10 cm diameter glass petri-dish at 70°C to produce wax thicknesses of 3, 5 or 10 mm. The weight of wax required to produce a given thickness was noted. Samples were then allowed to solidify in the cold room (at approximately 3°C) for 1 hour prior to transfer to storage at 25 or 46 °C. Samples were removed at fixed time intervals of 0, 1, 2, 4, 7, 14, 28 or 90 days and

allowed to equilibrate at room temperature for 1 hour (see Section 6.3.1.3 below) and then analysed by the TA.XT2 Texture Analyser operated under the test conditions described in Section 2.4.11.2 (Page 64). Samples were penetrated by a sharp, clean and dry metal pointed probe (push pin) to a depth of 1 mm during a 10 second period. Six replicates of each wax sample were tested.

6.2.2 Effect of thermal annealing on GMS morphology assessed by polarised light microscopy and SEM

Untreated GMS samples were melted by heating at 70°C (higher than the melting point) and solidified at 3°C for 1 hour and then analysed by polarised light microscope (Section 2.4.8, Page 58) and SEM (Section 2.4.10, Page 61). Each sample was annealed in an air-tight amber glass container at 25 or 46°C for fixed time (0 or 28 days for polarised light microscopy studies as well as 0 or 4 days for SEM studies).

6.2.3 Effect of thermal annealing on GPS morphology assessed by SEM

Untreated GPS samples were melted by heating at 70°C (higher than the melting point) and solidified at 3°C for 1 hour and then analysed by SEM (Section 2.4.10, Page 61). Each sample was annealed in an air-tight amber glass container at 25 or 46°C for 0 or 7 days and then evaluated by SEM.

6.2.4 Effect of thermal annealing on GMS pellet formulations assessed by polarised light microscopy and SEM

For polarised light microscopy studies, the GMS–diltiazem mixtures were composed of 10% diltiazem HCl and 90% GMS. The wax was melted at a temperature above its melting point and drug was added gradually into the melted wax and solidified at 3°C for 1 hour and then analysed by polarised light microscope (Section 2.4.8, Page 58). Each sample was annealed in an air-tight amber glass container at 46°C for 0 or 28 days and then evaluated by polarised light microscope.

Pellets composed of 60% GMS, 30% DCP and 10% diltiazem HCl were prepared by following the general warm spheronisation method (Section 2.5, Page 65) using a spheronisation temperature of 50°C and a spheronisation time of 4 minutes. Pellets within the size range of 1001 to 1180 μm were annealed in an air-tight amber glass container at 25 or 46°C for 0 or 90 days and then analysed by SEM (Section 2.4.10, Page 61).

6.2.5 Effect of thermal annealing on GPS pellet formulations assessed by polarised light microscopy and SEM

For polarised light microscopy studies, the GPS–diltiazem mixtures were composed of 10% diltiazem HCl and 90% GPS. The wax was melted at a temperature above its melting point and drug was added gradually into the melted wax and solidified at 3°C for 1 hour and then analysed by polarised light microscope (Section 2.4.8, Page 58). Each sample was annealed in an air-tight amber glass container at 46°C for 0 or 28 days and then evaluated by polarised light microscope.

Pellets composed of 90% GPS and 10% diltiazem HCl were prepared by following the general warm spheronisation method (Section 2.5, Page 65) using a spheronisation temperature of 45°C and a spheronisation time of 5 minutes. Pellets within the size range of 1001 to 1180 μm were annealed in an air-tight amber glass container at 25 or 46°C for 0 or 28 days and then analysed by SEM (Section 2.4.10, Page 61).

6.3 Results and Discussion

6.3.1 Effect of thermal annealing in GMS or GPS materials on mechanical properties

The Texture Analyser can be used to perform a penetration test to measure the force during insertion of a probe into a sample to a specified depth. Hardness, defined as the force required to achieve a given deformation, is an important factor to

characterise mechanical and/or rheological properties of semi-solid products. A 'soft' sample will afford a low penetrating force whereas a 'hard' sample will yield higher forces (Jones et al., 2002).

6.3.1.1 Validation of test methodology using plasticine and balsa wood as models of plastic and brittle materials

The capability of the Texture Analyser to discriminate the structural properties of contrasting materials was evaluated using a material likely to undergo plastic deformation (plasticine) and a second material possessing a stratified structure likely to undergo a combination of plastic and brittle deformation (balsa wood). The resultant force-time curves are shown in Figures 6.1 and 6.2 below.

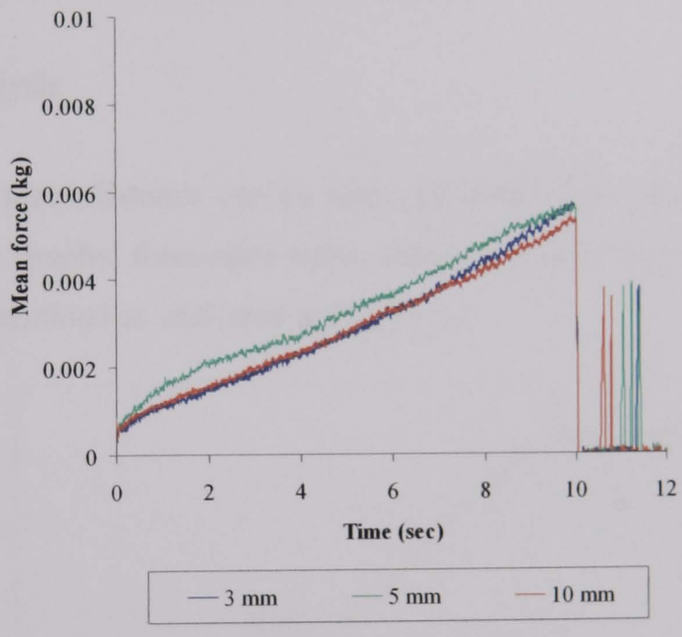

Figure 6.1. Relationship of mean (n = 6) force and time in plasticine during penetration test performed on different thicknesses.

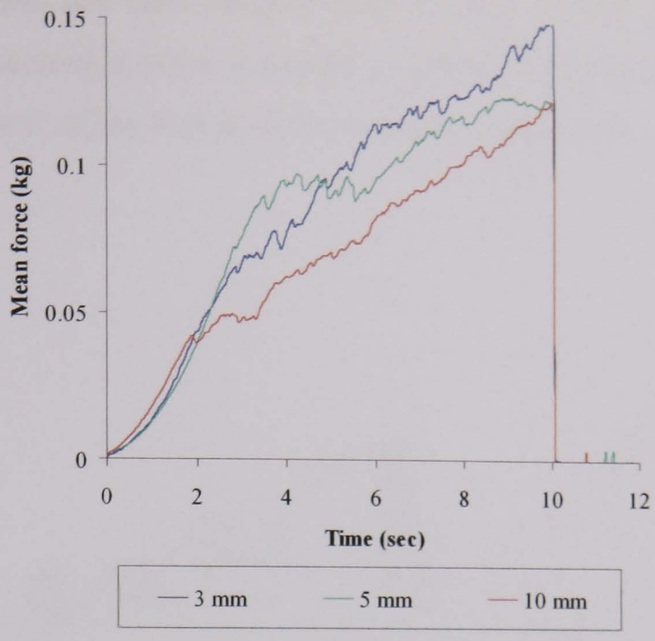

Figure 6.2. Relationship of mean (n = 6) force and time in balsa wood during penetration test performed on different thicknesses.

6.3.1.2 Data analysis

Force-time and force-distance curves were generated from individual experiments. From force-time graphs, force-time slope, maximum force and area under the curve (AUC) were determined as indicated in Figure 6.3.

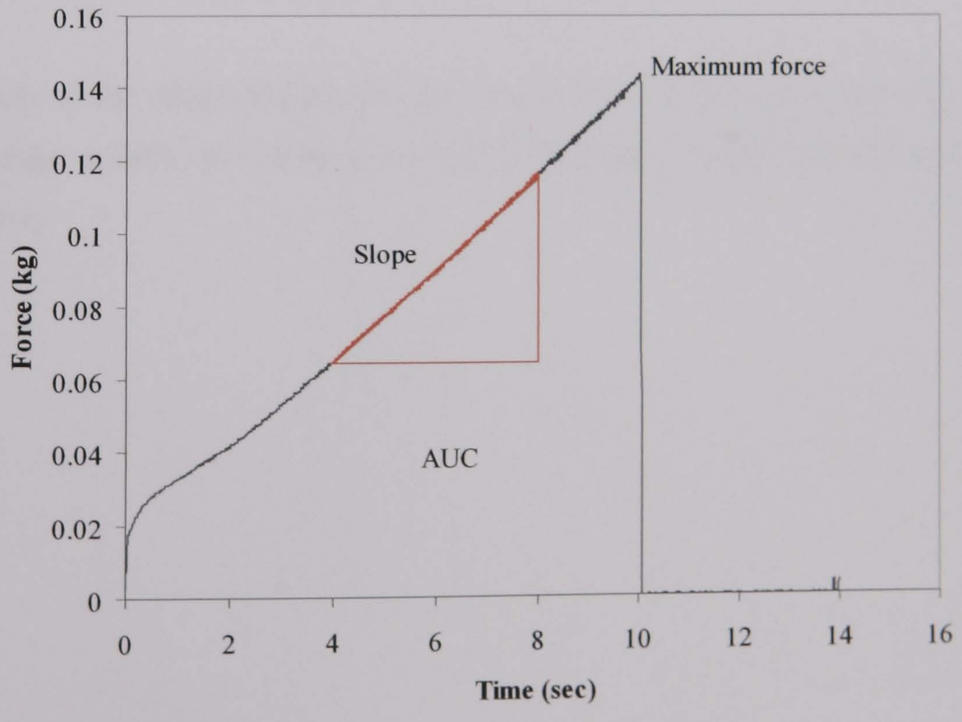

Figure 6.3. Typical force–time graph obtained for the duration of a 10 second experiment in which the probe penetrates a depth of 1mm.

Furthermore, in GMS and GPS samples aged 90 days at 46°C, the forces generated over 0.5 mm of penetration were examined in greater detail in an attempt to identify key structural features of the wax as demonstrated in Figure 6.4.

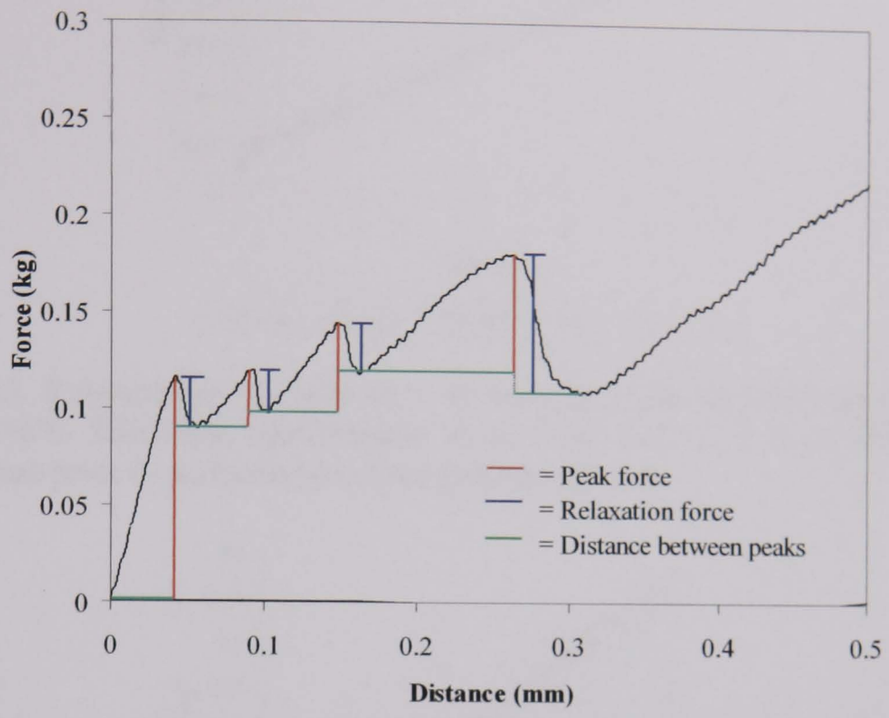

Figure 6.4. Typical graph plotted between force and distance (scale 0.5 mm) obtained following 1 mm penetration of probe into aged wax at room temperature.

6.3.1.3 Results and discussion of mechanical properties

The results of the effect of equilibration time at room temperature following removal from storage at 46°C for 14 days (no found fluctuation peaks) are shown in Figures 6.5 and 6.6.

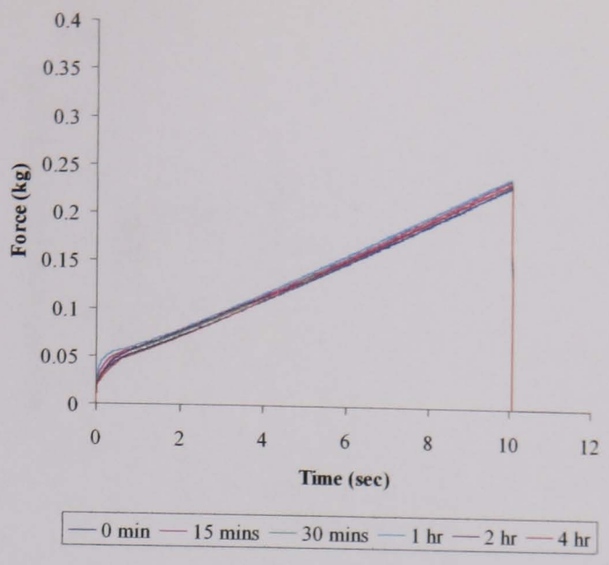

Figure 6.5. Relationship of mean (n = 6) force and time in GMS samples aged 14 days at 46°C following equilibration at 0, 0.25, 0.5, 1, 2 or 4 hours at room temperature prior to performance of the penetration test.

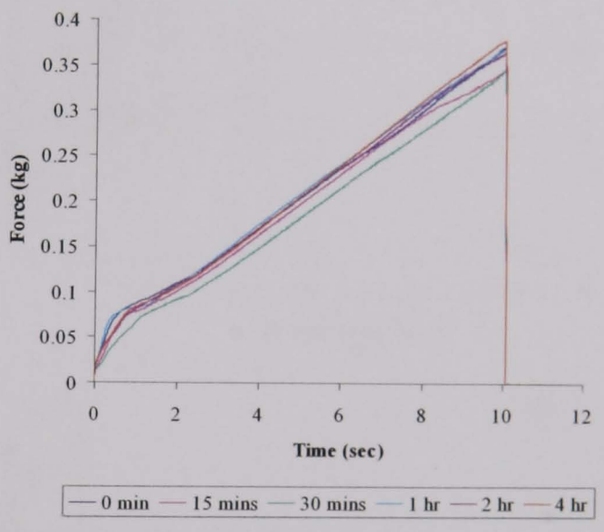

Figure 6.6. Relationship of mean (n = 6) force and time in GPS samples aged 14 days at 46°C following equilibration at 0, 0.25, 0.5, 1, 2 or 4 hours at room temperature prior to performance of the penetration test.

From Figures 6.5 and 6.6, the force-time profiles of both GMS and GPS aged 14 days at 46°C appeared to be independent of equilibration time. For future studies, an equilibration time of 1 hour was adopted. After establishing optimal temperature equilibration conditions, the effect of wax type, sample thickness and storage temperature were investigated using force-time slope, maximum force and area under the curve (AUC) as shown in Figures 6.7 to 6.9.

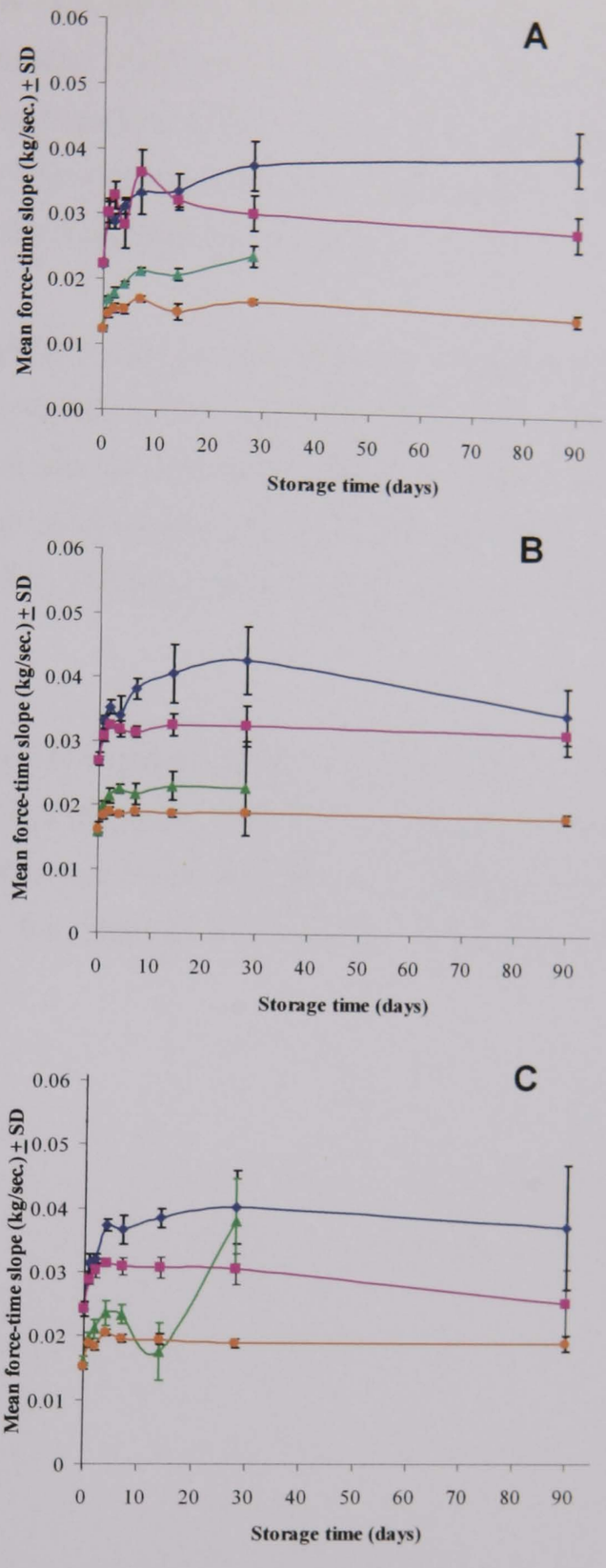

Figure 6.7. Relationship of mean force-time slope and storage time (n = 6) during penetration test performed on different wax thicknesses (A – 3 mm; B – 5 mm; C – 10 mm wax thickness). ◆ GPS 46°C; ■ GPS 25°C; ▲ GMS 46°C; ● GMS 25°C

From Figure 6.7 (A - C), the GPS samples exhibited higher slopes compared to the GMS samples, indicating it performed as a harder material in this test. The overall profiles were similar regardless of the thickness of the wax samples. Some variation in relation to time of storage was observed with the trend to rapidly plateau following an initial rise over the initial period (5 - 7 days).

For both GMS and GPS samples, the effect of storage at 46°C afforded a harder material than when stored at 25°C suggesting macroscopic structural reorganisation within the matrix at the elevated temperature. Previous workers have referred to similar development of structural changes on storage (Roussin and Duddu, 2001; Shimpi et al., 2004), although those authors did not attempt to quantify any mechanical effects.

In Figure 6.7C, the GMS sample stored at 46°C showed a different profile with a sudden increase in hardness after day 14. The reason for this remains uncertain; however it introduced considerable variability into the results from this point onwards such that it was not appropriate to derive mean data points for graphical representation.

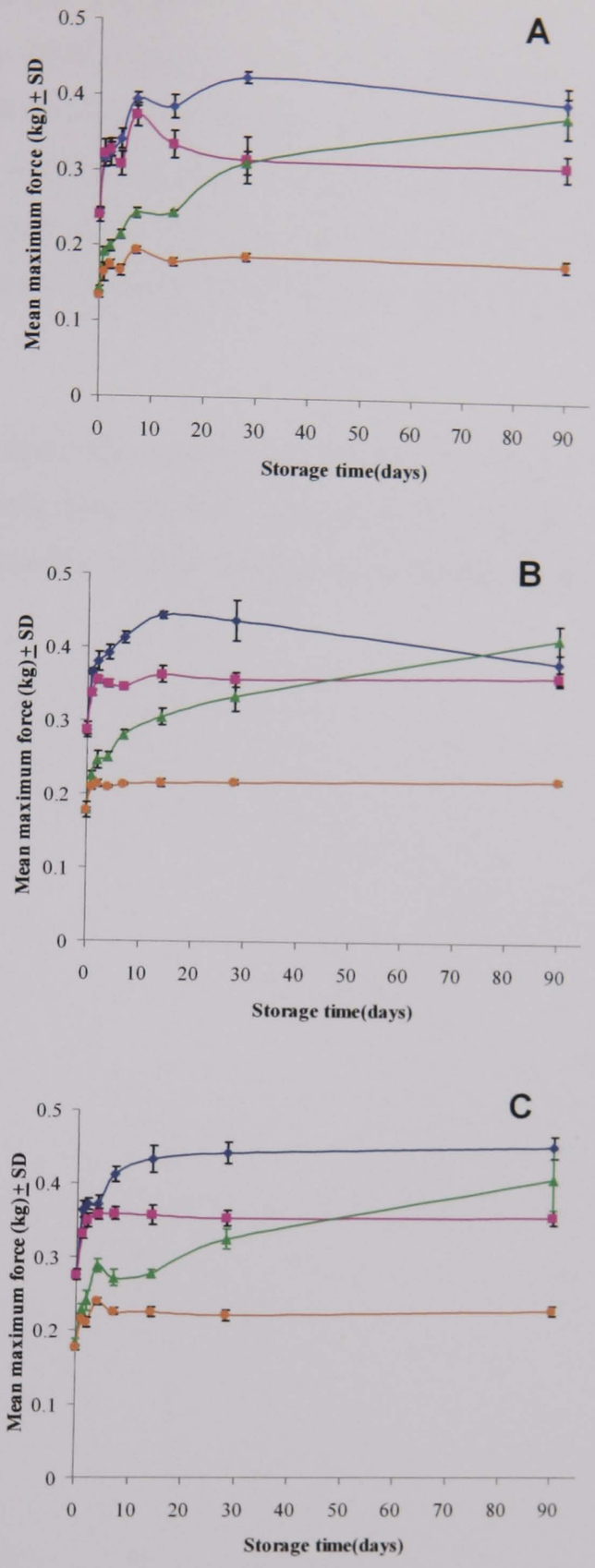

Figure 6.8. Relationship of mean maximum force and storage time (n = 6) during penetration test performed on different wax thicknesses (A – 3 mm; B – 5 mm; C – 10 mm wax thickness). ◆ GPS 46°C; ■ GPS 25°C; ▲ GMS 46°C; ● GMS 25°C

From Figure 6.8 (A - C), the GPS samples exhibited higher mean maximum forces compared to the GMS samples, indicating it performed as a harder material in this test. The overall profiles were similar regardless of the thickness of the wax samples. Some variation in relation to time of storage was observed with the trend to rapidly plateau following an initial rise over the initial period (5 - 7 days) with the exception of the GMS samples stored at 46°C where it continued to increase over the duration of the study.

For both GMS and GPS samples, the effect of storage at 46°C afforded a harder material than when stored at 25°C suggesting macroscopic structural reorganisation within the matrix at the elevated temperature as discussed previously.

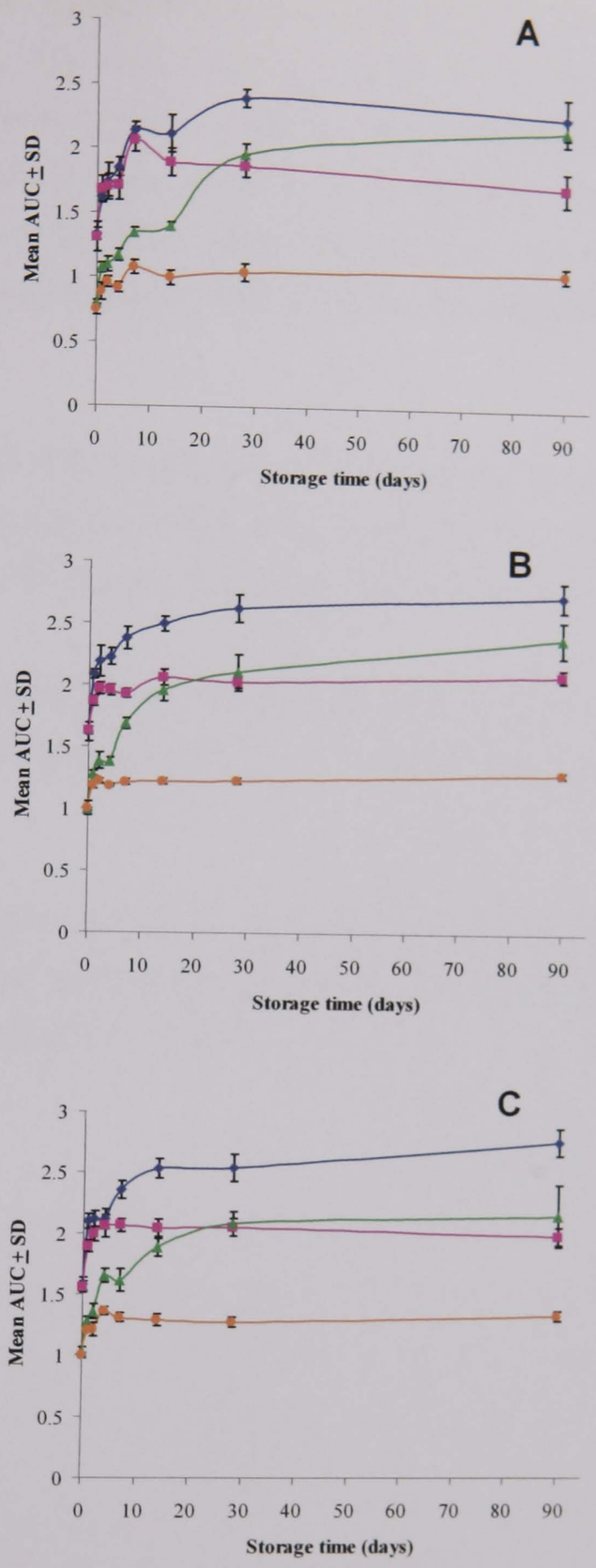

Figure 6.9. Relationship of mean AUC and storage time (n = 6) during penetration test performed on different wax thicknesses (A – 3 mm; B – 5 mm; C – 10 mm wax thickness). ◆ GPS 46°C; ■ GPS 25°C; ▲ GMS 46°C; ● GMS 25°C

From Figure 6.9 (A - C), the GPS samples exhibited higher mean AUCs compared to the GMS samples. The overall profiles were similar regardless of the thickness of the wax samples. Some variation in relation to time of storage was observed with the trend to rapidly plateau following an initial rise over the initial period (5 - 7 days) with the exception of the GMS samples stored at 46°C which continued to increase, albeit at a more modest rate than that observed when considering mean maximum force.

For both GMS and GPS samples, the effect of storage at 46°C afforded a harder material than when stored at 25°C suggesting macroscopic structural reorganisation within the matrix at the elevated temperature as discussed previously.

Each of the three parameters would equally appear appropriate for characterising the development of structural changes in wax samples that have different thermal histories.

The data over the initial compression period were analysed more closely to determine any structural changes taking place for samples of GMS and GPS stored for 90 days at 46°C as shown in Figure 6.10 below.

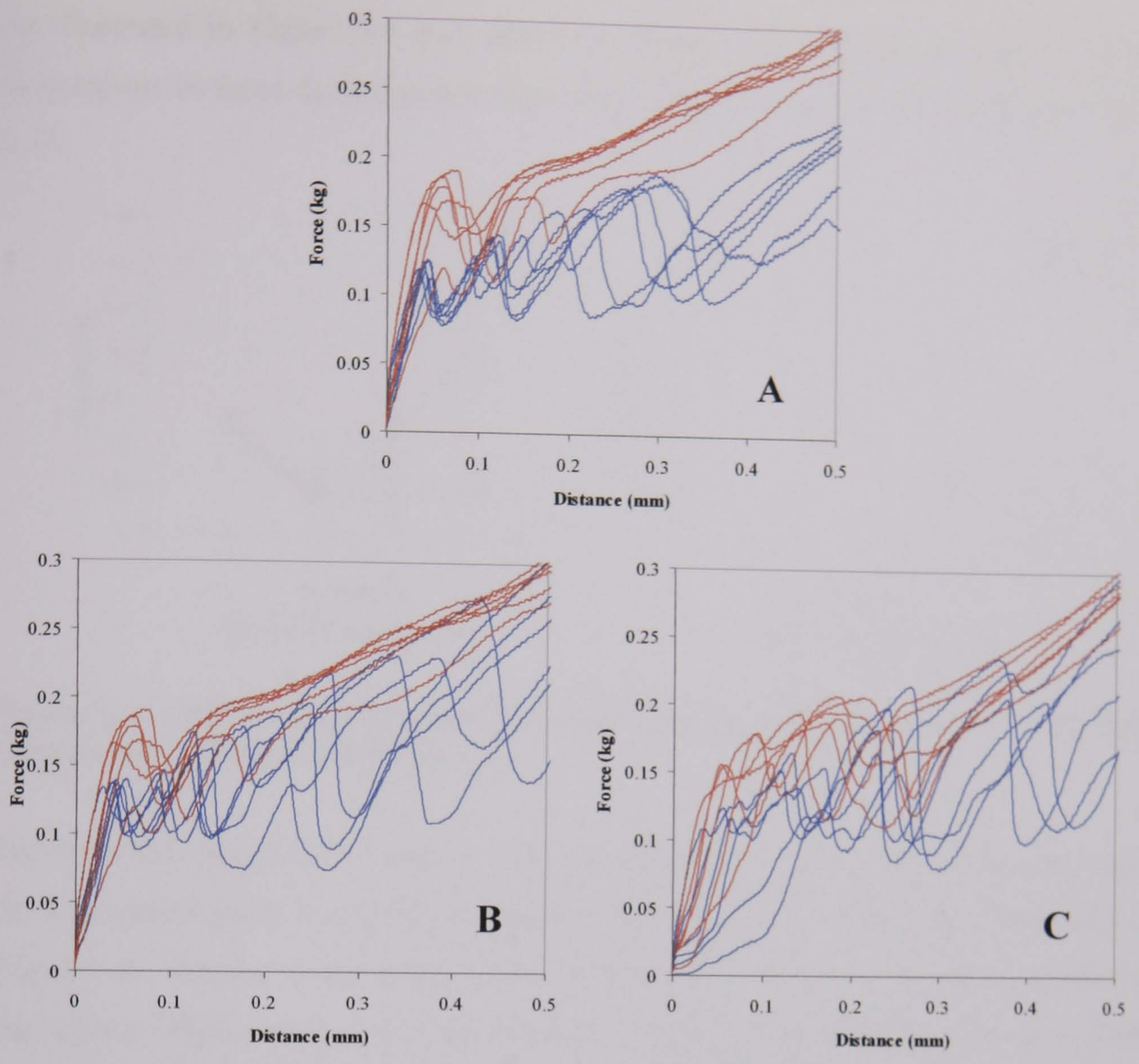

Figure 6.10. Relationship of force and distance in GMS (—) or GPS (—) samples aged 90 days at 46°C during penetration test performed on (**A**) 3 mm; (**B**) 5 mm or (**C**) 10 mm wax thickness.

In Figure 6.10A, the 3 mm GMS samples had noticeably more substructure in the matrix with 3 – 4 discrete layers as reflected by force-distance profiles. In contrast, this was noticeably absent in the GPS samples where force rose steadily following an initial sharper rise. From Figure 6.10B, in the 5 mm thick samples of GMS, a similar multi-peaked profile was observed. The GPS sample was characterised by a single peak, although one analysis revealed twin-peaks. There was no discernable difference between the 5 and 10 mm GMS samples, however, the 10 mm GPS material exhibited multi-peaked traces, which were not observed in the 5 mm sample.

As illustrated in Figure 6.4 and data from Figure 6.10, a detailed analysis of the fluctuations in force during penetration can be observed as shown in Figures 6.11 – 6.13.

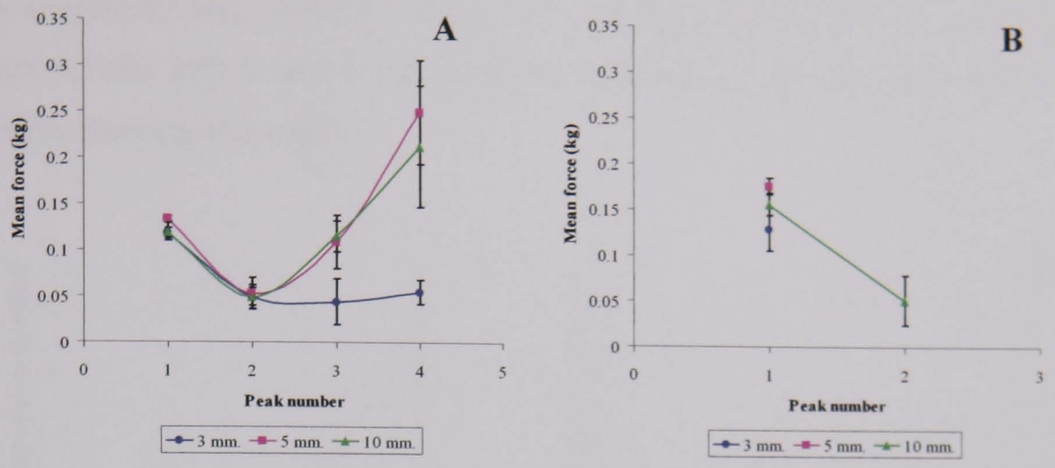

Figure 6.11. Relationship of mean force and peak number in (**A**) GMS or (**B**) GPS samples aged 90 days at 46°C (n = 6).

For all GMS samples (3, 5 and 10 mm thicknesses) the peak force values decreased from observed peak 1 to peak 2 (Figure 6.11A) using the convention described in Figure 6.4. For the 3 mm GMS thickness the values reached a plateau, whereas for the thicker GMS samples successive peaks revealed greater values. However, GPS samples exhibited fewer peaks (Figure 6.11B) with 3 and 5 mm thicknesses showing a single peak whereas 10 mm thickness showed two peaks. For both GMS and GPS samples, the first and second peaks had similar numerical values.

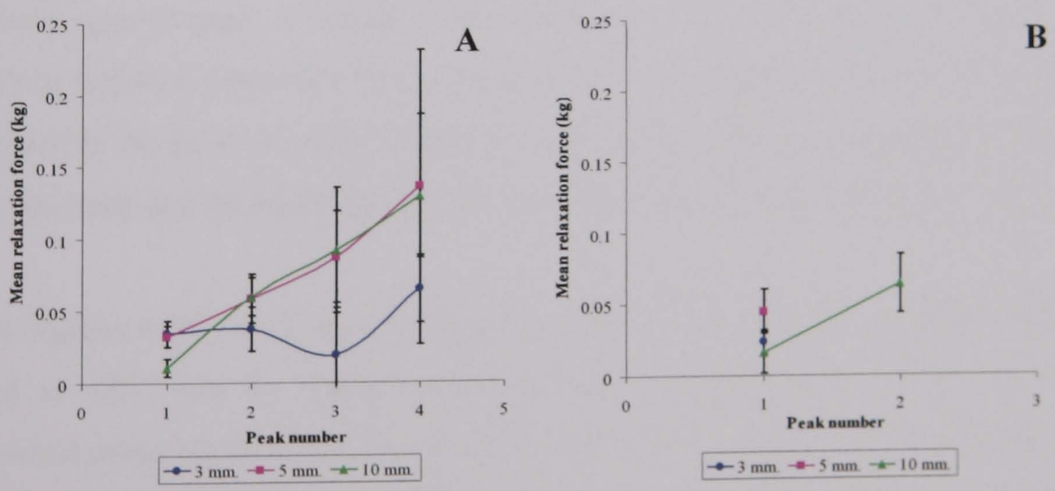

Figure 6.12. Relationship of mean relaxation force and peak number in (**A**) GMS or (**B**) GPS samples aged 90 days at 46°C (n = 6).

For 3 mm GMS samples the mean relaxation force between successive peaks remained reasonably constant whereas for the 5 and 10mm GMS thicknesses the values showed a near linear increase in mean relaxation force between successive peaks (Figure 6.12A). Analysis of the GPS samples is hindered by the lack of peaks (Figure 6.11B) with 3 and 5 mm thicknesses showing only one peak and 10 mm thickness showing two peaks.

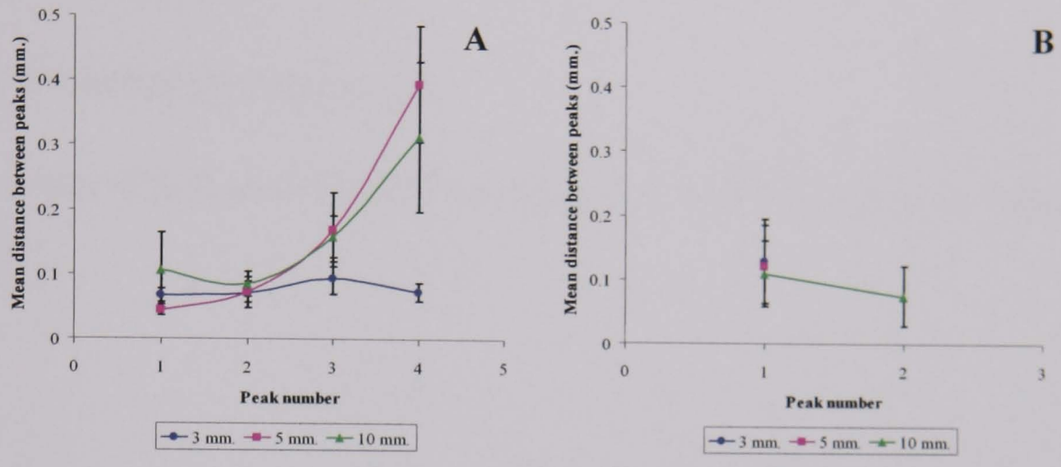

Figure 6.13. Relationship of mean distance between peaks and peak number in (**A**) GMS or (**B**) GPS samples aged 90 days at 46°C (n = 6).

The data for distance between successive peaks revealed that the 3 mm GMS thickness had a reproducible structure characterised by near constant distances of approximately 69 μm between successive 'layers' as determined by force measurement. However, with thicker GMS samples while the first two 'layers' were similarly spaced apart, as depth of penetration increased, increasing distances were observed between successive layers (Figure 6.13A). Analysis of the GPS samples is hindered by the lack of peaks (Figure 6.13B) with 3 and 5 mm thicknesses showing only one peak and 10 mm thickness showing two peaks, spaced apart by 77 μm.

From Figures 6.10 – 6.13, it is apparent that the internal structure of GMS melted and stored at 46°C can be characterised as having discrete layers that give rise to individual peaks on the force–distance plots developed during the TA penetration test. Whereas the 3 mm thick wax samples appear to provide a more consistent structure, the thicker 5 and 10 mm samples appeared to have a more developed internal structure and to greater depths within the wax matrix.

However, GPS samples exhibited less development of internal structure after annealing at 46°C than observed with GMS samples. Whether these observations are a true reflection of internal 'structure' or an artifact arising from sample thickness or from the test procedure itself requires further investigation.

6.3.2 Effect of thermal annealing on GMS morphology assessed by polarised light microscopy and SEM

6.3.2.1 Polarised light microscopy

The results of melt-solidified GMS annealed at 25 or 46°C are shown in Figure 6.14 below.

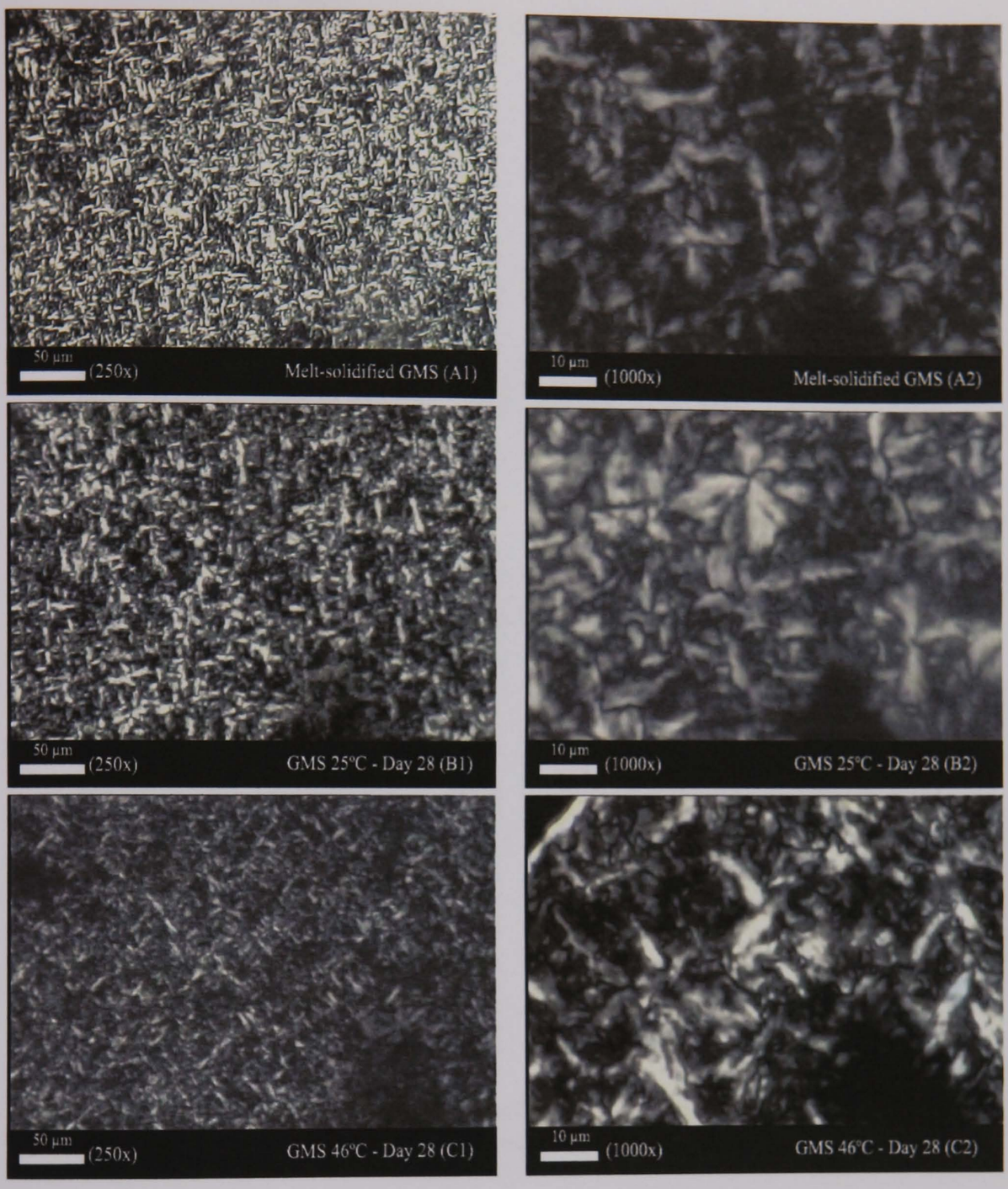

Figure 6.14. Polarised light microscopy photographs at magnification (**1**) 250X or (**2**) 1000X of melt-solidified GMS following (**A**) no annealing, (**B**) annealing for 28 days at 25°C or (**C**) annealing for 28 days at 46°C.

The melt-solidified GMS (Figure 6.14(A1-2)) appeared as needle-shaped crystals. When samples were annealed at 25 or 46°C for 28 days (Figure 6.14(B1-2) or (C1-2)), morphologically all samples appeared similar when observed using polarised light microscopy.

6.3.2.2 Scanning electron microscope (SEM)

The results of untreated, melt-solidified and samples annealed at 25 or 46°C are shown in Figures 6.15 - 6.16.

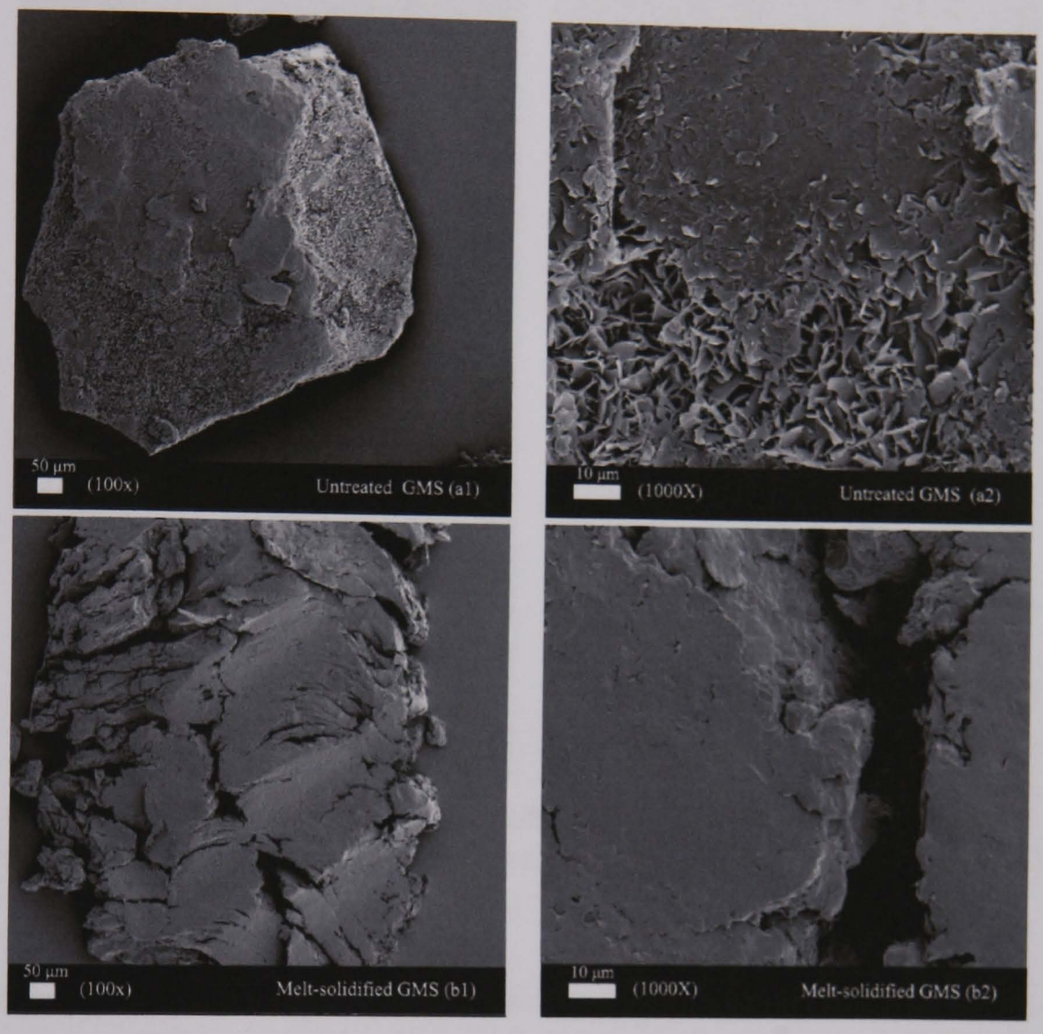

Figure 6.15. SEM photographs at magnification (**1**) 100X or (**2**) 1000X of GMS obtained from (**a**) untreated or (**b**) melt-solidified samples.

The untreated GMS (Figure 6.15(a1-2)) showed crystalline structure with cracks and fissures, whereas melt-solidified sample (Figure 6.15(b1-2)) exhibited smooth surfaces. These microscopic details are consistent with the observations of Garti and Sato (1988) who noted that the ß-form of saturated monoacid triglycerides (similar crystal packing as GMS) appeared as large crystals, whereas the α-form showed smooth homogeneous surfaces with smaller crystalline domains. It can be concluded that untreated GMS (ß-form) transforms to the unstable α-form following melt-solidification. These microscopic changes correlated to the physicochemical changes of GMS reported in Section 4.3.5.

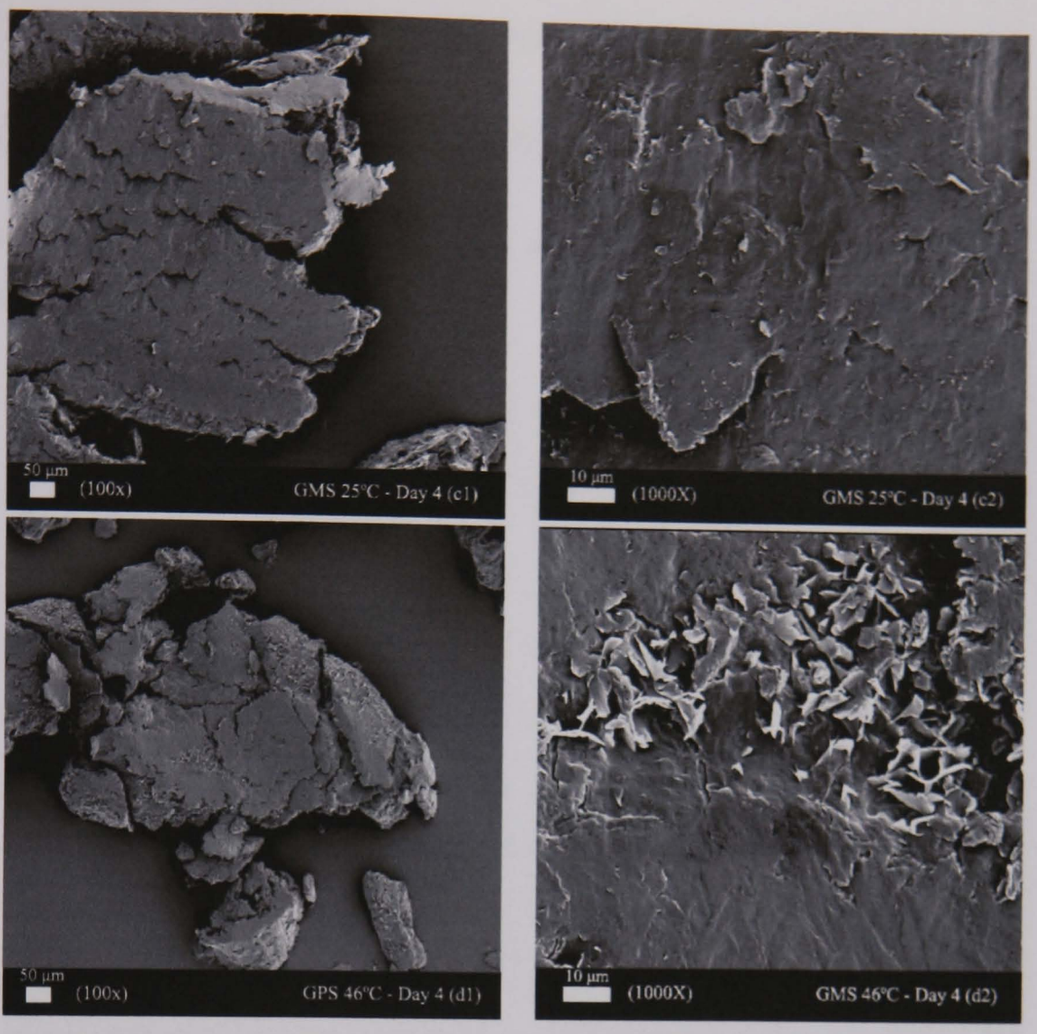

Figure 6.16. SEM photographs at magnification (**1**) 100X or (**2**) 1000X of melt-solidified GMS following (**c**) annealing for 4 days at 25°C or (**d**) annealing for 4 days at 46°C.

When melt-solidified GMS were annealed at 25°C for 4 days (Figure 6.16(c1-2)), SEM photographs showed the development of surface crystals. With annealed samples (46°C for 4 days, Figure 6.16(d1-2)), the surface changes reflected a transformation to the ß-form. Moreover, higher annealing temperature of 46°C accelerated polymorphic transformation to the stable form compared to lower temperature annealing (25°C) confirming findings previously reported using FT-IR, DSC and XRPD in Section 4.3.5.

Roussin and Duddu (2001) described a similar study in SEM photographs of Gelucire 50/13 in which form I (the unstable form) showed a smooth surface, while the form I' presented cracks, fissures, gaps and spaces on the surface. The form I converted to form I' during storage.

6.3.3 Effect of thermal annealing on GPS morphology assessed by SEM

6.3.3.1 Scanning electron microscope (SEM)

The results of untreated, melt-solidified and samples annealed at 25 or 46°C are shown in Figures 6.17 - 6.18.

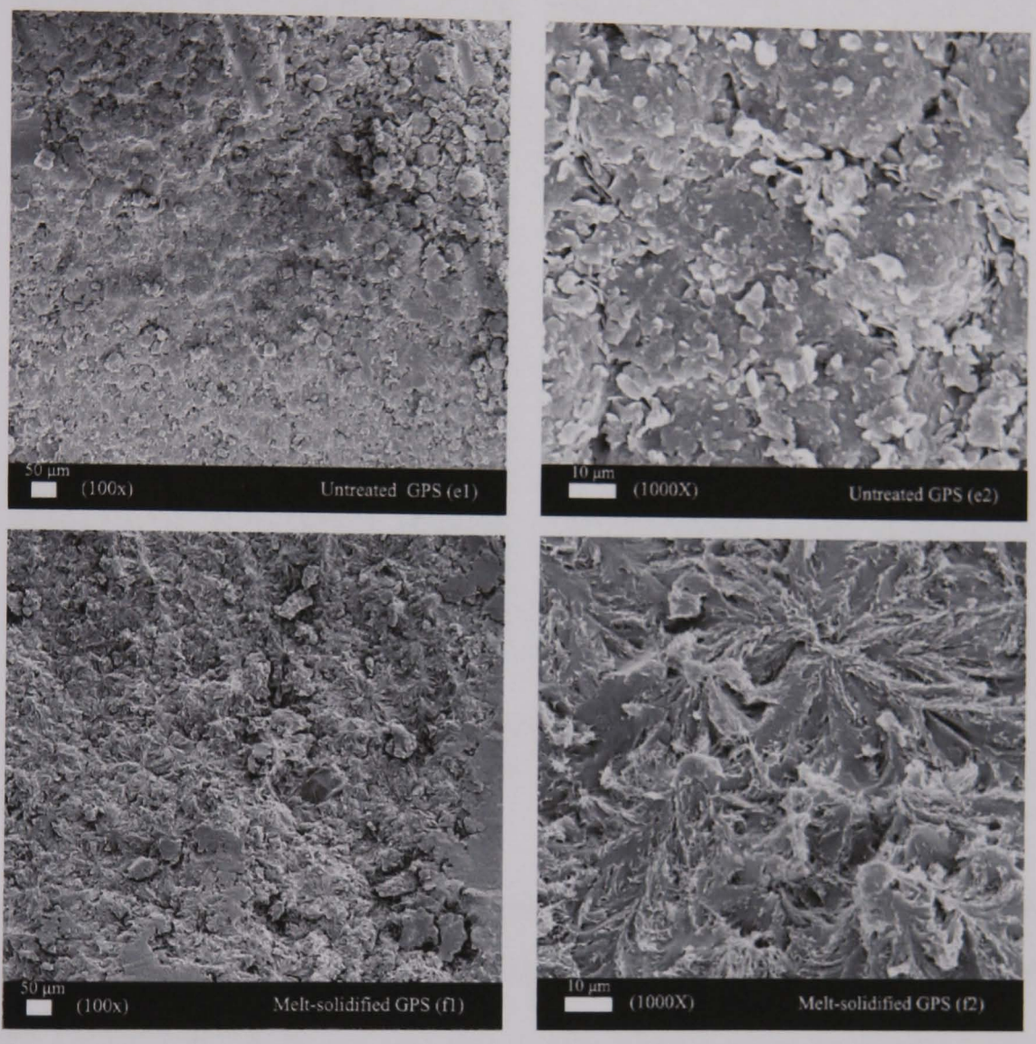

Figure 6.17. SEM photographs at magnification (**1**) 100X or (**2**) 1000X of GPS obtained from (**e**) untreated or (**f**) melt-solidified samples.

The untreated GPS presented with small particles on the surface, while the melt-solidified samples showed the presence of a more ordered 'floral' structure, which differed to the smooth surface obtained by melt-solidification of GMS.

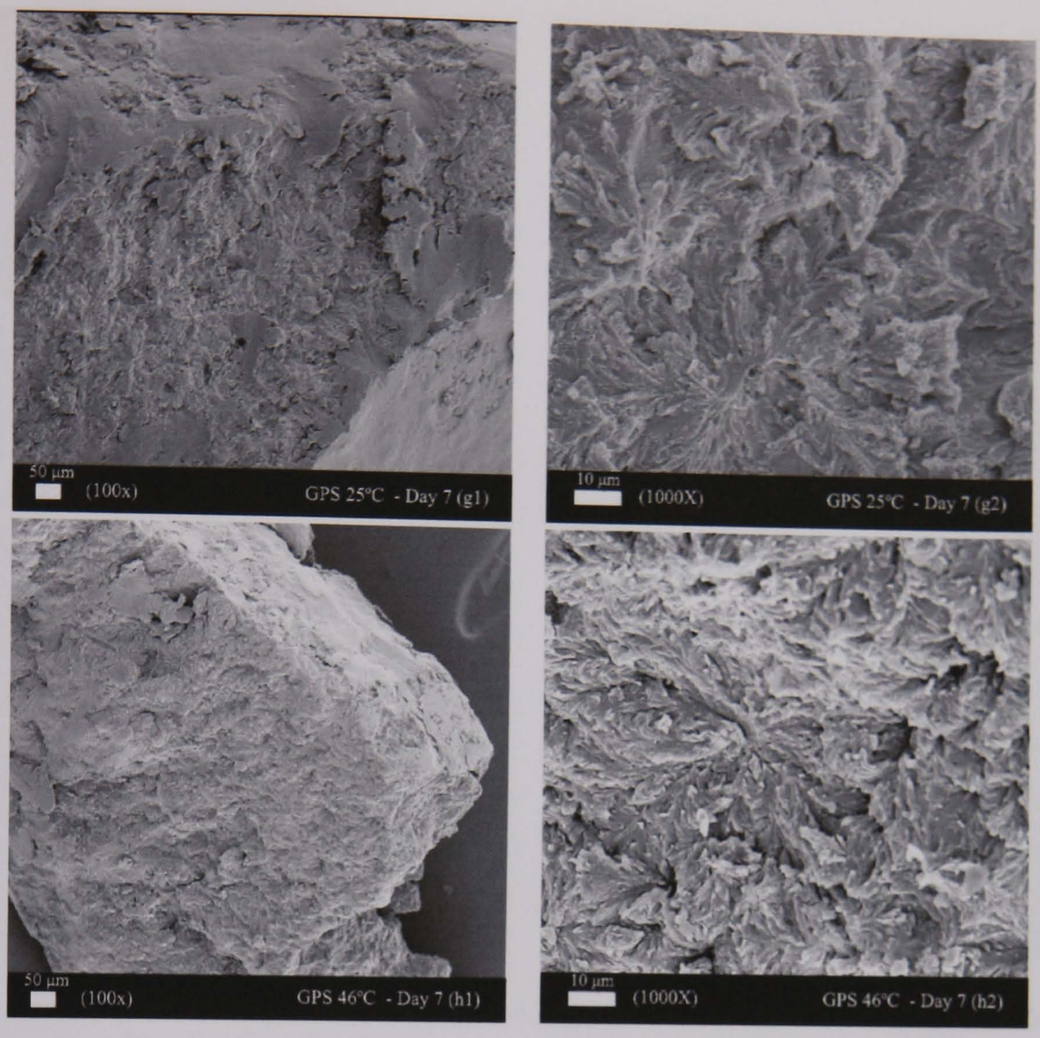

Figure 6.18. SEM photographs at magnification (**1**) 100X or (**2**) 1000X of melt-solidified GPS following (**g**) annealing for 7 days at 25°C or (**h**) annealing for 7 days at 46°C.

When melt-solidified GPS samples were annealed for 7 days at 25°C (Figure 6.18(g1-2)) or 46°C (Figure 6.18(h1-2)), the surfaces which presented 'floral' structure were not changed.

6.3.4 Effect of thermal annealing on GMS pellet formulations assessed by polarised light microscopy and SEM

6.3.4.1 Polarised light microscopy

The results of melt-solidified GMS-diltiazem mixtures after annealing at 46°C are shown in Figure 6.19.

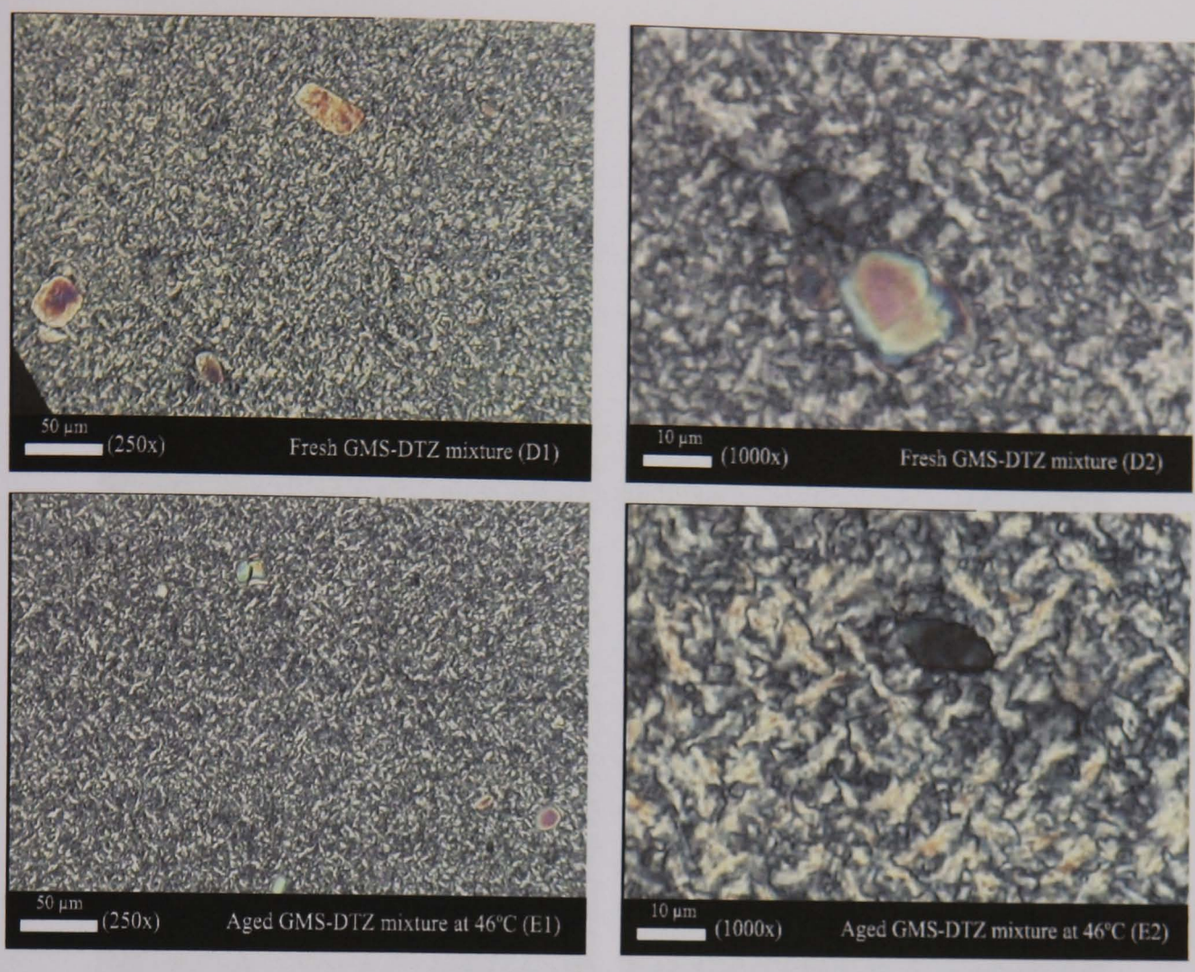

Figure 6.19. Polarised light microscopy photographs at magnification (**1**) 250X or (**2**) 1000X of melt-solidified GMS-diltiazem mixtures obtained from (**D**) fresh or (**E**) annealed for 28 days at 46°C.

The diltiazem crystals were clearly identifiable using polarised light. The formulations appear to exist as solid dispersions as observed by the existence of birefringent crystals. From Figure 6.19(D1-2), the melt-solidified GMS-diltiazem mixtures showed the drug crystals which dispersed in the needle-shaped crystals of GMS. When samples were annealed at 46°C for 28 days (Figure 6.19(E1-2)), morphologically all samples appeared similar.

6.3.4.2 Scanning electron microscope (SEM)

The results of GMS pellets containing DCP and diltiazem HCl after annealing at 25 or 46°C are shown in Figure 6.20.

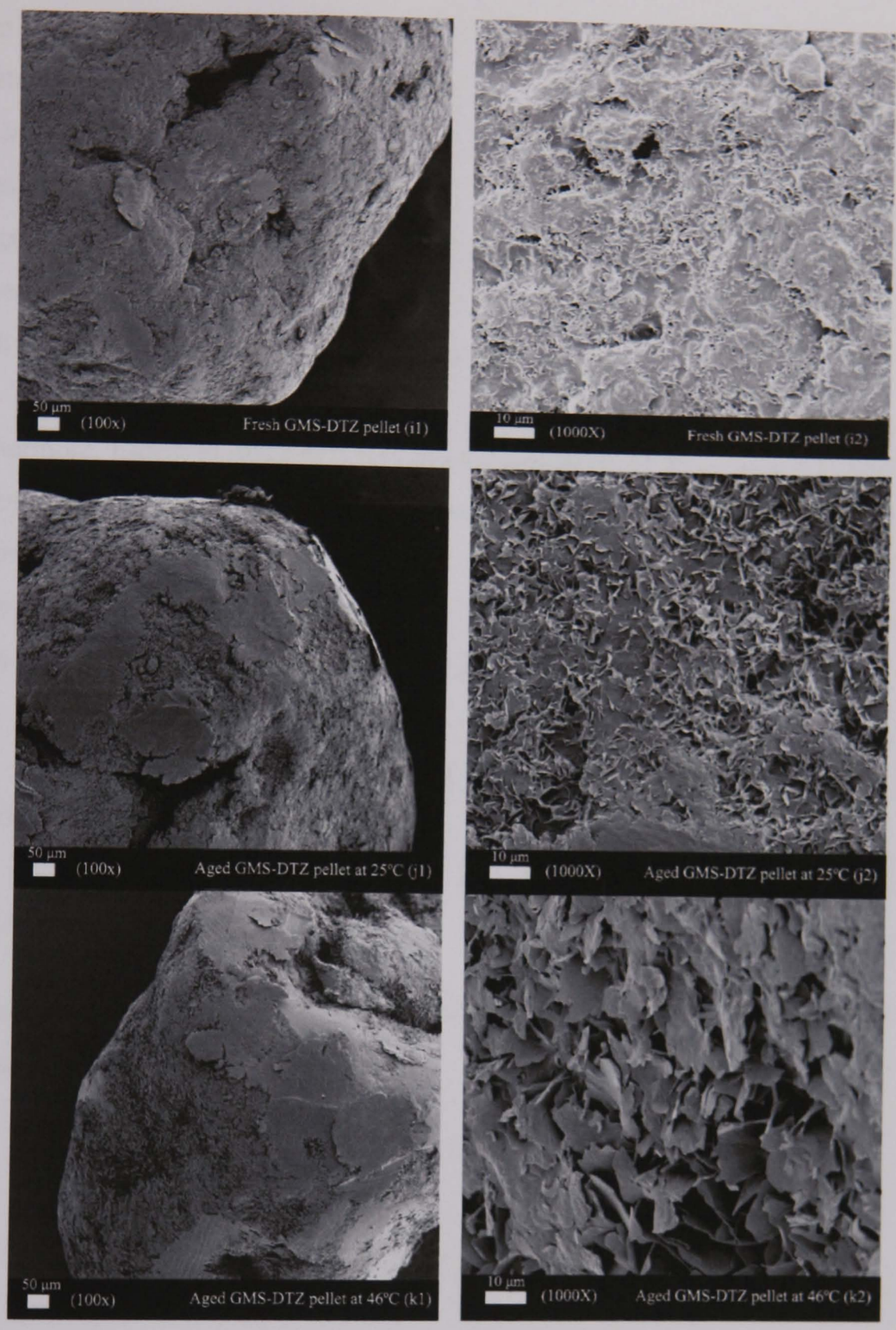

Figure 6.20. SEM photographs at magnification (**1**) 100X or (**2**) 1000X of GMS-diltiazem pellets obtained from (**i**) fresh, (**j**) annealed for 90 days at 25°C or (**k**) annealed for 90 days at 46°C.

Whereas the freshly prepared GMS pellets (containing DCP and diltiazem HCl) appeared to have a rather regular surface, after annealing the surface developed a more structured crystalline appearance corresponding to the change from α- to the stable ß-form.

From Section 6.3.2.2, the melt-solidified GMS (α-form) were converted gradually to the stable form (ß-form) during annealing. The α-form of GMS had better wetting and lower melting point than the ß-form (Yajima et al., 2002). Although thermal annealing of GMS pellet resulted in a more clearly defined crystalline surface (with an apparent greater surface area), the polymorphic transformation to ß-form (with poorer wetting property) has a more dominant effect on drug dissolution with the result that dissolution rates decrease following annealing.

Furthermore, Eldem et al. (1991) described a similar SEM study in which spray lipid micropellets containing wax (GDB or glycerol tristearate), lecithin and estradiol 17-ß cypionate showed spherical smooth surfaces with very thin crystal size corresponding to a less stable wax form. This unstable form was transformed to a stable form exhibiting larger crystals after storage at elevated temperatures.

6.3.5 Effect of thermal annealing on GPS pellet formulations assessed by polarised light microscopy and SEM

6.3.5.1 Polarised light microscopy

The results of melt-solidified GPS-diltiazem mixtures after annealing at 46°C are shown in Figure 6.21.

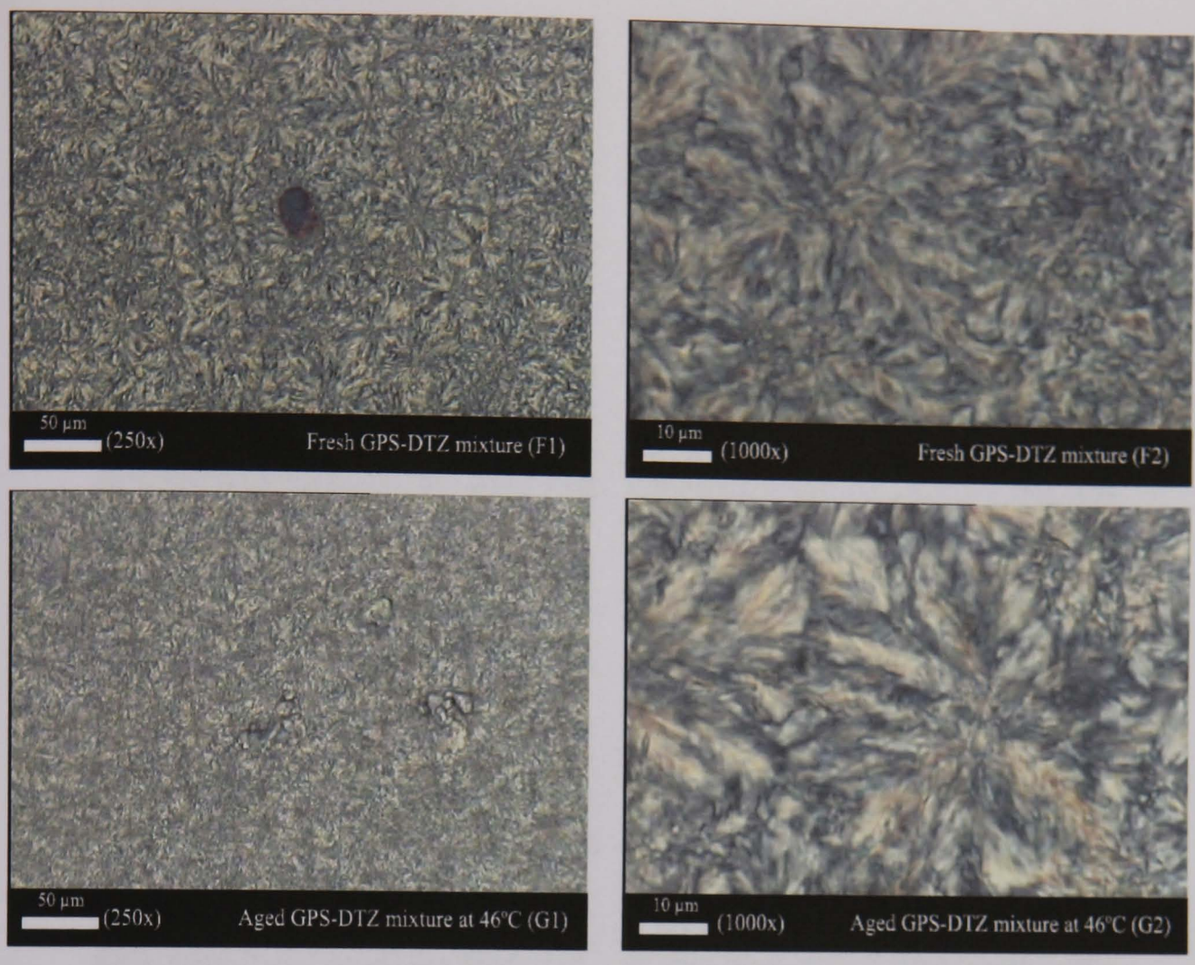

Figure 6.21. Polarised light microscopy photographs at magnification (**1**) 250X or (**2**) 1000X of melt-solidified GPS-diltiazem mixtures obtained from (**F**) fresh or (**G**) annealed for 28 days at 46°C.

The diltiazem crystals were identifiable using polarised light. The formulations would exist as solid dispersions as observed by the existence of birefringent crystals. From Figure 6.21(F1-2), the melt-solidified GPS-diltiazem mixtures showed the drug crystals which dispersed in the floral-shaped crystals of GPS. When samples were annealed at 46°C for 28 days (Figure 6.21(G1-2)), morphologically all samples appeared similar.

6.3.5.2 Scanning electron microscope (SEM)

The results of the surface of GPS-diltiazem pellets after annealing at 25 or 46°C are shown in Figure 6.22.

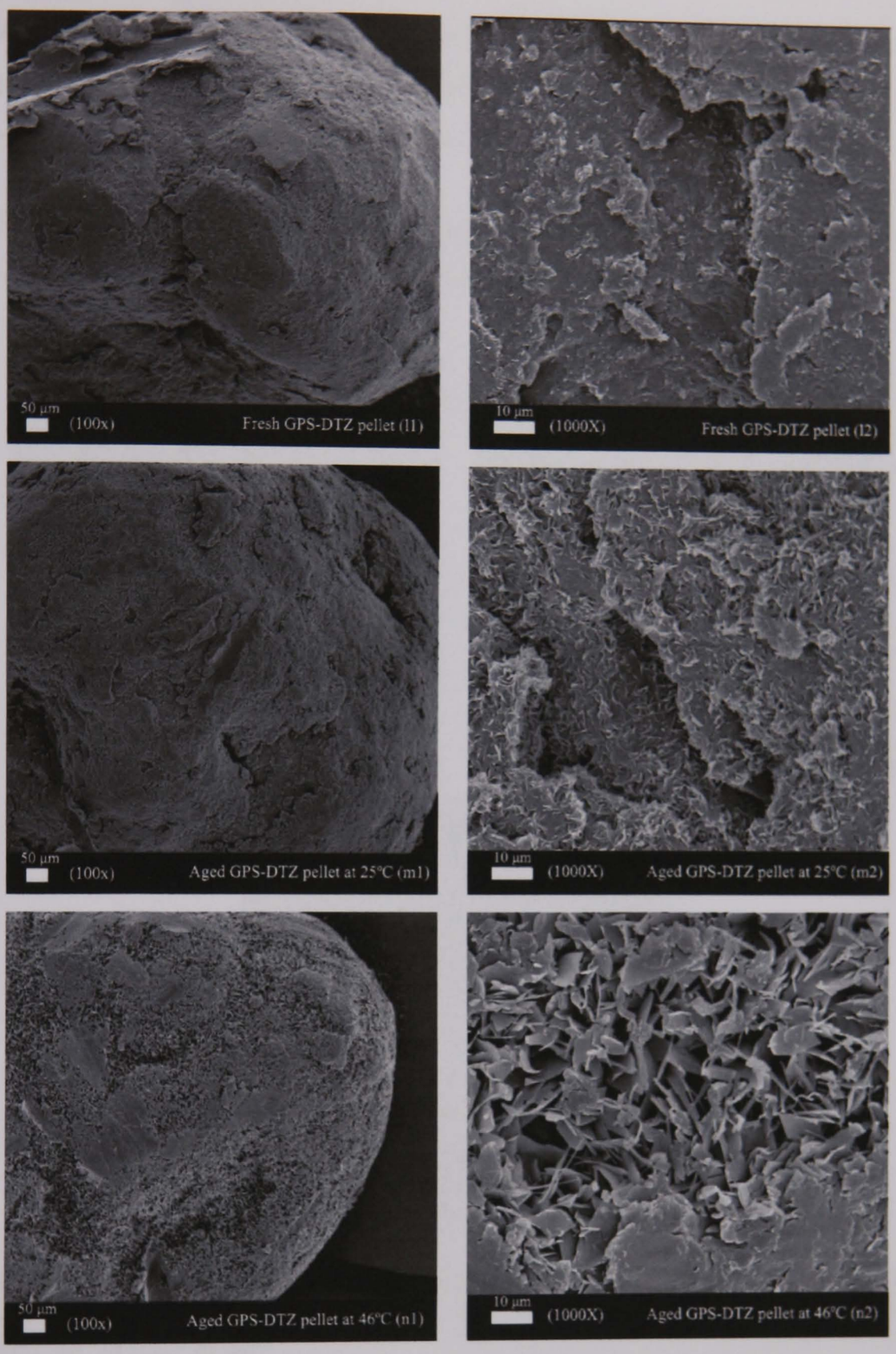

Figure 6.22. SEM photographs at magnification (**1**) 100X or (**2**) 1000X of GPS-diltiazem pellets on surface obtained from (**l**) fresh, (**m**) annealed for 28 days at 25°C or (**n**) annealed for 28 days at 46°C.

Following annealing the surface of the GPS-diltiazem pellets showed the development of a more pronounced crystalline nature.

Similarly, with Gelucire 50/13-drug (paracetamol or caffeine) dispersions, Khan and Craig (2004) suggested a general mechanism of morphological change with small scale-like crystals transforming to leaf-like structures during storage at 37°C.

The SEM photographs of the cross-section of GPS-diltiazem pellets after annealing at 25 or 46°C are shown in Figure 6.23 below.

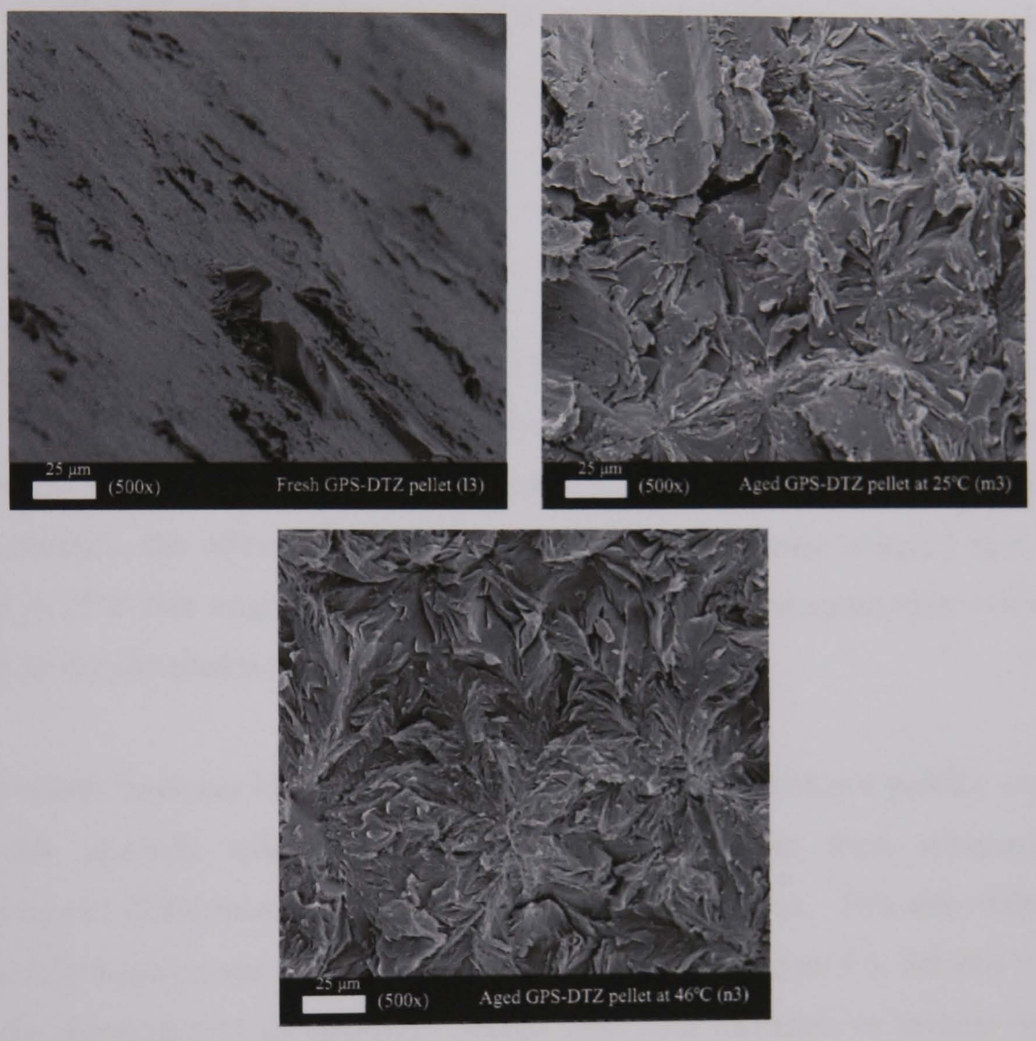

Figure 6.23. SEM photographs at magnification (**3**) 500X of GPS-diltiazem pellets on cross section obtained from (**l**) fresh, (**m**) annealed for 28 days at 25°C or (**n**) annealed for 28 days at 46°C.

Whereas the fresh GPS pellets (Figure 6.23(l3)) showed a generally smooth surface, annealed pellets showed the development of defined crystalline structures. It is possible that the presence of this internal crystalline nature exerts an influence on structure porosity that may lead to enhancement in dissolution rate as reported in Section 5.3.2.

Shimpi et al. (2004) and Chauhan et al. (2005a) reported similar findings for granules containing drug (diltiazem HCl or risedronate sodium) and Gelucire 43/01, with SEM photographs of fresh granules showing smooth surfaces without crystal formation. However, aged samples exhibited rougher surfaces due to phase induced transformations. Moreover, Roussin and Duddu (2001) and Galal et al. (2004) reported that fresh Gelucire 50/13 matrix formulations had smooth homogeneous surfaces whereas aged samples showed cracks and fissures on the surface. In that instance, the formation of cracks and fissures led to easier penetration of dissolution medium which expedited drug release.

6.4 Conclusion

Using the novel Texture Analyser method described above, GPS samples were found to be harder materials than GMS samples, having higher mean slopes, maximum forces and AUCs as determined by the probe penetration test. For both GMS and GPS samples, the effect of storage at 46°C afforded a harder material than when stored at 25°C that might cause by macroscopic structural reorganisation within the matrix at the elevated temperature.

The Texture Analyser identified sub-strata from the force–distance profiles over the first few seconds with zones exhibiting fluctuations in force measurements suggestive of differences in internal structures within the wax. This may reflect the reduced dissolution rate observed in aged GMS samples (Figure 5.3, Section 5.3.1.2) with the development of structure perhaps reflecting diffusion or erosion barriers associated with polymorphic transitions within the matrix. The reasons for the acceleration of dissolution rate observed for GPS formulations (Figure 5.9, Section 5.3.2.2) is not apparent from Texture Analyser studies since little development of structure was observed during ageing. This would suggest that microscopic structure is not the only determinant of dissolution rate changes for such GPS formulations.

Using SEM, the untreated GMS appeared as large crystals indicating the ß-form but in melt-solidified GMS, they showed smooth homogeneous surface indicating the α-form which transformed gradually during annealing to the ß-form. Moreover, the

melt-solidified GPS showed a rougher surface which differed to the smooth surface obtained from melt-solidified GMS. However, these morphological changes could not observed by polarised light microscopy.

Thermal annealing at 46°C in both GMS and GPS pellet formulations had a greater effect on surface morphology than at 25°C. Even though thermal annealing of GMS pellet induced the formation of large wax crystals, the transformation from α- to ß-form (poorer wetting property) had a greater influence on drug release.

However, in order to substantiate whether the increased dissolution rate of GPS pellets following annealing is related to enhanced porosity following the formation of large wax crystals, further studies using mercury porosimetry were considered. However, accessibility to this technique was limited. Whether mercury penetration would be unimpeded to all pores within the matrix thereby giving a true porosity value was considered doubtful and sample deformation under the test conditions was considered a possibility which would further detract from such an experimental approach.

CHAPTER 7

IMPACT OF THERMAL ANNEALING AND STABILISATION EXCIPIENTS ON DISSOLUTION PROPERTIES OF WAX MATRIX PELLETS

7.1 Introduction

From Chapter 5, thermal annealing at 46°C for up to 14 days would be sufficient to stabilise the dissolution performance of pellet formulations containing 90% GPS and 10% diltiazem HCl. However, since thermal annealing is an impractical method for industry, the addition of nucleation inhibitors [e.g. polyvinyl pyrrolidone (PVP), carboxy methyl cellulose (CMC), Cab-O-Sil (fumed silica) or hydroxylpropyl methyl cellulose (HPMC)] or nucleation enhancers (e.g. glyceryl monostearate (GMS), polyethylene glycol (PEG) 1450, PEG ester mixture, stearate 1500 and other long chain fatty acids) was explored as a mechanism for bypassing the requirement to anneal product thereby providing reproducible dissolution performance (Roussin and Duddu, 2001). The aim of this chapter was therefore to investigate mechanisms for stabilising dissolution performance during thermal annealing and/or by the addition of some of the above stabilisation excipients. Diltiazem HCl was chosen as a model drug since it had optimal analytical properties and provided comparison with previously experimental data. In vitro dissolution of GPS-diltiazem pellet formulations was investigated using four dissolution media at pH 1.2; pH 5.0; pH 7.4 to simulate changing pH environment throughout the GI tract as well as in distilled water.

7.2 Methods

Sample preparation and analysis methods are provided below and referenced where appropriate to Chapter 2.

7.2.1 Effect of nucleation inhibitors on response to thermal annealing

$HPMC_{K15M}$ (Methocel® K15 M Premium; high viscosity) was used as a nucleation inhibitor in this study. Pellets composed of 4.5% $HPMC_{K15M}$, 85.5% GPS and 10% diltiazem HCl were prepared by following the general direct warm spheronisation method (Section 2.5, Page 65) using a spheronisation temperature of 45°C and a spheronisation time of 5 minutes. GPS pellets of size range 1001 to 1180 μm were annealed in the air-tight amber glass container at 25 or 46°C for fixed times (0, 7, 14 or 28 days) and then evaluated by dissolution test (Section 2.4.3, Page 50).

7.2.2 Effect of nucleation enhancers on response to thermal annealing

GMS and PEG 1450 were selected as nucleation enhancers. Pellet compositions are shown in Table 7.1 below. Pellets were prepared by following the general direct warm spheronisation method (Section 2.5, Page 65) using a spheronisation temperature of 45°C and a spheronisation time of 5 minutes.

Table 7.1. Pellet formulations containing 10% diltiazem HCl and 90% excipient incorporating the nucleation enhancers.

Formulation	DTZ content (%w/w)	GPS content (%w/w)	GMS content (%w/w)	PEG 1450 content (%w/w)
I	10	85.5	2.25	2.25
II	10	85.5	4.5	-
III	10	81	9	-

GPS pellets of size range 1001 to 1180 μm were annealed in the air-tight amber glass container at 25 or 46°C for fixed times (0, 7, 14 or 28 days) and then evaluated by dissolution test (Section 2.4.3, Page 50).

7.2.3 In vitro dissolution of GPS-diltiazem pellet formulations in various dissolution media

Pellets composed of 90% GPS and 10% diltiazem HCl were prepared following the general direct warm spheronisation method (Section 2.5, Page 65) using a spheronisation temperature of 45°C and a spheronisation time of 5 minutes. Pellets within the size range of 1001 to 1180 μm were used for subsequent dissolution studies (Section 2.4.3, Page 50). The pellets were performed in different pH media which were distilled water, hydrochloric acid buffer solution pH 1.2, phosphate buffer solution pH 5.0 and pH 7.4.

7.3 Results and Discussion

7.3.1 Effect of nucleation inhibitor on response to thermal annealing

7.3.1.1 Dissolution studies

The result of the effect of $HPMC_{K15M}$ on the dissolution performance of GPS pellets thermally annealed at 46°C is shown in Figure 7.1 below.

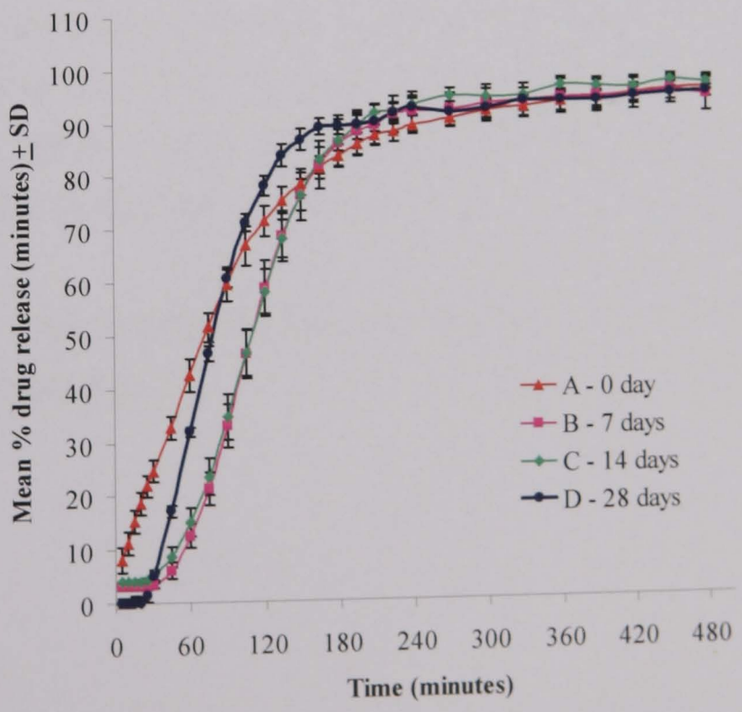

Figure 7.1. Dissolution profiles of pellets containing 4.5% $HPMC_{K15M}$, 85.5% GPS and 10% diltiazem HCl after annealing for 7, 14 or 28 days at 46°C (n = 6).

As annealing time increased from 0 to 7 days, there was a decrease in drug dissolution rate (Figure 7.1). Between days 7 – 14 no significant changes occurred in dissolution rate (Fit factor for statistical analysis with $f_1 < 15\%$ and $f_2 > 50\%$; Appendix I, Table I.3.1). After 14 days, an increase in drug release was observed when analysed using Fit factor (with $f_1 > 15\%$ and $f_2 < 50\%$). In comparison when pellets were annealed at 25°C for 28 days, no significant change in drug release was observed (data not shown).

Fresh GPS pellets containing $HPMC_{K15M}$ reached 80% drug release within 3 hours which was faster than that observed for pellets containing 90% GPS and 10% diltiazem HCl (~ 14 hours, Figure 5.9 in Section 5.3.2.2). This is attributable to $HPMC_{K15M}$ being a hydrophilic excipient which acts to enhance the penetration of dissolution medium into pellets accelerating drug release.

Similarly, Roussin and Duddu (2001) reported that nucleation inhibitors such as PVP (5 - 10% w/w), CMC (5% w/w) or Cab-O-Sil (1.25% w/w) in Gelucire 50/13–theophylline mixtures had no effects on drug release during storage at 25 or 40°C. In contrast, Jannin et al. (2006) noted that inclusion of 25% w/w poloxamer 407 (Lutrol® F127; hydrophilic polymer) in theophylline capsules containing 14.7% drug and 60.3% GPS inhibited changes in drug release profiles upon 6 months storage. Moreover, Galal et al. (2004) reported that incorporation of 10% w/w PVP in Gelucire 33/01 matrix formulations decreased physical changes and stabilised dissolution profiles during storage at room temperature for one year.

From Figure 7.1, the relationship between annealing time and mean times to drug release is shown in Figure 7.2.

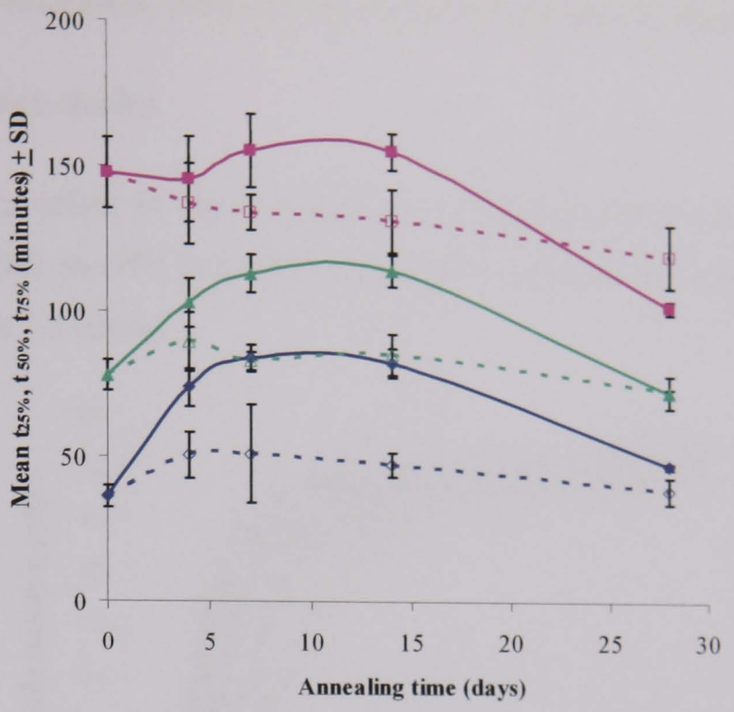

Figure 7.2. Effect of pellet annealing on mean times to 25%, 50% or 75% drug release ($t_{25\%}$, $t_{50\%}$ or $t_{75\%}$) of formulations containing 4.5% $HPMC_{K15M}$, 85.5% GPS and 10% diltiazem HCl after annealing for 7, 14 or 28 days at 46°C (solid lines) or 25°C (dotted lines) (n = 6) (—◆— $t_{25\%}$ at 46°C; - ◇ - $t_{25\%}$ at 25°C; —▲— $t_{50\%}$ at 46°C; - △ - $t_{50\%}$ at 25°C; —■— $t_{75\%}$ at 46°C; - □ - $t_{75\%}$ at 25°C).

Annealing at 46°C affected the $t_{25\%}$, $t_{50\%}$ and $t_{75\%}$ data in a similar manner with small increases being observed over the first 7 days, followed by a plateau then a decrease by day 28. However, the $t_{25\%}$, $t_{50\%}$ and $t_{75\%}$ in pellets annealed at 25°C were generally constant. The reasons for the observed decrease in the dissolution profile followed by a return to initial values are not understood. In conclusion, $HPMC_{K15M}$ was not a suitable excipient to incorporate in the wax formulation because it could not prevent dissolution changes from occurring during thermal annealing at 46°C. Hence, a nucleation enhancer was investigated in the following section.

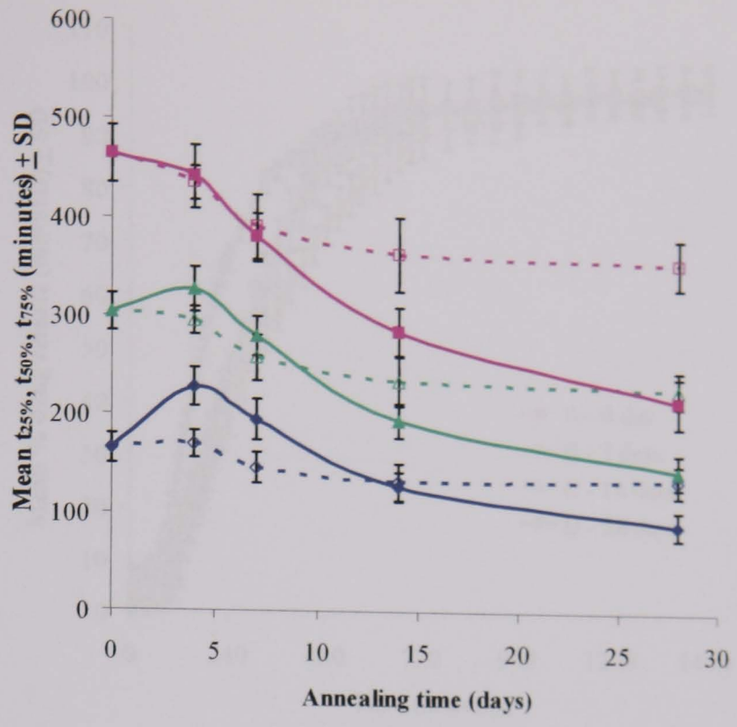

Figure 7.4. Effect of pellet annealing on mean times to 25%, 50% or 75% drug release ($t_{25\%}$, $t_{50\%}$ or $t_{75\%}$) of Formulation I containing 2.25% PEG 1450, 2.25% GMS, 85.5% GPS and 10% diltiazem HCl after annealing for 7, 14 or 28 days at 46°C (solid lines) or 25°C (dotted lines) (n = 6) (—◆— $t_{25\%}$ at 46°C; - ◇ - $t_{25\%}$ at 25°C; —▲— $t_{50\%}$ at 46°C; - △ - $t_{50\%}$ at 25°C; —■— $t_{75\%}$ at 46°C; - □ - $t_{75\%}$ at 25°C).

The observed profiles of annealing at 46°C for $t_{25\%}$, $t_{50\%}$ and $t_{75\%}$ were generally similar with a progressive increase in dissolution rate (reduction in t values) being observed after 4 days. However, the $t_{25\%}$, $t_{50\%}$ and $t_{75\%}$ in pellets annealed at 25°C were near constant.

The result of the effect of 4.5% GMS alone as a nucleation enhancer in GPS pellets following thermal annealing at 46°C is shown in Figure 7.5 below.

7.3.2 Effect of nucleation enhancer on response to thermal annealing

7.3.2.1 Dissolution studies

The result of the effect of incorporation of nucleation enhancers (2.25% GMS and 2.25% PEG 1450) on GPS pellet dissolution following thermal annealing at 46°C is shown in Figure 7.3 below.

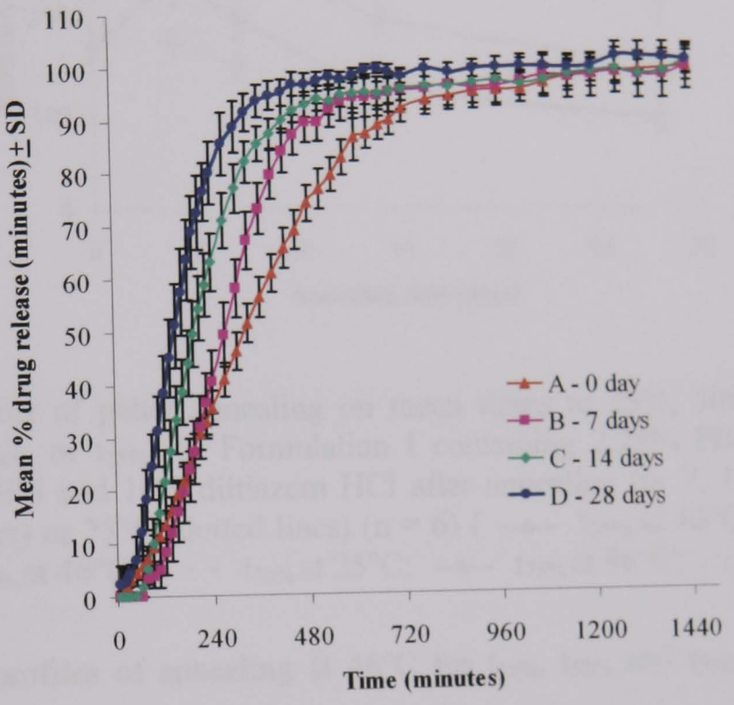

Figure 7.3. Dissolution profiles of Formulation I containing 2.25% PEG 1450, 2.25% GMS, 85.5% GPS and 10% diltiazem HCl after annealling for 7, 14 or 28 days at 46°C (n = 6).

The dissolution performance of GPS pellets containing nucleation enhancers were broadly similar to that observed in 90% GPS-10% diltiazem pellets (Figure 5.9, Section 5.3.2.2) with increasing annealing time resulting in increased dissolution rates (with f_1 >15% and f_2 < 50%; Appendix I, Table I.3.2.1). However, samples annealed at 25°C for 28 days were not found to significantly affect dissolution (data not shown).

From Figure 7.3, the relationship between annealing time and mean times to drug release is shown in Figure 7.4.

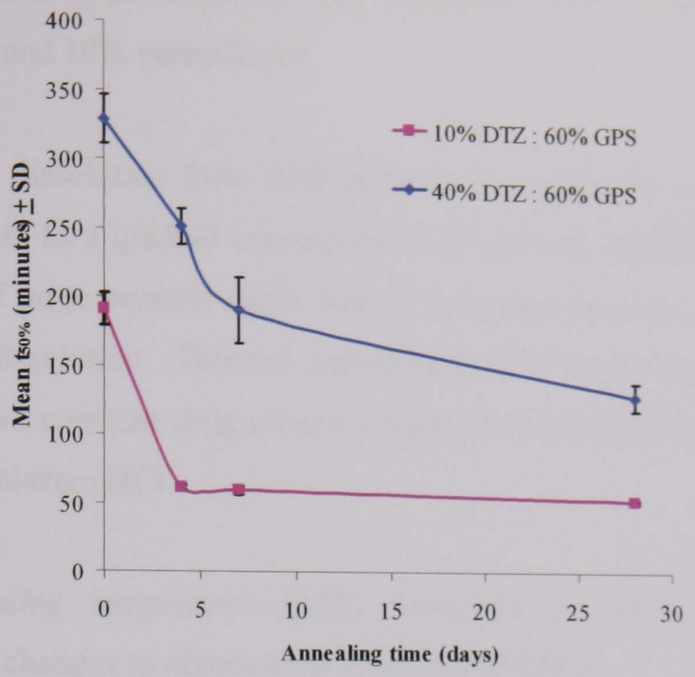

Figure 5.24. Effect of drug content on mean time to 50% drug release ($t_{50\%}$) of formulations containing GPS (60%), DCP (0 - 30%) and DTZ (10 – 40%) after annealing for 4, 7 or 28 days at 46°C (n = 6).

Pellets containing 10% drug content had a noticeably more rapid release compared to those containing 40% diltiazem HCl. This was completely unexpected and no explanation is offered even after consideration of the potential role of the DCP excipient. In both samples, the $t_{50\%}$ decreased upon annealing with the 10% formulation plateauing after 4 days whereas the 40% formulation continued to fall progressively over the 28 day period.

5.4 Conclusion

The physicochemical changes observed in GMS and GPS formulations during thermal annealing were monitored by DSC, HSM, XRPD as well as dissolution testing. Thermal annealing at 46°C produced divergent effects on GMS and GPS pellets with decreased release rates in GMS formulations and increased release rates in GPS formulations.

Annealing was associated with physicochemical transformations to the more stable GMS polymorph which has poorer wetting properties. The optimal annealing time

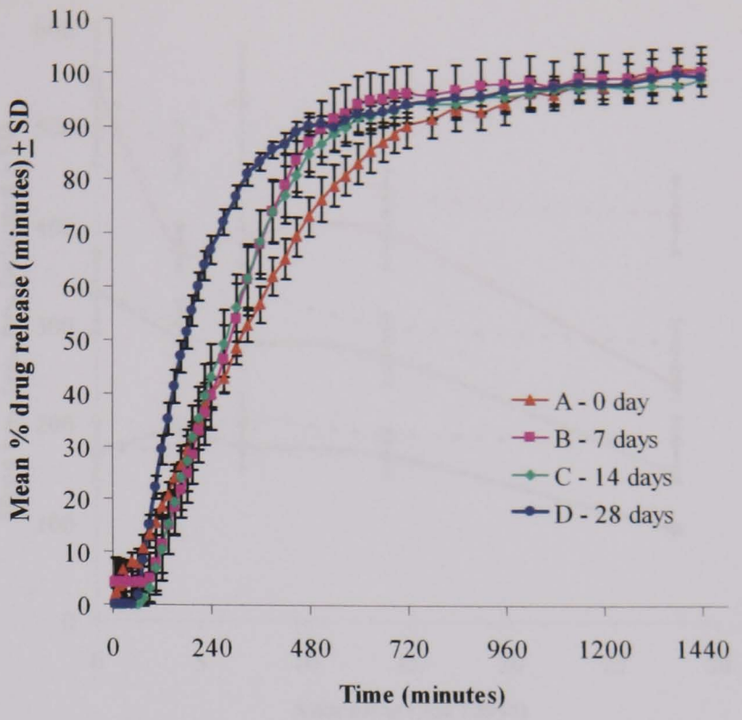

Figure 7.5. Dissolution profiles of Formulation II containing 4.5% GMS, 85.5% GPS and 10% diltiazem HCl after annealing for 7, 14 or 28 days at 46°C (n = 6).

Increasing annealing time over 14 days resulted in little change in dissolution profiles, however longer annealing time significantly increased drug dissolution rate (with f_1 >15% and f_2 < 50%; Appendix I, Table I.3.2.2) as shown in Figure 7.5. Thermal annealing of Formulation II at 25°C for 28 days had no effect on drug release changes (data not shown).

From Figure 7.5, the relationship between annealing time and mean times to drug release is shown in Figure 7.6.

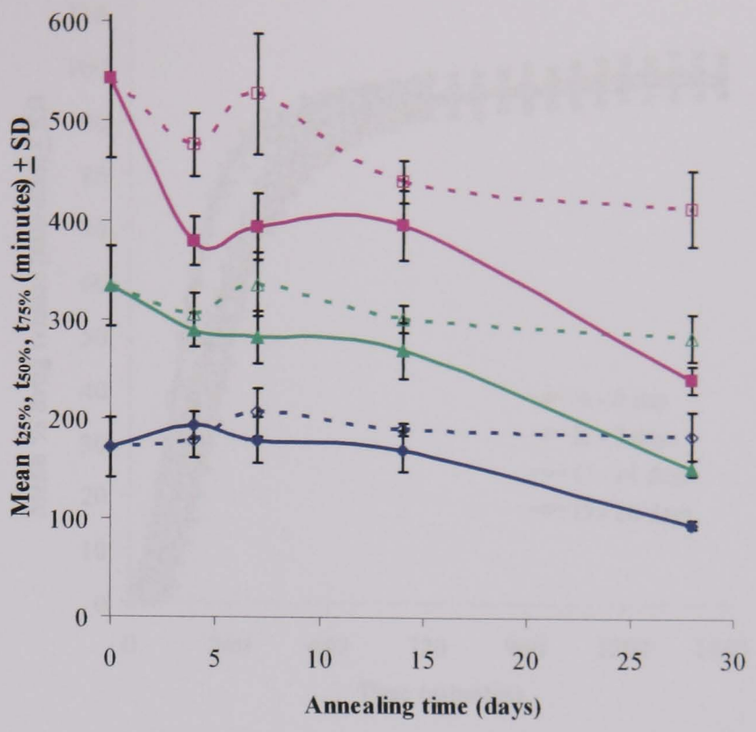

Figure 7.6. Effect of pellet annealing on mean times to 25%, 50% or 75% drug release ($t_{25\%}$, $t_{50\%}$ or $t_{75\%}$) of Formulation II containing 4.5% GMS, 85.5% GPS and 10% diltiazem HCl after annealing for 7, 14 or 28 days at 46°C (solid lines) or 25°C (dotted lines) (n = 6) (—◆— $t_{25\%}$ at 46°C; - ◇ - $t_{25\%}$ at 25°C; —▲— $t_{50\%}$ at 46°C; - △ - $t_{50\%}$ at 25°C; —■— $t_{75\%}$ at 46°C; - □ - $t_{75\%}$ at 25°C).

Following annealing at 46°C for $t_{25\%}$, $t_{50\%}$ and $t_{75\%}$ values were generally similar with a plateau being observed over the first 14 days, followed by a decrease. This suggested that addition of 4.5% GMS as a nucleation enhancer in Formulation II was capable of preventing dissolution changes for the first 14 days after which an increase in dissolution rate occurred. However, the $t_{25\%}$, $t_{50\%}$ and $t_{75\%}$ values in pellets annealed at 25°C were similar.

The result of the effect of 9% GMS as a nucleation enhancer in GPS pellets following thermal annealing at 46°C is shown in Figure 7.7 below.

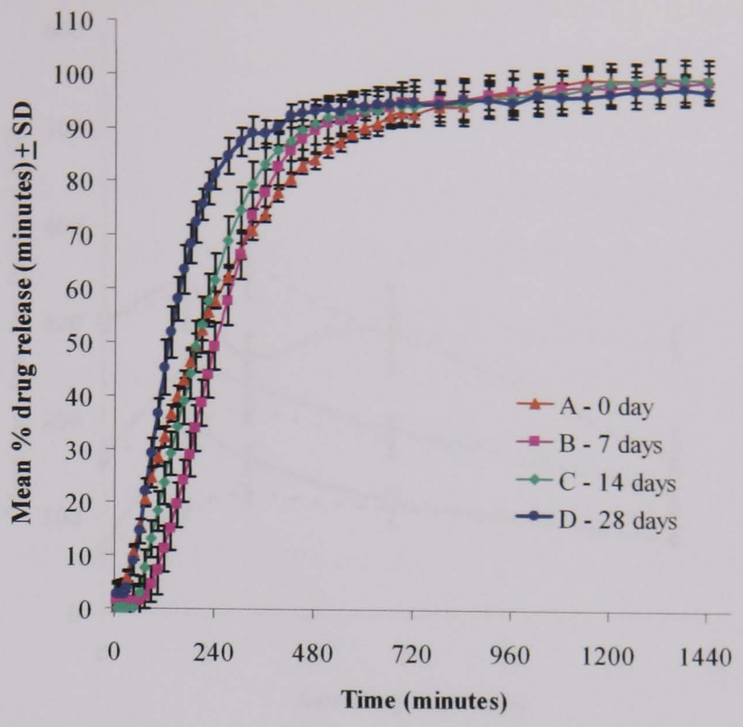

Figure 7.7. Dissolution profiles of Formulation III containing 9% GMS, 81% GPS and 10% diltiazem HCl after annealing for 7, 14 or 28 days at 46°C (n = 6).

Over 0 – 14 days annealing, similar dissolution profiles were observed. However after 28 days the dissolution rate had significantly increased (with $f_1 > 15\%$ and $f_2 < 50\%$; Appendix I, Table I.3.2.3) as shown in Figure 7.8. Thermal annealing of Formulation III at 25°C for 28 days had no effect on drug release changes (data not shown).

Fresh Formulation III reached 80% drug release within ~ 7 hours which was marginally faster than fresh pellets of Formulations I and II (Figures 7.3 and 7.5 respectively). This may be due to the reduction in GPS content by replacement with more hydrophilic GMS allowing easier penetration of dissolution medium into pellets and accelerating drug release.

From Figure 7.7, the relationship between annealing time and mean times to drug release is shown in Figure 7.8.

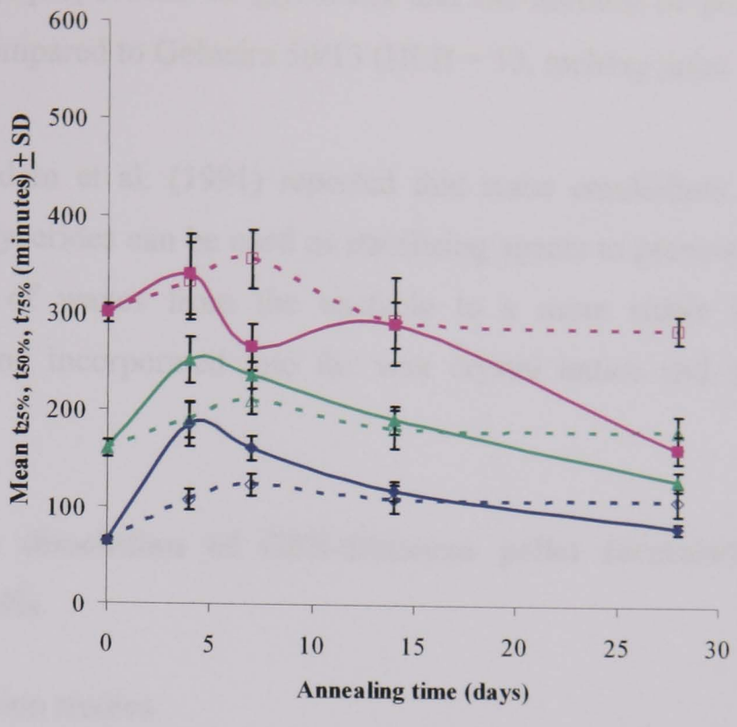

Figure 7.8. Effect of pellet annealing on mean times to 25%, 50% or 75% drug release ($t_{25\%}$, $t_{50\%}$ or $t_{75\%}$) of Formulation III containing 9% GMS, 81% GPS and 10% diltiazem HCl after annealing for 7, 14 or 28 days at 46°C (solid lines) or 25°C (dotted lines) (n = 6) (—◆— $t_{25\%}$ at 46°C; - ◇ - $t_{25\%}$ at 25°C; —▲— $t_{50\%}$ at 46°C; - △ - $t_{50\%}$ at 25°C; —■— $t_{75\%}$ at 46°C; - □ - $t_{75\%}$ at 25°C).

Annealing at 46°C resulted in the $t_{25\%}$, $t_{50\%}$ and $t_{75\%}$ values having generally similar profiles with an initial increase followed by a gradual decrease. The $t_{25\%}$, $t_{50\%}$ and $t_{75\%}$ values in pellets annealed at 25°C were constant.

From Formulations I – III, no formulations were capable of preventing alterations in dissolution following thermal annealing at 46°C over 28 days. However, Formulations II and III were capable of reducing dissolution changes over the first 14 days but not thereafter. However, Formulation III fundamentally influenced the whole profile. Hence the most promising formulation was Formulation II.

Although the addition of nucleation enhancers such as GMS and PEG 1450 could inhibit drug release from Gelucire 50/13–theophylline formulations during storage at 25 and 40°C for up to 2 months (Roussin and Duddu, 2001), this method was not appropriate in preventing changes in dissolution performance in GPS-diltiazem formulations. This might be a consequence of GPS (HLB = 2, melting point = 54°C)

having different proportions of glycerides and the absence of polyethylene glycol (PEG) esters compared to Gelucire 50/13 (HLB = 13, melting point = 50°C).

In addition, Eldem et al. (1991) reported that some emulsifiers such as lecithin, mono- and diglycerides can be used as stabilising agents to prevent the polymorphic transformation of waxes from the unstable to a more stable form due to the emulsifiers being incorporated into the wax crystal lattice and molecular spacial arrangements.

7.3.3 In vitro dissolution of GPS-diltiazem pellet formulations in various dissolution media

7.3.3.1 Dissolution studies

The result of the effect of pH medium on drug release from GPS pellets is shown in Figure 7.9 below.

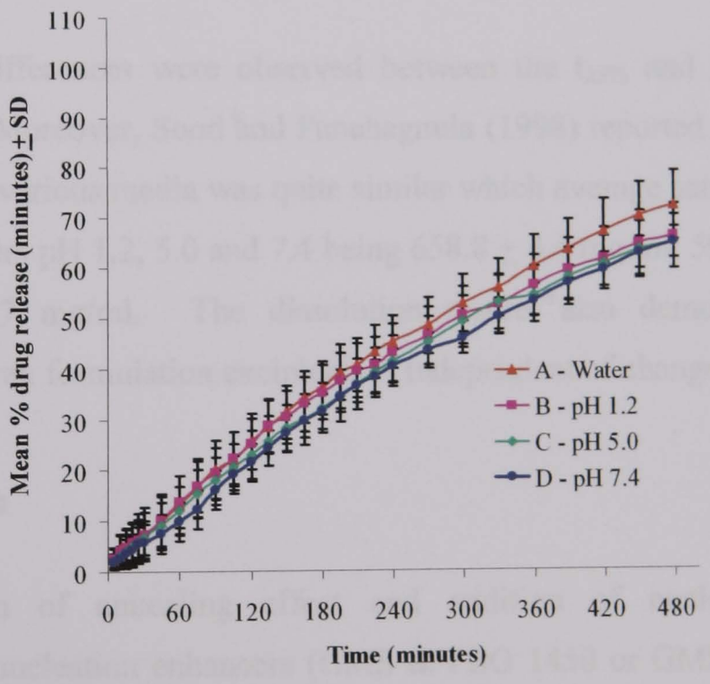

Figure 7.9. Dissolution profiles of pellets containing 90% GPS and 10% diltiazem HCl in different dissolution media (n = 6).

The different pH media had no significant effect on diltiazem HCl release from GPS pellets when analysed using Fit factors (with $f_1 < 15\%$ and $f_2 > 50$; Appendix I, Table

drug release. Addition the nucleation enhancers (2.25% GMS and 2.25% PEG 1250) in Formulation I was unable to prevent dissolution changes over time. However the inclusion of 4.5% GMS in Formulation II had a transient effect on dissolution profiles following 14 days annealing but was ineffective over 28 days. Increasing GMS content to 9% GMS in Formulation III failed to yield an additional advantage and also resulted in more rapid drug release. In conclusion, 4.5% GMS was observed to be the preferred concentration of excipient to stabilise drug dissolution changes following thermal annealing at 46°C. The inclusion of stabilisation excipients to prolong the stabilisation period warrants further study.

The independence of pH of the dissolution performance of the wax matrix pellets was encouraging and supports the further development of this formulation concept.

I.3.3). From Figure 7.9, the relationship between pH condition and mean times to drug release can be obtained as shown in Figure 7.10.

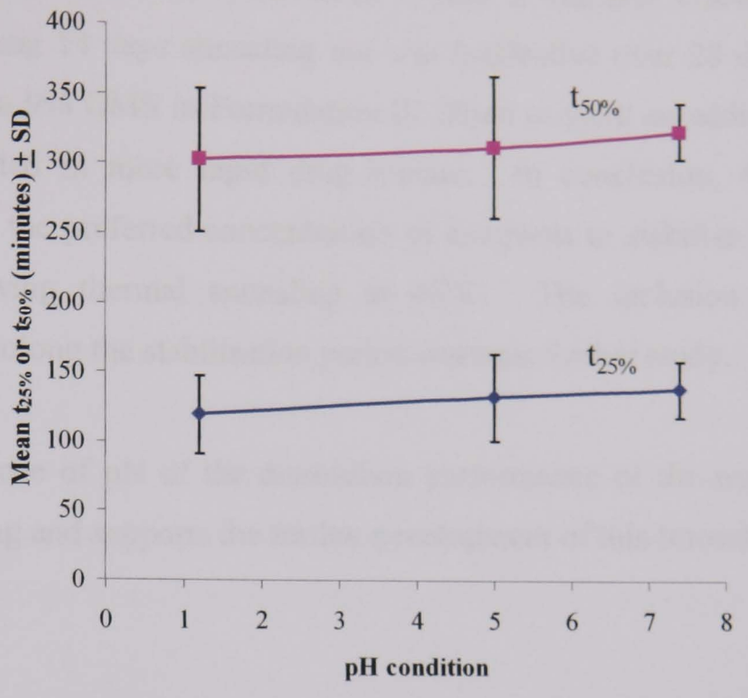

Figure 7.10. Effect of pH condition on mean times to 25% or 50% drug release ($t_{25\%}$ or $t_{50\%}$) from formulations containing 90% GPS and 10% diltiazem HCl (n = 6).

No significant differences were observed between the $t_{25\%}$ and $t_{50\%}$ values as a function of pH. Moreover, Sood and Panchagnula (1998) reported that solubility of diltiazem HCl in various media was quite similar which average saturation solubility at 37.5°C in buffers pH 1.2, 5.0 and 7.4 being 658.8 ± 4.4 mg/ml, 597.5 ± 1.5 mg/ml and 593.2 ± 3.7 mg/ml. The dissolution results also demonstrate that the functionality of wax formulation excipients is independent of changes in media pH.

7.4 Conclusion

The combination of annealing effect and addition of nucleation inhibitors ($HPMC_{K15M}$) or nucleation enhancers (GMS & PEG 1450 or GMS alone) in GPS-diltiazem pellet formulations were studied as potential strategies to stabilise pellet dissolution performance.

The incorporation the $HPMC_{K15M}$ was incapable of inhibiting dissolution changes following thermal annealing at 46°C and furthermore was observed to accelerate

CHAPTER 8

SUMMARY OF CONCLUSIONS AND FUTURE WORK

8.1 General discussion

Wax matrix pellets have been produced via a direct warm spheronisation method without extrusion. Melt solidification followed by milling then warm spheronisation techniques afforded sustained release matrix pellets. The yield of granules in the desirable size range was dependent on the blender milling time. In the spheronisation process, spheronisation time, speed and temperature all affected spheronicity, size distribution and dissolution performance of pellets.

The physicochemical properties of GMS and GPS materials changed during melt-solidification and subsequent ageing. These changes were monitored by FT-IR spectroscopy, differential scanning calorimetry (DSC), hot stage microscopy (HSM), X-ray powder diffraction (XRPD), Texture Analyser, polarised light microscopy and scanning electron microscopy (SEM), with varying degrees of success. In interpretation of the experimental data collected within this thesis, one should be cautious in generalising the findings due to the diversity in chemical composition of pharmacopoeia waxes which are permitted to exhibit significant heterogeneity in their composition. Therefore although the trends reported herein are likely to be applicable between batches, the absolute attributes of each are likely to deviate appreciably.

FT-IR spectroscopy identified changes in the spatial arrangement of the alcohol C-O and CH_3 of both GMS and GPS on storage following melting. These changes were temperature dependent and only manifested at temperatures of 25 and 50°C. DSC and FT-IR spectroscopy were complementary and indicated that a temperature of 3°C would prevent such changes; however this condition would not represent a useful pharmaceutical strategy.

DSC highlighted that fast cooling of GMS materials affected the recombination of wax components and accelerated the change to the stable form, however slow cooling led to fractionation of wax components into different melting fractions. A temperature of 46°C was found to be the optimal for the annealing process to afford rapid conversion to the stable form.

For GMS, it could be concluded that the untreated GMS (ß-form) when melted and cooled provides the α-form which reverts progressively back to the stable ß-form after annealing as demonstrated by FT-IR spectroscopy, DSC, XRPD and SEM. During thermal annealing of GPS, it could be concluded that the melt-solidified GPS also progressively crystallised as observed by FT-IR spectroscopy, DSC, XRPD and SEM. Moreover, high temperature thermal annealing (46°C) of both GMS and GPS had more pronounced affects on structure and physicochemical properties than when annealing was performed at low temperature (25°C) with melt-solidified GMS (composed of smaller molecular weight substances) taking noticeably less annealing time compared to melt-solidified GPS (composed of larger molecular weight substances).

Using the Texture Analyser, GPS samples were found to be harder materials than GMS samples, having higher mean slopes, maximum forces and AUCs. For both GMS and GPS samples, the effect of storage at 46°C afforded a harder material than when stored at 25°C that might cause by macroscopic structural reorganisation within the matrix at the elevated temperature.

The Texture Analyser also identified sub-strata from the force–distance profiles over the first few seconds of probe penetration with zones exhibiting fluctuations in force measurements suggestive of differences in internal structures within the wax. These initial investigations suggest that the Texture Analyser may be a useful technique for identifying micro-changes within a matrix structure which might be applicable to the study of other pharmaceutical forms.

The physicochemical changes observed in GMS and GPS formulations during thermal annealing were monitored by DSC, HSM, XRPD, polarised light microscopy, SEM as well as dissolution testing. Thermal annealing at 46°C produced divergent effects on GMS and GPS pellets with decreased release rates in GMS formulations and increased release rates in GPS formulations. Subsequent dissolution performance was dependent on wax type & content as well as drug type & content with each of these parameters responding differently to annealing.

Even though thermal annealing of GMS pellet resulted in the formation of large wax crystals, the transformation from α- to ß-form (poorer wetting property) had a more dominant influence on the decrease in drug release. The optimal annealing time was found to be 4 days at 46°C to effectively stabilise drug release profiles of GMS pellets containing GMS, with 30% DCP and 10% paracetamol.

In contrast, drug dissolution from GPS pellets was accelerated after annealing at 46°C, associated with a gradual crystallisation of GPS resulting more porous structure. Thermal annealing at 46°C for up to 14 days was sufficient to afford constant drug release profiles from GPS pellets containing GPS and 10% diltiazem HCl.

The incorporation the $HPMC_{K15M}$ in diltiazem–GPS formulations resulted in rapid drug release and had no effect on subsequent changes in the wax following thermal annealing at 46°C. The addition the 4.5% GMS was the preferred concentration of excipient to stabilise dissolution changes after thermal annealing at 46°C for 14 days.

The different pH media had no effects on diltiazem HCl release from GPS pellets containing GPS and 10% diltiazem HCl.

This research project was designed to develop wax matrix pellets based on a direct warm spheronisation method. In parallel physicochemical changes in GMS and GPS both as raw materials and in pellet formulations were investigated.

As discussed in the Introduction, pharmaceutical waxes are ill defined and this leads to irreproducible performance outcomes. This thesis reinforces the need for greater consistency in their compositions if their application in oral controlled release technology is to be more widely exploited. The utilisation of a spectrum of analytical techniques affords an opportunity for detailed characterisation of these types of materials and leads to an understanding of their behaviour following thermal stress which will be useful in monitoring consistency as manufacturers strive to improve product performance.

8.2 Suggested future work

The following future work is proposed:

- Investigate the effect of processing and thermal annealing on other pharmaceutical waxes (such as Gelucire 43/01, 50/02, 50/13, 44/14 or 55/18) and formulations containing alternative model drug substances. The properties can be assessed by FT-IR spectroscopy, DSC, HSM, XRPD, Texture Analyser, SEM, polarised light microscopy and dissolution testing.

- Investigate other techniques to produce wax matrix pellets such as spray congealing, melt pelletisation, extrusion-spheronisation and hot melt extrusion-spheronisation and investigate the incidence of changes in physicochemical and morphological properties (compared to those produced by the direct warm spheronisation method).

- Quantitatively measure pellet porosity or wettability based on mercury porosimeter density and pycnometric density or pellet contact angle to investigate the mechanism of dissolution changes following annealing

- Investigate the in vivo performance of freshly prepared and annealed formulations to determine the in vivo-in vitro correlation (IVIVC) of

formulations which appear to change significantly using in vitro analytical techniques.

- Investigate the effect of other stabilisation excipients such as polyvinyl pyrrolidone (PVP), carboxy methyl cellulose (CMC), poloxamer 407 (Lutrol® F127), lecithin, mono- and diglycerides on thermal annealing in the GPS-diltiazem pellet formulation to eliminate changes in drug release profiles.

- Investigate the behaviour of highly purified components of waxes to determine the relative importance of each component in the performance of pharmacopoeia waxes.

- Investigate the applicability of the Texture Analysis probe penetration technique as a more general analytical tool for characterisation of pharmaceutical systems.

REFERENCES

Abrahamsson, B., Alpsten, M., Jonsson, U. E., Lundberg, P. J., Sandberg, A., Sundgren, M., Svenheden, A., and Tolli, J. (1996). Gastro-intestinal transit of a multiple-unit formulation (metoprolol CR/ZOK) and a non-disintegrating tablet with the emphasis on colon. *International Journal of Pharmaceutics* **140**, 229-235.

Acemoglu, M. (2004). Chemistry of polymer biodegradation and implications on parenteral drug delivery. *International Journal of Pharmaceutics* **277**, 133-139.

Akiyama, Y., Yoshioka, M., Horibe, H., Hirai, S., Kitamori, N., and Toguchi, H. (1993). Mechanism of drug release from polyglycerol ester of fatty acid-based microspheres. *Journal of Controlled Release* **27**, 37-45.

Albertini, B., Passerini, N., Gonzalez-Rodriguez, M. L., Perissutti, B., and Rodriguez, L. (2004). Effect of aerosil on the properties of lipid controlled release microparticles. *Journal of Controlled Release* **100**, 233-246.

Alhamami, O. M. O. (2002). The effects of some physico-chemical factors and pharmaceutical excipients on the bioavailability of nitrofurantoin oily and aqueous suspensions in rats. *Drug Development and Industrial Pharmacy* **28**, 305-316.

Amidon, G. L., Lennernas, H., Shah, V. P., and Crison, J. R. (1995). A theorectical basis for a biopharmaceutic drug classification: the correlation of in vitro drug product dissolution and in vivo bioavailability. *Pharmaceutical Research* **12**, 413-420.

Attwood, D. (2007). Disperse systems. In *Aulton's pharmaceutics: The design and manufacture of medicines* (M. E. Aulton, Ed.), pp. 70-98. Elsevier Limited, Philadelphia.

Baert, L., and Remon, J. P. (1993). Influence of amount of granulation liquid on the drug release rate from pellets made by extrusion spheronisation. *International Journal of Pharmaceutics* **95**, 135-141.

Barker, S. A., Yap, S. P., Yuen, K. H., McCoy, C. P., Murphy, J. R., and Craig, D. Q. M. (2003). An investigation into the structure and bioavailability of [alpha]-tocopherol dispersions in Gelucire 44/14. *Journal of Controlled Release* **91**, 477-488.

Barrau, J. P., Bataille, B., and Jacob, M. (1993). The influence of spheroniser load in extrusion-spheronisation. *Pharm. Tech. Int. Biophys.* **5**, 66-70.

Berger, K. G., and Hamilton, R. J. (1995). Lipids and oxygen: is rancidity avoidable in practice? In *Developments in oils and fats* (R. J. Hamilton, Ed.), pp. 192-203. Blackie Academic and Professional, Suffolk.

Blanque, D., Sternagel, H., Podczeck, F., and Newton, J. M. (1995). Some factors influencing the formation and in vitro drug release from matrix pellets prepared by extrusion/spheronization. *International Journal of Pharmaceutics* **119**, 203-211.

Bodea, A., and Leucuta, S. E. (1997). Optimization of hydrophilic matrix tablets using a D-optimal design. *International Journal of Pharmaceutics* **153**, 247-255.

Bresson, S., El Marssi, M., and Khelifa, B. (2006). Conformational influences of the polymorphic forms on the C-O and C-H stretching modes of five saturated monoacid triglycerides studied by Raman spectroscopy at various temperatures. *Vibrational Spectroscopy* **40**, 263.

British Pharmacopoeia (1999). In *British Pharmacopoeia*, pp. 515-516, 1088-1089. The stationery office, London.

Buckton, G., Beezer, A. E., Chatham, S. M., and Patel, K. K. (1989). In vitro dissolution testing of oral controlled release preparations in the presence of artificial foodstuffs. II. Probing drug/food interactions using microcalorimetry. *International Journal of Pharmaceutics* **56**, 151-157.

Caraballo, I., Millan, M., Rabasco, A. M., and Leuenberger, H. (1996). Zero-order release periods in inert matrices: Influence of the distance to the percolation threshold. *Pharmaceutica Acta Helvetiae* **71**, 335-339.

Chambin, O., Berard, V., Rochat-Gonthier, M. H., and Pourcelot, Y. (2002). Dry adsorbed emulsion: 2. Dissolution behaviour of an intricate formulation. *International Journal of Pharmaceutics* **235**, 169-178.

Chariot, M., Frances, J., Lewis, G. A., Mathieu, D., Luu, R. P. T., and Stevens, H. N. E. (1987). A factorial approach to process variables of extrusion-spheronisation of wet powder masses. *Drug Development and Industrial Pharmacy* **13**, 1639 - 1649.

Chatchawalsaisin, J., Podczeck, F., and Newton, J. M. (2005). The preparation by extrusion/spheronization and the properties of pellets containing drugs, microcrystalline cellulose and glyceryl monostearate. *European Journal of Pharmaceutical Sciences* **24**, 35-48.

Chauhan, B., Shimpi, S., Mahadik, K. R., and Paradkar, A. (2005a). Preparation and evaluation of floating Risedronate sodium-Gelucire® 43/01 formulations. *Drug Development and Industrial Pharmacy* **31**, 851 - 860.

Chauhan, B., Shimpi, S., and Paradkar, A. (2005b). Preparation and evaluation of glibenclamide-polyglycolized glycerides solid dispersions with silicon dioxide by spray drying technique. *European Journal of Pharmaceutical Sciences* **26**, 219-230.

Chidambaram, N., Porter, W., Flood, K., and Qiu, Y. (1998). Formulation and characterization of new layered diffusional matrices for zero-order sustained release. *Journal of Controlled Release* **52**, 149-158.

Chien, Y. W. (1992). Novel drug delivery systems, pp. 1-3. Marcel Dekker, New York.

Choy, Y. W., Khan, N., and Yuen, K. H. (2005). Significance of lipid matrix aging on in vitro release and in vivo bioavailability. *International Journal of Pharmaceutics* **299**, 55-64.

Clarke, G. M., Newton, J. M., and Short, M. B. (1995). Comparative gastrointestinal transit of pellet systems of varying density. *International Journal of Pharmaceutics* **114**, 1-11.

Costa, P., and Sousa Lobo, J. M. (2001). Modeling and comparison of dissolution profiles. *European Journal of Pharmaceutical Sciences* **13**, 123-133.

Craig, D. Q. M. (1995). The use of glycerides as controlled release matrices. In *Excipient and delivery systems for pharmaceutical formulations* (D. R. Karsa, Stephenson, R.A., Ed.), pp. 148-173. The royal society of chemistry, Cambridge.

Crowley, M. M., Schroeder, B., Fredersdorf, A., Obara, S., Talarico, M., Kucera, S., and McGinity, J. W. (2004). Physicochemical properties and mechanism of drug release from ethyl cellulose matrix tablets prepared by direct compression and hot-melt extrusion. *International Journal of Pharmaceutics* **269**, 509-522.

Danckwerts, M. P. (1994). Development of a zero-order release oral compressed tablet with potential for commercial tabletting production. *International Journal of Pharmaceutics* **112**, 37-45.

Davis, S. S., Khosia, R., Wilson, C. G., and Washington, N. (1987). Gastrointestinal transit of a controlled-release pellet formulation of tiaprofenic acid and the effect of food. *International Journal of Pharmaceutics* **35**, 253-258.

Dennis, A. B., Farr, S. J., Kellaway, I. W., Taylor, G., and Davidson, R. (1990). In vivo evaluation of rapid release and sustained release Gelucire capsule formulations. *International Journal of Pharmaceutics* **65**, 85-100.

Devereux, J. E., Newton, J. M., and Short, M. B. (1990). The influence of density on the gastrointestinal transit of pellets. *Journal of pharmacy and pharmacology* **42**, 500-501.

Duclos, R., Bourret, E., and Brossard, C. (1999). Rheology of polyol behenates and drug release from matrix monolithic capsules. *International Journal of Pharmaceutics* **182**, 145-154.

Ehtezazi, T., Washington, C., and Melia, C. D. (2000). First order release rate from porous PLA microspheres with limited exit holes on the exterior surface. *Journal of Controlled Release* **66**, 27-38.

Eldem, T., Speiser, P., and Altorfer, H. (1991). Polymorphic behavior of sprayed lipid micropellets and its evaluation by differential scanning calorimetry and scanning electron microscopy. *Pharmaceutical Research* **8**, 178-184.

Emas, M., and Nyqvist, H. (2000). Methods of studying aging and stabilization of spray-congealed solid dispersions with carnauba wax. 1. Microcalorimetric investigation. *International Journal of Pharmaceutics* **197**, 117-127.

European Pharmacopoeia (2007). In *European Pharmacopoeia*, pp. 1990-1991, 1996-1997. Directorate for the Quality of Medicines of the Council of Europe, Nordlingen.

FDA (1997). Guidance for industry: Dissolution testing of immediate release solid oral dosage forms. (Center of Drug Evaluation and Research, Ed.).

Ford, J. L., and Timmins, P. (1989). Instrumentation for thermal analysis. In *Pharmaceutical thermal analysis: Techniques and applications*, pp. 7-24. Ellis Horwood Limited, West Sussex.

Frenning, G., and Stromme, M. (2003). Drug release modeled by dissolution, diffusion, and immobilization. *International Journal of Pharmaceutics* **250**, 137-145.

Galal, S., Massik, M. A. E., Abdallah, O. Y., and Daabis, N. A. (2004). Study of in-vitro release characteristics of carbamazepine extended release semisolid matrix filled capsules based on Gelucires. *Drug Development and Industrial Pharmacy* **30**, 817 - 829.

Gandhi, R., Lal Kaul, C., and Panchagnula, R. (1999). Extrusion and spheronization in the development of oral controlled-release dosage forms. *Pharmaceutical Science & Technology Today* **2**, 160-170.

Garti, N. and Sato, K. (1988). *Crystallization and polymorphism of fats and fatty acids*. Marcel Dekkar, New York.

Garti, N., Sato, K., and Yano, J. (2001). The role of emilsifiers in fat crystallization. In *Crystallization process in fats and lipid systems* (N. Garti, and K. Sato, Eds.), pp. 211-250. Marcel Dekkar, New York.

Grant, D. J. W. (1999). Theory and origin of polymorphism. In *Polymorphism in pharmaceutical solids* (H. G. Brittain, Ed.), pp. 1-33. Marcel Dekkar, New York.

Gren, T., and Nystrom, C. (1999). Porous cellulose matrices containing lipophilic release modifiers-a potential oral extended-release system. *International Journal of Pharmaceutics* **184**, 7-19.

Griffin, W. C. (1949). Classification of surface-active agents by HLB. *Journal of the Society of Cosmetic Chemists* **1**, 311-326.

Gunstone, F. D., and Norris, F. A. (1983). Oxidation. In *Lipids in foods: Chemistry, biochemistry and technology* (F. D. Gunstone, and F. A. Norris, Eds.), pp. 58-69. Pergamon Press Ltd., Exeter.

Hamdani, J., Moes, A. J., and Amighi, K. (2002). Development and evaluation of prolonged release pellets obtained by the melt pelletization process. *International Journal of Pharmaceutics* **245**, 167-177.

Hamdani, J., Moes, A. J., and Amighi, K. (2003). Physical and thermal characterisation of Precirol and Compritol as lipophilic glycerides used for the preparation of controlled-release matrix pellets. *International Journal of Pharmaceutics* **260**, 47-57.

Hatakeyama, T., and Quinn, F. X. (1999). Thermal analysis. In *Thermal analysis: Fundamentals and applications to polymer science*, pp. 1-4. John Wiley & Sons Ltd., West sussex.

Hellen, L., Yliruusi, J., Merkku, P., and Kristoffersson, E. (1993a). Process variables of instant granulator and spheroniser: I. Physical properties of granules, extrudate and pellets. *International Journal of Pharmaceutics* **96**, 197-204.

Hellen, L., Yliruusi, J., and Kristoffersson, E. (1993b). Process variables of instant granulator and spheroniser: II. Size and size distributions of pellets. *International Journal of Pharmaceutics* **96**, 205-216.

Hemming, F. M., and Hawthorne, J. N. (1996). Basic techniques. In *Lipid analysis*, pp. 5-72. BIOS Scientific Publishers Limited, Oxford.

Himawan, C., Starov, V. M., and Stapley, A. G. F. (2006). Thermodynamic and kinetic aspects of fat crystallization. *Advances in Colloid and Interface Science* **122**, 3-33.

Hoener, B., and Benet, L. Z. (2002). Factors influencing drug absorption and drug availabilty. In *Modern pharmaceutics* (G. S. Banker, Ed.), pp. 93-117. Marcel Dekkar, New York.

Jannin, V., Pochard, E., and Chambin, O. (2006). Influence of poloxamers on the dissolution performance and stability of controlled-release formulations containing Precirol® ATO 5. *International Journal of Pharmaceutics* **309**, 6-15.

Jenkins, R., and Snyder, R. L. (1996). *Introduction to X-ray powder diffractometry*. John Wiley & Sons, Inc., New York.

Jones, D. S., Lawlor, M. S., and Woolfson, A. D. (2002). Examination of the flow rheological and textural properties of polymer gels composed of poly(methyl vinylether-co-maleic anhydride) and poly(vinylpyrrolidone): Rheological and mathematical interpretation of textural parameters. *Journal of Pharmaceutical Sciences* **91**, 2090-2101.

Kaneko, F. (2001). Polymorphism and phase transitions of fatty acids and agylglycerols. In *Crystallization process in fats and lipid systems* (N. Garti, Sato, K., Ed.), pp. 53-97. Marcel Dekkar, New York.

Khaili, E., and Sallam, A. (2000). Content uniformity and dissolution characteristics of prednisolone Avicel PH 200 interactive powder mixture: a comparative study with Emcompress and lactose granules. *STP Pharma Sciences* **10**, 149-155.

Khan, N., and Craig, D. Q. M. (2003). The influence of drug incorporation on the structure and release properties of solid dispersions in lipid matrices. *Journal of Controlled Release* **93**, 355-368.

Khan, N., and Craig, D. Q. M. (2004). Role of blooming in determining the storage stability of lipid-based dosage forms. *Journal of Pharmaceutical Sciences* **93**, 2962-2971.

Kim, C. J. (1995). Compressed donut-shaped tablets with zero-order release kinetics. *Pharmaceutical Research* **12**, 1045-1048.

Laine, E., Auramo, P., and Kahela, P. (1988). On the structural behaviour of triglycerides with time. *International Journal of Pharmaceutics* **43**, 241-247.

Larsson, K. (1994). Physical properties-structural and physical characteristics. In *The lipid handbook* (F. D. Gunstone, J. L. Harwood, and F. B. Padley, Eds.), pp. 321-375. Chapman and Hall, London.

Lawler, P. J., and Dimick, P. S. (2002). Crystallization and polymorphism of fats. In *Food lipids: chemistry, nutrition and biochemistry* (C. C. Akoh, and D. B. Min, Eds.), pp. 229-247. Marcel Dekker Inc., New York.

Lee, J. N. N. (2003). Investigations into sustained-release hydrophobic matrix pellet formulations. In *Department of Pharmaceutical sciences*, University of Strathclyde, Glasgow.

Lee, J. N. N., Mullen, A. B., and Stevens, H. N. E. (2001). Effect of HLB on drug release from a hydrophobic matrix pellet delivery system. *Proceed. Intern. Symp. Control. Rel. Bioact. Mater.* **28**, 742-743.

Liu, J., Zhang, F., and McGinity, J. W. (2001). Properties of lipophilic matrix tablets containing phenylpropanolamine hydrochloride prepared by hot-melt extrusion. *European Journal of Pharmaceutics and Biopharmaceutics* **52**, 181-190.

Liversidge, G. G., Grant, D. J. W., and Padfield, J. M. (1981). Influence of physicochemical interactions on the properties of suppositories I. Interactions

between the constituents of fatty suppository bases. *International Journal of Pharmaceutics* **7**, 211-223.

Lu, R., and Abbott, J. A. (2004). Force/deformation techniques for measuring texture. In *Texture in food Vol. 2: Solid food* (D. Kilcast, Ed.), pp. 109-145. Woodhead Publishing limited and CRC Press LLC, Boca Raton.

Luttton, E. S., and Jackson, F. L. (1948). The polymorphism of 1-monostearin and 1-monopalmitin. *Journal of the American Oil Chemists' Society* **70**, 2445-2449.

Maejima, T., Osawa, T., Nakajima, K., and Kobayashi, M. (1997). Effect of species of non-meltable and meltable materials and their physical properties on granulatability in tumbling melt granulation method. *Chemical & pharmaceutical bulletin* **45**, 1833-1839.

Maruyama, T., Niiya, L., Imamura, M., Okada, M., and Matsumoto, T. (1973). Study on polymorphism of monoglyceride. II. thermodynamic considerations on transition. *Yukagaku* **22**, 85-88.

Maruyama, T., Niiya, L., Imamura, M., Okada, M., Matsumoto, T., Horisawa, M., and Mastumoto, T. (1971). Polymorphism of monoglycerides. I. Transition of crystal modifications of 1-monolaurin, 1-monomyristn, 1-monopalmitin and 1-monostearin. *Yukagaku* **20**, 395-402.

Mayersohn, M. (2002). Principles of drug absorption. In *Modern pharmaceutics* (G. S. Banker, Ed.), pp. 23-66. Marcel Dekkar, New York.

Metzler, C. M. (1991). Statistical criteria. In *Pharmaceutical bioequivalence* (P. G. Welling, F. L. S. Tse, and S. V. Dighe, Eds.), pp. 35-66. Marcel dekker Inc., New york.

Meyer, J. H., Dressman, J., and Amidon, G. (1985a). Effect of size and density on canine gastric emptying of nondigestible solids. *Gastroenterology* **89**, 805-813.

Meyer, J. H., Gu, Y. G., Dressman, J., and Amidon, G. L. (1985b). Effect of viscosity and flow rate on gastric empyting of solid. *Gastroenterology* **88**, 1501.

Meyer, J. H., Elahoff, J., Porter-Fink, V., Dressman, J., and Amidon, G. L. (1988). Human postprandial gastric emptying of 1-3 millimeters spheres. *Gastroenterology* **94**, 1315-1325.

Mills, B. (2006). Skeletal formula of paracetamol (N-(4-hydroxyphenyl)ethanamide, $C_8H_9NO_2$). user-created image.

Miyagawa, Y., Okabe, T., Yamaguchi, Y., Miyajima, M., Sato, H., and Sunada, H. (1996). Controlled-release of diclofenac sodium from wax matrix granule. *International Journal of Pharmaceutics* **138**, 215-224.

Moffat, A. C., Osselton, M. P., and Widdop, B. (2004). In *Clarke's analysis of drugs and poisons in pharmaceuticals, body fluids, and post-mortem material* (L. Galichet, Ed.), pp. 925-926, 1391-1393. The Pharmaceutical press, London.

Montousse, C., Pruvost, M., Rodriguez, F., and Brossard, C. (1999). Extrusion-spheronization manufacture of Gelucire® matrix beads. *Drug Development and Industrial Pharmacy* **25**, 75 - 80.

Moore, J. W., and Flanner, H. H. (1996). Mathematical comparison of dissolution profiles. *Pharmaceutical Technology* **20**, 64-74.

Mullin, J. W. (1996). Sieving of pharmaceuticals. In *Encyclopedia of pharmaceutical technology* (J. Swarbick, Bylan, J.C., Ed.), pp. 63-85. Marcel Dekker, New York.

Mulye, N. V., and Turco, S. J. (1995). A simple model based on first order kinetics to explain release of highly water soluble drugs from porous dicalcium phosphate dihydrate matrices. *Drug Development and Industrial Pharmacy* **21**, 943 - 953.

Nakahara, N. (1964). Methods and apparatus for making spherical. In *United States Patent 3 277 520*, United States.

Newton, J. M., Chapman, S. R., and Rowe, R. C. (1995). The influence of process variables on the preparation and properties of spherical granules by the process of extrusion and spheronisation. *International Journal of Pharmaceutics* **120**, 101-109.

Nur, A. O., and Zhang, J. S. (2000). Captopril floating and/or bioadhesive tablets: Design and release kinetics. *Drug Development and Industrial Pharmacy* **26**, 965-969.

Passerini, N., Perissutti, B., Albertini, B., Voinovich, D., Moneghini, M., and Rodriguez, L. (2003). Controlled release of verapamil hydrochloride from waxy microparticles prepared by spray congealing. *Journal of Controlled Release* **88**, 263-275.

Patzelt, W. J. (1985). In *Polarized light microscopy: Principals, instruments, applications*, pp. 1-102. Ernst Leitz Wetzlar GmbH, Wetzlar.

Peh, K. K., Wong, C. F., and Yuen, K. H. (2000). Possible mechanism for drug retardation from glyceryl monostearate matrix system. *Drug Development and Industrial Pharmacy* **26**, 447-450.

Phuapradit, W., Shah, N. H., Lou, Y., Kundu, S., and Infeld, M. H. (2002). Critical processing factors affecting rheological behavior of a wax based formulation. *European Journal of Pharmaceutics and Biopharmaceutics* **53**, 175-179.

Qiu, Y., Chidambaram, N., and Flood, K. (1998). Design and evaluation of layered diffusional matrices for zero-order sustained-release. *Journal of Controlled Release* **51**, 123-130.

Rao, P. R., Ramakrishna, S., and Diwan, P. V. (2000). Drug release kinetics from polymeric films containing propranolol hydrochloride for transdermal use. *Pharmaceutical Development and Technology* **5**, 465 - 472.

Reitz, C., and Kleinebudde, P. (2007). Solid lipid extrusion of sustained release dosage forms. *European Journal of Pharmaceutics and Biopharmaceutics* **67**, 440.

Remunan, C., Bretal, M. J., Nunez, A., and Vila Jato, J. (1992). Accelerated stability study of sustained-release nifedipine tablets prepared with Gelucire. *International Journal of Pharmaceutics* **80**, 151-159.

Rinaki, E., Valsami, G., and Macheras, P. (2003). The power law can describe the 'entire' drug release curve from HPMC-based matrix tablets: A hypothesis. *International Journal of Pharmaceutics* **255**, 199-207.

Rodriguez, L., Passerini, N., Cavallari, C., Cini, M., Sancin, P., and Fini, A. (1999). Description and preliminary evaluation of a new ultrasonic atomizer for spray-congealing processes. *International Journal of Pharmaceutics* **183**, 133-143.

Roussin, P., and Duddu, S. (2001). Sustained release theophylline formulations, excipient systems and methods of production. In *United States Patent 6 171 615 B1*, Gattefosse (Saint Priest, FR) SmithKline Beecham Corp. (Philadelphia, PA), United States.

Rowe, R. C. (1985). Spheronisation: A novel pill-making process? *Pharm. Int.* **6**, 119-123

Rowe, R. C., Sheskey. P. J., and Weller, P. J. (2003). In *Handbook of pharmaceutical excipients*, pp. 260-261, 264-268. Pharmaceutical press, Bath.

Roy, S., and Xu, W. (2001). Modeling of diffusion in the presence of damage in polymer matrix composites. *International Journal of Solids and Structures* **38**, 115-126.

Rubinstein, A., Li, V. H. K., Gruber, P., and Robinson, J. R. (1988). Gastrointestinal-physicological variables affecting the performance of oral sustained release dosage forms. In *Oral sustained release formulations: design and evaluation* (A. Yacobi, Halperin-Walega, E., Ed.), pp. 125-156. Pergamon Press, New York.

Sallam, E., Ibrahim, H., Takieddin, M., Abushamat, M., and Baghal, T. (1988). Dissolution characteristics of interactive powder mixtures. Part two: Effect of surface characteristics of excipients. *Drug Development and Industrial Pharmacy* **14**, 1277-1302.

Sallam, E., Ibrahim, H., Takieddin, M., Baghal, T., Saket, M., Awad, R., and Arafat, T. (1991). Dissolution characteristics of interactive powder mixtures. 4. Effects of additives on the dissolution of griseofulvin from Emcompress carrier. *International Journal of Pharmaceutics* **67**, 247.

San Vicente, A., Hernandez, R. M., Gascon, A. R., Calvo, M. B., and Pedraz, J. L. (2000). Effect of aging on the release of salbutamol sulfate from lipid matrices. *International Journal of Pharmaceutics* **208**, 13-21.

Sato, K. (1988). Crystallization of fats and fatty acids. In *Crystallization and polymorphism of fats and fatty acids* (N. Garti, and K. Sato, Eds.), pp. 227-266. Mercel Dekker, New York.

Shen, E., Kipper, M. J., Dziadul, B., Lim, M.-K., and Narasimhan, B. (2002). Mechanistic relationships between polymer microstructure and drug release kinetics in bioerodible polyanhydrides. *Journal of Controlled Release* **82**, 115-125.

Shimpi, S., Chauhan, B., Mahadik, K. R., and Paradkar, P. (2004). Preparation and evaluation of diltiazem hydrochloride-Gelucire 43/01 floating granules prepared by melt granulation. *AAPS PharmSciTech* **5**, article 43.

Siepmann, J., and Peppas, N. A. (2001). Modeling of drug release from delivery systems based on hydroxypropyl methylcellulose (HPMC). *Advanced Drug Delivery Reviews* **48**, 139-157.

Slayter, E. M., and Slayter, H. S. (1992). Scanning microscopes. In *Light and electron microscopy*, pp. 212-227. Cambridge University Press, Cambridge.

Smith, B. C. (1999). The basis of infrared interpretation. In *Infrared spectral interpretation: A systematic approach*, pp. 1-29. CRC Press, Washington.

Sood, A., and Panchagnula, R. (1998). Drug release evaluation of diltiazem CR preparations. *International Journal of Pharmaceutics* **175**, 95-107.

Srivastava, S. P., Tandon, R. S., Pandey, D. C., Madhwal, D. C., and Goyal, S. K. (1993). Phase transitions in petroleum waxes: Correlation with properties. *Fuel* **72**, 1345-1349.

Sutananta, W., Craig, D. Q. M., and Newton, J. M. (1994a). An investigation into the effect of preparation conditions on the structure and mechanical properties of pharmaceutical glyceride bases. *International Journal of Pharmaceutics* **110**, 75-91.

Sutananta, W., Craig, D. Q. M., and Newton, J. M. (1994b). The effects of ageing on the thermal behaviour and mechanical properties of pharmaceutical glycerides. *International Journal of Pharmaceutics* **111**, 51-62.

Sutananta, W., Craig, D. Q. M., and Newton, J. M. (1995a). An investigation into the effect of preparation conditions and storage on the rate of drug release from pharmaceutical glyceride bases. *Journal of pharmacy and pharmacology* **47**, 355-359.

Sutananta, W., Craig, D. Q. M., and Newton, J. M. (1995b). An evaluation of the mechanisms of drug release from glyceride bases. *Journal of pharmacy and pharmacology* **47**, 182-187.

The United States Pharmacopeia (2000). In *The United States Pharmacopeia: The National Formulary,* pp. 17-20, 573-575, 2462-2463. United states pharmacopeial convention Inc., Philadelphia.

Thorburn Burns, D. (1993). Principles of spectrophotometric measurements with particular reference to the UV-visble region. In *UV spectroscopy techniques, instrumentation, data handling* (B. J. Clark, T. Frost, and M. A. Russell, Eds.), pp. 1-16. Chapman & Hall, London.

Timms, R. E. (1995). Crystallisation of fats. In *Developments in oils and fats* (R. J. Hamilton, Ed.), pp. 204-223. Blackie Academic and Professional, Suffolk.

Varelas, C. G., Dixon, D. G., and Steiner, C. A. (1995). Zero-order release from biphasic polymer hydrogels. *Journal of Controlled Release* **34**, 185-192.

Vergote, G. J., Vervaet, C., Van Driessche, I., Hoste, S., De Smedt, S., Demeester, J., Jain, R. A., Ruddy, S., and Remon, J. P. (2001). An oral controlled release matrix pellet formulation containing nanocrystalline ketoprofen. *International Journal of Pharmaceutics* **219**, 81-87.

Vervaet, C., Baert, L., and Remon, J. P. (1995). Extrusion-spheronisation: A literature review. *International Journal of Pharmaceutics* **116**, 131-146.

Vippagunta, S. R., Brittain, H. G., and Grant, D. J. W. (2001). Crystalline solids. *Advanced Drug Delivery Reviews* **48**, 3-26.

Vippagunta, S. R., Maul, K. A., Tallavajhala, S., and Grant, D. J. W. (2002). Solid-state characterization of nifedipine solid dispersions. *International Journal of Pharmaceutics* **236**, 111-123.

Voinovich, D., Moneghini, M., Perissutti, B., Filipovic-Grcic, J., and Grabnar, I. (2000). Preparation in high-shear mixer of sustained-release pellets by melt pelletisation. *International Journal of Pharmaceutics* **203**, 235-244.

Wan, L. S. C., Heng, P. W. S., and Liew, C. V. (1993). Spheronization conditions on spheroid shape and size. *International Journal of Pharmaceutics* **96**, 59-65.

Washington, N., and Wilson, C. G. (1994). Behaviour of multiparticulate systems versus monolithic systems in the gastrointesitinal tract. I. Oesophagus and stomach. In *Multiparticulate controlled release oral dosage forms: Technology and biopharmaceutics* (C. D. Melia, N. Washington, and C. G. Wilson, Eds.), pp. 77-99. C & N Comminications Ltd., Edinburgh.

Watt, I. M. (1997). The electron microscopy family. In *The principles and practice of electron microscopy*, pp. 59-135. The Press Syndicate of the University of Cambridge, Cambridge.

West, R. J., Boehm, G., Dwyer, M., Williams, D. B., Sansom, L. N., and Penna, A. C. (1990). Bioavailbility of a new sustained-release theophylline capsule in fasted and non-fasted healthy subjects: single and multiple dosing studies. *Biopharmaceutics & drug disposition* **11**, 165-177.

Whittam, J. H., and Rosano, H. L. (1975). Physical aging of even saturated monoacid triglycerides. *Journal of the American Oil Chemists' Society* **52**, 128-133.

Wilding, I. R., Hardy, J. G., Maccari, M., Ravelli, V., and Davis, S. S. (1991). Scintigraphic and pharmacokinetic assessment of a multiparticulate sustained release formulation of diltiazem. *International Journal of Pharmaceutics* **76**, 133-143.

Wilding, I. R., Sparrow, R. A., Davis, S. S., and Horton, R. J. (1992). The role of gastric emptying in the absorption and metabolism of nifedipine given in a modified release pellet formulation. *International Journal of Pharmaceutics* **84**, 59-67.

Wu, P.-C., Tsai, M.-J., Huang, Y.-B., Chang, J.-S., and Tsai, Y.-H. (2002). In vitro and in vivo evaluation of potassium chloride sustained release formulation prepared with saturated polyglycolyed glycerides matrices. *International Journal of Pharmaceutics* **243**, 119-124.

Yajima, T., Itai, S., Takeuchi, H., and Kawashima, Y. (2002). Determination of optimum processing temperature for transformation of glyceryl monostearate. *Chemical & pharmaceutical bulletin* **50**, 1430-1433.

Yajima, T., Itai, S., Takeuchi, H., and Kawashima, Y. (2003). Optimum heat treatment conditions for masking the bitterness of the clarithromycin wax matrix. *Chemical & pharmaceutical bulletin* **51**, 1223-1226.

Young, C. R., Koleng, J. J., and McGinity, J. W. (2002). Production of spherical pellets by a hot-melt extrusion and spheronization process. *International Journal of Pharmaceutics* **242**, 87-92.

Yu, L. X., Amidon, G. L., Polli, J. E., Zhao, H., Mehta, M. U., Conner, D. P., Shah, V. P., Lesko, L. J., Chen, M., Lee, V. H. L., and Hussain, A. S. (2002). Biopharmaceutic classification system: The scientific basis for biowaiver extension. *Pharmaceutical Research* **19**, 921-925.

Yu, L. X., Crison, J. R., and Amidon, G. L. (1996). Compartmental transit and dispersion model analysis of small intestinal transit flow in humans. *International Journal of Pharmaceutics* **140**, 111-118.

Yuen, K. H., Deshmukh, A. A., Newton, J. M., Short, M., and Melchor, R. (1993). Gastrointestinal transit and absorption of theophylline from a multiparticulate controlled release formulation. *International Journal of Pharmaceutics* **97**, 61-77.

Yuksel, N., Karatas, A., Ozkan, Y., Savaser, A., Ozkan, S. A., and Baykara, T. (2003). Enhanced bioavailability of piroxicam using Gelucire 44/14 and Labrasol: In vitro and in vivo evaluation. *European Journal of Pharmaceutics and Biopharmaceutics* **56**, 453-459.

Zhou, F., Vervaet, C., and Remon, J. P. (1996). Matrix pellets based on the combination of waxes, starches and maltodextrins. *International Journal of Pharmaceutics* **133**, 155-160.

Zhou, F., Vervaet, C., and Remon, J. P. (1997). Influence of processing on the characteristics of matrix pellets based on microcrystalline waxes and starch derivatives. *International Journal of Pharmaceutics* **147**, 23-30.

Zhou, F., Vervaet, C., Schelkens, M., Lefebvre, R., and Remon, J. P. (1998). Bioavailability of ibuprofen from matrix pellets based on the combination of waxes and starch derivatives. *International Journal of Pharmaceutics* **168**, 79-84.

APPENDIX I

FIT FACTORS STATISTICAL ANALYSIS ON DISSOLUTION PROFILES

Fit Factors (difference factor f_1 and similarity factor f_2), calculated in percentage were used to compare the significance difference between two dissolution profiles at the same time. One graph was set as the reference graph while the other was assigned the test graph.

Dissolution profiles are determined to be significant difference when $f_1 \geq 15\%$ and $f_2 \leq 50\%$. When f_1 and f_2 values contradict significant results, the f_2 value was principally used to define the significant differences between two dissolution profiles. Tables I.1 to I.3 show the f_1, f_2 and overall results for various dissolution profile comparisons. Overall, profiles which are significantly different from each other statistically are assigned (√) but profiles which have no significantly different from each other statistically are assigned (X).

I.1 Chapter 3 The influence of processing on the characteristics of wax matrix pellets

I.1.1 Effect of spheronisation time on pellet dissolution

Table I.1.1 (from Figure 3.2)

Difference factor (f_1)

Time	initial	1 mins	2 mins	3 mins	4 mins	5 mins	6 mins
Initial		27.23	48.6	66.63	71.96	65.27	67.27
1 min			26.04	51.19	59.56	50.53	54.28
2 min				30.52	42.15	31.69	38.00
3 min					14.69	3.62	13.49
4 min						10.95	1.21
5 min							11.41
6 min							

Similarity factor (f_2)

Time	initial	1 min	2 mins	3 mins	4 mins	5 mins	6 mins
Initial		36.13	23.82	17.02	15.26	17.47	16.81
1 min			42.16	27.05	23.44	27.14	25.46
2 min				39.95	32.52	38.34	34.14
3 min					57.45	73.77	54.47
4 min						65.19	68.18
5 min							62.69
6 min							

Overall result

Time	initial	1 min	2 mins	3 mins	4 mins	5 mins	6 mins
Initial		√	√	√	√	√	√
1 min			√	√	√	√	√
2 min				√	√	√	√
3 min					X	X	X
4 min						X	X
5 min							X
6 min							

I.1.2 Effect of spheronisation speed on pellet dissolution

Table I.1.2 (from Figure 3.5)

Difference factor (f_1)

Speed	Speed 4	Speed 5	Speed 6	Speed 7
Speed 4		44.23	32.60	37.48
Speed 5			17.74	6.61
Speed 6				8.33
Speed 7				

Similarity factor (f_2)

Speed	Speed 4	Speed 5	Speed 6	Speed 7
Speed 4		30.17	37.85	34.65
Speed 5			57.06	68.45
Speed 6				69.23
Speed 7				

Overall result

Speed	Speed 4	Speed 5	Speed 6	Speed 7
Speed 4		√	√	√
Speed 5			X	X
Speed 6				X
Speed 7				

I.1.3 Effect of GMS content on pellet dissolution

Table I.1.3 (from Figure 3.7)

Difference factor (f_1)

% w/w	30 %	40 %	50 %	60 %	70 %	90 %
30 %		28.23	14.72	9.23	13.02	32.39
40 %			16.27	34.99	38.16	51.67
50 %				28.29	33.05	69.55
60 %					1.59	21.19
70 %						19.84
90 %						

Similarity factor (f_2)

% w/w	30 %	40 %	50 %	60 %	70 %	90 %
30 %		42.08	60.38	57.28	60.08	41.17
40 %			54.06	36.40	35.41	28.55
50 %				46.09	45.89	34.63
60 %					78.99	50.42
70 %						50.47
90 %						

Overall result

% w/w	30 %	40 %	50 %	60 %	70 %	90 %
30 %		√	X	X	X	√
40 %			X	√	√	√
50 %				√	√	√
60 %					X	X
70 %						X
90 %						

I.1.4 Effect of GMS pellet ageing on dissolution performance

Table I.1.4 (from Figure 3.9)

Difference factor (f_1)

% w/w	30 %, initial	40 %, initial	50 %, Initial	60 %, initial	70 %, initial	90 %, initial
30 %, day 75	59.06					
40 %, day 75		55.95				
50 %, day 75			162.95			
60 %, day 75				45.93		
70 %, day 75					130.11	
90 %, day 75						31.77

Similarity factor (f_2)

% w/w	30 %, initial	40 %, initial	50 %, Initial	60 %, initial	70 %, initial	90 %, initial
30 %, day 75	27.22					
40 %, day 75		26.04				
50 %, day 75			25.09			
60 %, day 75				31.21		
70 %, day 75					26.66	
90 %, day 75						39.33

Overall result

% w/w	30 %, initial	40 %, initial	50 %, Initial	60 %, initial	70 %, initial	90 %, initial
30 %, day 75	√					
40 %, day 75		√				
50 %, day 75			√			
60 %, day 75				√		
70 %, day 75					√	
90 %, day 75						√

I.1.5 Effect of wax compositions of identical HLB on pellet dissolution

Table I.1.5.1 (from Figure 3.10)

Difference factor (f_1)

Composition	60% GMS (4 mins)	51.6%GDB : 8.4% PG8BX (4 mins)	54.6%GDB : 5.4% Gelucire 50/13 (4 mins)
60% GMS (4 mins)		19.68	160.07
51.6%GDB : 8.4% PG8BX (4 mins)			55.84
54.6%GDB : 5.4% Gelucire 50/13 (4 mins)			

Similarity factor (f_2)

Composition	60% GMS (4 mins)	51.6%GDB : 8.4% PG8BX (4 mins)	54.6%GDB : 5.4% Gelucire 50/13 (4 mins)
60% GMS (4 mins)		45.15	21.57
51.6%GDB : 8.4% PG8BX (4 mins)			33.52
54.6%GDB : 5.4% Gelucire 50/13 (4 mins)			

Overall result

Composition	60% GMS (4 mins)	51.6%GDB : 8.4% PG8BX (4 mins)	54.6%GDB : 5.4% Gelucire 50/13 (4 mins)
60% GMS (4 mins)		√	√
51.6%GDB : 8.4% PG8BX (4 mins)			√
54.6%GDB : 5.4% Gelucire 50/13 (4 mins)			

Table I.1.5.2 (from Figure 3.11)

Difference factor (f_1)

Composition	51.6%GDB : 8.4% PG8BX (2 mins)	51.6%GPS : 8.4% PG8BX (2 mins)
51.6%GDB : 8.4% PG8BX (2 mins)		41.31
51.6%GPS : 8.4% PG8BX (2 mins)		

Similarity factor (f_2)

Composition	51.6%GDB : 8.4% PG8BX (2 mins)	51.6%GPS : 8.4% PG8BX (2 mins)
51.6%GDB : 8.4% PG8BX (2 mins)		37.87
51.6%GPS : 8.4% PG8BX (2 mins)		

Overall result

Composition	51.6%GDB : 8.4% PG8BX (2 mins)	51.6%GPS : 8.4% PG8BX (2 mins)
51.6%GDB : 8.4% PG8BX (2 mins)		√
51.6%GPS : 8.4% PG8BX (2 mins)		

I.1.6 Effect of spheronisation time and temperature on pellet dissolution

Table I.1.6.1 (from Figure 3.12)

Difference factor (f_1)

Time	2 minutes	4 minutes	6 minutes
2 minutes		5.05	29.67
4 minutes			17.89
6 minutes			

Similarity factor (f_2)

Time	2 minutes	4 minutes	6 minutes
2 minutes		76.23	43.80
4 minutes			48.76
6 minutes			

Overall result

Time	2 minutes	4 minutes	6 minutes
2 minutes		X	√
4 minutes			√
6 minutes			

Table I.1.6.2 (from Figure 3.13)

Difference factor (f_1)

Temperature	50°C	55°C	58°C	60°C
50°C		14.58	39.11	26.90
55°C			27.35	18.35
58°C				14.02
60°C				

Similarity factor (f_2)

Temperature	50°C	55°C	58°C	60°C
50°C		53.02	31.46	39.36
55°C			41.07	56.78
58°C				54.55
60°C				

Overall result

Temperature	50°C	55°C	58°C	60°C
50°C		X	√	√
55°C			√	X
58°C				X
60°C				

I.1.7 Effect of GDB-PG8BX pellet ageing on dissolution performance

Table I.1.7 (from Figure 3.15)

Difference factor (f_1)

Composition	51.6%GDB : 8.4%PG8BX, initial
51.6%GDB : 8.4%PG8BX , day 75	4.65

Similarity factor (f_2)

Composition	51.6%GDB : 8.4%PG8BX, initial
51.6%GDB : 8.4%PG8BX , day 75	76.73

Overall result

Composition	51.6%GDB : 8.4%PG8BX, initial
51.6%GDB : 8.4%PG8BX , day 75	X

I.2 Chapter 5 Physicochemical evaluations of wax matrix formulations

I.2.1 Effect of thermal annealing on GMS pellet formulations containing paracetamol

Table I.2.1 (from Figure 5.3)

Difference factor (f_1)

Time	initial	Day 1	Day 2	Day 3	Day 4	Day 5	Day 6	Day 7	Day 28
Initial		69.52	65.75	67.00	70.07	67.17	62.36	63.71	56.08
Day 1			6.67	11.24	18.68	15.56	8.47	9.27	3.88
Day 2				5.35	12.99	10.20	2.69	4.32	8.28
Day 3					8.07	5.12	2.80	1.26	15.19
Day 4						3.20	10.65	10.17	25.30
Day 5							7.78	6.75	21.41
Day 6								1.56	11.96
Day 7									13.73
Day 28									

Similarity factor (f2)

Time	initial	Day 1	Day 2	Day 3	Day 4	Day 5	Day 6	Day 7	Day 28
Initial		22.48	25.03	22.83	21.90	22.65	24.29	27.61	30.34
Day 1			60.87	53.74	48.67	48.46	50.85	49.68	51.80
Day 2				75.05	62.74	62.99	68.44	65.92	65.50
Day 3					77.78	79.00	81.58	80.61	65.40
Day 4						90.03	73.15	75.64	58.20
Day 5							79.34	83.55	60.94
Day 6								94.79	71.54
Day 7									68.50
Day 28									

Overall result

Time	initial	Day 1	Day 2	Day 3	Day 4	Day 5	Day 6	Day 7	Day 28
Initial		√	√	√	√	√	√	√	√
Day 1			X	X	√	√	X	√	X
Day 2				X	X	X	X	X	X
Day 3					X	X	X	X	X
Day 4						X	X	X	X
Day 5							X	X	X
Day 6								X	X
Day 7									X
Day 28									

I.2.2 Effect of thermal annealing on GPS pellet formulations containing diltiazem HCl

Table I.2.2.1 (from Figure 5.9)

Difference factor (f_1)

Time	initial	Day 4	Day 7	Day 14	Day 28
Initial		11.50	55.88	104.34	139.13
Day 4			39.25	93.99	147.55
Day 7				29.48	58.60
Day 14					15.38
Day 28					

Similarity factor (f2)

Time	initial	Day 4	Day 7	Day 14	Day 28
Initial		49.46	35.94	29.60	26.72
Day 4			43.92	31.59	26.77
Day 7				48.79	38.19
Day 14					64.13
Day 28					

Overall result

Time	initial	Day 4	Day 7	Day 14	Day 28
Initial		√	√	√	√
Day 4			√	√	√
Day 7				√	√
Day 14					X
Day 28					

Table I.2.2.2 (from Figure 5.10)

Difference factor (f_1)

Time	initial	Day 4	Day 7	Day 14	Day 28
Initial		7.21	12.98	13.30	10.36
Day 4			6.25	5.71	5.58
Day 7				0.58	0.21
Day 14					1.57
Day 28					

Similarity factor (f2)

Time	initial	Day 4	Day 7	Day 14	Day 28
Initial		61.80	52.69	53.45	52.35
Day 4			70.25	72.48	60.56
Day 7				88.98	75.15
Day 14					76.77
Day 28					

Overall result

Time	initial	Day 4	Day 7	Day 14	Day 28
Initial		X	X	X	X
Day 4			X	X	X
Day 7				X	X
Day 14					X
Day 28					

I.2.3 Effect of thermal annealing on GPS pellet formulations with high diltiazem HCl loading

Table I.2.3.1 (from Figure 5.13)

Difference factor (f_1)

Time	initial	Day 4	Day 7	Day 28	Adizem® XL
Initial		5.50	15.17	64.29	19.02
Day 4			9.48	85.33	36.43
Day 7				64.69	39.51
Day 28					133.30
Adizem® XL					

Similarity factor (f_2)

Time	initial	Day 4	Day 7	Day 28	Adizem® XL
Initial		48.08	43.37	30.98	56.51
Day 4			66.76	31.75	44.82
Day 7				35.84	43.28
Day 28					28.67
Adizem® XL					

Overall result

Time	initial	Day 4	Day 7	Day 28	Adizem® XL
Initial		√	√	√	X
Day 4			X	√	√
Day 7				√	√
Day 28					√
Adizem® XL					

Table I.2.3.2 (from Figure 5.14)

Difference factor (f_1)

Time	initial	Day 4	Day 7	Day 28	Adizem® XL
Initial		31.89	40.15	22.59	19.02
Day 4			6.95	9.60	63.70
Day 7				13.79	74.38
Day 28					58.40
Adizem® XL					

Similarity factor (f_2)

Time	initial	Day 4	Day 7	Day 28	Adizem® XL
Initial		42.76	38.90	45.34	56.51
Day 4			72.36	69.29	39.33
Day 7				59.86	35.89
Day 28					39.83
Adizem® XL					

Overall result

Time	initial	Day 4	Day 7	Day 28	Adizem® XL
Initial		√	√	√	X
Day 4			X	X	√
Day 7				X	√
Day 28					√
Adizem® XL					

I.2.4 Effect of wax type on thermal annealing

Table I.2.4 (from Figure 5.20)

Difference factor (f_1)

Time	GMS Initial	GMS day7	GMS day28	GPS Initial	GPS day7	GPS day28	GDB Initial	GDB day7	GDB day28
GMS Initial		50.86	52.49	82.96			71.73		
GMS day7			12.09		29.03			116.43	
GMS day28						13.02			61.59
GPS Initial					203.40	222.05	7.52		
GPS day7						6.49		43.41	
GPS day28									50.44
GDB Initial								7.04	7.18
GDB day7									13.28
GDB day28									

Similarity factor (f2)

Time	GMS Initial	GMS day7	GMS day28	GPS Initial	GPS day7	GPS day28	GDB Initial	GDB day7	GDB day28
GMS Initial		22.66	21.77	11.51			15.22		
GMS day7			57.18		46.16			24.71	
GMS day28						49.79			22.18
GPS Initial					23.13	21.95	42.15		
GPS day7						63.31		28.77	
GPS day28									26.32
GDB Initial								76.48	76.53
GDB day7									63.42
GDB day28									

Overall result

Time	GMS Initial	GMS day7	GMS day28	GPS Initial	GPS day7	GPS day28	GDB Initial	GDB day7	GDB day28
GMS Initial		√	√	√			√		
GMS day7			X		√			√	
GMS day28						√			√
GPS Initial					√	√	√		
GPS day7						X		√	
GPS day28									√
GDB Initial								X	X
GDB day7									X
GDB day28									

I.2.5 Effect of wax content on thermal annealing

Table I.2.5.1 (from Figure 5.21)

Difference factor (f_1)

Time	40%GMS Initial	40% GMS day7	40% GMS day28	60%GMS Initial	60% GMS day7	60% GMS day28	90% GMS Initial	90% GMS day7	90% GMS day28
40% GMS Initial		66.23	62.22	25.08			7.24		
40% GMS day 7			6.18		2.93			15.07	
40% GMS day28						9.27			23.12
60% GMS Initial					55.20	57.85	25.67		
60% GMS day 7						5.32		17.56	
60% GMS day28									12.67
90% GMS Initial								60.74	57.80
90% GMS day 7									1.89
90% GMS day28									

Similarity factor (f_2)

Time	40%GMS Initial	40% GMS day7	40% GMS day28	60%GMS Initial	60% GMS day7	60% GMS day28	90% GMS Initial	90% GMS day7	90% GMS day28
40% GMS Initial		21.67	22.97	48.03			69.01		
40% GMS day 7			78.77		84.07			60.83	
40% GMS day28						72.05			54.64
60% GMS Initial					26.08	25.21	42.68		
60% GMS day 7						78.02		57.06	
60% GMS day28									67.08
90% GMS Initial								24.37	25.28
90% GMS day 7									86.19
90% GMS day28									

Overall result

Time	40%GMS Initial	40% GMS day7	40% GMS day28	60%GMS Initial	60% GMS day7	60% GMS day28	90% GMS Initial	90% GMS day7	90% GMS day28
40% GMS Initial		√	√	√			X		
40% GMS day 7			X		X			X	
40% GMS day28						X			X
60% GMS Initial					√	√	√		
60% GMS day 7						X		X	
60% GMS day28									X
90% GMS Initial								√	√
90% GMS day 7									X
90% GMS day28									

Table I.2.5.2 (from Figure 5.22)

Difference factor (f_1)

Time	60%GPS Initial	60% GPS day 4	60%GPS day14	60% GPS day28	90% GPS Initial	90% GPS day 4	90%GPS day14	90% GPS day28
60% GPS Initial		61.37	67.04	65.94	57.50			
60% GPS day 4			15.72	12.94		74.76		
60% GPS day14				3.24			122.50	
60% GPS day28								54.04
90% GPS Initial						12.31	47.75	115.27
90% GPS day 4							48.45	59.60
90% GPS day14								15.38
90% GPS day28								

Similarity factor (f_2)

Time	60%GPS Initial	60% GPS day 4	60%GPS day14	60% GPS day28	90% GPS Initial	90% GPS day 4	90%GPS day14	90% GPS day28
60% GPS Initial		24.83	23.13	23.96	35.46			
60% GPS day 4			60.10	55.99		19.74		
60% GPS day14				65.85			27.83	
60% GPS day28								28.00
90% GPS Initial						48.67	29.48	26.50
90% GPS day 4							31.59	26.77
90% GPS day14								55.38
90% GPS day28								

Overall result

Time	60%GPS Initial	60% GPS day 4	60%GPS day14	60% GPS day28	90% GPS Initial	90% GPS day 4	90%GPS day14	90% GPS day28
60% GPS Initial		√	√	√	√			
60% GPS day 4			X	X		√		
60% GPS day14				X			√	
60% GPS day28								√
90% GPS Initial						√	√	√
90% GPS day 4							√	√
90% GPS day14								X
90% GPS day28								

I.2.6 Effect of drug type and content on thermal annealing

Table I.2.6.1 (from Figure 5.23)

Difference factor (f_1)

Time	10%PCM Initial	10%PCM day4	10%PCM day7	10%PCM day28	10%DTZ Initial	10%DTZ day4	10%DTZ day7	10%DTZ day28
10%PCM Initial		70.07	63.71	56.08	173.48			
10%PCM day 4			10.17	25.30		85.70		
10%PCM day7				13.73			81.96	
10%PCM day28								293.77
10%DTZ Initial						157.27	50.86	52.49
10%DTZ day 4							13.12	1.88
10%DTZ day7								12.09
10%DTZ day28								

Similarity factor (f_2)

Time	10%PCM Initial	10%PCM day4	10%PCM day7	10%PCM day28	10%DTZ Initial	10%DTZ day4	10%DTZ day7	10%DTZ day28
10%PCM Initial		21.90	27.61	30.34	16.88			
10%PCM day 4			75.64	58.20		26.51		
10%PCM day7				68.50			17.43	
10%PCM day28								18.95
10%DTZ Initial						18.45	22.66	21.77
10%DTZ day 4							57.32	56.59
10%DTZ day7								57.18
10%DTZ day28								

Overall result

Time	10%PCM Initial	10%PCM day4	10%PCM day7	10%PCM day28	10%DTZ Initial	10%DTZ day4	10%DTZ day7	10%DTZ day28
10%PCM Initial		√	√	√	√			
10%PCM day 4			X	X		√		
10%PCM day7				X			√	
10%PCM day28								√
10%DTZ Initial						√	√	√
10%DTZ day 4							X	X
10%DTZ day7								X
10%DTZ day28								

Table I.2.6.2 (from Figure 5.24)

Difference factor (f_1)

Time	10%DTZ Initial	10%DTZ day4	10%DTZ day7	10%DTZ day28	40%DTZ Initial	40%DTZ day4	40%DTZ day7	40%DTZ day28
10%DTZ Initial		61.37	67.04	65.94	21.84			
10%DTZ day 4			15.72	12.94		70.14		
10%DTZ day7				3.24			73.40	
10%DTZ day28								53.33
40%DTZ Initial						3.87	14.26	65.41
40%DTZ day 4							8.66	72.82
40%DTZ day7								53.95
40%DTZ day28								

Similarity factor (f_2)

Time	10%DTZ Initial	10%DTZ day4	10%DTZ day7	10%DTZ day28	40%DTZ Initial	40%DTZ day4	40%DTZ day7	40%DTZ day28
10%DTZ Initial		24.83	23.13	23.96	44.39			
10%DTZ day 4			60.10	55.99		21.45		
10%DTZ day7				65.85			20.79	
10%DTZ day28								28.92
40%DTZ Initial						49.03	44.19	31.56
40%DTZ day 4							66.76	33.20
40%DTZ day7								37.78
40%DTZ day28								

Overall result

Time	10%DTZ Initial	10%DTZ day4	10%DTZ day7	10%DTZ day28	40%DTZ Initial	40%DTZ day4	40%DTZ day7	40%DTZ day28
10%DTZ Initial		√	√	√	√			
10%DTZ day 4			X	X		√		
10%DTZ day7				X			√	
10%DTZ day28								√
40%DTZ Initial						√	√	√
40%DTZ day 4							X	√
40%DTZ day7								√
40%DTZ day28								

I.3 Chapter 7 Impact of thermal annealing and stabilisation excipients on dissolution properties of wax matrix pellets

I.3.1 Effect of nucleation inhibitors on response to thermal annealing

Table I.3.1 (from Figure 7.1)

Difference factor (f_1)

Time	initial	Day 7	Day 14	Day 28
Initial		31.41	29.06	18.84
Day 7			3.29	38.19
Day 14				24.39
Day 28				

Similarity factor (f_2)

Time	initial	Day 7	Day 14	Day 28
Initial		37.21	38.72	45.77
Day 7			88.09	41.01
Day 14				42.02
Day 28				

Overall result

Time	initial	Day 7	Day 14	Day 28
Initial		√	√	√
Day 7			X	√
Day 14				√
Day 28				

I.3.2 Effect of nucleation enhancers on response to thermal annealing

Table I.3.2.1 (from Figure 7.3)

Difference factor (f_1)

Time	initial	Day 7	Day 14	Day 28
Initial		8.12	51.15	53.25
Day 7			34.37	58.66
Day 14				48.90
Day 28				

Similarity factor (f_2)

Time	initial	Day 7	Day 14	Day 28
Initial		54.47	39.13	38.63
Day 7			42.47	28.92
Day 14				43.29
Day 28				

Overall result

Time	initial	Day 7	Day 14	Day 28
Initial		X	√	√
Day 7			√	√
Day 14				√
Day 28				

Table I.3.2.2 (from Figure 7.5)

Difference factor (f_1)

Time	initial	Day 7	Day 14	Day 28
Initial		1.80	1.09	43.57
Day 7			2.82	51.24
Day 14				55.99
Day 28				

Similarity factor (f_2)

Time	initial	Day 7	Day 14	Day 28
Initial		58.27	57.09	37.81
Day 7			75.50	37.46
Day 14				39.20
Day 28				

Overall result

Time	initial	Day 7	Day 14	Day 28
Initial		X	X	√
Day 7			X	√
Day 14				√
Day 28				

Table I.3.2.3 (from Figure 7.7)

Difference factor (f_1)

Time	initial	Day 7	Day 14	Day 28
Initial		23.36	6.21	33.48
Day 7			21.30	51.84
Day 14				52.51
Day 28				

Similarity factor (f_2)

Time	initial	Day 7	Day 14	Day 28
Initial		44.64	57.47	42.22
Day 7			50.71	29.07
Day 14				39.16
Day 28				

Overall result

Time	initial	Day 7	Day 14	Day 28
Initial		√	X	√
Day 7			X	√
Day 14				√
Day 28				

I.3.3 In vitro dissolution of GPS-diltiazem pellet formulations in various dissolution media

Table I.3.3 (from Figure 7.9)

Difference factor (f_1)

Media	Water	pH 1.2	pH 5.0	pH 7.4
Water		4.65	9.27	12.75
pH 1.2			5.09	9.28
pH 5.0				3.99
pH 7.4				

Similarity factor (f_2)

Media	Water	pH 1.2	pH 5.0	pH 7.4
Water		78.75	70.95	65.91
pH 1.2			84.70	75.70
pH 5.0				87.88
pH 7.4				

Overall result

Media	Water	pH 1.2	pH 5.0	pH 7.4
Water		X	X	X
pH 1.2			X	X
pH 5.0				X
pH 7.4				